Fisheries and Oceans Canada | Pêches et Océans Canada
Ecosystems and Oceans Science | Sciences des écosystèmes et des océans

Canadian Science Advisory Secretariat (CSAS)

Research Document 2024/007

Quebec Region

Results of Comparative Fishing Between the CCGS *Teleost* and CCGS *John Cabot* in the Estuary and Northern Gulf of St. Lawrence in 2021 and 2022

Hugues P. Benoît[1], Yihao Yin[2] and Hugo Bourdages[1]

[1]Fisheries and Oceans Canada
Maurice Lamontagne Institute
Mont Joli, QC G5H 3Z4

[2] Fisheries and Oceans Canada
Bedford Institute of Oceanography
Dartmouth, NS B2Y 4A2

April 2024

Foreword

This series documents the scientific basis for the evaluation of aquatic resources and ecosystems in Canada. As such, it addresses the issues of the day in the time frames required and the documents it contains are not intended as definitive statements on the subjects addressed but rather as progress reports on ongoing investigations.

Published by:

Fisheries and Oceans Canada
Canadian Science Advisory Secretariat
200 Kent Street
Ottawa ON K1A 0E6

http://www.dfo-mpo.gc.ca/csas-sccs/
csas-sccs@dfo-mpo.gc.ca

ISSN 1919-5044
ISBN 978-0-660-70787-7 Cat. No. Fs70-5/2024-007E-PDF

Correct citation for this publication:

Benoît, H.P., Yin, Y., and Bourdages, H. 2024. Results of Comparative Fishing Between the CCGS *Teleost* and CCGS *John Cabot* in the Estuary and Northern Gulf of St. Lawrence in 2021 and 2022. DFO Can. Sci. Advis. Sec. Res. Doc. 2024/007. xvii + 229 p.

Aussi disponible en français :

Benoît, H.P., Yin, Y., et Bourdages, H. 2024. Résultats de la pêche comparative entre le NGCC Teleost *et le NGCC* John Cabot *dans l'estuaire et le nord du golfe du Saint-Laurent en 2021 et 2022. Secr. can. des avis sci. du MPO. Doc. de rech. 2024/007. xix + 233 p.*

TABLE OF CONTENTS

LIST OF TABLES

LIST OF FIGURES

ABSTRACT

Bottom-trawl surveys provide key inputs to stock assessments for groundfish stocks and other taxa, for ecosystem monitoring and reporting, and for research. These surveys can produce annual indices of abundance that are proportional to stock size, provided that the proportionality constant, typically called catchability, does not change over time. This is typically achieved through the use of standardized survey design and procedures. Periodically it becomes necessary or desirable to change one or more aspects of the protocol, and calibration experiments are typically required to estimate adjustments for possible changes in catchability. From 2004 to 2022, the CCGS *Teleost* fishing a Campelen 1800 bottom-trawl was used for the annual survey of the Estuary and northern Gulf of St. Lawrence (EnGSL). This vessel will soon be retired and is being replaced by the CCGS *John Cabot*, fishing a slightly modified Campelen 1800 trawl. Paired-trawl comparative fishing experiments involving these two vessels and gear pairs were conducted in August 2021 and August and September 2022 to obtain catch data required to estimate their relative fishing efficiency for a large number of fish and invertebrate taxa that are routinely sampled in this survey. In this document we briefly describe these comparative fishing experiments and report on analyses of the resulting data for over 125 fish and invertebrate taxa routinely sampled by the EnGSL survey. The analyses employed a suite of contemporary statistical models used previously in extended comparative fishing analyses in the eastern United States and which were recently extensively tested using simulations. Relative catchability as a function of individual lengths (fishes, shrimps and squid) or carapace width (crabs) was evaluated and estimated for 50 taxa, whereas size-aggregated estimates were derived for the others. Given the large similarities between the old and replacement survey vessel and gear, and consequent expected similarity in catchability, and in some cases due to modest sample sizes, estimates of relative catchability were not statistically significant for many taxa. Recommendations for the application of the conversion factors are provided. Use of these conversion factors will maintain the integrity of the over four decade long time series for various northern Gulf marine taxa.

1. INTRODUCTION

Worldwide, bottom-trawl surveys provide key inputs to stock assessments for groundfish stocks and other taxa, for ecosystem monitoring and reporting, and for research. These surveys can produce annual indices of abundance that are proportional to stock size, provided that the proportionality constant, typically called catchability, does not change over time. Failure to achieve this consistency via proper sampling design and standardization increases the risk of confounding changes in abundance with changes in catchability. Maintaining consistency in survey protocols, and the survey vessel and gear (hereafter in the Introduction, simply the protocol) is key to maintaining a constant catchability. However, periodically it becomes necessary or desirable to change one or more aspects of the protocol, and calibration experiments are typically required to estimate adjustments for possible changes in catchability. The most common and effective form of these experiments is comparative fishing, which usually involves paired trawling of vessels constituting the former and replacement protocol as close together as safety permits. This design minimizes the difference in fish densities sampled by the trawls, such that differences in catches over replicates of paired-trawl sampling will reflect the difference in catchability.

Fisheries and Oceans Canada (DFO) is undertaking comparative fishing in each of its six Atlantic bottom-trawl surveys from 2021 to 2023 to calibrate two new offshore fisheries survey vessels that will replace two retiring longstanding vessels. In some surveys, the change in vessel will also be accompanied by a change in survey trawl and survey procedures (e.g., tow duration), and the joint effect of all of these factors on relative catchability should be reflected in results of the comparative fishing experiments. In the survey of the Estuary and northern Gulf of St. Lawrence (EnGSL), which has taken place annually in August since 1984, the CCGS John Cabot (63.0 m; 2 975 t gross tonnage) will replace the CCGS Teleost (63 m; 2 405 t gross tonnage), which has been used to conduct the survey since 2004. During the EnGSL survey, the CCGS Teleost fished using the Campelen 1800 trawl (Walsh et al. 2009), and a version of that trawl, modified slightly to make it less susceptible to damage and to improve repairability, will be used by the CCGS John Cabot (details in Appendix I). No other changes to the survey protocol were introduced with the arrival of the CCGS John Cabot. Comparative fishing between the two vessels, with their respective trawls, took place during the regular survey of the EnGSL in 2021, and principally in 2022. The design employed, sometimes termed a shadow survey design (Thiess et al. 2018), involved paired trawling at sites selected as part of the routine stratified random design for the survey (Fig. 1). Such a design best ensures that comparative fishing results will reflect the environmental conditions of the survey area which can affect catchability, principally depths and bottom substrate. It also ensures that data will be available to estimate relative catchability adjustment factors for as many as possible of the taxa that are sampled by the survey and for which standardization is required for ongoing research and reporting.

In this document, we describe the 2021-2022 comparative fishing experiments for the EnGSL and report on analyses of the resulting data for over 125 fish and invertebrate taxa routinely sampled by the EnGSL survey. The analyses employed contemporary statistical models used previously in extended comparative fishing analyses in the eastern United State (Miller et al. 2010; Miller 2013), and applied recently to analyses of past comparative fishing data for some stocks in the Gulf of St. Lawrence (Yin and Benoît 2022a; Benoît et al. 2022). These models were extensively tested in a simulation context and were confirmed appropriate for analyses such as those employed in the present case (Yin and Benoît 2022b). As part of the analyses, estimates of relative catchability as a function of individual lengths (fish, squid and decapod shrimps) or carapace width (crabs) were derived for 50 taxa, whereas size-aggregated

estimates were derived for the others. Given the large similarities between the old and replacement survey protocols and consequent expected similarity in catchability, and in some cases due to modest sample sizes, estimates of relative catchability were not statistically significant for many taxa. We recommend that the estimates in these instances not be applied for survey standardization.

2. METHODS

2.1. COMPARATIVE FISHING

Comparative fishing was constrained to August 13 to 18 in 2021 due to the availability of the CCGS John Cabot. Twenty-one valid paired tows were completed that year (Table 1; Fig. 2). In 2022, 161 valid paired tows were completed between August 11th and September 13th. In both years, comparative fishing was undertaken at regular survey stations chosen according to the stratified random design (Fig. 1).

At pre-selected stations, the CCGS John Cabot and the CCGS Teleost fished as close together in space and in time as was safe and practical. The majority of paired sets were done side-by-side, and across stations, the vessels alternated between having the other vessel on their port or starboard side. Efforts were made to ensure similar depths between the two locations fished at a station. The distance separating the vessels was typically 1 km or less, and didn't exceed 2 km. The difference in the start times for paired tows averaged 10 minutes, and exceeded 1 hour (but not 2 hours) for only seven set pairs. At eight stations at which suitable bottom could only be found for one vessel, or where depth contours were strong, the vessels fished the same track sequentially, alternating across stations as to which vessel fished first. These stations are indicated in Table 1.

Both vessels fished standard tows targeting a tow time of 15 minutes at 3.0 knots. Tow durations of at least 10 minutes were considered acceptable. Tow time was measured from the time the trawl was on bottom and began fishing, to the time it lifted off bottom. Both vessels employed an auto-trawl system using Scanmar sensors in which trawl geometry is dynamically adjusted during the tow to keep the trawl square to the trawl path. The data from the Scanmar sensors were additionally used to monitor trawl performance and to potentially invalidate a tow, but were not used to calculate the swept area of each tow for use in the data analyses. Instead, tow distance was used as the sole standardizing factor for swept area of individual tows. A brief analysis of the Scanmar data is presented in Appendix II. Based on that analysis, the swept area (wingspread) of an average survey tow is 16.71 m with the new protocol, compared to 16.94 m with the Teleost-Campelen protocol.

Catch processing followed the standard protocols for the EnGSL survey (Bourdages et al. 2022), with the exception that some detailed biological sampling such as the collection of data on fish maturities and individual weights, and the collection of otoliths for some species, was only undertaken aboard the CCGS Teleost during comparative tows.

2.2. COMPARATIVE FISHING DATA ANALYSIS

2.2.1. Binomial models

In the analysis of comparative fishing data, the goal is to estimate the relative fishing efficiency between a pair of vessels-gear combinations (referred to as vessel in this section for simplicity). We assume the expected catch from vessel v ($v \in \{A, B\}$) at length l and at station i is

$$E[C_{vi}(l)] = q_{vi}(l) D_{vi}(l) f_{vi}$$

where, $q_{vi}(l)$ is the catchability of vessel v, D_{vi} is the underlying population density sampled by vessel v, and f_{vi} is a standardization term which usually includes the swept area of a tow, and if applicable, the proportion of sub-sampling for size measurement on-board. In a binomial model (e.g., Miller 2013), the catch from vessel A at station i, conditioning on the combined catch from both vessels at this station, $C_i(l) = C_{Ai}(l) + C_{Bi}(l)$, is binomial-distributed

$$C_{Ai}(l) \sim BI(C_i(l), p_{Ai}(l))$$

where $p_{Ai}(l)$ is the expected proportion of catch from vessel A. Tows in a pair are generally assumed to fish the same underlying densities at the station, as the paired vessels typically fish within a small distance of each other: $D_{Ai}(l) = D_{Bi}(l) = D_i(l)$. Then the logit-probability of catch by vessel A is

$$logit(p_{Ai}(l)) = log(\frac{E[C_{Ai}(l)]}{E[C_{Bi}(l)]}) = log(\rho_i(l)) + o_i$$

Where $\rho_i(l)$ is the ratio of catchabilities between vessels A and B at length l and at station i, or the conversion factor, the quantity of interest,

$$\rho_i(l) = q_{Ai}(l)/q_{Bi}(l)$$

and $o_i = log(f_{Ai}/f_{Bi})$ is an offset term derived from known standardization terms for tow length relative to the standard tow length and for subsampling.

For a length-based conversion factor, we consider a smooth length effect based on a general additive smooth function,

$$log(\rho(l)) = \sum_{k=0}^{K} \beta_k X_k(l) = \mathbf{X}^T\boldsymbol{\beta},$$

where $\boldsymbol{\beta}$ are the coefficient parameters and are estimated, $\mathbf{X}$, or $\{X_k(l), k = 0,1,\cdots,K\}$, are a set of smoothing basis functions, and K is the dimension of the basis that controls the number of coefficient parameters and is usually pre-defined. Here a cubic spline smoother was used (Hastie et al. 2009), with the basis functions and penalty matrices generated by the R package mgcv for R (Wood 2011; R core team 2021).

The estimation of a cubic spline smoother is based on the penalized sum of squares smoothing objective, but in practice, this is usually replaced by a penalized likelihood objective (Green and Silverman 1993):

$$\mathcal{L}(\boldsymbol{\beta}, \lambda) = f(\mathbf{Y}|\mathbf{X}, \boldsymbol{\beta})e^{-\frac{\lambda}{2}\boldsymbol{\beta}^T\mathbf{S}\boldsymbol{\beta}}$$

$\mathcal{L}$ denotes the likelihood objective function. $f(\mathbf{Y}|\mathbf{X}, \boldsymbol{\beta})$ is the joint probability function of the survey data $\mathbf{Y}$ conditional on the basis functions and coefficient parameters. $\mathbf{S}$ is the penalty matrix defined by the smoother and the dimension of the basis, and λ is the smoothness parameter. This smoothness parameter is estimated by maximum likelihood along with other model parameters but may be sensitive to the data. In such cases, it can be determined by other criteria such as generalized cross-validation (Wood 2000).

The penalized maximum likelihood smoother can also be re-parameterized into a mixed effects model (Verbyla et al. 1999; Wood 2017) to facilitate implementation as well as incorporation of additional random effects:

$$log(\rho_i(l)) = \mathbf{X}_f^T\boldsymbol{\beta}_f + \mathbf{X}_r^T\mathbf{b}$$

where $\boldsymbol{\beta}_f$ are fixed effects and $\mathbf{b}$ are random effects. $\mathbf{X}_f$ and $\mathbf{X}_r$ are transformed from the basis functions $\mathbf{X}$ and an eigen-decomposition of the penalty matrix $\mathbf{S}$, $\mathbf{X}_f = \mathbf{U}_f^T\mathbf{X}$ and $\mathbf{X}_r = \mathbf{U}_r^T\mathbf{X}$, where $\mathbf{U}_f$ and $\mathbf{U}_r$ are the eigenvectors that correspond to the zero and positive eigenvalues of $\mathbf{S}$. The random effects $b \sim \mathrm{N}(0, \mathbf{D}_+^{-1}/\boldsymbol{\lambda})$ where D_+ is the diagonal matrix of the positive eigenvalues of S. In the mixed effects model representation of the cubic spline smoother, the number of fixed effects is 2 and the number of random effects is bounded by $K - 2$. Smoothing effects are transformed into shrinkage of random effects in the fitting of random deviations, and can be integrated into complex mixed effects models commonly used in fisheries science (Thorson and Minto 2015).

Additional random effects can be incorporated into the mixed effects model to address variations in the relative catch efficiency related to each station,

$$log(\rho_i(l)) = \mathbf{X}_f^T(\boldsymbol{\beta}_f + \boldsymbol{\delta}_i) + \mathbf{X}_r^T(\mathbf{b} + \boldsymbol{\epsilon}_i).$$

where $\boldsymbol{\delta}_i \sim \mathrm{N}(\mathbf{0}, \boldsymbol{\Sigma})$ and $\boldsymbol{\epsilon}_i \sim \mathrm{N}(\mathbf{0}, \mathbf{D}_+^{-1}/\xi)$. From a similar re-parameterization of the cubic spline smoother, these random effects allow for deviations of the length-based conversion at each station. $\boldsymbol{\Sigma}$ is the covariance matrix of the random effects corresponding to the random deviations and contains three parameters. ξ controls the degree of smoothness of the random smoothers and the smoother at each station can differ.

A summary of the above binomial mixed model is as follows,

$$C_i(l) = C_{Ai}(l) + C_{Bi}(l)$$
$$C_{Ai}(l) \sim BI(C_i(l), p_{Ai}(l))$$
$$logit(p_{Ai}(l)) = log(\rho_i(l)) + o_i$$
$$log(\rho_i(l)) = \mathbf{X}_f^T(\boldsymbol{\beta}_f + \boldsymbol{\delta}_i) + \mathbf{X}_r^T(\mathbf{b} + \boldsymbol{\epsilon}_i)$$

The model is estimated via maximum likelihood and the marginal likelihood integrating out random effects is

$$\mathcal{L}(\boldsymbol{\beta}_f, \boldsymbol{\Sigma}, \lambda, \xi) = \int \left(\prod_{i=1}^{m} \int \int f(\mathbf{Y}_i|\mathbf{X}_f, \mathbf{X}_r, \boldsymbol{\beta}_f, \mathbf{b}, \boldsymbol{\delta}_i, \boldsymbol{\epsilon}_i) f(\boldsymbol{\delta}_i|\boldsymbol{\Sigma}) f(\boldsymbol{\epsilon}_i|\xi) \mathrm{d}\boldsymbol{\delta}_i \mathrm{d}\boldsymbol{\epsilon}_i \right) f(\mathbf{b}|\lambda) \mathrm{d}\mathbf{b}$$

The binomial mixed model can be adapted for various assumptions on the smoother and potential station variation to accommodate different underlying density of a species and data limitations especially in length measurements. A set of binomial models considered in the present analyses is provided in Table 2.

2.2.2. Beta-binomial models

The binomial assumption of the catch can be extended to a beta-binomial distribution to explain over-dispersion at the stations (Miller 2013):

$$C_{A,i}(l) \sim BB(C_i(l), p_{A,i}(l), \phi_i(l)).$$

The beta-binomial distribution is a compound of the binomial distribution and a prior beta distribution. More specifically, it assumes a beta-distributed random effect in the expected proportion of catch from vessel A across stations. As a result, the expected catch by vessel A has a variance of

$$var(C_{A,i}) = C_i p_i (1 - p_i) \frac{\phi_i + C_i}{\phi_i + 1}$$

where ϕ is the over-dispersion parameter that captures the extra-binomial variation.

The same smoothing length effect can be applied to the over-dispersion parameter,

$$log(\phi_i(l)) = \mathbf{X}_f^T\boldsymbol{\gamma} + \mathbf{X}_r^T\mathbf{g}$$

where $\boldsymbol{\gamma}$ are fixed effects and $\mathbf{g}$ are random effects, $\mathbf{g} \sim \mathrm{N}(0, \mathbf{D}_+^{-1}/\tau)$. This length effect models the variance heterogeneity and is particularly useful for projecting uncertainty to poorly sampled lengths. However, estimation of a length-based variance parameter typically requires sufficient catch at length data, which is usually not available for less abundant species.

A summary of the beta-binomial mixed model is as follows,

$$C_i(l) = C_{Ai}(l) + C_{Bi}(l)$$
$$C_{Ai}(l) \sim BB(C_i(l), p_{Ai}(l), \phi_i(l))$$
$$logit(p_{Ai}(l)) = log(\rho_i(l)) + o_i$$
$$log(\rho_i(l)) = \mathbf{X}_f^T(\boldsymbol{\beta}_f + \boldsymbol{\delta}_i) + \mathbf{X}_r^T(\mathbf{b} + \boldsymbol{\epsilon}_i)$$
$$log(\phi_i(l)) = \mathbf{X}_f^T\boldsymbol{\gamma} + \mathbf{X}_r^T\mathbf{g}$$

The marginal likelihood is

$$\mathcal{L}(\boldsymbol{\beta}_f, \boldsymbol{\gamma}, \boldsymbol{\Sigma}, \lambda, \xi, \tau)$$
$$= \int\int \left(\prod_{i=1}^{m} \int\int f(\mathbf{Y}_i|\mathbf{X}_f, \mathbf{X}_r, \boldsymbol{\beta}_f, \mathbf{b}, \boldsymbol{\gamma}, \mathbf{g}, \boldsymbol{\delta}_i, \boldsymbol{\epsilon}_i) f(\boldsymbol{\delta}_i|\boldsymbol{\Sigma}) f(\boldsymbol{\epsilon}_i|\xi) \mathrm{d}\boldsymbol{\delta}_i \mathrm{d}\boldsymbol{\epsilon}_i \right) f(\mathbf{b}|\lambda) f(\mathbf{g}|\tau) \mathrm{d}\mathbf{b}\mathrm{d}\mathbf{g}$$

Likewise, various smoothing assumptions can be applied to the variance parameter. Table 3 presents a set of beta-binomial mixed models.

2.2.3. Tweedie model for biomass data

The binomial and beta-binomial models are appropriate for data constituted of catch counts, but are not appropriate for catch weight or biomass. Biomass indices are routinely derived from survey data for population trend monitoring. For taxa that are measured, biomass values adjusted for the change in relative catchability are most reliably derived by applying the results of the analyses described above to length specific catch numbers and employing a length-weight conversion. However, individual measurements are not made for numerous invertebrate taxa, and were not made for some years or some specific survey hauls for many of the remaining taxa. Estimates of relative catchabilities were therefore required for size-aggregated catch weights for all taxa.

The analysis of catch weights required a probability distribution with a mass at zero, but that is otherwise continuous and can accommodate some overdispersion in catch weights. Unlike the models for catch counts, it was not possible to condition model estimates on the total catch. We employed the following model, which assumed that catch weights were a Tweedie (TW) distributed random variable:

$$W_{i,v} \sim TW(\mu_{i,v}, \varphi, \tau)$$
$$E[W_{i,v}] = \mu_{i,v} = \exp(v + S_i + o_{i,v})$$
$$Var[W_{i,v}] = \varphi(\mu_{i,v})^{\tau}$$

where $W_{i,v}$ is the catch weight at station *i* by vessel *v*, $\mu_{i,v}$ is the expected catch weight at station *i* for vessel *v,* φ is the dispersion parameter of the Tweedie distribution,τ is a power parameter,

restricted to the interval 1< τ <2 (Dunn and Smyth 2005), *v* is the fixed vessel effect, where *exp*(*v*) = ρ, S_i is a fixed effect that accounts for the biomass at station *i*, and $o_{i,v}$ is the offset. Unlike the model for catch numbers in which the offset term was the log of the ratio of sampling efforts (tow distance and catch sampling fraction), the offset term in the Tweedie model is the log of sampling effort at station *i* for vessel *v*, relative to the standard effort for that vessel.

A version of the model in which the station effect was treated as a random effect of the following form was initially investigated:

$$E[W_{i,v}] = \mu_{i,v} = \exp(v + \delta_i + o_{i,v})$$

$$\delta_i \sim N(0, \sigma^2)$$

However, the assumed normal distribution for the random effect in the linear predictor was found to be inappropriate.

2.2.4. Model fitting, selection and validation

The binomial and beta-binomial models in Tables 2 and 3 for analyses of length-disaggregated catches were implemented using the Template Model Builder (TMB) package (Kristensen et al. 2016). TMB uses the Laplace approximation to integrate the joint negative loglikelihood (nll) over the random effects to calculate the marginal nll (mnll). Optimization of the mnll is then undertaken in R using the *nlminb()* function. The basis functions for the cubic smoothing spline and the corresponding penalty matrices were generated using the R package mgcv (Wood 2011) based on 10 equally-spaced knots ($K = 9$) within the pre-specified length range depending on the range of lengths observed proper to each taxon. TMB automatically calculates a standard error for the maximum likelihood estimation of the conversion factor via the delta method (Kristensen et al. 2016).

Analyses were also undertaken for length-aggregated catch numbers, for those taxa or instances where length-aggregated conversion factors are required. Contrary to the analyses described above that treat the catch of a taxon at a station and in a length class as the basic datum, these length-aggregated analyses model the total catch numbers at each station. For simplicity, these analyses were implemented using the glmmTMB function from the homonymous R package (Brooks et al. 2017). Models BI0, BI1, BB0 and BB1 (Tables 2 and 3) were fitted by specifying family=binomial(link = "logit") or family=betabinomial(link = "logit"), as appropriate, maintaining the same assumptions as the length-disaggregated models. Note that conversion factor estimates for these four models obtained from the length-aggregated analyses are likely to differ from those obtained from the length-disaggregated analyses when there is strong underlying length-dependency in relative catchability between the two vessels. Furthermore, because sample sizes are greater in the length-disaggregated analyses, standard errors on the correction factors are generally expected to be smaller.

The analyses of catch weights were also implemented using the glmmTMB function. The option family = tweedie was specified.

Length-disaggregated models were fitted only for taxa for which there were data for at least 25 relevant set pairs (pairs with catch by at least one vessel). Size-aggregated model were only fitted for taxa for which there were data for at least 15 relevant set pairs. While these thresholds are somewhat arbitrary, they are reasonable in light of the complexity of the models (number of fixed and random parameters estimated) and are consistent with minimum requirements evident from the simulation study of Yin and Benoît (2022b).

There were in total 13 candidate models of length-disaggregated catches for estimating the conversion factors, although convergence could not be attained for any of the taxa for the most

complex model, BB7, and convergence was attained for a single taxon using model BB6. There were four candidate models for length-aggregated catch numbers. The best model for each set of analyses was selected by BIC (Bayesian information criterion) to maximize model fitting, while avoiding over-fitting of more complicated models, especially in cases without adequate data. We also examined values for AIC (Akaike information criterion), which tends to select slightly more complex models compared to BIC (Hastie et al. 2009), but which in the present applications, largely supported decisions based on BIC.

In each length-disaggregated analysis, the estimated μ function (length-dependent expected proportion of catch by vessel A) from all converged models were compared along with the sample proportions (aggregated by stations and averaged for each length) to provide a more rigorous interpretation of the results. The estimated $\rho(l)$ (expected relative catch efficiency, or conversion factor function) and associated approximate 95% confidence interval from the best model is then shown over the range of lengths contained in the input data. Normalized quantile model residuals (Dunn and Smyth 1996) were produced and plotted using boxplots against length and survey station to visually assess the adequacy of model fit. Given possible concerns about inconsistent fishing during the first sets undertaken in 2021 (assumed here to be the first five sets), and of possible depletion effects in comparative tows that were done one vessel at a time over the same trawl path (n=8), the residuals for these station were distinguished in the latter plot. Furthermore, given the potentially large number of stations for some species which would otherwise generate a crowded boxplot, we plot only the residuals for the first 60 tows of 2022 to provide an indication of possible lack of fit. Finally, we plotted model residuals against depth and the time at which a station was fished, two factors known to affect catchability (e.g., Benoît and Swain 2003), to evaluate whether these effects might interact with the vessel effect under study. To flag possible cases where these effects may have been influential we also fit the following gaussian models (presented using pseudo equations) to the normalized quantile model residuals (NQR):

i) NQR ~ s(depth) + (1|station)

ii) NQR ~ s(time) + (1|station)

iii) NQR ~ factor(day) + (1|station)

where s(*x*) denotes a smooth function of variable *x*, (1|station) denotes a random effect for the station and factor(day) is a factor delineating day and night, where day = 6:00 < time ≤ 20:00. Both smoothed and discrete effects of time were considered to flag cases of a possible diel effect on relative catchability (e.g., Benoît and Swain 2003). We examined the p-values associated with the effects of depth, time and day, and further investigated the residuals patterns in cases with $p < 0.01$.

The fit of catch-aggregated analyses for counts and weights was assessed by plotting the conversion factor and associated approximate 95% confidence interval in biplots of the catch of one vessel over the other. Additionally, we examined the scaled quantile residuals obtained using the R package DHARMa (Hartig 2021). Unlike the normalized quantile residuals used in the length-disaggregated analyses above, which have an expected Gaussian distribution when model fit is adequate, the quantile residuals from DHARMa have an expected uniform distribution. The choice was dictated in part by the fact that it was easier to examine residuals using boxplots in the former case, which has more residual values. Residuals for the catch-aggregated analyses were examined for uniformity and possible overdispersion, and plotted as a function of the fitted values, station depth and time. The evaluation of residuals in size-aggregated analyses was limited to a visual inspection.

2.2.5. Data treatment prior to analysis

Data for some taxa were grouped prior to analysis due to perceived inconsistencies in identification during the surveys or due to small sample sizes amongst related and morphologically similar taxa. These groupings are outlined in Table 4.

In a very small number of instances, the catch of one or two individuals at the very smallest or very largest lengths had undue influence on the shape of the length-dependent conversion factor function at and around those lengths. This results from the flexibility inherent in the cubic spline functions and is a known problem for these models (Cadigan et al. 2022). Although Cadigan et al. (2022) present an alternative and likely more robust approach, it is only applicable to monotonic length-dependent relative catchability functions, thereby limiting the application. Furthermore, we were unable to obtain converged fits in attempts made with data from two of the more data-rich taxa, American plaide (*Hippoglossoides platessoides*) and Greenland halibut (*Reinhardtius hippoglossoides*), and consequently did not pursue that approach. Instead we excluded the catches for these extreme lengths from the analysis. These cases are summarized in Table 5.

Sorting procedures for large redfish (roughly >33 cm) differed between the two vessels during the second leg of the comparative fishing experiment in 2022, during which the majority of paired comparative sets were made. Aboard the CCGS John Cabot, these fish were sampled randomly as part of the catch of fish roughly >20 cm, while aboard the CCGS Teleost, the large fish were explicitly separated from the abundant catch of fish roughly 20-28 cm prior to biological sampling. Given the overwhelming abundance of redfish measuring 20-28 cm in the trawl catches, this difference in procedures resulted in catches of large redfish that were much more frequent in the data for the CCGS Teleost. Given the inability to disentangle the effect of this difference in procedure from possible vessel effects, data for redfish >33 cm were excluded from the analyses.

2.2.6. Interpretation of analysis results and application of conversion factors

Two general patterns observed in the model selection and model results motivated the adoption of additional screening criteria in determining whether a conversion factor (function) should be applied, and which should be chosen for application in future analyses of the survey data. First, there were some cases in which a length-dependent model was selected yet the 95% confidence intervals for the conversion factor function overlapped with a value of one over the entire length range, indicating no statistical difference with the case of equivalent vessel catchability. In these cases, we examined the results for non-length dependent analyses but found that these were typically not statistically significant either and therefore conclude that conversions are not required for these taxa. Similarly, for taxa for which size-aggregated analyses were exclusively undertaken, we interpreted cases in which the confidence intervals for the estimates contain the value one as not statistically significant.

As noted above, the estimation of length-specific conversion factor functions can be sensitive to the sparseness of data in the tails of the length frequencies. Despite eliminating some extreme lengths, there were still cases were conversion factor values diverged considerably from the overall length-dependent trend as lengths tended toward the smallest and largest lengths. We therefore adopted the following procedure. We first identified the lengths that constituted the 0.5^{th} and 99.5^{th} percentiles of the taxon-specific total length frequency distribution for the 2021-2022 experiment for taxa with at least 20 length classes (either cm or mm classes), and used the 2.5^{th} and 97.5^{th} percentiles for taxa with fewer classes. We then identified the conversions factor function values at these percentiles for each taxon, and assumed these values as constants for lengths below and above these percentiles, respectively. These constant values

were projected respectively to the taxon-specific smallest and largest lengths observed since 1984 in the survey.

3. RESULTS

The results of the various analyses for the numerous taxa covered in this report are simply too voluminous to interpret in detail. Instead we aimed to provide detailed figures and tables that describe the results and support decisions for the application of conversion factors, and provide some interpretation of results only for key harvested species and species of conservation concern. These species, which are reported on annually (e.g., Bourdages et al. 2022), are ones for which reporting on survey results is likely to be most consequential, and therefore where the need for careful examination and interpretation of comparative fishing results is arguably greatest. We begin by explaining the structure for the presentation of results, and then address results for these specific species.

3.1. PRESENTATION OF RESULTS

The following tables and figures provide taxon-specific results.

Table 6 provides the total number of relevant set pairs (i.e., pairs in which the taxon was caught by at least one of the two vessels), the number of pairs for which only the CCGS John Cabot caught the taxon, and the number of pairs for which only the CCGS Teleost caught the taxon. Notably, the table provides a reference to the number for the figure(s) in which the results are presented for that taxon. Taxa for which length-disaggregated analyses were supported are presented first, followed by those for which size-aggregated analyses were employed.

Table 7 provides details of the model evidence and selection (ΔAIC and ΔBIC values) for the length-disaggregated analyses.

Table 8 presents the p-values for the smooth effect of depth, the smooth effect of time and the fixed effect of day on the normalized quantile residuals from the best length-disaggregated model. Values ≤ 0.01 are indicated in bold.

Table 9 provides details of the model evidence and selection (AIC and BIC values) for the length-aggregated analyses of catch numbers, and the estimated conversion factors (rho) and 95% confidence intervals for the analyses of catch numbers and of catch weights for taxa that were otherwise also considered in length-disaggregated analyses.

Table 10 provides the same types of results as Table 9, but for those taxa that were not considered in length-disaggregated analyses, either because representative length sampling was not undertaken or because the total number of relevant set pairs was $15 \leq n < 25$.

Plots for the results of the length-disaggregated analyses are presented in multiple panels across three pages for each taxon. Figures 3-5 provide an explanation of the content of each page. Briefly, the first page (labelled a.) provides a summary of the data from a spatial, size-aggregated and length-specific perspective (details in Fig. 3). Results for the size-aggregated analyses are plotted in one of the panels in an effort to reduce the total number of figures contained in this report. The second page (labelled b.) provides a plot of the fit of all converged models and a plot of the selected conversion factor function and 95% confidence interval, along with the projected constant values we propose for the smallest and largest lengths (details in Fig. 4). Finally, the third page (labelled c.) provides various boxplots for the normalized quantile residual values for the selected model (details in Fig. 5).

Plots for the results of the length-aggregated analyses, including the fitted model and model quantile residuals, are presented on a single page for each taxon for the analyses of catch

counts (left column) and catch weighted (right column) (details in Fig. 6). Figures are presented only for taxa that were not subjected to length-disaggregated analyses to reduce the total number of figures in this report. Nonetheless, fits of the selected length-aggregated model for catch for the remaining taxa are presented in the plots for length-disaggregated analyses and the estimated conversion factor values are in Table 9. Detailed residual plots were created and examined even though they are not formally presented here.

3.2. SOME SPECIFIC RESULTS

3.2.1. Atlantic cod (*Gadus morhua*)

Catches of Atlantic cod were remarkably similar between the two vessels, with the exception of one haul in 2021 in which the CCGS Teleost made a very significant catch (Fig. 15a, see biplot and length frequencies). The overall species composition also differed between vessels in this pair (results not shown), including the relative catches of redfish, suggesting that the two vessels had fished different habitats. Converged models suggested that the relative efficiency of the two vessels was very similar and that any length dependency was weak. Nonetheless model BB5 was selected by BIC, although the confidence intervals associated with the correction factor function overlapped with one across all lengths (Fig. 15b). There were no patterns in the residuals that would indicate an important model lack of fit (Fig. 15c). The application of a correction factor in future analysis of the survey data is not recommended for Atlantic cod.

3.2.2. Silver hake (Merluccius bilinearis)

Silver hake were principally captured during the 2022 experiment. Catches by the two vessel were very similar across a range of catch amounts (Fig. 18a). The length frequencies were similar between vessels, although like for White hake (see below), there was a tendency for the CCGS Teleost to catch more larger silver hake. However, both AIC and BIC favoured the non length-dependent model BB1 (Table 7). Furthermore, confidence intervals for the estimate suggest that the relative efficiency of the two vessels did not differ significantly (Fig. 18b). Model fit appeared to be adequate (Fig. 18c). The application of a correction factor in future analysis of the survey data is not recommended for silver hake.

3.2.3. White hake (*Urophycis tenuis*)

White hake were captured in both years, and catch amounts and the length frequencies were very similar between vessels, although the CCGS John Cabot seemed to catch more smaller individuals < 35 cm and slightly fewer larger individuals (Fig. 17a.). Nonetheless, both AIC and BIC favoured the non length-dependent model BI1 (Table 7). Furthermore, confidence intervals for the estimate suggest that the relative efficiency of the two vessels did not differ significantly (Fig 17b). Model fit appeared to be adequate (Fig. 17c). The application of a correction factor in future analysis of the survey data is not recommended for white hake.

3.2.4. Longfin hake (*Phycis chesteri*)

Few longfin hake were caught in 2021; the majority of catches were made in the eastern portion of the Laurentian channel in 2022 (Fig. 16a). Catches by the two vessels were remarkably similar in 2022. While there were some indications that the relative efficiency of the CCGS Teleost declined with length, model BB0 was selected by BIC, and with support by AIC (Table 7). The confidence intervals of the selected model overlapped with a value of one (Fig. 16b.). There was a slight tendency for model residuals to be positive for lengths <30 cm, although the magnitude of the normalized quantile residuals was small (Fig. 16c.) and there was

little support for length-dependent models based on AIC (Table 7). The application of a correction factor in future analysis of the survey data is not recommended for longfin hake.

3.2.5. Atlantic wolffish (*Anarhichas lupus*) and spotted wolffish (*A. minor*)

Atlantic wolffish were principally caught in 2022 along the coast of western Newfoundland (Fig. 23a). Although catches were somewhat variable between vessels, the CCGS John Cabot tended to catch more individuals across most lengths. Nonetheless, a length-independent model was selected (BI1) by both AIC and BIC, with confidence intervals on the estimate indicating no significant difference between vessels (Fig. 23b). There was a slight pattern in model residuals plotted against length indicating a small possible lack of model fit (Fig. 23c), although there was only slight support for a length-dependent model based on AIC (BI3 and BB4, with delta-AIC values of 4 and 6 respectively), and no support based on BIC. The application of a correction factor in future analysis of the survey data is not recommended for Atlantic wolffish.

Although spotted wolffish (*Anarhichas minor*) is a species of conservation concern that is occasionally captured in the survey, too few individuals were captured during the comparative fishing to estimate a relative catchability.

3.2.6. Redfish (*Sebastes sp.*)

There was one pair in 2021, the same one as identified for Atlantic cod, in which the CCGS Teleost caught many more redfish than its counterpart, likely as a result of fishing a different habitat than the CCGS John Cabot (Fig. 29a). Catches of redfish can be particularly abundant and consequently variable, nonetheless the two vessels generally caught very similar amounts. There was a slight tendency for the CCGS Teleost to catch more redfish of lengths between 10 and 15 cm. This was reflected in a significantly different relative catch efficiency at those lengths for the selected model BB5, although the difference in catchability was not significant at larger lengths (Fig. 29b). The model estimated that the CCGS Teleost was significantly less efficient at catching redfish < 8 cm, although these lengths represent an insignificant fraction of the catch. Model residuals suggested an adequate model fit (Fig. 29c). The relative efficiency function defined by the black dashed line in the lower panel of Figure 29b is recommended for redfish.

3.2.7. Lumpfish (Cyclopterus lumpus)

Lumpfish were not caught frequently, and catches comprised one or two individuals (Fig. 37a). Model BI0 was selected, although there was some support for some of the other models based on AIC, but not BIC (Table 7). Confidence intervals for the estimated conversion approached but did not overlap with a relative efficiency of 1 (Fig. 37b). Estimates from the best length-independent model and from the analyses of length-aggregated catch weights (biplot in Fig. 37a; Table 9) suggest that the CCGS John Cabot may be more efficient at catching lumpfish. The estimate from model BI0 is recommended.

3.2.8. American plaice (Hippoglossoides platessoides)

Catches of American plaice were remarkably similar between vessels in both years (Fig. 39a). There was a clear pattern of increasing relative efficiency of the CCGS John Cabot with increasing lengths. Although the magnitude of the effect was modest, the length dependency was statistically significant (Fig. 39b). The selected model, BB5, appeared to fit the data well (Fig. 39c). Adoption of the length-dependent conversion is recommended for American plaice.

3.2.9. Witch flounder (Glyptocephalus cynoglossus)

Catches of witch flounder were very similar between vessels in both years (Fig. 40a). There was a clear tendency for the CCGS John Cabot to catch more witch flounder across all lengths sampled. Confidence intervals for the estimated conversion factor function for the selected model based on BIC, BB1, indicate a significant difference from equal catchability between vessels, independent of length (Fig. 40b). The selected model fit the data well (Fig. 40c). Adoption of the length-independent conversion is recommended for witch flounder.

3.2.10. Greenland halibut (Reinhardtius hippoglossoides)

With the exception of one set pair, catches of Greenland halibut were remarkably similar between vessels in both years (Fig. 41a). There appeared to be a tendency for the CCGS John Cabot to catch more small Greenland halibut (< 20 cm), although confidence intervals for the conversion factor function for the selected model, BB5, suggest the difference may not be statistically significant (Fig. 41b). Overall, the evidence for a significant length-dependent conversion is weak (Fig. 41b), and both length-independent (see biplot in Fig 41a) and length-aggregated model results (Table 9) indicated that the vessel effect is not statistically significant. Consequently, the application of a correction factor in future analysis of the survey data is not recommended for Greenland halibut.

3.2.11. Atlantic halibut (*Hippoglossus hippoglossus*)

Although Atlantic halibut catch amount were generally small and lengths variable in individual tows, the vessels generally caught similar amount and similar lengths in paired sets (Fig. 42a). Model BI1 was selected, and appeared to fit the data well (Fig. 42b). However, the relative catch efficiency was not significantly different from a value of one (Fig. 42b). A correction factor is not recommended in future analysis of the survey data for Atlantic halibut.

3.2.12. Thorny skate (*Amblyraja radiata*)

Thorny skate were captured in similar amounts by the two vessels, although the CCGS Teleost tended to catch more individuals <25 cm, particularly in 2021 (Fig. 9a). Model BB1 was selected by both AIC and BIC, although there was support for the length-dependent BB4 based on AIC (Fig. 9b). The estimated relative catch efficiency did not differ from a value of 1. Model BB1 appeared to provide an adequate fit (Fig. 9c). A correction factor is not required in future analysis of the survey data for thorny skate.

3.2.13. Smooth skate (*Malacoraja senta*)

Catches of smooth skate tended to be more variable between vessels, although the CCGS John Cabot was clearly more efficient at most lengths (Fig. 10a). Model BI1 was selected and appeared to provide an adequate fit (Fig. 10b,c). Confidence intervals on the estimate approached but did not overlap with a value of 1, as was the case for the catch-aggregated analysis (Table 9). These results confirm that the CCGS John Cabot was significantly more efficient and application of the conversion factor is recommended.

3.2.14. Black dogfish (*Centroscyllium fabricii*)

Although black dogfish were only captured in a small number of paired tows along the Laurentian channel and in the Estuary, catches and catch lengths were very similar between vessels (Fig. 8a). The correction factor function for the selected model, BB1, was not statistically significant from equivalent efficiency for the two vessels (Fig. 8b). Application of a conversion factor in future analyses is not recommended for black dogfish.

3.2.15. Atlantic herring (*Clupea harengus*)

Catches of herring were similar between vessels in most pairs, but much less so when one vessel made a large catch (Fig. 11a). With the exception of BI2, all models suggest that that the relative efficiency of the vessel is very similar or equal. Confidence intervals for the selected model, BB1, indicate that there was no significant difference in catchability between the vessels (Fig. 11b), consequently application of a conversion is not recommended.

3.2.16. Capelin (*Mallotus villosus*)

Catches of capelin were quite variable in the comparative fishing data, although the CCGS Teleost appeared to be more efficient at catching capelin between about 12-15 cm, which were by far the most common lengths in the catches (Fig. 12a). This was confirmed by the length-dependent modelling, where model BB4 was selected indicating a significant difference at these sizes only (Fig. 12b). However, we cannot think of a basis for such a dome-shaped function, and suspect that it may be a spurious result. A length-aggregated conversion is supported based on the results of length-independent and length-aggregated modelling of weights (see biplot in Fig. 12a; Table 9). We recommend using for capelin the estimate from model BB1, the length-independent model with the most support based on AIC and BIC.

3.2.17. Northern shortfin squid (*Illex illecebrosus*)

Catches of northern shortfin squid were generally small and variable, yet similar between vessels (Fig. 44a). Although the CCGS Teleost appeared to be more efficient, the difference was not statistically significant for the selected length-dependent model (Fig. 44b), nor for the length-independent and length-aggregated modelling (Fig. 44a.; Table 9). A conversion factor is not recommended for this species.

3.2.18. Northern shrimp (*Pandalus borealis*)

Northern shrimp were mainly caught in set pairs fished in the Estuary and in the northern tip of the Esquiman channel (Fig. 48a). The CCGS Teleost tended to catch more northern shrimp across all sizes, and especially individuals < 15 mm. Model BB5 was selected and appeared to provide an adequate fit to the data (Fig. 48b,c). Estimates from that model suggest that the CCGS Teleost was significantly more efficient (between approximately 50-75% more) at capturing both smaller and larger individuals. The adoption of the length-dependent correction factor function from model BB5 is recommended for this species.

3.2.19. Snow crab (*Chionoecetes opilio*)

Snow crab were principally captured in set pairs in the Estuary and along the Quebec north shore (Fig. 54a). The CCGS John Cabot was clearly more efficient at catching snow crab across the full range of sizes for this species. Model BB1 was selected by BIC, although there was support for BB5, which estimated a very slight convex function for the relative efficiency, based on AIC and BIC (Fig. 54b; Table 7). Model BB1 fit the data well, and indicates that the difference in efficiency is statistically significant. The conversion factor from BB1 is recommended for future analysis of snow crab catches from the survey.

3.2.20. Sea pens

There are four species of sea pens commonly captured by the survey: *Pennatula aculeata, Ptilella grandis, Balticina finmarchica* and *Anthoptilum grandiflorum*. There were sufficient catches of each during the comparative fishing to support analyses (Table 6). The CCGS John Cabot was statistically significantly more efficient at catching all four species based on catch

numbers, and generally also catch weights (Table 10; Figures 78-81). Estimated relative efficiencies were similar between species and should be applied in future analyses.

3.2.21. Other taxa with significant length-dependent relative efficiencies

In addition to the taxa considered above, there were four others for which there was evidence of a length-dependent difference in efficiency between the vessels.

The CCGS Teleost was more efficient at catching small hagfish (*Myxine limosa*) (<30 cm), but less efficient at catching larger hagfish (Fig. 7a). A length-dependent function based on model BI3 is well supported for this species (Fig. 7b,c).

Catches of argentine (*Argentina silus*) were somewhat variable, and across most lengths, neither vessel appeared more efficient (Fig. 13a). However, for lengths above 25 cm, and especially above 30 cm, the CCGS Teleost was more efficient. The selected model is consistent with equal efficiency up to about 28 cm, but estimates an extreme difference for larger lengths (Fig. 13b). Catches at these lengths were small but not rare either. However, there does not appear to be a basis for such large differences in relative efficiency. Given these observations, and that length-independent and length-aggregated relative efficiencies were not statistically significant (biplot in Fig, 13a; Table 9), we recommend against adopting a conversion for argentine.

Similar to the results for northern shrimp, somewhat concave relative efficiency functions were estimated for striped pink shrimp (*Pandalus montagui*) (Fig. 49b) and for Norwegian shrimp (*Pontophilus norvegicus*) (Fig. 51b).

3.2.22. Other measured taxa with significant length-independent relative efficiencies

In addition to the taxa considered above, there were three others with statistically significant length-independent effects: *Lycodes vahlii*, Liparidae and *Atlantopandalus propinqvus*. For the first two taxa, confidence intervals for the estimated relative efficiency extended very close to, but did not overlap with a value of 1 (Figs. 27b, 38b). In both cases, the estimates based on size-aggregated catches were not significant (Table 9), and based on these results, the application of a conversion factor is not recommended. In contrast, both the length-independent (Fig. 50b) and size-aggregated analyses (Table 9) for *A. propinqvus* identified a significant difference in relative efficiency, with the CCGS Teleost producing larger catches.

Taxa that were considered in the length-dependent analyses and that were not specifically mentioned in this section or a preceding one of the Results, are considered to have been associated with a non-significant difference in efficiency between vessels and therefore do not require the application of conversion factors. In every case, the estimates for the length-aggregated analysis of catch numbers corroborate these conclusions. However there are a few taxa for which the analyses of aggregated catch weights indicate a significant difference: *Arctozenus risso, Nezumia bairdii, Scomber scombrus, Leptoclinus maculatus, Triglops murrayi, Lithodes maja* and *Hyas alutaceus* (Table 9). Given the absence of evidence for a length-dependent effect that could generate these contrasting results, and given that the models used for catch weights were not simulation tested for use in comparative fishing analyses, unlike the models for catch numbers (Yin and Benoît 2022b), and may therefore not be fully reliable, we recommend against applying conversions for these taxa.

3.2.23. Significant covariate effects

For taxa included in the length-disaggregated analyses, normalize quantile residuals from the selected model were associated with depth for two taxa, and with time of day for two others (Table 8).

For fourbeard rockling (*Enchelyopus cimbrius*), residuals tended to be positive for depths <150 m, and negative for depths >400 m (Fig. 19c). We re-fitted the suite of binomial and beta-binomials treating depth rather than length as a covariate. The best fitting model, BB4, provided a better fit to the data than the best fitting length-dependent model based on both AIC (2249 vs. 2258) and BIC (2282 vs. 2284) (note these are absolute values note reported in the tables, in contrast to the delta values in Table 7). The CCGS Teleost was more efficient at catching fourbeard rockling at depths shallower than about 220m, and less efficient at deeper depths (Fig. 19d). The model fit the data adequately, with no apparent pattern in the residuals as a function of depth, length or time of day (Fig. 19e). For this species, a depth-specific correction factor is recommended.

Catches of Arctic shrimp (*Argis dentata*) tended to be somewhat variable and confined to shallow and midwater depths (Fig. 52a). Although there appears to be a decline in the value of the quantile residuals with depth, the magnitude of the median change is small (Fig. 52c). Given the wide confidence intervals on the estimate from the best model (Fig. 52b), there wasn't a strong basis for a depth effect and further analyses were not pursued.

For the sea poacher (*Leptagonus decagonus*), residuals were positive around midnight, 4 am and 8 pm, and negative or neutral otherwise (Fig. 34c). This pattern, which emerges from a model fit to sparse catches, with many instances of nil catch by one vessel or the other (Fig. 34b), does not conform with typical patterns for diel variation in catchability (Benoît and Swain 2003) or crepuscular activity, suggesting the result may be spurious.

Catches of pink glass shrimp (*Pasiphea multidentata*) were quite consistent between vessels across numerous set pairs (Fig. 45a). Quantile residual values for set pairs fished just after midnight were strongly negative and those for set pairs fished prior to 8 am were generally negative (Fig. 45c). Meanwhile, values for set pairs fished in the evening and up to midnight were generally positive. These patterns are not consistent with a strong effect of the diel cycle and consequently further analyses were not pursued.

3.2.24. Interpretation of results for taxa exclusively in size-aggregated analyses

With the exception of two fish species, most of the taxa for which size-aggregated analyses were exclusively undertaken were invertebrates (Table 10). Results for this ensemble of taxa are too numerous to interpret individually. Instead we highlight some of the patterns that are apparent in the results.

For many colonial taxa, results often differed between the analyses of numbers and weights (e.g., Porifera, Fig. 59; *Gersemia rubiformis*, Fig 76; Table 10). This was also true for fragile invertebrates such as heart urchins (*Brisaster fragilis*, Fig. 117) and brittle stars (e.g, *Ophiura sarsii*, Fig. 129). These results are not surprising, given that the weight is a measured quantity, while the numbers are derived of what are considered to be relatively intact individuals or fragments and sometimes even derived using a small sub-sample that is both weighed and enumerated. There is therefore additional sampling variability for catch numbers, and a potential to underestimate numbers in samples in which a high proportion of individuals are reduced to small fragments. Furthermore, in hauls in which there are no intact individuals or fragments, no inference on catch numbers is made, resulting in a difference in sample size between count and weight based analyses. Given the greater uncertainty for catch numbers, we recommend

applying conversion factors only when the analysis for catch weights is significant, and to apply the conversion factor from the weight-based analysis to both the weights and the numbers. More generally, we question the benefit of deriving catch numbers for these taxa given the uncertainty inherent in their derivation. The taxa for which the derived counts are likely not reliable are: Porifera, Hydrozoa, Scyphozoa, *Epizoanthus erdmanni, Gersemia rubiformis, Drifa glomerata,* Nephtheidae, Bryozoa, Polychaeta, Polynoidae, *Brisaster fragilis, Ophiura sarsii* and *Ascidia* sp.

In contrast to the colonial and fragile taxa, there was good agreement between number- and weight-based analyses for well sampled single organism taxa (Table 10). Notable examples include the jellyfish *Cyanea capillata* (Fig. 67), the anemones *Bolocera tuediae* (Fig. 71) and *Actinostola callosa* (Fig. 73), the four seapen species previously mentioned (Figs. 78-81), the small crustacean *Syscenus infelix* (Fig. 106), the pelicanfoot *Arrhoges occidentalis* (Fig. 85) and the urchin *Strongylocentrolus* sp. (Fig. 116). For the single organism taxa we recommend applying both the respective corrections to weights and numbers when either or both are statistically significant, provided the estimates appear reasonable, that is, that they are not associated with an unusually large standard error, for instance. This approach will ensure there is consistency in the corrections that are applied, especially in cases where lower sample size and variability in the data likely underly a lack of significance for one of the two measures (e.g., *Cucumaria frondosa*, Fig. 115). For an example of a statistically significant correction for which the estimate does not appear reasonable and should therefore not be applied, see the results for the count-based analysis for the shrimp *Eualus fabricii* (Fig. 108).

4. DISCUSSION

Overall, the data obtained in 2021-2022 appear sufficient to reliably test for differences in relative efficiency between vessels and to estimate conversion factors and length-dependent conversion factor functions for the most commonly captured taxa in the survey, which includes most commercially important species. While additional comparative fishing would improve the precision of estimates, particularly for infrequently captured taxa or those with variable catches, the benefits appear small relative to the financial and logistical costs of additional comparative fishing. The peer review meeting of the results of these comparative fishing experiments concluded that no additional comparative fishing was warranted based on these considerations.

The experiments in the northern Gulf of St. Lawrence employed a shadow survey design, which helps ensure that the estimated relative catchabilities are relevant for the habitat conditions in the survey area. Furthermore, based on analyses of the model residuals and upon further consideration, we concluded that there was a single instance where relative catchability was affected by depth or time of day, key factors that can affect overall survey catchability (e.g., Benoît and Swain 2003). These conditions lend support to the reliability of the conversion factor estimates.

The relative efficiency of the CCGS Teleost and CCGS John Cabot, which fished a slightly modified Campelen 1800 trawl, was expected to be similar *a priori*. The results were generally consistent with this expectation as non-significant relative efficiency estimates were obtained for most taxa. For those where results were significant and judged to be reliable, the difference in relative efficiency were small. Although not explored in detail, there appeared to be a tendency across taxa for those that are more closely associated with the bottom to be more catchable by the CCGS John Cabot. This is evident, for instance, in the results for hagfish American plaice and witch flounder, three of the crab species and a number of benthic invertebrates, including sea pens.

5. ACKNOWLEDGEMENTS

Numerous DFO Science and CCG staff participated in the planning and implementation of comparative fishing in the EnGSL. We are indebted to Jordan Ouellette-Plante for providing R Markdown code that greatly simplified the process of compiling the numerous figures into the document, and to Paul Regular and Andrea Perreault for identifying and correcting an error in the calculation of AIC and BIC values in earlier analyses. We wish to thank Truong Nguyen for providing details on the changes made to the Campelen 1800 trawl, and Laurie Isabel for recommendations on the appropriate taxa groupings for the analysis. Finally, we thank Jordan and Laurie for their careful review of the penultimate draft of this document.

6. REFERENCES CITED

Benoît, H.P., and Swain, D.P. 2003. Accounting for length and depth-dependent diel variation in catchability of fish and invertebrates in an annual bottom-trawl survey. ICES J. Mar. Sci. 60: 1297-1316.

Benoît, H.P., Ouellette-Plante, J., Yin, Y, and Brassard, C. 2022. Review of the assessment framework for Atlantic cod in NAFO 3Pn4RS: Fishery independent surveys. DFO Can. Sci. Advis. Sec. Res. Doc. 2022/049. xiii + 130 p.

Bourdages, H., Brassard, C., Chamberland, J.-M., Desgagnés, M., Galbraith, P., Isabel, L. and Senay, C. 2022. Preliminary results from the ecosystemic survey in August 2021 in the Estuary and northern Gulf of St. Lawrence. DFO Can. Sci. Advis. Sec. Res. Doc. 2022/011. iv + 95 p.

Brooks, M.E., Kristensen, K., van Benthem, K.J., Magnusson, A., Berg, C.W., Nielsen, A., Skaug, H.J., Mächler, M., and Bolker, B.M. 2017. glmmTMB balances speed and flexibility among packages for zero-inflated generalized linear mixed modeling. R Journal, 9(2):378-400.

Cadigan, N.G., Yin, Y., Benoît, H.P., and Walsh, S.J. 2022. A nonparametric-monotone regression model and robust estimation for paired-tow bottom-trawl survey comparative fishing data. Fish. Res. 254: 106422.

Dunn, P.K., and Smyth, G.K. 1996. Randomized quantile residuals. J. Comput. Graph. Stat 5: 236-244.

Dunn, P.K., and Smyth, G.K. 2005. Series evaluation of Tweedie exponential dispersion model densities. Statis. Comput. 15:267-280.

Green, P.J., and Silverman, B.W. 1993. Nonparametric regression and generalized linear models. Chapman and Hall/CRC, 184 p.

Hartig, F. 2021. DHARMs: Residual diagnostics for hierarchical (multi-level.mixed) regression models. R package version 0.4.1

Hastie, T., Tibshirani, R., and Friedman, J. 2009. The elements of statistical learning: data mining, inference, and prediction. Springer Science and Business Media.

Kristensen, K., Nielsen, A., Berg, C.W., Skaug, H., and Bell, B.M. 2016. TMB: Automatic differentiation and Laplace approximation. J. Stat. Softw. 70: 1-21.

Miller, T.J. 2013. A comparison of hierarchical models for relative catch efficiency based on paired-gear data for US Northwest Atlantic fish stocks. Can. J. Fish. Aquat. Sci. 70: 1306-1316.

Miller, T.J., Das, C., Politis, P.J., Miller, A.S., Lucey, S.M., Legault, C.M., Brown, R.W., and Rago, P.J. 2010. Estimation of Albatross IV to Henry B. Bigelow calibration factors. Fish. Sci. Cent. Ref. Doc. 10-05; 233 p.

R Core Team. 2021. R: A language and environment for statistical computing. R Foundation for Statistical Computing, Vienna, Austria.

Thiess, M.E., Benoit, H., Clark, D.S., Fong, K., Mello, L.G.S., Mowbray, F., Pepin, P., Cadigan, N.G., Miller, T., Thirkell, D., and Wheeland, L. 2018. Proceedings of the national comparative trawl workshop, November 28-30, 2017, Nanaimo, BC. Can. Tech. Rep. Fish. Aquat. Sci. 3254: x + 40 p.

Thorson, J.T., and Minto, C. 2015. Mixed effects: a unifying framework for statistical modelling in fisheries biology. ICES J. Mar. Sci. 72:1245-1256.

Verbyla, A.P., Cullis, B.R., Kenward, M.G, and Welham, S.J. 1999. The analysis of designed experiments and longitudinal data by using smoothing splines. J. Roy. Stat. Soc. Ser. C 48: 269-311.

Walsh, S.J., Hickey, W.H., Porter, J., Delouche, H., and McCallum, B.R. 2009. NAFC survey trawl operations manual: version 1.0. Fisheries and Oceans, Northwest Atlantic Fisheries Centre, Newfoundland Region, St. John's.

Wood, S.N. 2000. Modelling and smoothing parameter estimation with multiple quadratic penalties. J. Royal. Statist. Soc. Ser. B Stat. Methodol. 62: 413–428.

Wood, S.N. 2011. Fast stable restricted maximum likelihood and marginal likelihood estimation of semiparametric generalized linear models. J. R. Stat. Soc. Ser. B Stat. Methodol. 73: 3–36.

Wood, S.N. 2017. Generalized additive models: An introduction with R, 2nd ed. Chapman and Hall/CRC Press, 496 p.

Yin, Y., and Benoît, H.P. 2022a. Re-analysis of comparative fishing experiments in the Gulf of St. Lawrence and other analyses to derive stock-wide bottom-trawl survey indices beginning in 1971 for 4RST Greenland halibut, *Reinhardtius hippoglossoides*. DFO Can. Sci. Advis. Sec. Res. Doc. 2022/002. vii + 45 p.

Yin, Y., and Benoît, H.P. 2022b. A comprehensive simulation study of a class of analysis methods for paired-tow comparative fishing experiments. Can. Tech. Rep. Fish. Aquat. Sci. 3466: vi + 99 p.

7. TABLES

Table 1. Details for the relevant set pairs in the 2021 and 2022 comparative fishing of the EnGSL, where columns indicated by TEL represent values for the CCGS Teleost and those indicated by CA represent values for the CCGS John Cabot Tow start times (Time) are expressed in decimal hours, starting latitudes and longitudes are expressed in decimal degrees, the Distance values represent the trawled distance for each vessel in nm and Separation is the distance between the starting positions of the tow for the two vessels in km. The date is that of the beginning of the tow by the CCGS Teleost, and the entry for CA Time denoted by [1] indicates that the tow by the CCGS John Cabot was started the day previous just before midnight. Footnotes in the column for Separation indicate cases for which the hauls were done on the same trawl track, with [2] indicating the CCGS John Cabot fished first and [3] indicating the CCGS Teleost fished first.

Date	Set no.	Stratum	TEL Depth (m)	CA Depth (m)	TEL Time	CA Time	TEL Distance (nm)	CA Distance (nm)	TEL Latitude	TEL Longitude	Separation (km)
2021-08-13	85	830	192	-	14.98	15.13	0.65	0.78	49.636	-64.355	1.54
2021-08-13	86	818	247	-	17.12	17.28	0.75	0.78	49.615	-64.461	0.72
2021-08-14	92	406	393	-	11.52	12.12	0.75	0.80	49.393	-64.923	1.39
2021-08-14	93	805	328	-	15.85	15.93	0.75	0.70	49.547	-65.222	0.78
2021-08-15	98	805	331	-	7.88	7.92	0.80	0.70	49.504	-66.323	0.63
2021-08-15	99	410	294	-	10.43	10.62	0.75	0.75	49.334	-66.143	1.20
2021-08-15	100	409	181	-	13.25	13.35	0.75	0.78	49.291	-66.028	1.39
2021-08-15	101	409	228	-	16.53	16.53	0.80	0.70	49.277	-66.192	0.62
2021-08-16	105	851	68	-	6.58	6.62	0.93	0.75	48.871	-67.573	0.68
2021-08-16	106	852	130	-	10.22	10.23	0.75	0.48	48.717	-68.197	0.56
2021-08-16	107	851	66	-	11.58	11.75	0.80	0.75	48.647	-68.326	0.49
2021-08-16	108	852	139	-	13.62	13.67	0.75	0.75	48.635	-68.451	0.56
2021-08-16	109	413	343	-	15.82	15.85	0.75	0.75	48.671	-68.706	0.81
2021-08-17	113	854	80	-	6.28	6.35	0.75	0.75	48.673	-68.974	1.64
2021-08-17	114	414	171	-	9.35	9.58	0.75	0.83	48.708	-68.8	1.16
2021-08-17	116	411	323	-	14.78	14.8	0.75	0.80	48.947	-68.223	1.79
2021-08-17	117	412	282	-	17.00	17.07	0.75	0.75	49.001	-68.091	1.97
2021-08-17	118	855	119	-	18.77	18.77	0.80	0.80	49.026	-68.122	1.05
2021-08-18	122	817	276	-	7.82	7.78	0.80	0.75	49.509	-66.595	1.41
2021-08-18	123	805	249	-	10.50	10.60	0.75	0.78	49.633	-66.686	0.73
2021-08-18	124	817	213	-	13.57	13.48	0.75	0.78	49.675	-66.88	1.01
2022-08-11	2	401	219	192	23.58	23.58	0.80	0.80	47.541	-60.449	0.56
2022-08-12	4	404	345	328	11.48	11.50	0.75	0.76	47.885	-60.64	0.41
2022-08-12	5	407	481	478	14.73	14.72	0.80	0.80	47.883	-60.281	0.32
2022-08-12	7	803	474	473	18.90	18.93	0.80	0.78	48.05	-60.216	0.79
2022-08-12	8	802	448	452	23.17	23.13	0.73	0.75	48.089	-59.955	0.52
2022-08-13	9	810	330	327	2.95	3.02	0.80	0.78	48.212	-59.842	1.1
2022-08-13	10	810	334	347	7.17	7.18	0.75	0.73	48.012	-59.682	0.67
2022-08-13	12	802	521	519	13.43	13.47	0.65	0.83	47.677	-59.73	0.3
2022-08-13	13	811	272	247	16.65	16.67	0.75	0.80	47.655	-59.433	1.52
2022-08-13	14	820	173	174	21.77	22.33	0.80	0.74	48.004	-59.494	0.6

Date	Set no.	Stratum	TEL Depth (m)	CA Depth (m)	TEL Time	CA Time	TEL Distance (nm)	CA Distance (nm)	TEL Latitude	TEL Longitude	Separation (km)
2022-08-14	15	820	109	101	1.98	2.02	0.83	0.74	48.359	-58.959	0.81
2022-08-14	16	821	109	85	5.43	5.45	0.85	0.74	48.349	-59.358	0.2
2022-08-14	17	821	100	86	8.25	8.27	0.70	0.72	48.255	-59.491	1.88
2022-08-14	18	811	266	274	11.23	11.15	0.70	0.79	48.379	-59.735	0.38
2022-08-14	21	835	54	52	21.33	21.38	0.75	0.76	48.962	-59.061	1.1
2022-08-15	22	836	81	69	0.13	0.17	0.75	0.74	49.119	-58.767	0.39
2022-08-15	23	836	45	57	3.27	3.28	0.80	0.75	49.375	-58.395	1.2
2022-08-15	24	836	90	87	7.75	7.73	0.75	0.75	49.656	-58.429	0.86
2022-08-15	25	822	137	142	10.42	10.25	0.80	0.76	49.745	-58.563	0.29
2022-08-15	26	822	112	106	16.67	16.57	0.75	0.75	49.943	-58.231	1.28
2022-08-15	27	823	159	163	19.32	19.33	0.78	0.75	50.113	-57.906	0.82
2022-08-15	28	813	252	248	22.12	22.12	0.78	0.70	50.349	-57.974	0.72
2022-08-16	29	813	254	249	0.93	0.98	0.60	0.60	50.446	-57.909	1.05
2022-08-16	30	823	144	132	3.52	3.53	0.80	0.76	50.474	-57.563	0.90
2022-08-16	31	823	171	147	6.83	6.85	0.75	0.75	50.593	-57.501	1.01
2022-08-16	32	824	156	157	9.42	9.43	0.75	0.75	50.760	-57.577	0.99
2022-08-16	33	837	91	101	12.37	12.43	0.75	0.76	50.955	-57.324	0.57
2022-08-16	34	837	78	71	14.62	14.58	0.75	0.74	51.036	-57.196	0.61
2022-08-16	35	838	60	59	0.07	0.33	0.78	0.75	51.493	-56.450	0.05
2022-08-17	36	838	67	62	2.85	2.88	0.80	0.76	51.542	-56.311	0.31
2022-08-17	37	838	37	38	8.80	9.12	0.75	0.75	51.622	-55.686	0.39
2022-08-17	38	840	131	112	14.62	14.62	0.80	0.75	51.878	-55.768	1.07
2022-08-17	40	838	76	68	22.95	23.30	0.75	0.70	51.578	-56.569	0.52
2022-08-18	45	813	205	183	17.77	17.92	0.78	0.78	50.507	-58.161	0.78
2022-08-18	46	824	164	158	21.7	21.65	0.75	0.74	50.488	-58.318	0.11
2022-08-19	47	813	237	212	0.15	0.18	0.77	0.55	50.368	-58.409	0.30
2022-08-19	50	801	320	325	7.17	7.17	0.60	0.62	50.225	-58.577	0.39
2022-08-19	51	813	213	214	10.63	10.62	0.75	0.77	49.909	-58.688	0.81
2022-08-19	52	812	219	214	13.6	13.58	0.75	0.71	49.807	-59.059	0.68
2022-08-19	53	812	212	210	18.75	18.2	0.78	0.75	49.473	-59.171	0.49
2022-08-20	54	822	144	140	0.17	23.82[1]	0.64	0.56	49.117	-59.178	0.25
2022-08-20	55	812	231	230	2.85	2.87	0.80	0.75	49.117	-59.444	0.56
2022-08-20	56	812	260	257	5.30	5.35	0.80	0.55	49.149	-59.591	0.89
2022-08-20	57	809	296	298	8.02	8.00	0.70	0.76	49.097	-59.779	1.15
2022-08-20	58	808	326	323	11.62	11.63	0.80	0.75	48.889	-60.020	0.60
2022-08-20	59	809	286	280	14.37	14.30	0.75	0.54	48.807	-59.763	0.84
2022-08-20	61	809	309	313	19.75	19.23	0.78	0.76	48.519	-59.896	0.27
2022-08-20	62	808	339	343	22.05	21.98	0.80	0.76	48.554	-60.076	1.04
2022-08-21	63	808	345	350	0.63	0.65	0.75	0.74	48.568	-60.239	1.03
2022-08-21	64	803	428	435	4.07	4.10	0.80	0.61	48.310	-60.188	0.93
2022-08-21	65	803	442	443	7.25	7.27	0.75	0.79	48.286	-60.629	0.53
2022-08-21	66	401	287	261	14.03	14.03	0.75	0.77	48.105	-61.204	0.53
2022-08-21	67	407	374	376	17	17.05	0.75	0.81	48.220	-61.347	0.63

Date	Set no.	Stratum	TEL Depth (m)	CA Depth (m)	TEL Time	CA Time	TEL Distance (nm)	CA Distance (nm)	TEL Latitude	TEL Longitude	Separation (km)
2022-08-21	68	404	344	352	20.22	20.20	0.83	0.74	48.195	-61.382	0.99
2022-08-21	69	408	383	379	23.12	23.10	0.78	0.77	48.307	-61.627	0.00
2022-08-22	70	405	327	339	2.52	2.57	0.66	0.78	48.346	-61.955	0.47
2022-08-22	71	402	261	225	5.65	5.63	0.60	0.64	48.345	-62.081	0.38
2022-08-22	72	408	408	412	9.4	9.87	0.75	0.76	48.456	-62.090	0.90
2022-08-25	77	403	260	276	0.22	0.25	0.78	0.70	48.893	-63.790	0.24
2022-08-25	78	406	298	301	3.33	3.38	0.83	0.70	49.015	-64.094	0.77
2022-08-25	79	406	332	319	5.93	5.95	0.75	0.75	49.129	-64.168	0.74
2022-08-25	80	818	270	282	9.70	9.73	0.75	0.74	49.397	-63.868	0.68
2022-08-25	81	830	175	170	13.73	13.25	0.75	0.74	49.557	-63.993	0.45
2022-08-25	82	841	65	58	18.08	17.77	0.80	0.70	49.695	-64.290	0.55
2022-08-25	83	818	223	229	21.38	21.77	0.75	0.82	49.621	-64.443	0.23
2022-08-26	84	806	349	359	1.33	1.40	0.75	0.75	49.478	-64.482	0.52
2022-08-26	85	806	310	312	4.20	4.20	0.75	0.60	49.606	-64.821	0.26
2022-08-26	87	804	381	378	8.12	9.32	0.75	0.76	49.436	-65.011	1.24
2022-08-26	88	805	324	328	11.30	12.27	0.75	0.75	49.559	-65.221	0.35
2022-08-26	89	805	330	333	15.62	16.05	0.75	0.75	49.385	-65.579	0.41
2022-08-26	90	410	295	278	19.42	19.38	0.88	0.75	49.350	-65.657	0.62
2022-08-26	91	805	329	328	22.48	22.45	0.85	0.74	49.512	-65.762	0.65
2022-08-27	92	409	237	209	1.55	1.58	0.80	0.75	49.309	-65.96	0.77
2022-08-27	94	409	252	240	9.78	9.83	0.75	0.76	49.175	-66.71	0.24
2022-08-27	95	411	308	307	14.30	14.35	0.75	0.76	49.164	-67.409	0.19
2022-08-27	96	412	220	220	18.12	18.12	0.78	0.74	49.205	-67.798	0.27
2022-08-27	97	855	130	97	22.08	22.02	0.80	0.75	49.016	-68.142	0.47
2022-08-27	98	854	65	67	0.07	1.15	0.80	0.75	49.035	-68.204	0.43
2022-08-28	99	855	133	122	4.32	4.33	0.78	0.74	48.879	-68.585	0.07
2022-08-28	100	854	71	89	7.57	7.60	0.75	0.75	48.745	-68.934	1.17
2022-08-28	101	414	194	202	10.62	10.03	0.75	0.75	48.700	-68.788	0.22
2022-08-28	103	413	317	308	15.93	15.95	0.75	0.75	48.535	-68.911	0.59
2022-08-28	104	852	142	172	19.67	19.68	0.80	0.74	48.342	-69.085	0.81
2022-08-28	105	851	80	51	0.05	0.10	0.83	0.80	48.603	-68.486	0.20
2022-08-29	107	852	127	151	4.25	4.30	0.80	0.74	48.643	-68.414	0.01
2022-08-29	109	411	348	347	9.32	9.33	0.75	0.78	48.844	-68.285	1.04
2022-08-29	110	412	258	231	12.62	12.62	0.80	0.74	48.832	-67.950	0.24
2022-08-29	111	851	75	89	15.12	15.10	0.75	0.70	48.859	-67.640	0.37
2022-08-29	112	411	302	300	17.97	17.90	0.83	0.72	48.996	-67.542	0.72
2022-08-29	113	805	306	304	22.98	22.98	0.85	0.75	49.337	-66.980	0.79
2022-08-30	114	817	195	198	3.90	3.95	0.75	0.75	49.673	-66.940	0.88
2022-08-30	115	832	165	156	7.00	7.02	0.75	0.75	49.737	-66.979	0.95
2022-08-30	116	805	298	300	10.95	10.95	0.75	0.74	49.684	-66.443	0.96
2022-08-30	117	805	338	353	13.72	13.77	0.75	0.75	49.694	-66.189	0.71
2022-08-30	118	817	234	247	17.98	18.02	0.80	0.75	49.922	-66.589	0.16
2022-08-30	119	817	269	269	20.73	20.73	0.80	0.78	49.880	-66.334	0.2

Date	Set no.	Stratum	TEL Depth (m)	CA Depth (m)	TEL Time	CA Time	TEL Distance (nm)	CA Distance (nm)	TEL Latitude	TEL Longitude	Separation (km)
2022-08-31	122	832	142	147	8.32	7.88	0.75	0.77	50.129	-65.811	0.15
2022-08-31	124	817	244	225	15.78	16.23	0.75	0.75	49.801	-65.244	0.45
2022-08-31	125	817	205	204	19.9	19.12	0.80	0.80	50.002	-65.201	0.12
2022-08-31	126	832	141	147	21.92	21.93	0.80	0.75	50.106	-65.163	0.40
2022-09-01	127	832	158	149	2.42	2.42	0.80	0.75	50.061	-64.548	0.52
2022-09-01	128	831	150	162	4.38	4.42	0.67	0.74	49.986	-64.442	0.19
2022-09-01	130	832	114	117	12.17	11.53	0.55	0.55	50.026	-64.196	0.45 [2]
2022-09-01	131	841	82	83	15.05	15.72	0.75	0.74	49.992	-63.914	0.04 [3]
2022-09-01	132	839	50	50	19.08	18.38	0.80	0.68	50.129	-63.774	0.18 [2]
2022-09-02	135	839	66	66	11.43	12.17	0.80	0.75	50.214	-62.873	0.33 [3]
2022-09-02	136	828	145	140	15.82	15.78	0.75	0.74	50.025	-62.698	1.19
2022-09-03	140	829	148	170	1.17	1.15	0.83	0.73	49.808	-63.102	0.02
2022-09-03	143	829	141	131	9.92	8.90	0.55	0.52	49.700	-62.698	0.96
2022-09-03	144	816	239	235	11.77	11.77	0.75	0.75	49.765	-62.585	0.95
2022-09-03	145	828	187	197	14.97	14.93	0.75	0.75	49.853	-62.273	0.10
2022-09-03	146	816	266	262	18.23	18.22	0.78	0.75	49.737	-62.007	0.16
2022-09-03	147	816	203	213	21.15	21.2	0.80	0.73	49.814	-61.820	0.28
2022-09-04	148	839	59	58	4.63	5.23	0.85	0.77	50.093	-61.867	0.04
2022-09-04	149	827	159	164	11.72	10.17	0.55	0.54	49.854	-61.418	0.01 [2]
2022-09-04	151	816	279	278	16.47	17.47	0.75	0.59	49.714	-61.245	0.80
2022-09-04	152	816	222	215	21.37	21.43	0.78	0.75	49.544	-61.770	0.13
2022-09-05	153	816	235	229	1.03	1.02	0.72	0.70	49.479	-61.300	0.48
2022-09-05	154	815	285	290	5.78	5.80	0.65	0.75	49.559	-60.803	0.58
2022-09-05	155	815	284	288	8.28	8.20	0.75	0.75	49.509	-60.666	0.87
2022-09-05	157	812	268	269	15.77	15.77	0.75	0.82	49.413	-59.627	0.95
2022-09-05	158	812	273	274	19.25	19.28	0.78	0.74	49.664	-59.588	0.90
2022-09-05	159	812	243	242	22.3	22.35	0.78	0.78	49.460	-59.421	0.99
2022-09-07	161	836	82	85	23.55	23.50	0.82	0.63	49.248	-58.572	0.91
2022-09-08	162	822	100	103	2.13	4.08	0.88	0.58	49.497	-58.615	1.23
2022-09-08	163	812	236	241	7.47	8.88	0.75	0.59	49.853	-59.192	0.04
2022-09-08	165	801	278	277	13.93	13.90	0.75	0.80	50.056	-58.844	0.79
2022-09-08	166	801	305	302	18.02	18.00	0.75	0.80	50.105	-58.672	0.32
2022-09-08	167	814	217	227	23.35	21.57	0.80	0.85	50.081	-59.155	0.49
2022-09-09	168	814	235	245	1.20	1.40	0.75	0.75	49.958	-59.357	0.30
2022-09-09	169	827	97	96	6.28	7.25	0.55	0.52	49.906	-60.058	0.33 [3]
2022-09-09	170	833	86	89	8.88	9.07	0.70	0.76	49.846	-60.069	1.09
2022-09-09	171	833	78	75	11.63	11.75	0.75	0.74	49.644	-60.126	0.22
2022-09-09	172	827	122	120	15.93	15.53	0.75	0.74	49.791	-60.367	0.04 [2]
2022-09-09	173	827	162	158	18.37	18.38	0.75	0.70	49.895	-60.634	0.27
2022-09-09	174	815	281	279	22.67	22.68	0.65	0.64	49.659	-60.656	0.91
2022-09-10	175	815	257	263	2.00	2.00	0.75	0.76	49.366	-60.804	0.19
2022-09-10	176	815	246	240	5.92	5.90	0.80	0.83	49.229	-60.659	0.69
2022-09-10	177	815	255	252	10.13	10.10	0.75	0.53	49.218	-60.052	0.99

Date	Set no.	Stratum	TEL Depth (m)	CA Depth (m)	TEL Time	CA Time	TEL Distance (nm)	CA Distance (nm)	TEL Latitude	TEL Longitude	Separation (km)
2022-09-10	178	808	277	278	12.45	12.40	0.75	0.66	49.165	-60.150	0.42
2022-09-10	179	815	281	287	14.68	14.60	0.75	0.54	49.086	-60.323	0.50
2022-09-10	180	829	92	91	19.07	19.48	0.80	0.73	49.041	-61.011	0.11 [3]
2022-09-10	181	830	133	134	22.12	22.07	0.80	0.71	48.903	-61.052	0.63
2022-09-11	182	819	234	250	0.65	0.63	0.80	0.75	48.848	-61.330	0.12
2022-09-11	183	807	317	313	2.98	3.00	0.75	0.81	48.776	-61.273	0.17
2022-09-11	184	819	266	276	5.6	5.57	0.75	0.57	48.762	-60.903	0.43
2022-09-11	185	819	253	252	9.00	9.00	0.60	0.57	48.828	-60.456	0.89
2022-09-11	188	803	399	393	17.37	17.28	0.75	0.71	48.465	-60.690	0.43
2022-09-11	189	803	406	408	20.40	20.73	0.75	0.75	48.344	-61.047	0.43
2022-09-11	190	407	410	408	23.63	23.47	0.75	0.82	48.204	-61.088	1.17
2022-09-12	191	803	422	421	3.33	3.27	0.80	0.55	48.450	-61.600	0.87
2022-09-12	192	803	421	426	6.47	6.42	0.75	0.82	48.578	-61.952	0.52
2022-09-12	193	804	412	411	9.15	9.13	0.75	0.78	48.629	-62.043	0.69
2022-09-12	194	807	358	348	11.60	11.62	0.80	0.82	48.774	-62.157	0.40
2022-09-12	195	807	363	365	14.27	14.27	0.65	0.71	48.795	-62.425	0.32
2022-09-12	196	807	283	279	16.68	16.85	0.65	0.76	48.906	-62.455	0.12
2022-09-12	197	830	129	143	18.77	18.77	0.60	0.56	49.013	-62.429	0.39
2022-09-12	198	818	268	259	20.82	20.82	0.80	0.81	48.942	-62.567	0.13
2022-09-13	199	408	384	391	0.60	0.62	0.75	0.76	48.710	-62.620	0.50
2022-09-13	200	405	356	363	3.83	3.87	0.80	0.78	48.528	-62.855	0.27
2022-09-13	201	402	249	264	6.43	6.57	0.80	0.78	48.470	-62.935	0.52

Table 2. A set of binomial models with various assumptions for the length effect and station effect in the relative catch efficiency. A smoothing length effect can be considered and the station effect can be added to the intercept, without interaction with the length effect, or added to both the intercept and smoother to allow for interaction between the two effects.

Model	$log(\rho)$	Length Effect	Station Effect
$BI0$	β_0	constant	not considered
$BI1$	$\beta_0 + \delta_{0,i}$	constant	intercept
$BI2$	$\mathbf{X}_f^T\boldsymbol{\beta}_f + \mathbf{X}_r^T\mathbf{b}$	smoothing	not considered
$BI3$	$\mathbf{X}_f^T\boldsymbol{\beta}_f + \mathbf{X}_r^T\mathbf{b} + \delta_{0,i}$	smoothing	intercept
$BI4$	$\mathbf{X}_f^T(\boldsymbol{\beta}_f + \boldsymbol{\delta}_i) + \mathbf{X}_r^T(\mathbf{b} + \boldsymbol{\epsilon}_i)$	smoothing	intercept, smoother

Table 3. A set of beta-binomial models with various assumptions for the length effect and station effect in the relative catch efficiency, and the length effect on the variance parameter. A smoothing length effect can be considered in both the conversion factor and the variance parameter. A possible station effect can be added to the intercept, without interaction with the length effect, or added to both the intercept and the smoother to allow for interaction between the two effects.

Model	$log(\rho)$	$log(\phi)$	Length Effects	Station Effect
$BB0$	β_0	γ_0	constant/constant	not considered
$BB1$	$\beta_0 + \delta_{0,i}$	γ_0	constant/constant	intercept
$BB2$	$\mathbf{X}_f^T\boldsymbol{\beta}_f + \mathbf{X}_r^T\mathbf{b}$	γ_0	smoothing/constant	not considered
$BB3$	$\mathbf{X}_f^T\boldsymbol{\beta}_f + \mathbf{X}_r^T\mathbf{b}$	$\mathbf{X}_f^T\boldsymbol{\gamma} + \mathbf{X}_r^T\mathbf{g}$	smoothing/smoothing	not considered
$BB4$	$\mathbf{X}_f^T\boldsymbol{\beta}_f + \mathbf{X}_r^T\mathbf{b} + \delta_{0,i}$	γ_0	smoothing/constant	intercept
$BB5$	$\mathbf{X}_f^T\boldsymbol{\beta}_f + \mathbf{X}_r^T\mathbf{b} + \delta_{0,i}$	$\mathbf{X}_f^T\boldsymbol{\gamma} + \mathbf{X}_r^T\mathbf{g}$	smoothing/smoothing	intercept
$BB6$	$\mathbf{X}_f^T(\boldsymbol{\beta}_f + \boldsymbol{\delta}_i) + \mathbf{X}_r^T(\mathbf{b} + \boldsymbol{\epsilon}_i)$	γ_0	smoothing/constant	intercept, smoother
$BB7$	$\mathbf{X}_f^T(\boldsymbol{\beta}_f + \boldsymbol{\delta}_i) + \mathbf{X}_r^T(\mathbf{b} + \boldsymbol{\epsilon}_i)$	$\mathbf{X}_f^T\boldsymbol{\gamma} + \mathbf{X}_r^T\mathbf{g}$	smoothing/smoothing	intercept, smoother

Table 4. Taxonomic groupings employed for the analyses of the EnGSL comparative fishing data. The codes are those used routinely in DFO's Quebec region, commonly called STRAP codes.

Taxon	Taxon code	Codes in group
Gadus morhua	438	430, 436, 438
Myctophidae	271	271, 272, 275, 278, 280, 281, 285, 290
Ammodytes sp.	696	693, 695, 696
Artediellus sp.	810	810, 811, 812
Eumicrotremus terraenovae	847	844, 845, 847
Liparidae	853	853, 856, 862, 865, 868, 874
Enchelyopus cimbrius	461	454, 461
Porifera	1101	1101 – 1165 (run separately including all sponges)
Polymastia sp.	1109	1107, 1109, 1122, 1126 (run separately from 1101)
Naticidae	3420	3420, 3422, 3437
Buccinum sp.	3516	3516, 3517, 3520, 3523
Colus sp.	3575	3575, 3576, 3577
Astarte sp.	4227	4227, 4231
Nymphon sp.	5961	5951, 5961
Pteraster sp.	8409	8409, 8410, 8411, 8412
Ophiura sarsii	8553	8553, 8552

Table 5. Summary of the catches at length excluded from the length-disaggregated analyses.

Taxon	**Lengths excluded**
Myxine limosa	<13 cm
Argentina silus	>35 cm
Urophycis tenuis	>85 cm
Ammodytes sp.	>20 cm
Sebastes sp.	>33 cm
Myoxocephalus scorpius	<13 cm
Gymnocanthus tricuspis	<9 cm
Leptagonus decagonus	<7 cm
Illex illecebrosus	<11 cm
Pandalus borealis	<6 mm
Pandalus montagui	<6 mm
Pontophilus norvegicus	<6 mm
Chionoecetes opilio	>130 mm

Table 6. Total number of relevant set pairs (those with at least one capture), and pairs in which the taxon was captured only by the CCGS John Cabot or only by the CCGS Teleost, along with a reference to the number of the figure in which results are plotted. The lists are sorted by the type of analysis (length-disaggregated vs size-aggregated) and roughly taxonomically.

Taxon	Code	Pairs	Cabot only	Teleost only	Figure number
Length-disaggregated analyses					
Fishes					
Myxine limosa	13	108	14	12	7
Centroscyllium fabricii	27	30	6	3	8
Amblyraja radiata	90	162	15	15	9
Malacoraja senta	91	135	33	27	10
Clupea harengus	150	121	19	24	11
Mallotus villosus	187	91	10	17	12
Argentina silus	193	30	6	11	13
Arctozenus risso	320	113	8	12	14
Gadus morhua	438	102	16	11	15
Phycis chesteri	444	43	7	8	16
Urophycis tenuis	447	109	14	22	17
Merluccius bilinearis	449	102	14	14	18
Enchelyopus cimbrius	461	140	15	24	19
Nezumia bairdii	478	111	7	10	20
Scomber scombrus	572	63	14	14	21
Ammodytes sp.	696	31	16	10	22
Anarhichas lupus	700	31	5	9	23
Lumpenus lampretaeformis	716	39	8	10	24
Leptoclinus maculatus	717	37	10	15	25
Lycodes lavalaei	728	32	8	9	26
Lycodes vahlii	730	49	6	13	27
Melanostigma atlanticum	745	56	10	11	28
Sebastes sp.	792	171	5	9	29
Artediellus sp.	810	47	14	12	30
Triglops murrayi	814	38	7	5	31
Myoxocephalus scorpius	819	34	9	7	32
Gymnocanthus tricuspis	823	39	6	15	33
Leptagonus decagonus	836	25	10	7	34
Aspidophoroides monopterygius	838	50	16	13	35
Eumicrotremus terraenovae	847	31	5	9	36
Cyclopterus lumpus	849	42	24	11	37
Liparidae	853	38	7	13	38
Hippoglossoides platessoides	889	169	9	12	39
Glyptocephalus cynoglossus	890	150	12	10	40
Reinhardtius hippoglossoides	892	156	18	14	41
Hippoglossus hippoglossus	893	85	19	24	42

Taxon	Code	Pairs	Cabot only	Teleost only	Figure number
Lophius americanus	966	34	12	16	43
Squid					
Illex illecebrosus	4753	81	19	26	44
Shrimps					
Pasiphaea multidentata	8057	90	10	8	45
Spirontocaris liljeborgii	8087	48	16	15	46
Lebbeus polaris	8093	57	22	21	47
Pandalus borealis	8111	152	7	9	48
Pandalus montagui	8112	84	10	13	49
Atlantopandalus propinqvus	8113	39	6	20	50
Pontophilus norvegicus	8135	111	12	13	51
Argis dentata	8138	33	6	8	52
Crabs					
Lithodes maja	8196	80	19	25	53
Chionoecetes opilio	8213	108	21	17	54
Hyas araneus	8217	26	8	8	55
Hyas alutaceus	8219	39	12	7	56
Size-aggregated analyses					
Fishes					
Myctophiformes	271	47	8	12	57
Eumesogrammus praecisus	711	24	4	11	58
Porifera					
Porifera sp.	1101	122	22	21	59
Tentorium semisuberites	1108	15	5	4	60
Polymastia sp.	1109	30	21	5	61
Stylocordyla borealis	1112	21	12	5	62
Hydrozoa and Scyphozoa					
Hydrozoa	1341	27	10	10	63
Ptychogena lactea	1353	35	10	12	64
Rhodaliidae	1380	26	5	9	65
Scyphozoa	2040	18	10	6	66
Cyanea capillata	2080	163	16	8	67
Periphylla periphylla	2096	57	19	18	68
Anthozoa					
Hormathia digitata	2150	49	20	12	69
Epizoanthus erdmanni	2156	33	14	17	70
Bolocera tuediae	2158	90	29	13	71
Stephanauge nexilis	2159	23	11	5	72
Actinostola callosa	2162	81	16	15	73
Stomphia coccinea	2173	40	10	15	74
Actinauge cristata	2182	67	11	15	75
Gersemia rubiformis	2184	32	4	14	76
Drifa glomerata	2191	28	10	10	77

Taxon	Code	Pairs	Cabot only	Teleost only	Figure number
Pennatula aculeata	2203	136	22	16	78
Ptilella grandis	2210	44	14	6	79
Halipteris finmarchica	2217	28	11	2	80
Anthoptilum grandiflorum	2218	51	18	9	81
Nephtheidae	2219	15	5	8	82
Tentaculata					
Pleurobrachia pileus	2255	16	4	6	83
Bryozoa	2670	15	6	8	84
Gastropoda					
Arrhoges occidentalis	3418	37	16	8	85
Cryptonatica affinis	3422	27	15	9	86
Buccinum sp.	3516	67	26	13	87
Neptunea despecta	3567	15	7	5	88
Colus sp.	3575	21	7	11	89
Scaphander punctostriatus	3715	23	5	11	90
Bivalvia					
Megayoldia thraciaeformis	4025	49	21	2	91
Mytilus sp.	4121	20	11	7	92
Chlamys islandica	4167	16	3	7	93
Astarte sp.	4227	48	18	11	94
Cuspidaria glacialis	4526	30	10	5	95
Rossia sp.	4557	32	7	20	96
Cephalopoda					
Stoloteuthis leucoptera	4587	27	13	11	97
Bathypolypus bairdii	4904	83	21	29	98
Polychaeta					
Polychaeta	4950	99	45	34	99
Aphrodita hastata	5002	31	17	11	100
Laetmonice filicornis	5003	49	10	15	101
Polynoidae	5007	41	12	20	102
Brada inhabilis	5755	16	5	9	103
Nymphon sp.	5961	56	17	17	104
Malacostraca					
Aega psora	6771	16	6	8	105
Syscenus infelix	6791	80	7	13	106
Epimeria loricata	7383	16	1	12	107
Eualus fabricii	8075	19	2	12	108
Eualus macilentus	8077	22	3	13	109
Spirontocaris sp.	8084	22	11	10	110
Spirontocaris spinus	8085	17	3	10	111
Sabinea septemcarinata	8128	23	6	7	112
Munidopsis curvirostra	8164	24	6	11	113
Pagurus sp.	8178	35	13	16	114

Taxon	Code	Pairs	Cabot only	Teleost only	Figure number
Holothuroidea and Echinoidea					
Cucumaria frondose	8312	16	5	5	115
Strongylocentrotus sp.	8363	62	7	13	116
Brisaster fragilis	8378	95	14	14	117
Asteroidea					
Ctenodiscus crispatus	8407	127	25	8	118
Pteraster militaris	8410	19	5	5	119
Ceramaster granularis	8429	33	5	12	120
Hippasteria phrygiana	8431	62	20	26	121
Pseudarchaster parelii	8433	27	12	5	122
Crossaster papposus	8447	27	5	10	123
Henricia sp.	8483	59	16	20	124
Leptasterias (Hexasterias) polaris	8511	16	6	7	125
Leptasterias groenlandica	8513	21	5	9	126
Psilaster andromeda	8520	29	5	2	127
Ophiuroidea					
Gorgonocephalus sp.	8540	33	10	8	128
Ophiura sarsii	8553	90	17	20	129
Ophiacantha bidentata	8575	40	4	20	130
Ophiopholis aculeata	8583	54	10	14	131
Ophioscolex glacialis	8585	33	6	17	132
Ascidiacea					
Ascidia sp.	8742	93	14	13	133
Eudistoma vitreum	8778	21	5	8	134
Boltenia ovifera	8792	19	5	3	135

Table 7. Relative evidence for length-disaggregated binomial and beta-binomial models based on delta values of A) the Aikaike Information Criterion (AIC) and B) the Bayesian Information Criterion (BIC). Entries with '–' indicate models that did not converge. Model BB7 did not converge for any taxon and results are therefore not included in the table. Similarly, model BB6 is excluded because convergence was achieved for a single taxon, Arctozenus risso, for which the fit was associated with the largest values of AIC and BIC relative to the other models.

A) ΔAIC

Code	Species	Bl0	Bl1	Bl2	Bl3	Bl4	BB0	BB1	BB2	BB3	BB4	BB5
13	*Myxine limosa*	465	87	336	1	-	345	81	243	246	0	1
27	*Centroscyllium fabricii*	46	22	49	24	-	13	0	17	17	3	3
90	*Amblyraja radiata*	175	22	166	24	-	95	0	89	80	1	-
91	*Malacoraja senta*	40	0	44	4	-	30	1	33	-	5	8
150	*Clupea harengus*	1716	30	1679	34	-	433	0	434	418	3	-
187	*Mallotus villosus*	1168	195	1078	136	-	192	28	181	180	0	6
193	*Argentina silus*	165	62	139	31	-	60	23	48	48	0	2
320	*Arctozenus risso*	47	1	43	0	-	36	-	35	38	-	-
438	*Gadus morhua*	2718	210	2707	206	-	1026	34	1028	1000	35	0
444	*Phycis chesteri*	11	6	12	7	-	2	0	3	6	1	4
447	*Urophycis tenuis*	117	0	111	1	-	86	2	83	86	3	-
449	*Merluccius bilinearis*	108	14	111	16	-	37	0	40	43	2	5
461	*Enchelyopus cimbrius*	162	30	155	20	68	88	7	82	81	0	3
478	*Nezumia bairdii*	101	10	105	13	-	61	0	64	68	3	7
572	*Scomber scombrus*	62	6	35	0	-	21	6	11	15	1	-
696	*Ammodytes sp.*	35	0	37	4	-	18	2	21	25	6	-
700	*Anarhichas lupus*	78	0	82	4	-	69	2	73	77	6	9
716	*Lumpenus lampretaeformis*	99	0	102	3	-	79	2	83	85	5	-
717	*Leptoclinus maculatus*	102	0	98	1	-	20	1	23	24	2	5
728	*Lycodes lavalaei*	69	1	64	0	-	56	-	54	58	-	-
730	*Lycodes vahlii*	210	109	199	96	-	50	8	41	-	0	3
745	*Melanostigma atlanticum*	79	0	83	3	-	45	2	49	52	5	-
792	*Sebastes sp.*	5902	1483	5834	1464	-	-	143	874	821	127	0
810	*Artediellus sp.*	56	7	51	1	-	24	4	21	-	0	-
814	*Triglops murrayi*	62	4	63	7	-	13	0	14	17	2	6
819	*Myoxocephalus scorpius*	20	0	20	1	-	16	1	18	19	2	5

Code	Species	BI0	BI1	BI2	BI3	BI4	BB0	BB1	BB2	BB3	BB4	BB5
823	*Gymnocanthus tricuspis*	165	0	168	1	-	73	0	77	80	1	-
836	*Leptagonus decagonus*	347	7	333	0	-	101	7	105	109	2	6
838	*Aspidophoroides monopterygius*	71	1	71	2	-	19	0	22	24	1	3
847	*Eumicrotremus terraenovae*	84	0	77	1	36	31	-	31	34	3	6
849	*Cyclopterus lumpus*	0	1	3	5	-	2	-	5	9	-	11
853	Liparidae	32	28	19	0	-	2	1	4	5	1	-
889	*Hippoglossoides platessoides*	802	138	789	132	-	329	33	319	305	25	0
890	*Glyptocephalus cynoglossus*	914	43	899	34	-	395	4	395	373	0	3
892	*Reinhardtius hippoglossoides*	782	230	771	190	-	390	47	389	381	38	0
893	*Hippoglossus hippoglossus*	1	0	5	4	-	3	2	7	-	-	-
966	*Lophius americanus*	4	6	0	2	-	-	8	2	-	-	-
4753	*Illex illecebrosus*	1	0	5	4	-	3	-	7	-	-	-
8057	*Pasiphaea multidentata*	676	63	680	51	-	317	10	320	304	0	-
8087	*Spirontocaris liljeborgii*	38	0	39	3	-	28	-	29	33	-	-
8093	*Lebbeus polaris*	140	2	109	0	-	80	3	74	78	2	-
8111	*Pandalus borealis*	11439	2486	10844	2252	-	1524	280	1456	1447	224	0
8112	*Pandalus montagui*	2537	242	2457	117	264	636	76	595	575	11	0
8113	*Atlantopandalus propinqvus*	148	0	151	4	-	78	2	82	84	-	-
8135	*Pontophilus norvegicus*	369	126	243	25	-	186	84	99	101	1	0
8138	*Argis dentata*	171	10	157	0	-	118	8	118	115	1	-
8196	*Lithodes maja*	13	0	16	4	-	15	-	18	21	-	-
8213	*Chionoecetes opilio*	527	98	520	64	-	226	14	228	212	2	0
8217	*Hyas araneus*	26	1	18	0	-	28	-	-	-	-	-
8219	*Hyas alutaceus*	50	0	54	0	-	41	1	44	-	1	-

B) ΔBIC

Code	Species	BI0	BI1	BI2	BI3	BI4	BB0	BB1	BB2	BB3	BB4	BB5
13	*Myxine limosa*	442	72	328	0	-	330	73	242	259	6	21
27	*Centroscyllium fabricii*	31	15	49	32	-	6	0	24	38	18	32
90	*Amblyraja radiata*	160	14	166	31	-	87	0	96	103	16	-
91	*Malacoraja senta*	33	0	51	18	-	30	9	48	-	27	44
150	*Clupea harengus*	1702	24	1679	41	-	426	0	441	438	17	-
187	*Mallotus villosus*	1145	177	1067	130	-	175	16	175	186	0	17
193	*Argentina silus*	139	43	126	24	-	41	10	42	54	0	15
320	*Arctozenus risso*	40	0	49	12	-	36	-	46	62	-	-
438	*Gadus morhua*	2672	171	2676	183	-	987	3	1005	992	20	0
444	*Phycis chesteri*	2	4	17	19	-	0	5	15	31	20	36
447	*Urophycis tenuis*	109	0	118	16	-	86	9	98	116	25	-
449	*Merluccius bilinearis*	94	7	111	23	-	30	0	47	64	16	33
461	*Enchelyopus cimbrius*	142	17	148	21	88	75	0	82	94	7	23
478	*Nezumia bairdii*	88	4	105	20	-	54	0	71	89	17	34
572	*Scomber scombrus*	49	0	36	8	-	15	8	19	36	16	-
696	*Ammodytes sp.*	29	0	43	16	-	18	8	33	49	24	-
700	*Anarhichas lupus*	70	0	89	19	-	69	9	88	107	28	47
716	*Lumpenus lampretaeformis*	92	0	109	16	-	79	9	96	111	25	-
717	*Leptoclinus maculatus*	96	0	104	13	-	20	7	34	47	19	34
728	*Lycodes lavalaei*	61	0	71	14	-	55	-	68	86	-	-
730	*Lycodes vahlii*	188	94	191	95	-	35	0	40	-	6	23
745	*Melanostigma atlanticum*	73	0	88	14	-	45	7	60	74	22	-
792	*Sebastes sp.*	5861	1450	5807	1444	-	-	116	854	815	114	0
810	*Artediellus sp.*	43	0	49	5	-	17	2	25	-	10	-
814	*Triglops murrayi*	53	0	65	15	-	9	2	21	37	16	32
819	*Myoxocephalus scorpius*	13	0	26	14	-	16	7	31	46	22	38
823	*Gymnocanthus tricuspis*	159	0	174	13	-	73	6	89	104	19	-
836	*Leptagonus decagonus*	334	0	332	5	-	94	6	110	126	13	28
838	*Aspidophoroides monopterygius*	64	0	76	13	-	18	5	32	46	18	31

Code	Species	BI0	BI1	BI2	BI3	BI4	BB0	BB1	BB2	BB3	BB4	BB5
847	*Eumicrotremus terraenovae*	78	0	82	13	66	31	-	42	57	21	35
849	*Cyclopterus lumpus*	0	8	17	26	-	9	-	26	44	-	52
853	Liparidae	24	26	23	11	-	0	5	15	30	19	-
889	*Hippoglossoides platessoides*	759	102	760	110	-	293	4	297	298	11	0
890	*Glyptocephalus cynoglossus*	896	32	894	37	-	383	0	398	391	10	28
892	*Reinhardtius hippoglossoides*	736	193	741	167	-	352	16	366	373	23	0
893	*Hippoglossus hippoglossus*	0	7	21	28	-	10	17	31	-	-	-
966	*Lophius americanus*	0	10	12	22	-	-	19	22	-	-	-
4753	*Illex illecebrosus*	0	4	16	20	-	8	-	24	-	-	-
8057	*Pasiphaea multidentata*	653	46	670	47	-	300	0	316	313	3	-
8087	*Spirontocaris liljeborgii*	32	0	45	14	-	28	-	40	55	-	-
8093	*Lebbeus polaris*	133	0	114	10	-	78	8	84	99	17	-
8111	*Pandalus borealis*	11400	2454	10819	2232	-	1492	254	1437	1440	211	0
8112	*Pandalus montagui*	2501	212	2434	100	266	607	53	578	570	0	1
8113	*Atlantopandalus propinqvus*	142	0	157	16	-	78	8	94	108	-	-
8135	*Pontophilus norvegicus*	345	108	231	19	-	168	71	93	106	0	11
8138	*Argis dentata*	155	0	154	3	-	109	4	122	131	11	-
8196	*Lithodes maja*	5	0	24	19	-	15	-	34	53	-	-
8213	*Chionoecetes opilio*	497	76	506	58	-	204	0	222	222	4	18
8217	*Hyas araneus*	17	0	24	14	-	26	-	-	-	-	-
8219	*Hyas alutaceus*	43	0	61	15	-	41	8	59	-	24	-

Table 8. P-values associated with tests for a smooth effect of depth, a smooth effect of time and a fixed effect of day on the normalized quantile residuals from the length-disaggregated selected best model. Values ≤0.01 are indicated in bold.

Taxon	s(depth)	s(time)	day
Myxine limosa	0.564	0.784	0.788
Centroscyllium fabricii	0.402	0.774	0.482
Amblyraja radiata	0.173	0.095	0.712
Malacoraja senta	0.341	0.697	0.320
Clupea harengus	0.392	0.268	0.245
Mallotus villosus	0.597	0.727	0.934
Argentina silus	0.497	0.156	0.730
Arctozenus risso	0.906	0.067	0.839
Gadus morhua	0.227	0.540	0.716
Phycis chesteri	0.026	0.752	0.143
Urophycis tenuis	0.933	0.991	0.248
Merluccius bilinearis	0.400	0.124	0.032
Enchelyopus cimbrius	**<0.001**	0.208	0.104
Nezumia bairdii	0.342	0.525	0.736
Scomber scombrus	0.925	0.487	0.570
Ammodytes sp.	0.049	0.737	0.625
Anarhichas lupus	0.490	0.843	0.519
Lumpenus lampretaeformis	0.547	0.016	0.418
Leptoclinus maculatus	0.978	0.360	0.545
Lycodes lavalaei	0.135	0.204	0.052
Lycodes vahlii	0.016	0.463	0.976
Melanostigma atlanticum	0.518	0.132	0.458
Sebastes sp.	0.864	0.579	0.680
Artediellus sp.	0.177	0.938	0.404
Triglops murrayi	0.857	0.451	0.539
Myoxocephalus scorpius	0.053	0.219	0.856
Gymnocanthus tricuspis	0.570	0.098	0.029
Leptagonus decagonus	0.567	**0.001**	0.400
Aspidophoroides monopterygius	0.176	0.193	0.840
Eumicrotremus terraenovae	0.900	0.352	0.035
Cyclopterus lumpus	0.551	0.515	0.190
Liparidae	0.760	0.812	0.361
Hippoglossoides platessoides	0.480	0.342	0.340
Glyptocephalus cynoglossus	0.179	0.440	0.551
Reinhardtius hippoglossoides	0.166	0.778	0.581
Hippoglossus hippoglossus	0.995	0.078	0.236
Lophius americanus	0.443	0.510	0.250
Illex illecebrosus	0.553	0.074	0.340
Pasiphaea multidentata	0.940	**0.004**	0.145
Spirontocaris liljeborgii	0.789	0.233	0.326

Taxon	s(depth)	s(time)	day
Lebbeus polaris	0.512	0.204	0.196
Pandalus borealis	0.044	0.169	0.615
Pandalus montagui	0.852	0.413	0.081
Atlantopandalus propinqvus	0.155	0.445	0.972
Pontophilus norvegicus	0.898	0.377	0.150
Argis dentata	0.178	0.283	0.807
Lithodes maja	**0.010**	0.978	0.473
Chionoecetes opilio	0.022	0.772	0.705
Hyas araneus	0.155	0.697	0.241
Hyas alutaceus	0.113	0.124	0.411

Table 9. Relative evidence for size-aggregated binomial and beta-binomial models for catch counts based on Aikaike's Information Criterion (AIC) and the Bayesian Information Criterion (BIC) values, and estimates of the conversion factor Rho, and approximate 95% confidence intervals, for catches in numbers and in weights for taxa for which length-disaggregated analyses were also undertaken. Recall that a single model was used for catch weights and thus AIC and BIC values are not shown. Entries with '–' indicate models that did not converge.

	AIC			BIC				
Taxon	**BI1**	**BB0**	**BB1**	**BI**	**BB0**	**BB1**	**Rho (numbers)**	**Rho (weights)**
Myxine limosa	626	624	626	632	629	634	0.88 (0.73-1.07)	0.76 (0.66-0.88)
Centroscyllium fabricii	187	187	189	189	189	193	1.00 (0.76-1.31)	0.94 (0.72-1.23)
Amblyraja radiata	747	745	747	753	751	756	1.02 (0.89-1.17)	0.97 (0.86-1.11)
Malacoraja senta	402	400	402	408	406	411	0.78 (0.63-0.97)	0.85 (0.68-1.07)
Clupea harengus	655	641	642	661	647	650	1.03 (0.83-1.30)	0.99 (0.79-1.23)
Mallotus villosus	657	646	646	662	651	654	1.26 (0.97-1.65)	1.42 (1.10-1.83)
Argentina silus	158	154	156	161	157	160	1.49 (0.86-2.59)	2.04 (1.39-3.01)
Arctozenus risso	454	453	455	459	459	463	1.12 (0.96-1.31)	1.13 (1.02-1.27)
Gadus morhua	793	782	781	799	787	789	1.02 (0.83-1.26)	1.16 (0.95-1.41)
Phycis chesteri	168	167	169	171	171	175	1.02 (0.80-1.31)	0.86 (0.71-1.04)
Urophycis tenuis	402	400	402	408	406	410	1.12 (0.92-1.36)	1.17 (1.00-1.37)
Merluccius bilinearis	433	432	434	438	437	442	1.01 (0.84-1.22)	1.13 (0.96-1.32)
Enchelyopus cimbrius	646	645	647	652	651	656	0.91 (0.77-1.06)	0.82 (0.72-0.93)
Nezumia bairdii	643	641	642	649	646	651	0.92 (0.81-1.03)	0.85 (0.79-0.92)
Scomber scombrus	202	201	203	207	205	209	0.91 (0.65-1.27)	0.64 (0.47-0.88)
Ammodytes sp.	88	85	87	91	88	91	0.77 (0.41-1.43)	1.05 (0.57-1.95)
Anarhichas lupus	126	125	127	129	128	132	0.90 (0.58-1.40)	0.67 (0.43-1.02)
Lumpenus lampretaeformis	162	161	163	165	164	168	0.96 (0.61-1.49)	0.86 (0.61-1.21)
Leptoclinus maculatus	113	109	111	116	112	115	1.47 (0.86-2.52)	1.97 (1.12-3.45)
Lycodes lavalaei	130	127	129	133	130	134	0.97 (0.58-1.61)	1.50 (0.91-2.47)
Lycodes vahlii	228	227	229	232	230	234	1.38 (0.97-1.95)	1.21 (0.93-1.57)
Melanostigma atlanticum	251	251	253	255	255	259	1.24 (0.94-1.64)	1.13 (0.96-1.34)
Sebastes sp.	2307	2285	2280	2313	2291	2290	0.99 (0.86-1.14)	0.98 (0.89-1.09)
Artediellus sp.	168	167	169	171	171	174	1.21 (0.78-1.89)	1.60 (1.12-2.29)
Triglops murrayi	198	198	200	201	201	204	0.81 (0.61-1.07)	0.73 (0.61-0.88)
Myoxocephalus scorpius	125	124	126	128	127	131	1.31 (0.83-2.07)	1.61 (1.05-2.46)
Gymnocanthus tricuspis	181	180	182	184	183	187	1.23 (0.78-1.94)	1.16 (0.81-1.65)
Leptagonus decagonus	97	95	97	100	97	100	0.89 (0.46-1.74)	0.80 (0.32-1.99)
Aspidophoroides monopterygius	144	142	144	148	146	150	0.93 (0.61-1.43)	1.30 (0.92-1.84)
Eumicrotremus terraenovae	125	124	126	127	126	130	1.36 (0.83-2.21)	0.93 (0.61-1.42)
Cyclopterus lumpus	74	73	75	77	77	81	0.59 (0.34-1.01)	0.43 (0.23-0.8)
Liparidae	103	102	104	106	105	109	1.41 (0.93-2.15)	1.20 (0.75-1.91)
Hippoglossoides platessoides	1127	1127	1129	1134	1133	1138	0.93 (0.84-1.03)	0.89 (0.83-0.96)
Glyptocephalus cynoglossus	922	920	922	928	926	931	0.88 (0.77-1.00)	0.88 (0.79-0.97)
Reinhardtius hippoglossoides	947	944	946	953	950	955	0.95 (0.85-1.08)	1.01 (0.93-1.1)
Hippoglossus hippoglossus	230	230	232	235	235	239	1.00 (0.77-1.30)	0.99 (0.76-1.31)

	AIC			BIC				
Taxon	**BI1**	**BB0**	**BB1**	**BI**	**BB0**	**BB1**	**Rho (numbers)**	**Rho (weights)**
Lophius americanus	58	58	-	61	61	-	0.93 (0.52-1.67)	1.76 (0.90-3.45)
Illex illecebrosus	216	216	218	221	220	225	1.23 (0.95-1.59)	1.24 (1.01-1.51)
Pasiphaea multidentata	826	815	814	831	820	822	0.85 (0.69-1.05)	1.15 (0.99-1.33)
Spirontocaris liljeborgii	147	142	144	151	146	150	0.93 (0.58-1.48)	0.64 (0.43-0.95)
Lebbeus polaris	181	177	179	185	181	185	1.11 (0.69-1.78)	1.39 (0.99-1.95)
Pandalus borealis	1784	1769	1770	1790	1775	1779	1.10 (0.94-1.29)	1.16 (1.01-1.33)
Pandalus montagui	700	689	689	705	693	696	1.13 (0.86-1.50)	1.03 (0.78-1.37)
Atlantopandalus propinqvus	129	128	130	132	131	135	1.81 (1.05-3.13)	1.95 (1.20-3.16)
Pontophilus norvegicus	720	713	714	725	719	722	1.19 (0.98-1.45)	1.21 (1.05-1.40)
Argis dentata	203	199	200	206	202	205	1.33 (0.80-2.19)	1.32 (0.84-2.07)
Lithodes maja	239	238	240	244	243	247	0.79 (0.60-1.04)	0.73 (0.58-0.91)
Chionoecetes opilio	551	547	549	556	552	557	0.71 (0.57-0.89)	0.69 (0.56-0.84)
Hyas araneus	83	81	83	85	83	86	1.14 (0.64-2.06)	1.03 (0.57-1.86)
Hyas alutaceus	143	142	144	146	145	149	0.78 (0.52-1.18)	0.54 (0.40-0.73)

Table 10. Relative evidence for size-aggregated binomial and beta-binomial models for catch counts based on Aikaike's Information Criterion (AIC) and the Bayesian Information Criterion (BIC) values, and estimates of the conversion factor Rho, and approximate 95% confidence intervals, for catches in numbers and in weights for taxa for which only size-aggregated analyses were also undertaken. Recall that a single model was used for catch weights and thus AIC and BIC values are not shown. Entries with '–' indicate models that did not converge.

	AIC			BIC				
Taxon	**Bl1**	**BB0**	**BB1**	**Bl1**	**BB0**	**BB1**	**Rho (numbers)**	**Rho (weights)**
Myctophiformes	142	141	143	146	145	149	1.21 (0.88-1.66)	1.19 (0.93-1.51)
Eumesogrammus praecisus	89	87	89	92	90	93	1.93 (1.01-3.69)	1.45 (0.85-2.46)
Porifera	116	115	117	120	118	122	0.53 (0.32-0.88)	0.88 (0.69-1.12)
Tentorium semisuberites	48	47	49	50	49	51	0.89 (0.40-1.98)	1.12 (0.54-2.32)
Polymastia sp.	56	64	66	59	67	70	0.00 (0.00-0.01)	0.36 (0.17-0.76)
Stylocordyla borealis	54	53	55	56	56	59	0.60 (0.27-1.36)	0.87 (0.41-1.87)
Hydrozoa	30	29	31	31	30	33	0.65 (0.24-1.76)	0.29 (0.13-0.64)
Ptychogena lactea	123	120	122	126	123	126	1.04 (0.61-1.76)	1.30 (0.71-2.37)
Rhodaliidae	96	95	97	98	98	101	0.80 (0.46-1.42)	0.89 (0.62-1.29)
Scyphozoa	21	21	23	22	22	24	0.26 (0.05-1.38)	0.69 (0.30-1.61)
Cyanea capillata	555	555	557	562	562	567	0.77 (0.68-0.87)	0.80 (0.70-0.91)
Periphylla periphylla	122	121	123	126	125	129	0.81 (0.53-1.22)	0.81 (0.51-1.27)
Hormathia digitata	159	157	159	163	161	165	0.59 (0.38-0.92)	0.73 (0.47-1.14)
Epizoanthus erdmanni	76	68	70	79	71	74	1.00 (0.50-2.01)	1.24 (0.63-2.45)
Bolocera tuediae	331	331	333	336	336	340	0.41 (0.28-0.62)	0.51 (0.39-0.66)
Stephanauge nexilis	70	69	71	72	71	75	0.55 (0.27-1.12)	0.52 (0.29-0.93)
Actinostola callosa	456	453	455	461	458	462	0.59 (0.46-0.77)	0.57 (0.44-0.73)
Stomphia coccinea	113	110	112	116	114	117	0.96 (0.56-1.65)	0.88 (0.54-1.43)
Actinauge cristata	429	427	429	434	432	436	0.78 (0.57-1.08)	0.53 (0.39-0.71)
Gersemia rubiformis	78	77	79	81	80	83	1.66 (0.93-2.96)	2.77 (1.68-4.55)
Drifa glomerata	51	49	51	53	51	54	0.70 (0.31-1.58)	1.18 (0.52-2.67)
Pennatula aculeata	783	772	774	788	778	782	0.71 (0.57-0.89)	0.44 (0.36-0.53)
Ptilella grandis	233	230	232	237	233	237	0.56 (0.37-0.86)	0.62 (0.41-0.92)
Halipteris finmarchica	86	86	88	89	89	92	0.42 (0.25-0.69)	0.51 (0.35-0.74)
Anthoptilum grandiflorum	284	281	283	287	285	289	0.64 (0.41-0.99)	0.57 (0.38-0.85)
Nephtheidae	-	20	22	-	21	24	1.34 (0.42-4.21)	2.13 (1.04-4.38)
Pleurobrachia pileus	42	41	-	43	43	-	1.23 (0.56-2.68)	0.97 (0.50-1.86)
Bryozoa	29	28	30	30	29	31	1.10 (0.37-3.29)	0.95 (0.33-2.74)
Arrhoges occidentalis	93	93	-	96	96	-	0.56 (0.45-0.69)	0.58 (0.47-0.72)
Cryptonatica affinis	55	54	56	57	56	60	0.59 (0.28-1.22)	0.43 (0.21-0.89)
Buccinum sp.	175	174	176	179	178	183	0.53 (0.39-0.72)	0.37 (0.27-0.50)
Neptunea despecta	27	-	-	28	-	-	0.79 (0.33-1.90)	0.75 (0.32-1.75)
Colus sp.	48	47	49	50	49	52	1.48 (0.68-3.23)	1.16 (0.60-2.22)
Scaphander punctostriatus	67	67	69	69	69	72	1.25 (0.63-2.47)	0.96 (0.54-1.71)
Megayoldia thraciaeformis	213	215	217	216	218	222	0.13 (0.06-0.28)	0.15 (0.11-0.22)
Mytilus sp.	42	40	42	44	42	45	0.54 (0.23-1.28)	0.73 (0.28-1.91)
Chlamys islandica	52	52	54	54	54	57	0.98 (0.50-1.91)	1.41 (0.71-2.81)

	AIC			BIC				
Taxon	**Bl1**	**BB0**	**BB1**	**Bl1**	**BB0**	**BB1**	**Rho (numbers)**	**Rho (weights)**
Astarte sp.	132	130	132	135	134	138	0.54 (0.34-0.86)	0.33 (0.21-0.50)
Cuspidaria glacialis	87	86	88	90	89	93	0.52 (0.31-0.87)	0.43 (0.28-0.66)
Rossia sp.	60	59	61	63	62	65	1.88 (0.97-3.65)	1.07 (0.52-2.20)
Stoloteuthis leucoptera	61	58	60	64	60	64	0.76 (0.37-1.55)	0.44 (0.24-0.82)
Bathypolypus bairdii	206	205	207	211	210	214	1.03 (0.76-1.41)	1.18 (0.88-1.60)
Polychaeta	249	240	242	255	245	250	0.62 (0.43-0.90)	0.27 (0.18-0.40)
Aphrodita hastata	64	62	64	67	65	69	0.60 (0.30-1.19)	0.54 (0.29-1.01)
Laetmonice filicornis	171	168	170	175	171	175	1.19 (0.78-1.81)	1.27 (0.88-1.84)
Polynoidae	93	91	93	97	95	98	1.40 (0.82-2.39)	1.00 (0.60-1.67)
Brada inhabilis	35	34	36	36	36	39	1.66 (0.68-4.09)	1.71 (0.86-3.41)
Nymphon sp.	169	168	170	173	172	176	1.22 (0.83-1.78)	1.26 (0.91-1.75)
Aega psora	30	30	32	31	31	34	1.18 (0.51-2.73)	1.37 (0.62-3.04)
Syscenus infelix	320	320	322	325	325	329	0.78 (0.62-0.98)	0.75 (0.63-0.90)
Epimeria loricata	28	28	-	30	30	-	7.58 (3.92-14.69)	4.74 (2.80-8.03)
Eualus fabricii	55	55	57	57	57	60	449.51 (1.15-1.7E6)	1.35 (0.57-3.20)
Eualus macilentus	97	95	97	99	98	101	3.05 (1.37-6.77)	3.87 (2.58-5.79)
Spirontocaris sp.	22	22	24	22	22	24	1.27 (0.34-4.75)	1.15 (0.54-2.45)
Spirontocaris spinus	60	60	61	61	61	64	2.55 (1.01-6.44)	0.73 (0.46-1.16)
Sabinea septemcarinata	106	105	107	109	107	110	1.03 (0.54-1.95)	1.52 (0.96-2.40)
Munidopsis curvirostra	57	57	59	59	59	62	1.86 (0.99-3.47)	2.12 (1.31-3.44)
Pagurus sp.	65	65	-	68	68	-	1.01 (0.61-1.69)	0.74 (0.43-1.27)
Cucumaria frondosa	41	41	43	43	43	45	0.52 (0.31-0.88)	0.80 (0.46-1.39)
Strongylocentrotus sp.	378	376	378	382	380	384	0.98 (0.72-1.34)	0.90 (0.71-1.15)
Brisaster fragilis	775	770	772	780	775	780	0.83 (0.65-1.05)	0.53 (0.43-0.65)
Ctenodiscus crispatus	997	993	995	1002	998	1003	0.60 (0.49-0.73)	0.49 (0.41-0.59)
Pteraster militaris	60	60	62	62	62	65	0.95 (0.49-1.84)	1.55 (0.80-3.00)
Ceramaster granularis	98	96	98	101	99	102	1.09 (0.64-1.87)	1.02 (0.55-1.87)
Hippasteria phrygiana	123	123	125	128	127	132	1.30 (0.89-1.91)	1.12 (0.77-1.65)
Pseudarchaster parelii	57	57	-	59	59	-	0.44 (0.28-0.68)	0.42 (0.25-0.72)
Crossaster papposus	84	83	85	87	86	89	1.04 (0.59-1.84)	0.57 (0.23-1.41)
Henricia sp.	141	141	143	145	145	149	0.87 (0.63-1.20)	0.66 (0.48-0.93)
Leptasterias (Hexasterias) polaris	40	39	41	42	41	44	1.21 (0.50-2.95)	1.35 (0.52-3.51)
Leptasterias groenlandica	55	54	56	57	56	59	1.00 (0.48-2.08)	0.74 (0.33-1.66)
Psilaster andromeda	163	162	164	166	165	168	0.39 (0.25-0.62)	0.22 (0.17-0.30)
Gorgonocephalus sp.	135	133	135	137	136	140	0.73 (0.46-1.16)	0.74 (0.49-1.11)
Ophiura sarsii	705	703	705	710	708	712	0.84 (0.63-1.12)	0.50 (0.39-0.65)
Ophiacantha bidentata	134	133	135	138	137	140	2.41 (1.45-4.00)	1.90 (1.12-3.20)
Ophiopholis aculeata	314	312	313	318	316	319	1.18 (0.83-1.68)	1.03 (0.80-1.32)
Ophioscolex glacialis	82	81	83	85	84	87	1.73 (0.97-3.07)	1.59 (0.95-2.65)
Ascidia sp.	422	420	422	427	425	429	0.97 (0.76-1.25)	1.28 (1.05-1.56)
Eudistoma vitreum	63	61	63	65	63	66	1.33 (0.66-2.66)	1.30 (0.64-2.64)
Boltenia ovifera	66	65	67	68	67	70	0.86 (0.47-1.56)	1.02 (0.55-1.89)

8. FIGURES

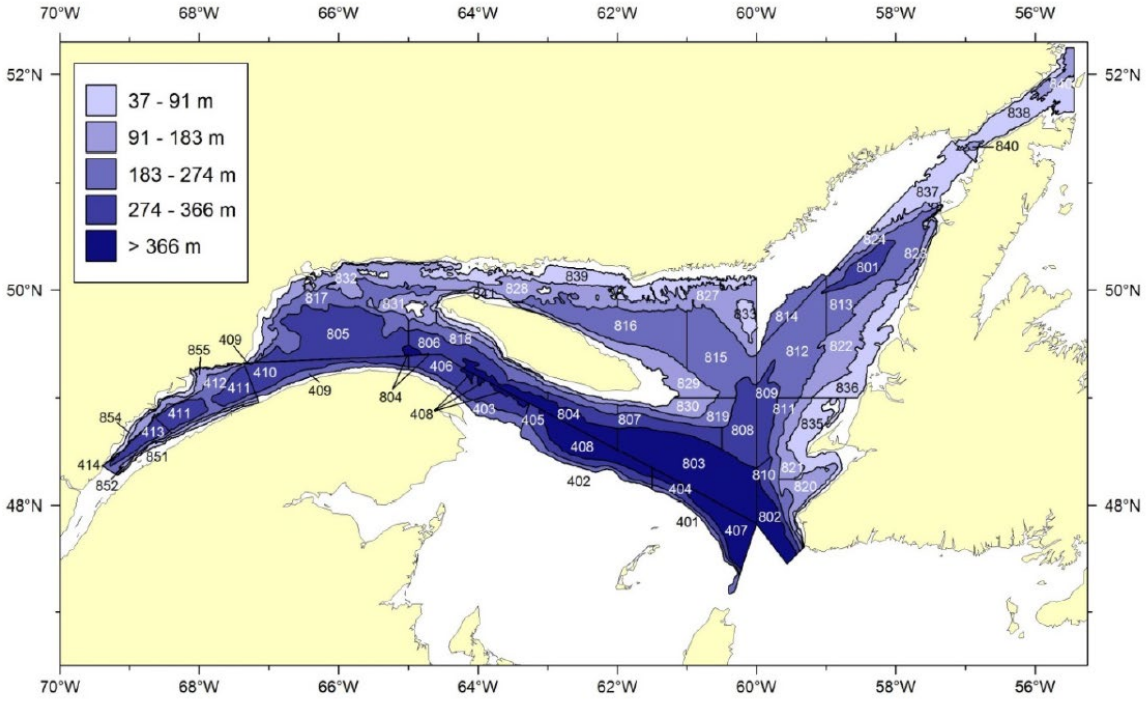

Figure 1. Stratification scheme for the Estuary and northern Gulf of St. Lawrence multi-species bottom-trawl survey.

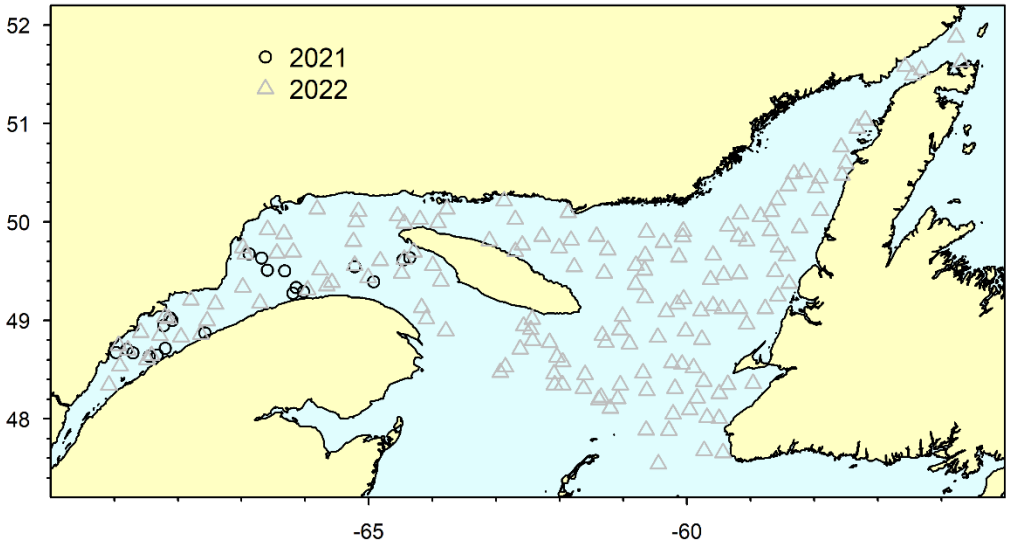

Figure 2. Location of comparative fishing set pairs fished in 2021 and in 2022.

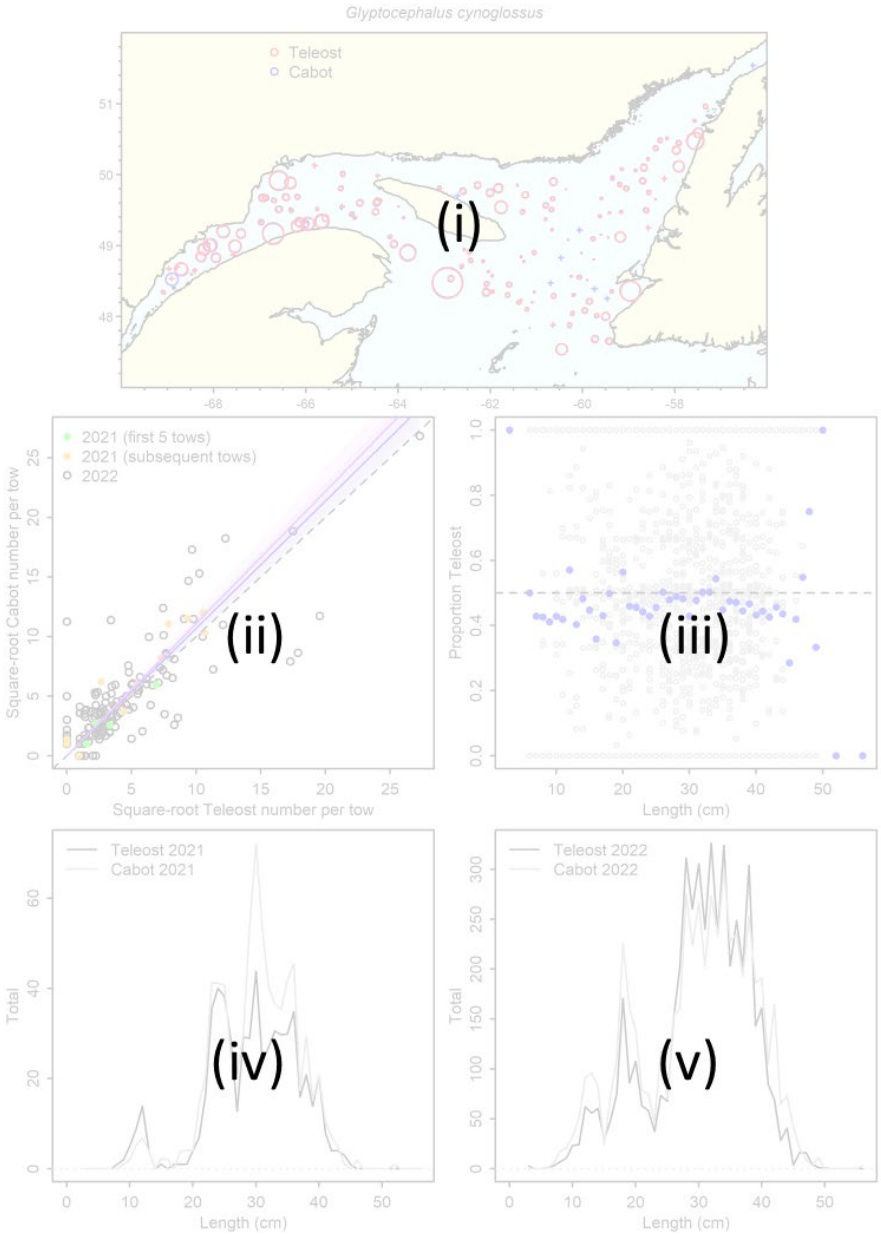

Figure 3.Interpretation for the first of three sets of figures presenting the data and results for taxa for which length-disaggregated analyses were undertaken. (i) Presents a map of catches by the CCGS Teleost (red circles) and by the CCGS John Cabot (blue circles) in comparative fishing sets, where circle size is proportional to the square root of the number caught and nil catches are indicated by +. (ii) Biplot of the square-root of CCGS John Cabot catch numbers against the square-root of CCGS Teleost catch numbers, where the blue line and shaded interval show the estimated conversion and approximate 95%CI from the best length-aggregated model, the purple line shows the estimated length-independent conversion and approximate 95%CI from the best length-based model, and where the first five sets in 2021 and the remaining sets in 2021 are indicate using filled symbols. (iii) Plot of the empirical proportion of total catch in a pair made by the CCGS Teleost as a function of length for each set pair (grey dots) and averaged across set pairs in each length interval (blue dots). (iv) Total length frequencies for catches made by the CCGS Teleost (black line) and by the CCGS John Cabot (grey line) in 2021. (v) Same as (iv) except for 2022.

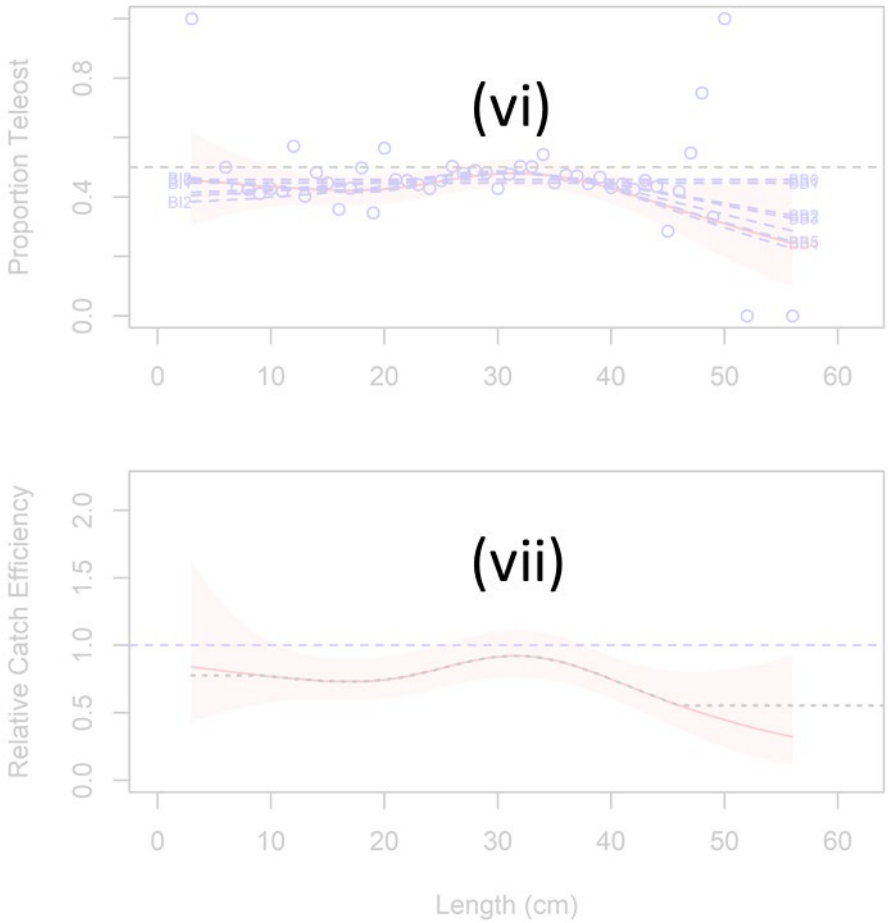

Figure 4. Interpretation for the second of three sets of figures presenting the data and results for taxa for which length-disaggregated analyses were undertaken. (vi) Estimated length-specific catch proportion functions, $logit(p_{Ai}(l))$, for each converged model, with the selected model plotted using a red line along with its approximate 95%CI (shaded area), as well as the length class-specific mean empirical proportion of total catch in a pair made by the CCGS Teleost (blue dots). (vii) Estimated relative catch efficiency (conversion factor) function from the best model (with 95% CI). The horizontal dashed blue line indicates equivalent efficiency between vessels and the dotted black line indicates the relative catch efficiency function that assumes a constant efficiency at small and large sizes.

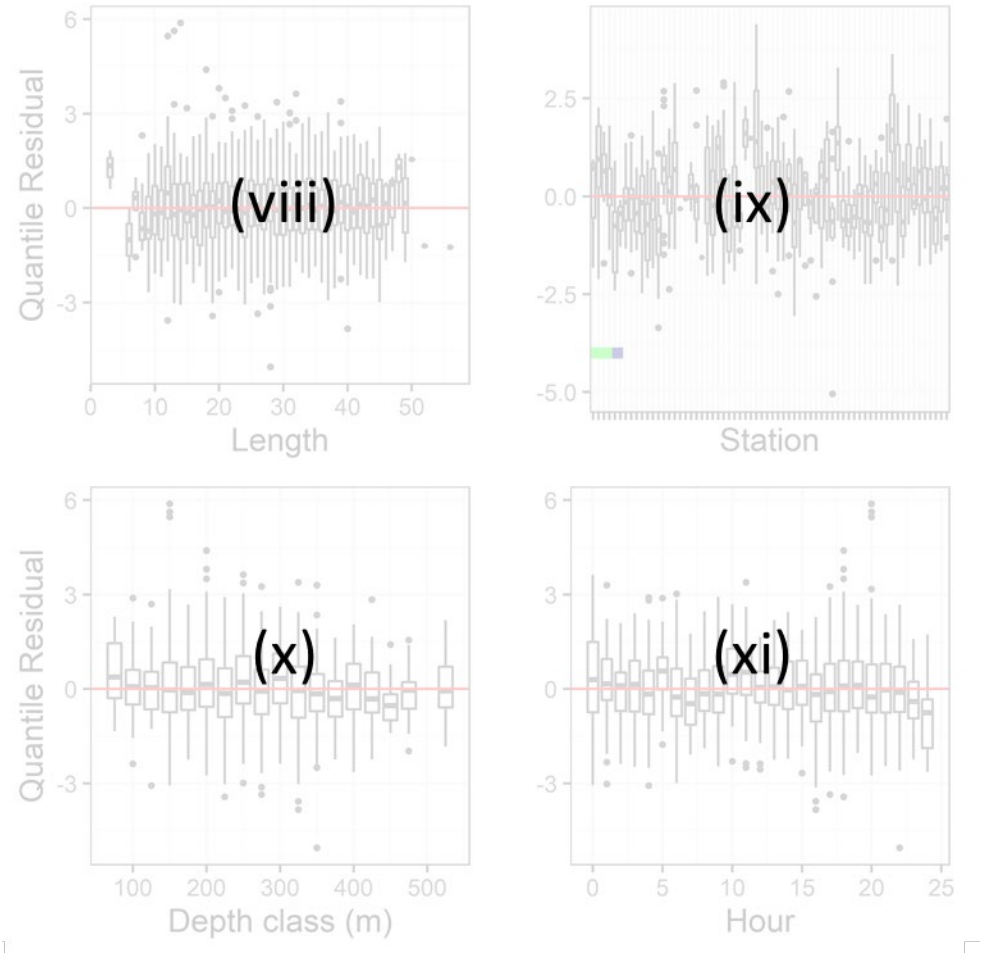

Figure 5. Interpretation for the third of three sets of figures presenting the data and results for taxa for which length-disaggregated analyses were undertaken. Boxplot of normalized quantile residuals from the selected model as a function of (viii) length, (ix) station, (x) depth class, and (xi) hour. In (ix), residuals associated with the first 5 pairs fished in 2021 are indicated by a green line, and those associated with pairs in which the vessels sequentially fished the same track are indicated by a colored line: CCGS John Cabot fished first (dark blue), CCGS Teleost fished first (light blue).

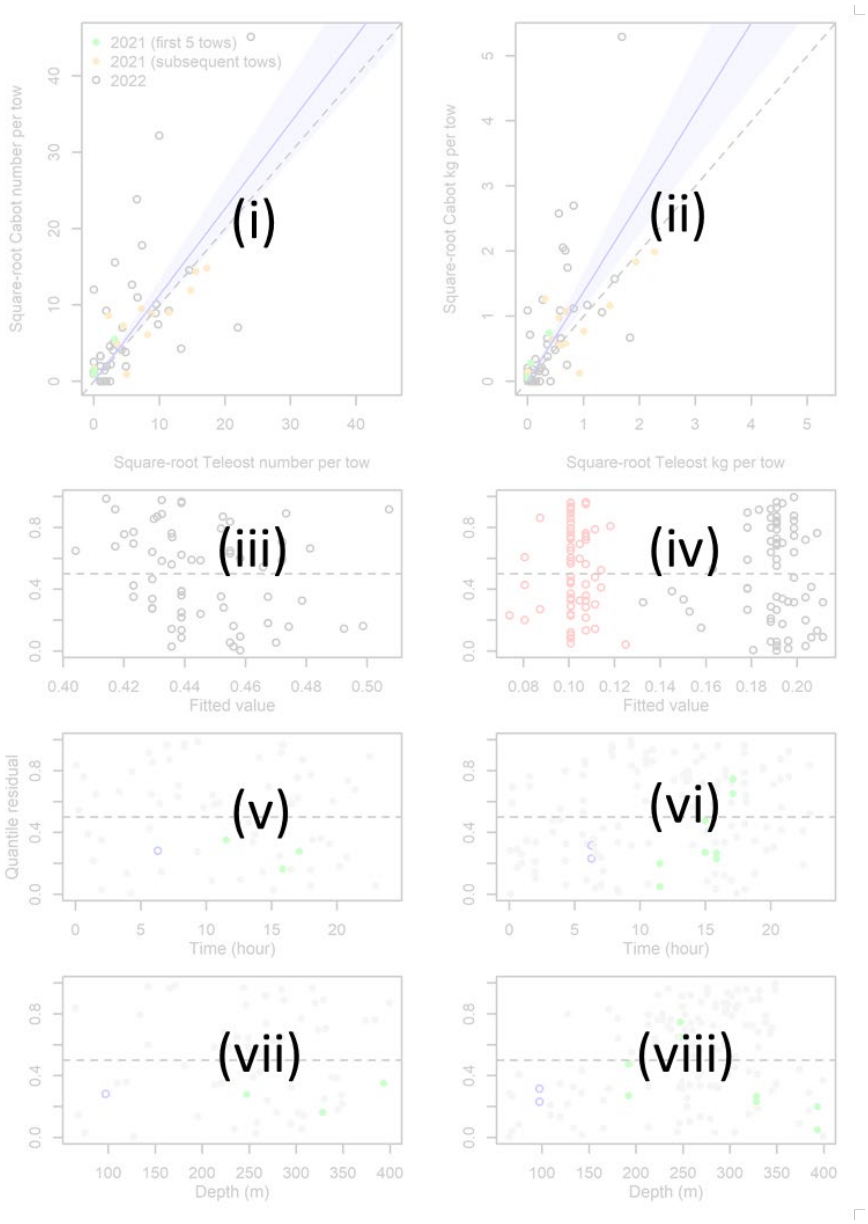

Figure 6.Interpretation for the figures presenting the data and results for taxa for which size-aggregated analyses were undertaken. (i) Biplot of the square-root of CCGS John Cabot catch numbers against the square-root of CCGS Teleost catch numbers, where the blue line and shaded interval show the estimated conversion and approximate 95%CI from the best size-aggregated model, and where the first five sets in 2021 and the remaining sets in 2021 are indicated using filled symbols. (ii) As in (i), except for catch weights. Quantile residuals for the selected model from the analysis of catch numbers are plotted as a function of (iii) fitted values, and the (v) time and (vii) depth of the paired set, where values are coloured according to the same scheme as in panel (i). Similarly, quantile residuals for the selected model from the analysis of catch weights are plotted as a function of (iv) fitted values, with values for the CCGS Teleost plotted with red circles and those for the CCGS John Cabot in black, and the (vi) time and (viii) depth of the paired set, again where values are coloured according to the same scheme as in panel (i).

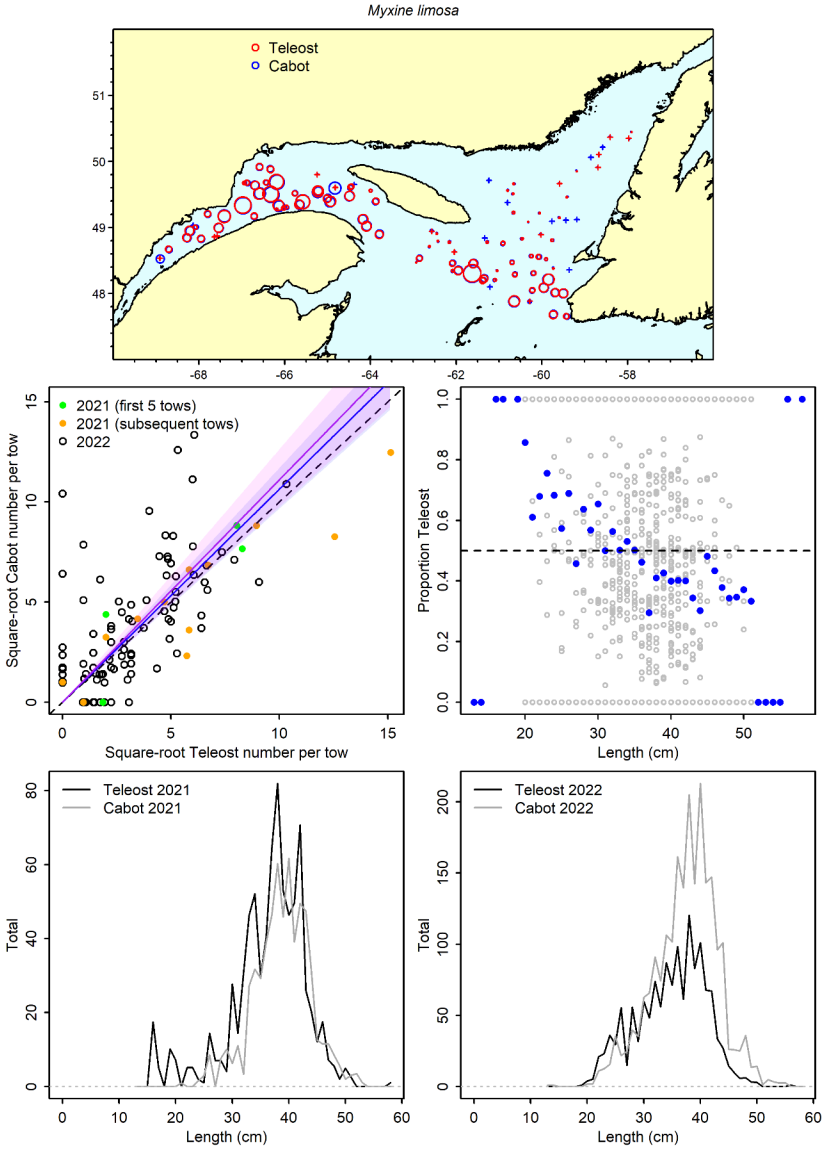

Figure 7a. Visualisation of comparative fishing data and size-aggregated model predictions for Myxine limosa.

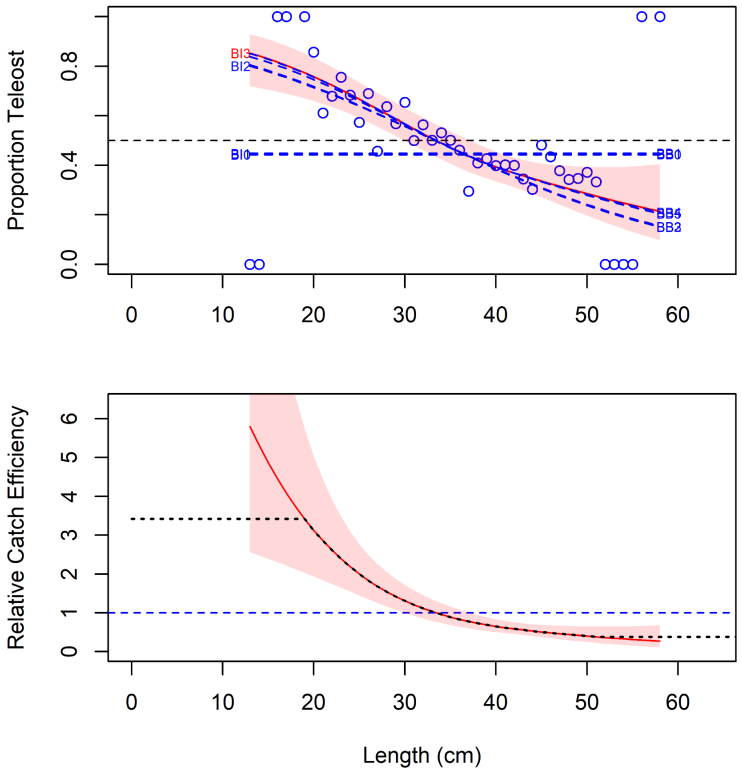

Figure 7b.Model fits and the selected length-based calibration for Myxine limosa.

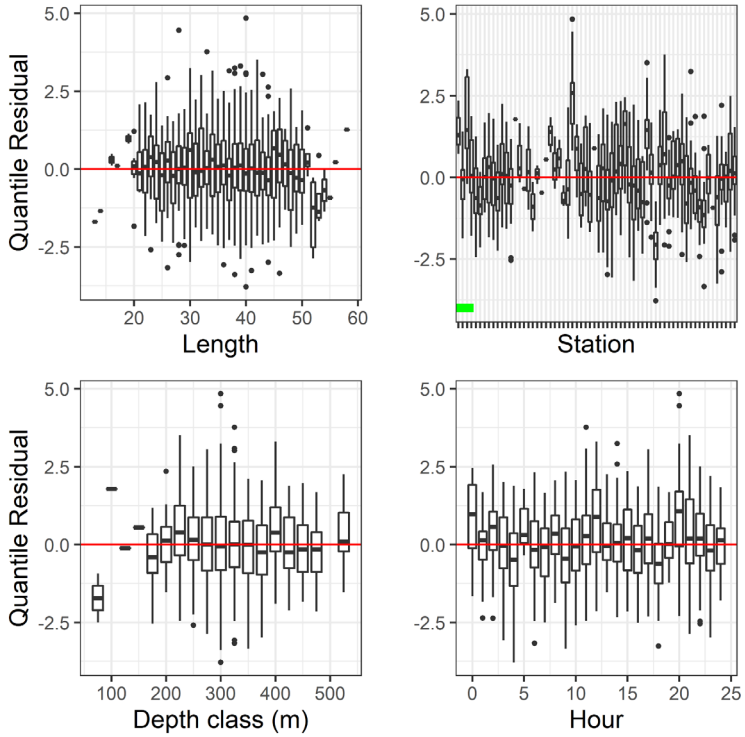

Figure 7c.Normalized quantile residuals for the selected model for Myxine limosa.

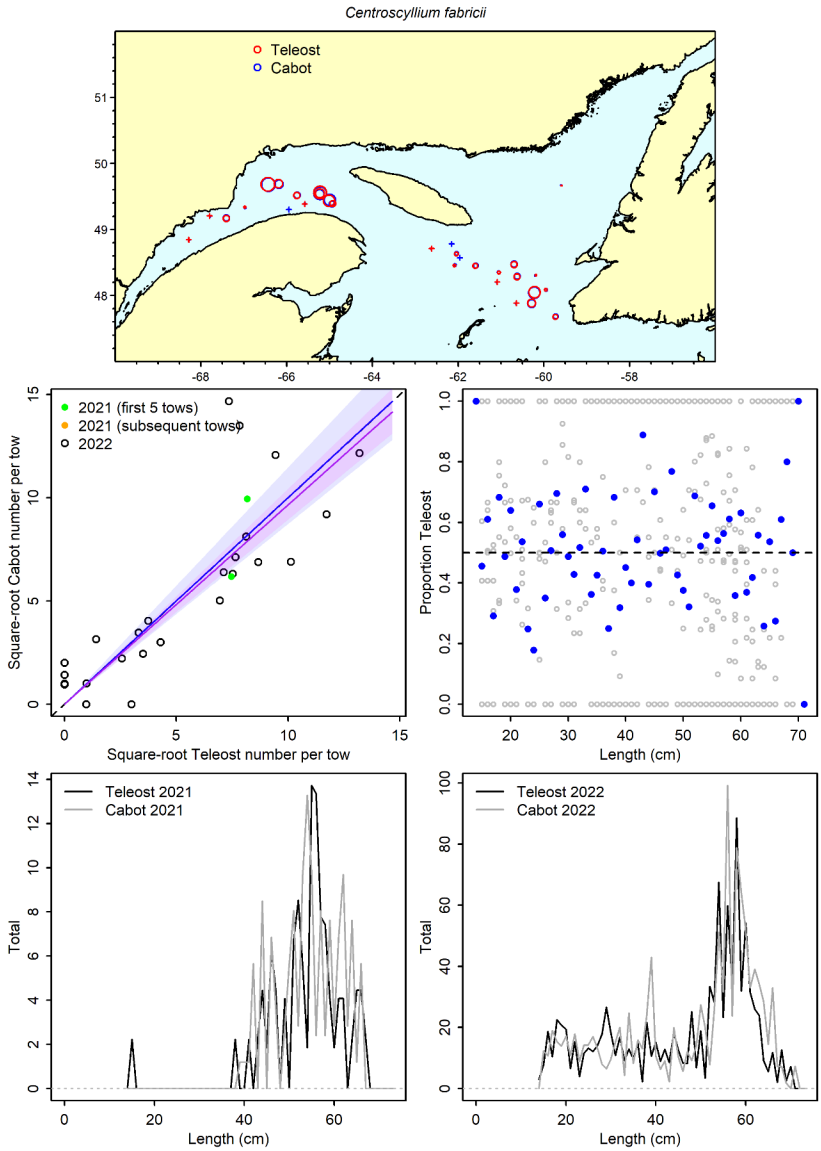

Figure 8a. Visualisation of comparative fishing data and size-aggregated model predictions for Centroscyllium fabricii.

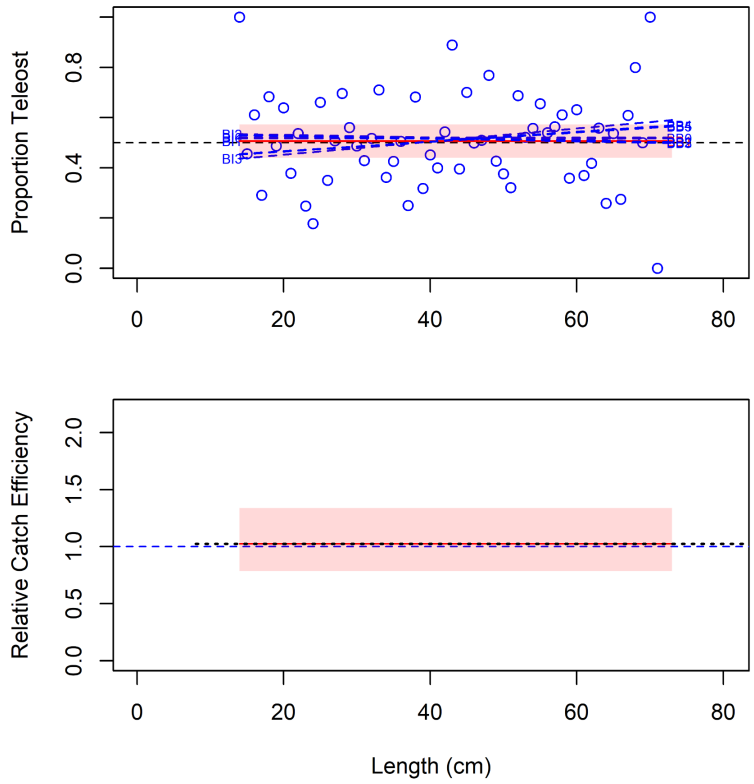

Figure 8b.Model fits and the selected length-based calibration for Centroscyllium fabricii.

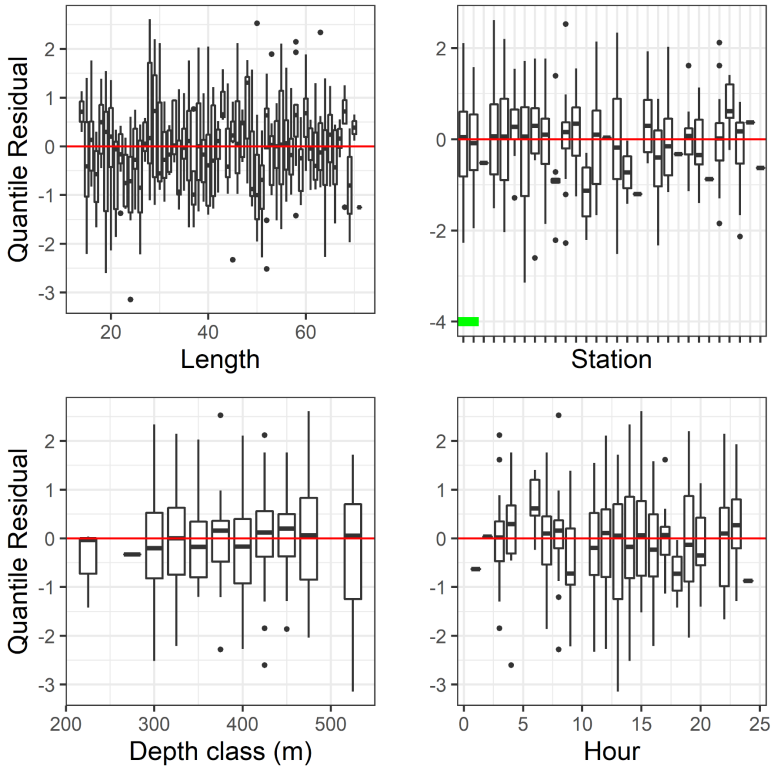

Figure 8c.Normalized quantile residuals for the selected model for Centroscyllium fabricii.

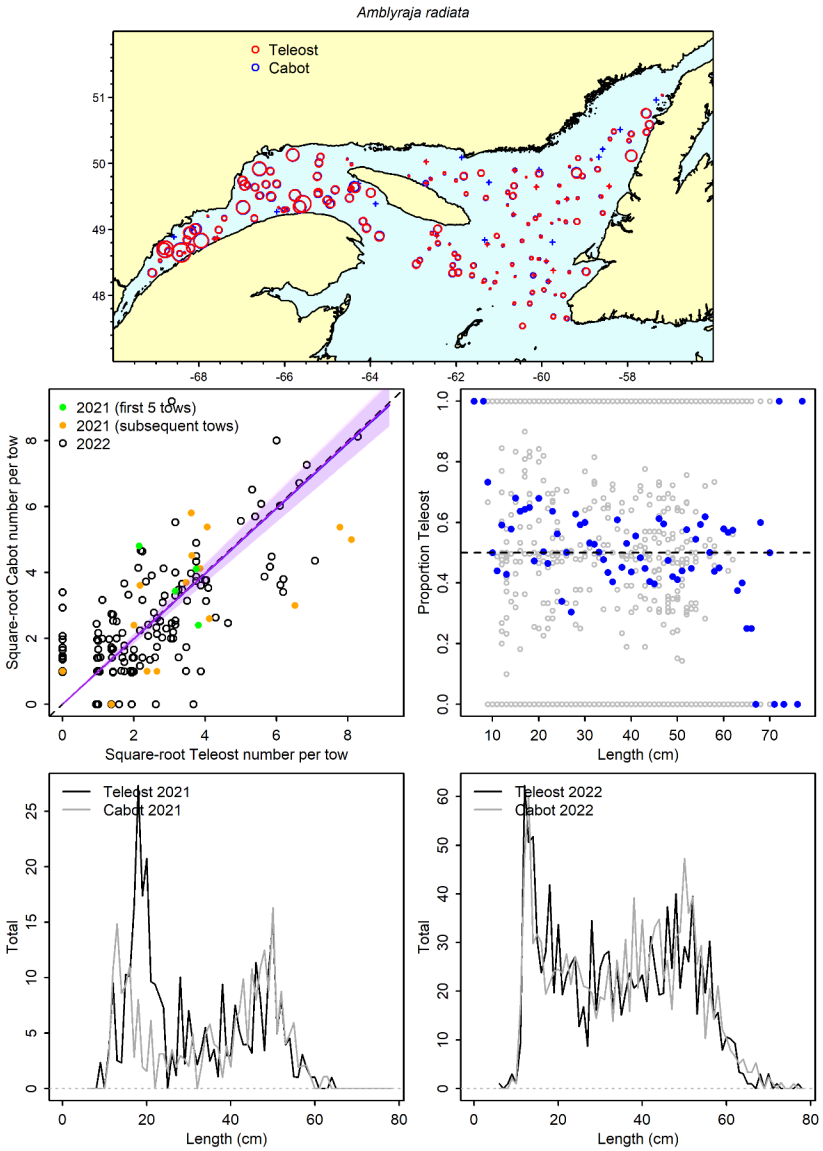

Figure 9a. Visualisation of comparative fishing data and size-aggregated model predictions for Amblyraja radiata.

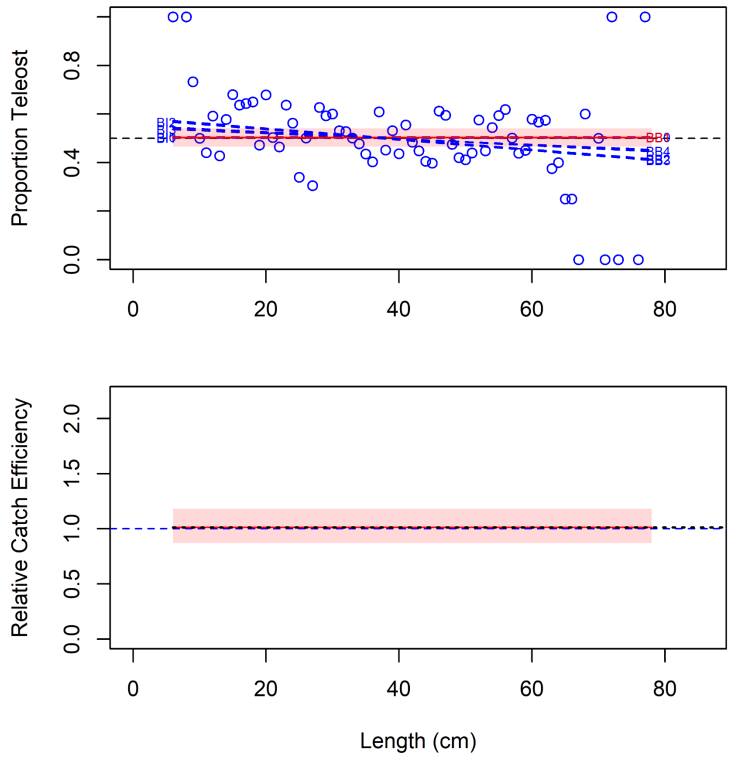

Figure 9b.Model fits and the selected length-based calibration for Amblyraja radiata.

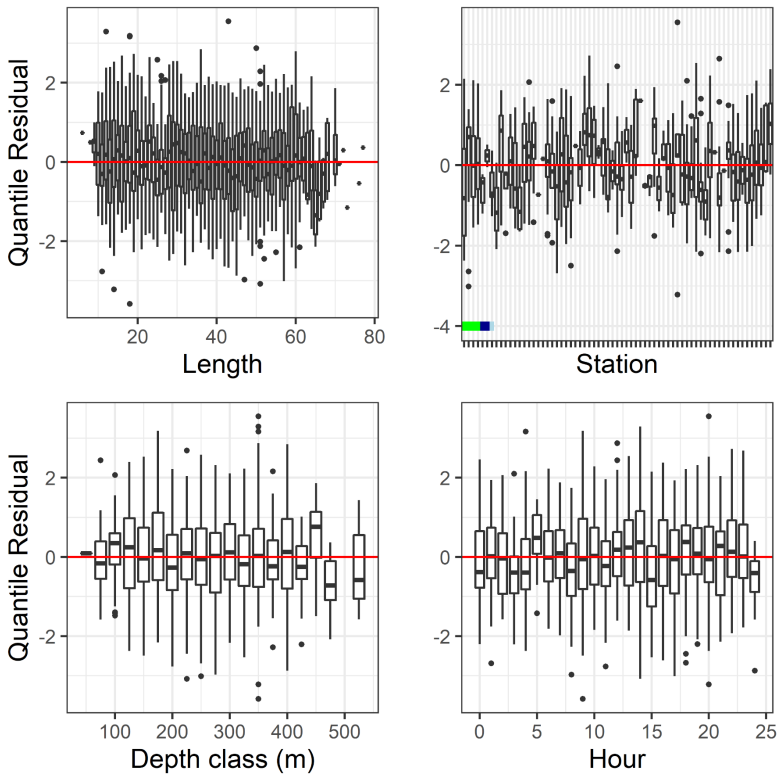

Figure 9c.Normalized quantile residuals for the selected model for Amblyraja radiata.

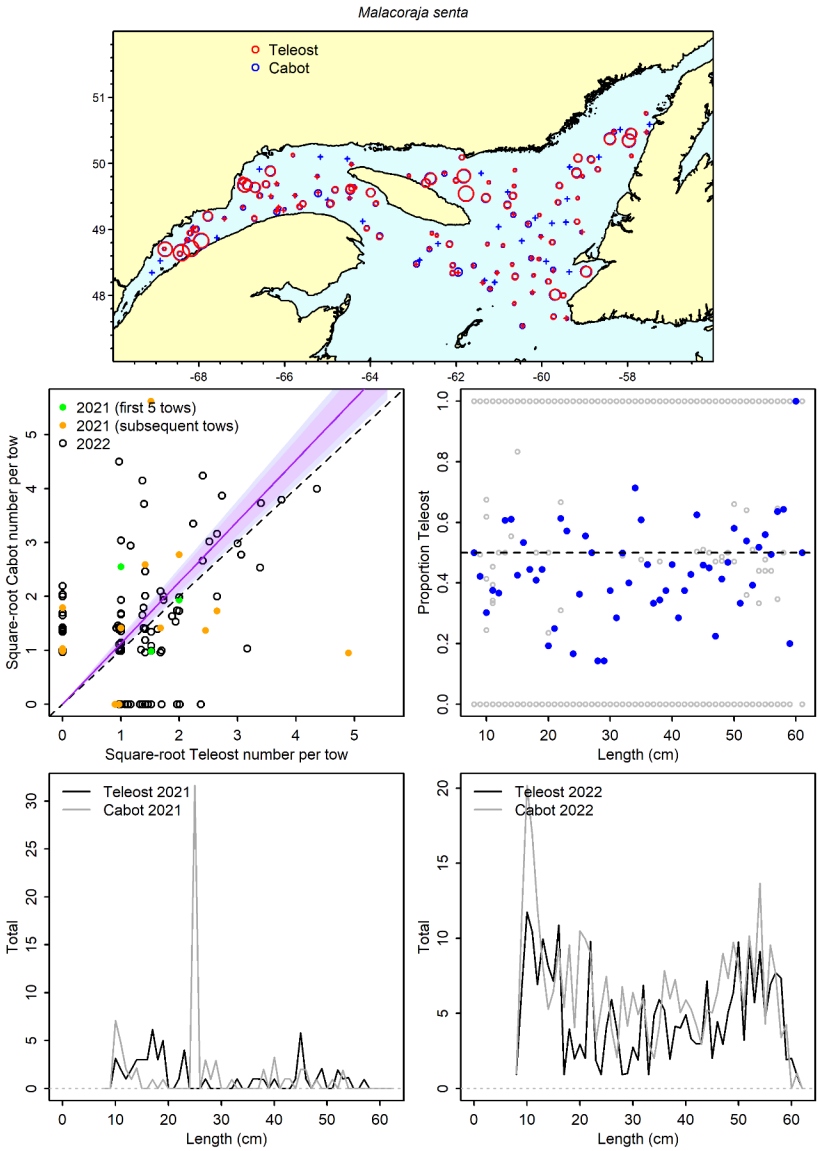

Figure 10a. Visualisation of comparative fishing data and size-aggregated model predictions for Malacoraja senta.

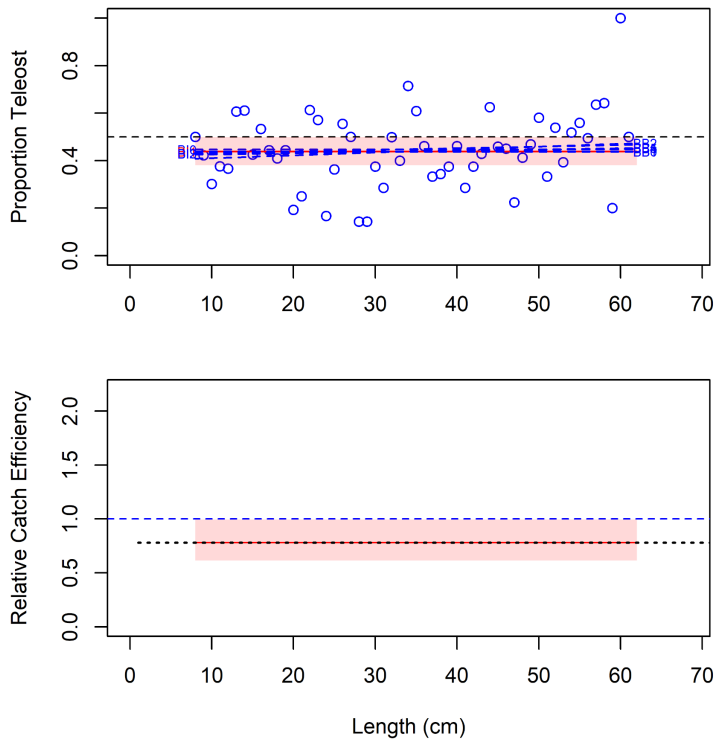

Figure 10b.Model fits and the selected length-based calibration for Malacoraja senta.

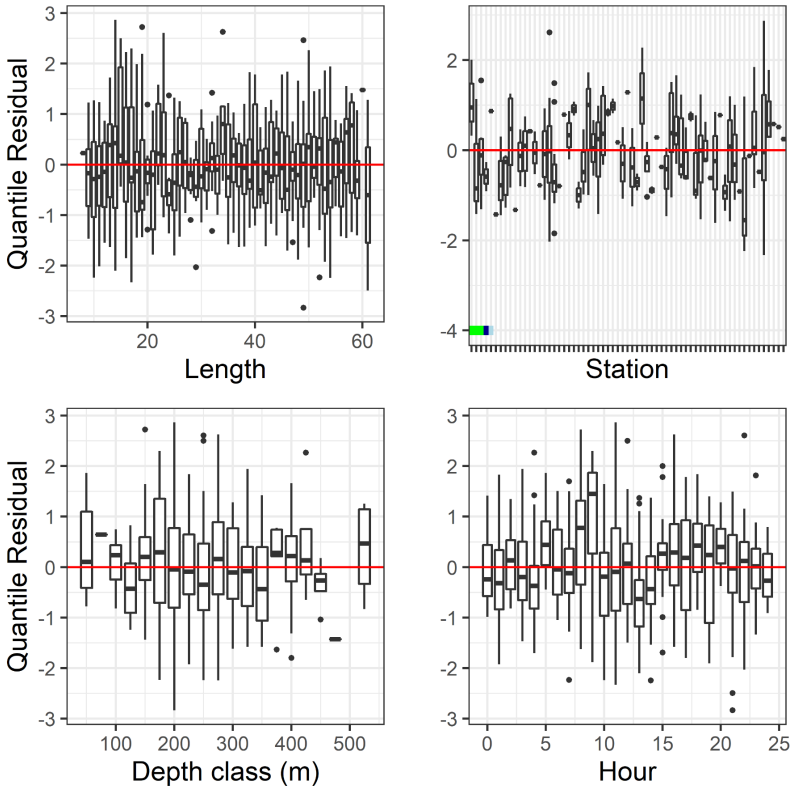

Figure 10c.Normalized quantile residuals for the selected model for Malacoraja senta.

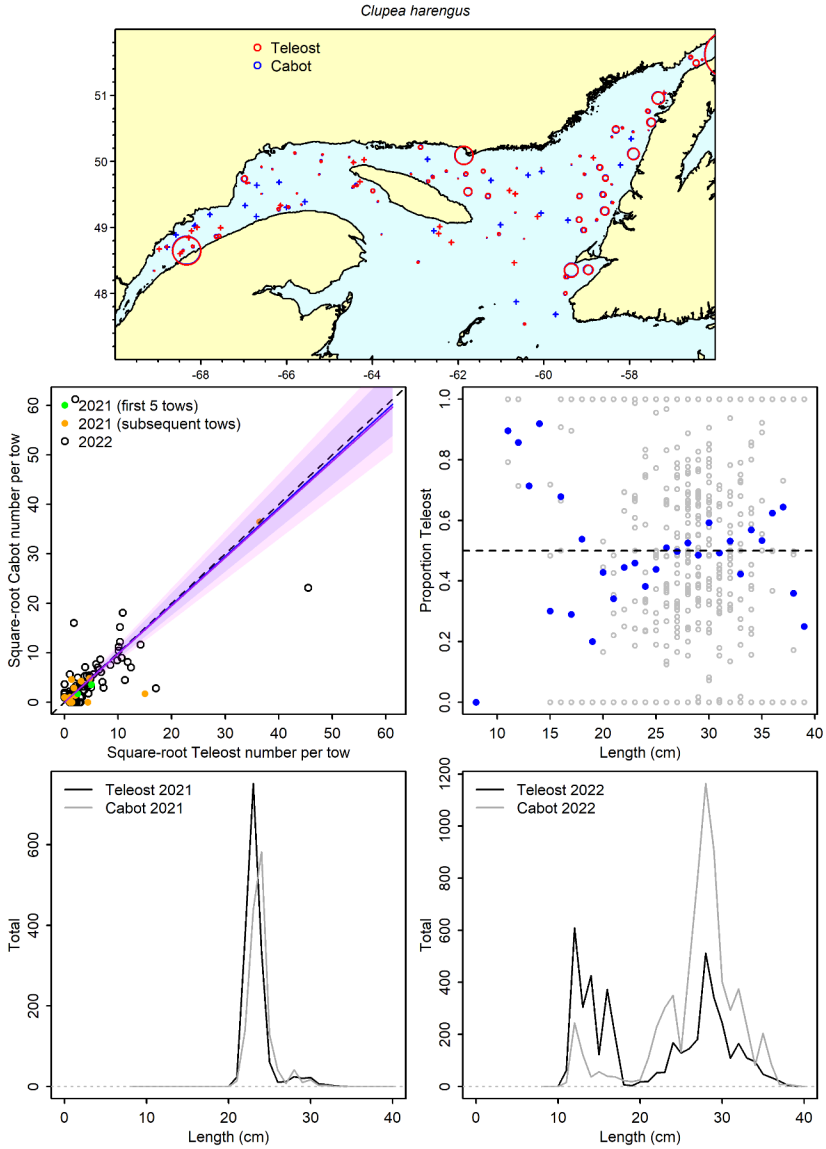

Figure 11a.Visualisation of comparative fishing data and size-aggregated model predictions for Clupea harengus.

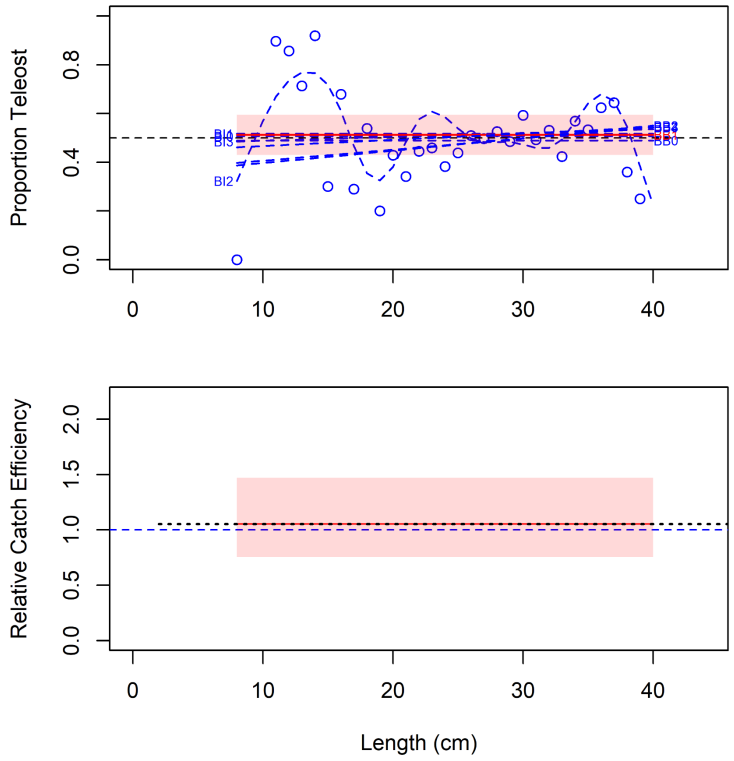

Figure 11b.Model fits and the selected length-based calibration for Clupea harengus.

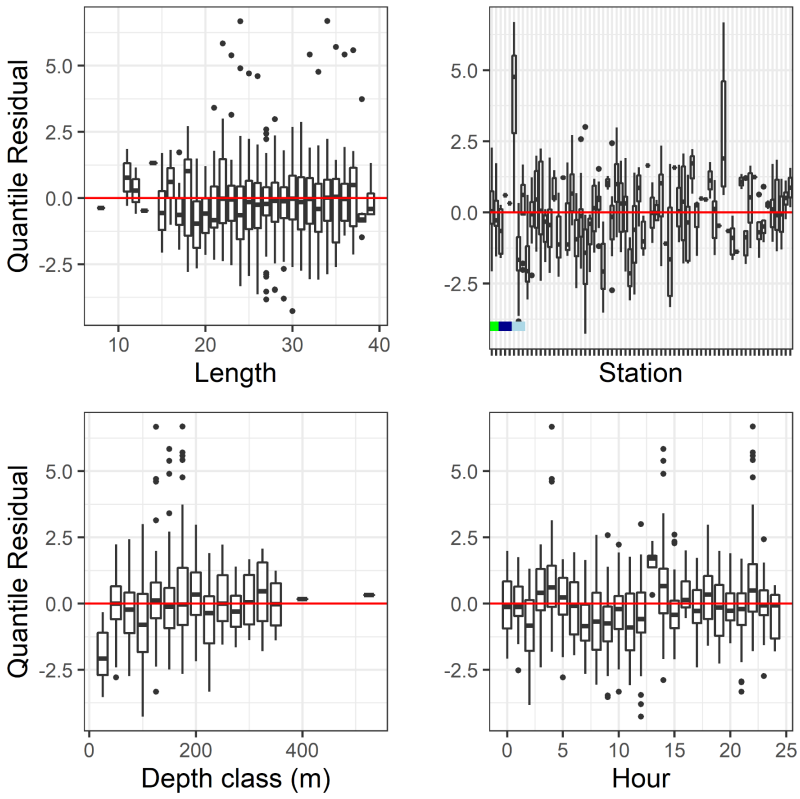

Figure 11c.Normalized quantile residuals for the selected model for Clupea harengus.

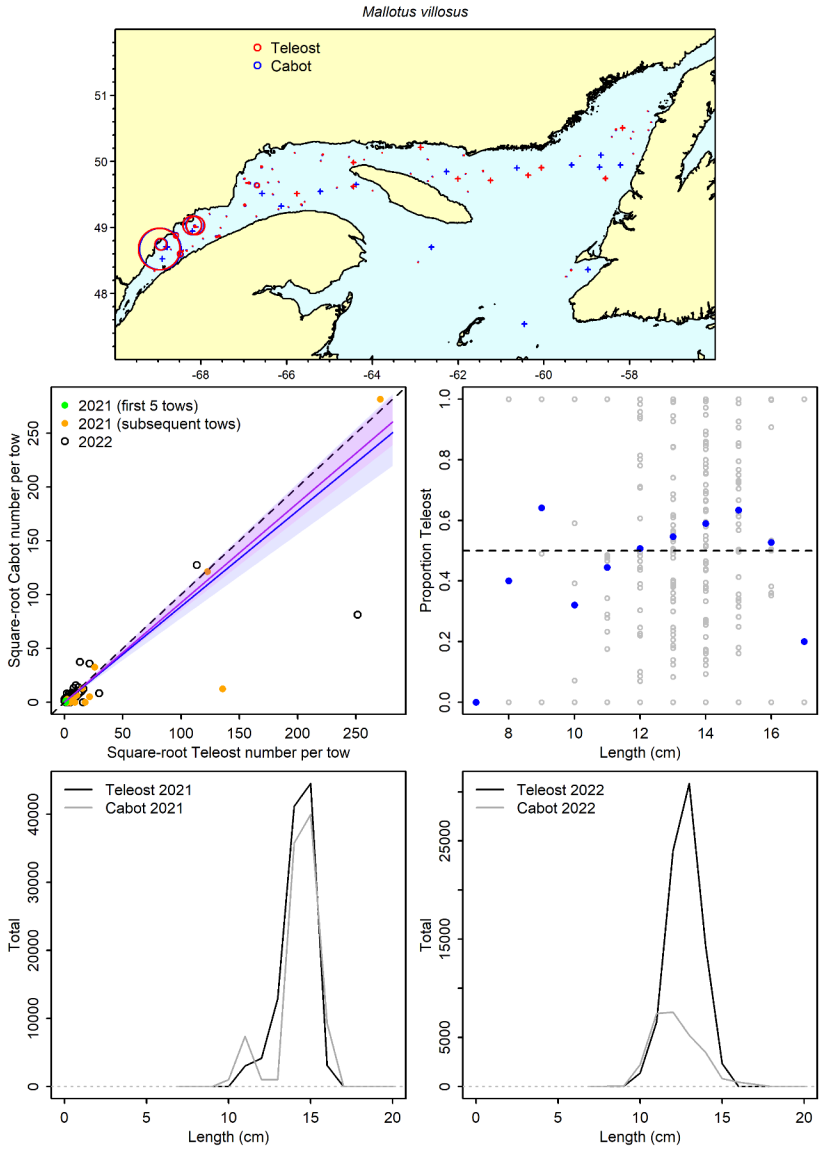

Figure 12a. Visualisation of comparative fishing data and size-aggregated model predictions for Mallotus villosus.

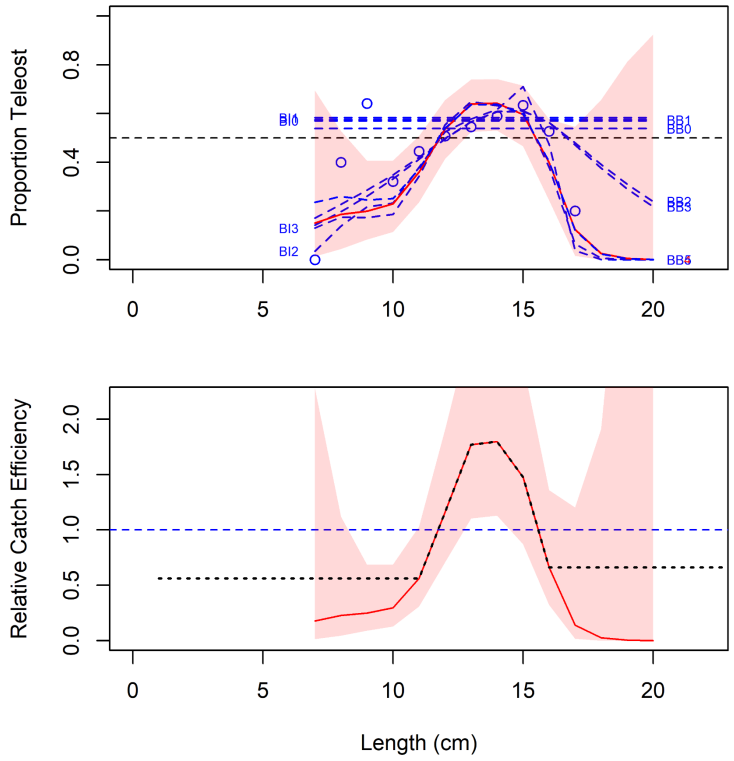

Figure 12b.Model fits and the selected length-based calibration for Mallotus villosus.

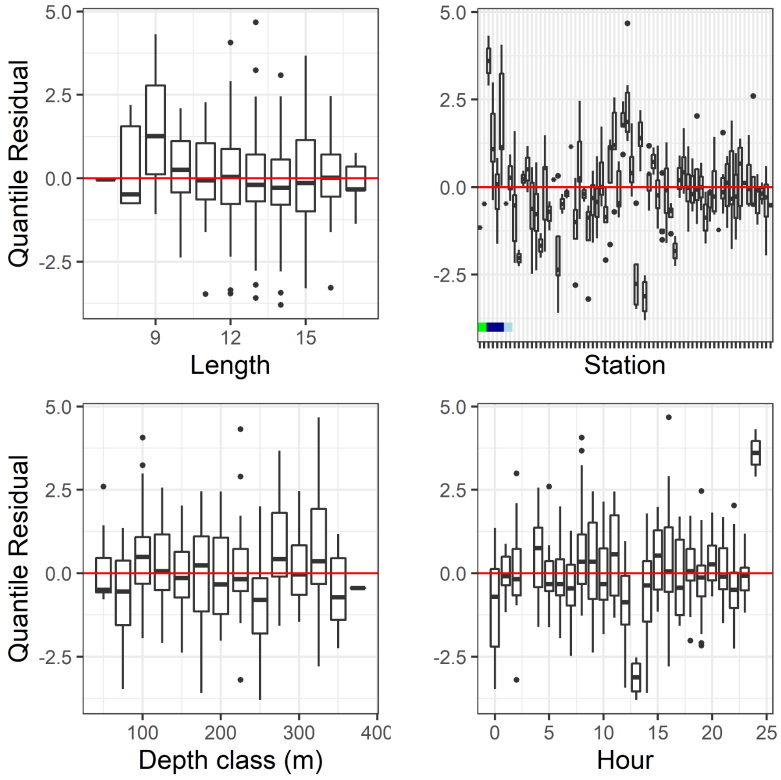

Figure 12c.Normalized quantile residuals for the selected model for Mallotus villosus.

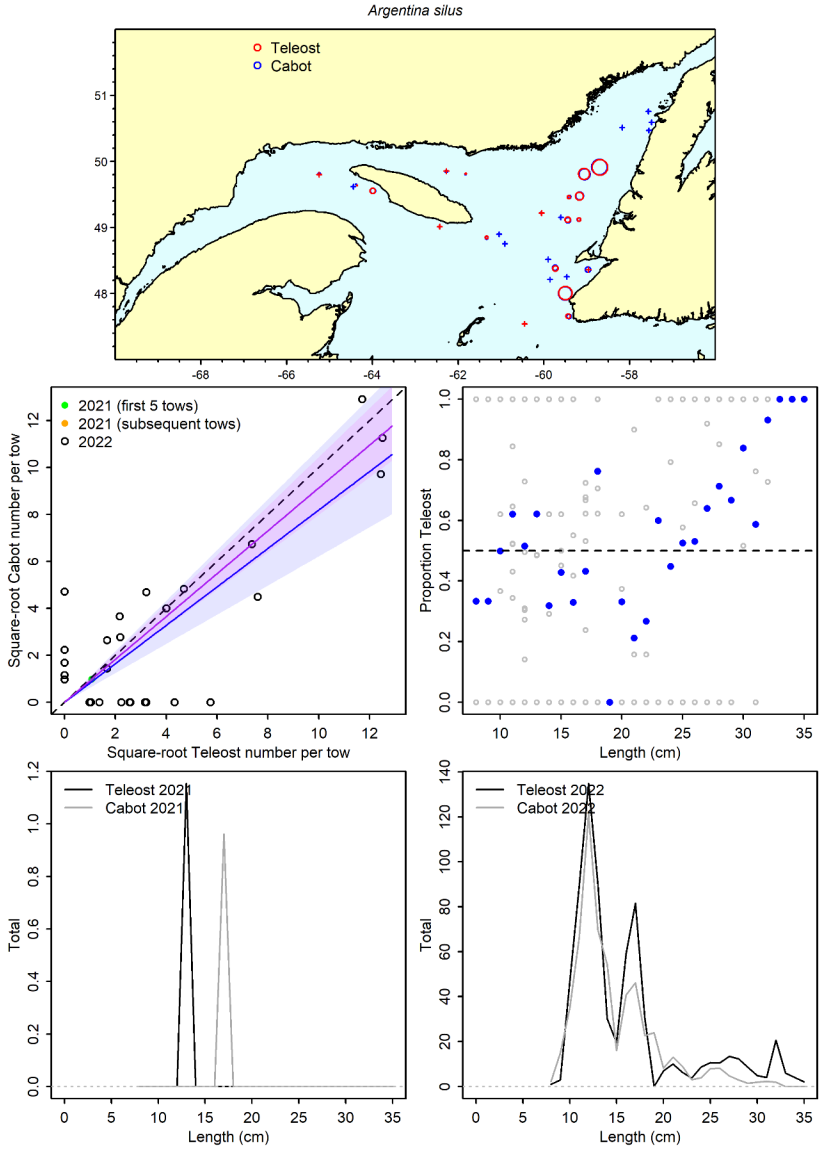

Figure 13a. Visualisation of comparative fishing data and size-aggregated model predictions for Argentina silus.

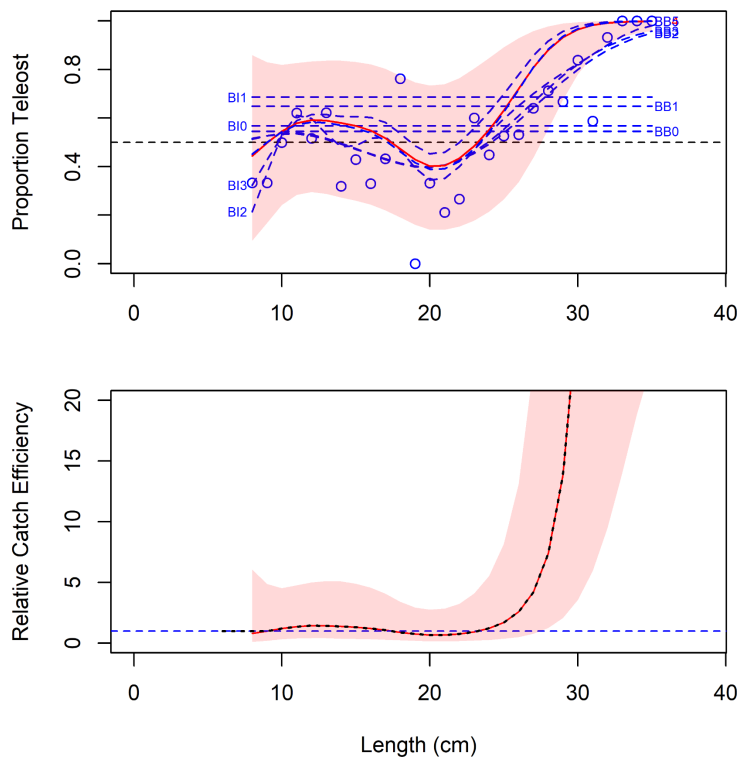

Figure 13b.Model fits and the selected length-based calibration for Argentina silus.

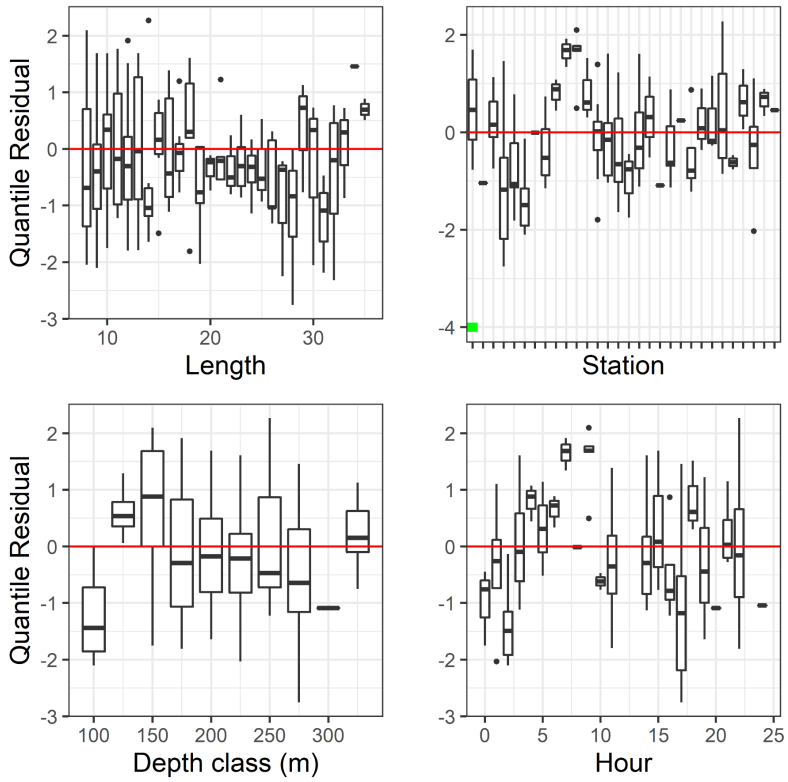

Figure 13c.Normalized quantile residuals for the selected model for Argentina silus.

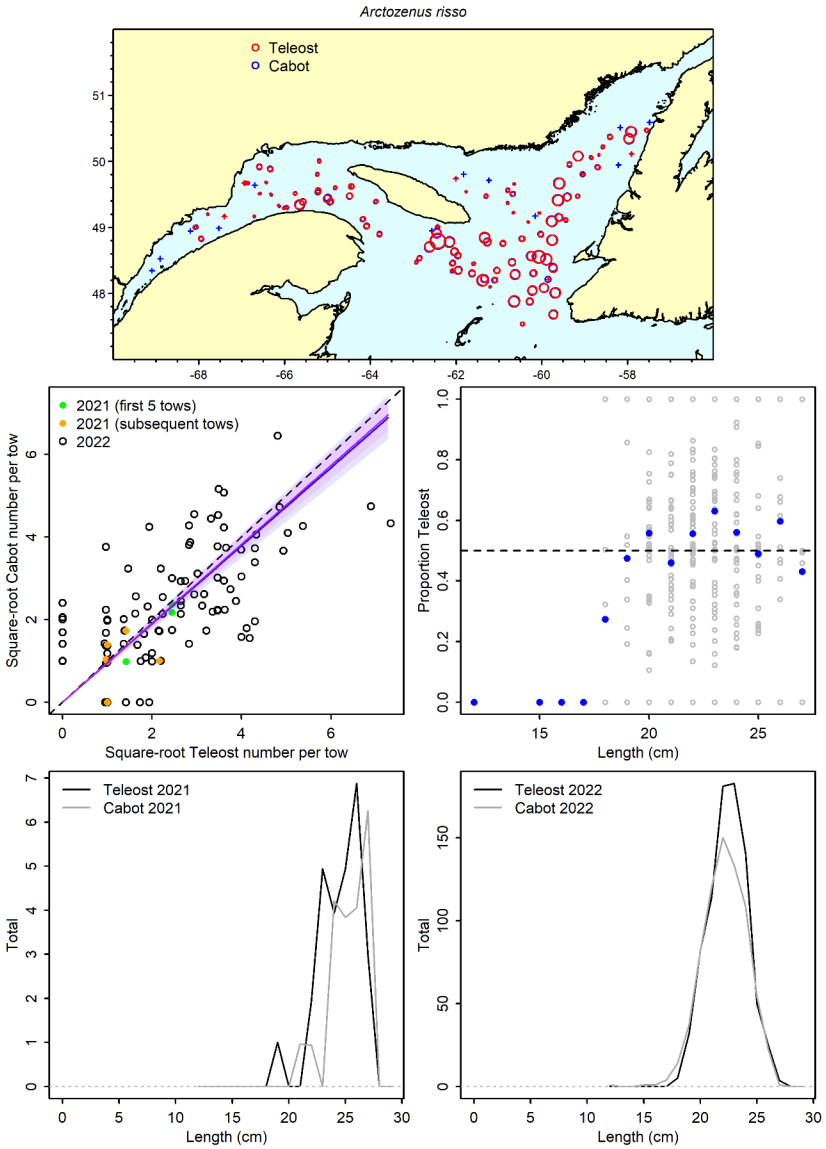

Figure 14a. Visualisation of comparative fishing data and size-aggregated model predictions for Arctozenus risso.

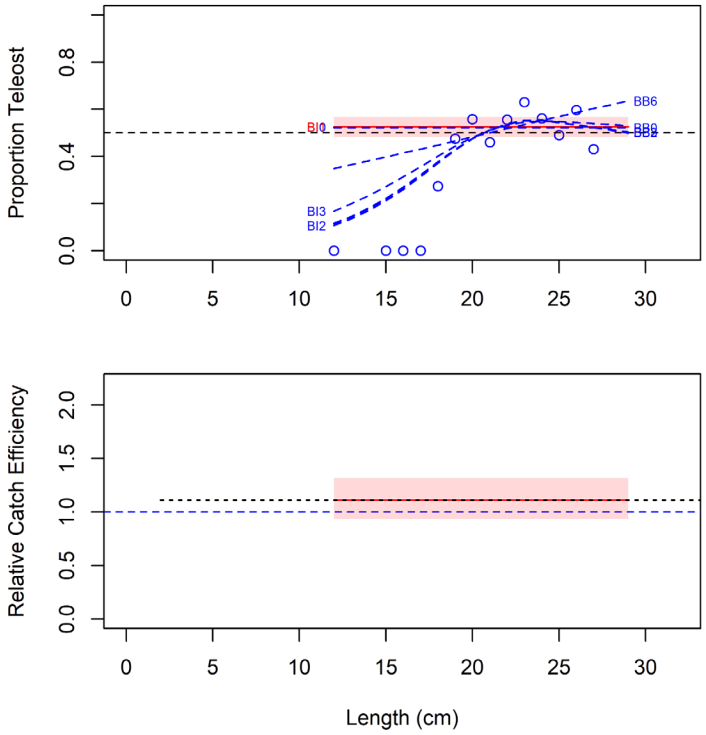

Figure 14b.Model fits and the selected length-based calibration for Arctozenus risso.

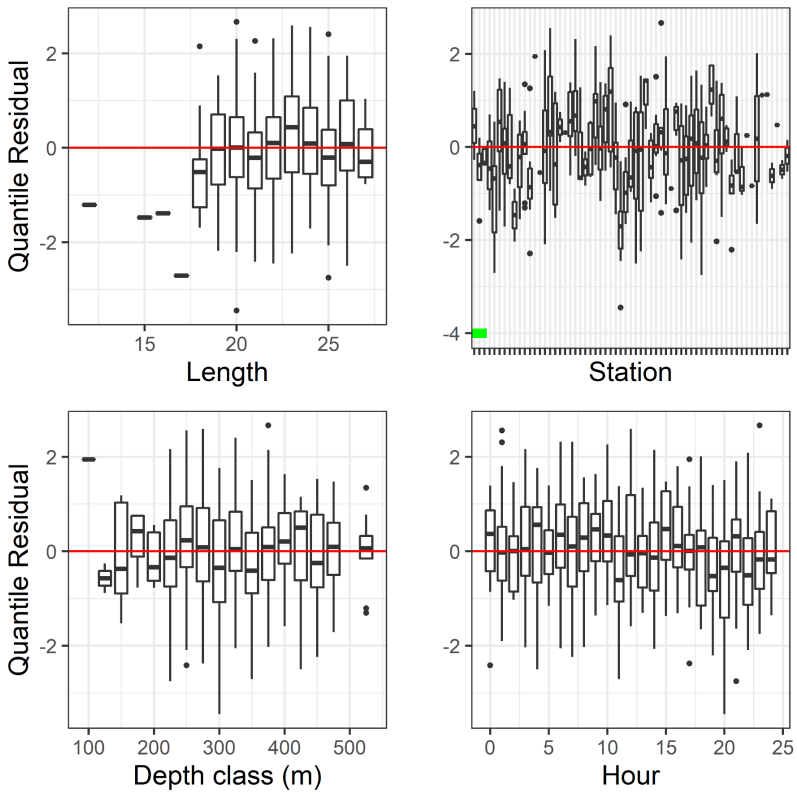

Figure 14c.Normalized quantile residuals for the selected model for Arctozenus risso.

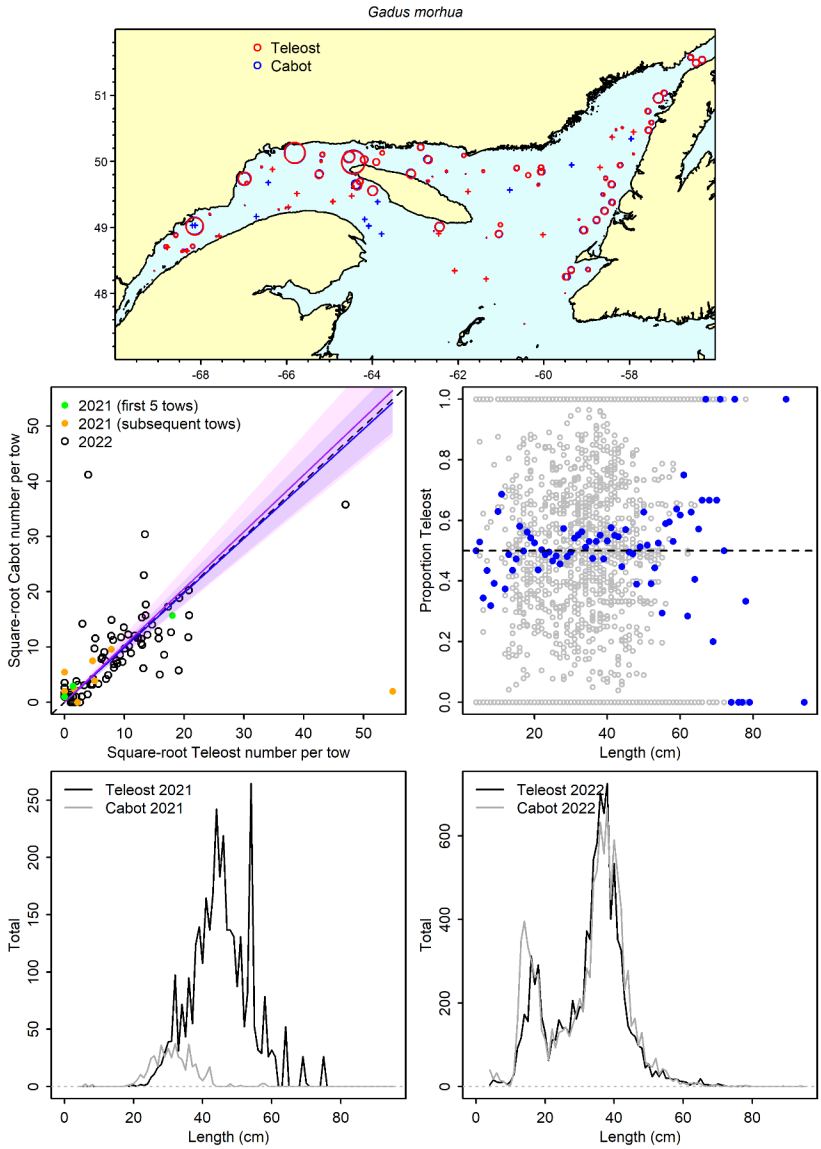

Figure 15a. Visualisation of comparative fishing data and size-aggregated model predictions for Gadus morhua.

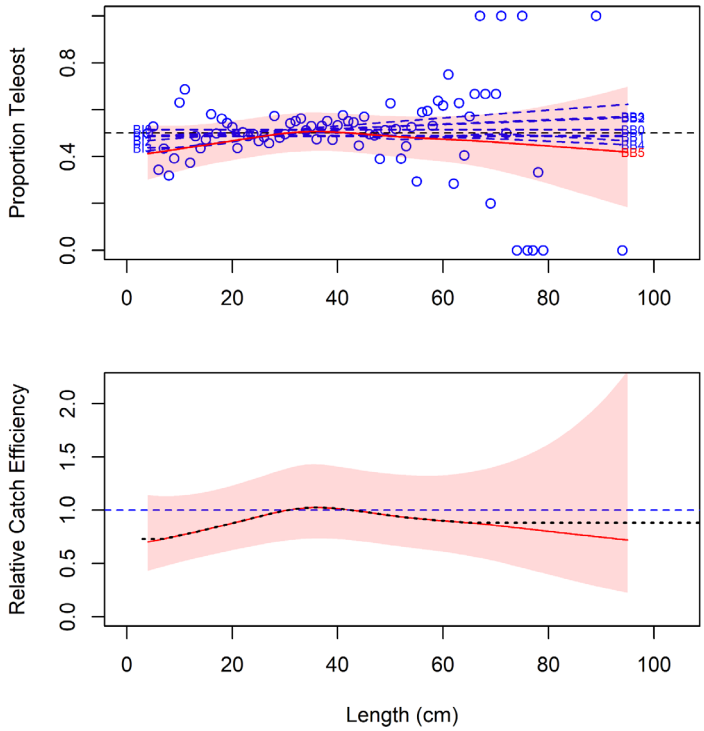

Figure 15b.Model fits and the selected length-based calibration for Gadus morhua.

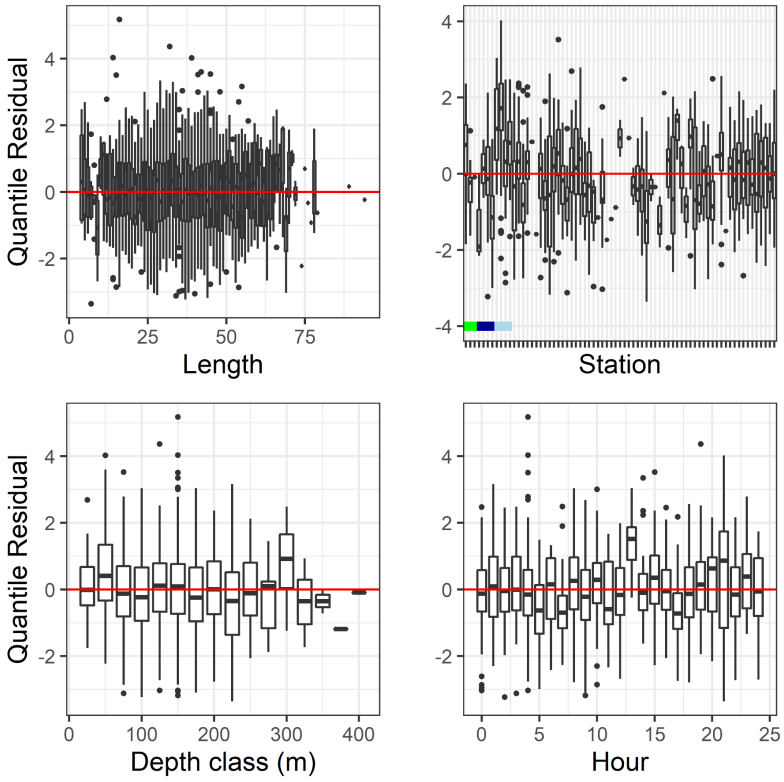

Figure 15c.Normalized quantile residuals for the selected model for Gadus morhua.

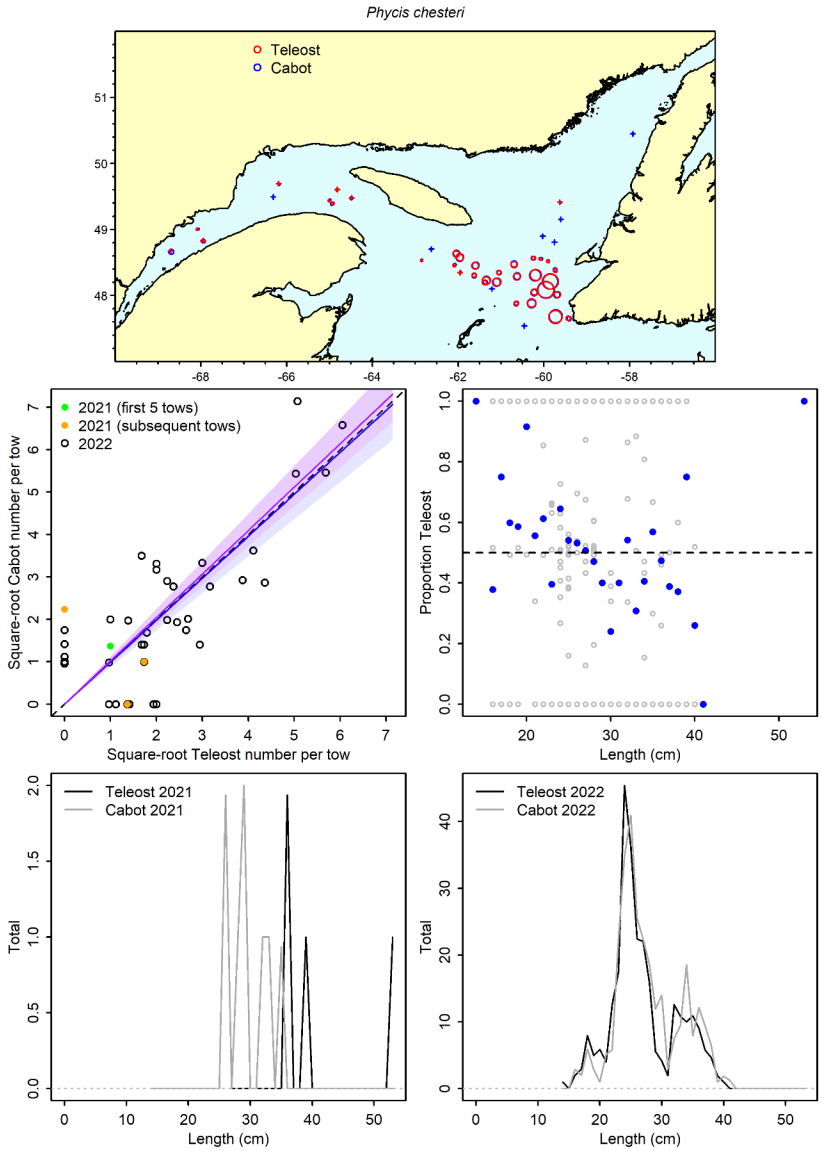

Figure 16a. Visualisation of comparative fishing data and size-aggregated model predictions for Phycis chesteri.

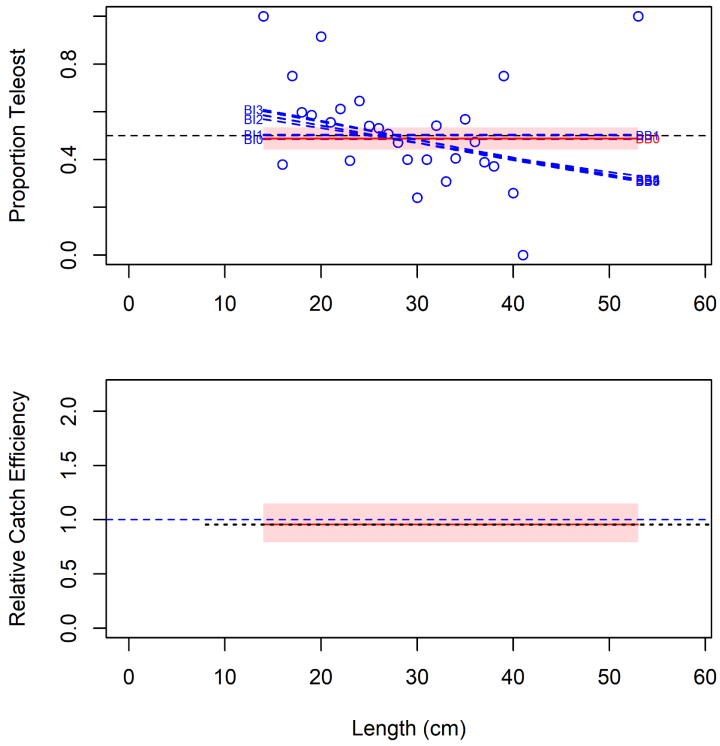

Figure 16b.Model fits and the selected length-based calibration for Phycis chesteri.

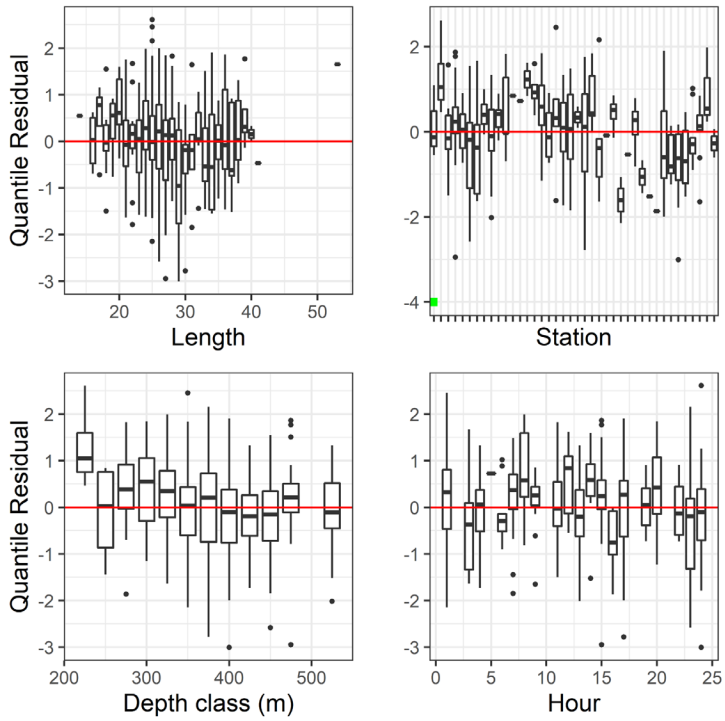

Figure 16c.Normalized quantile residuals for the selected model for Phycis chesteri.

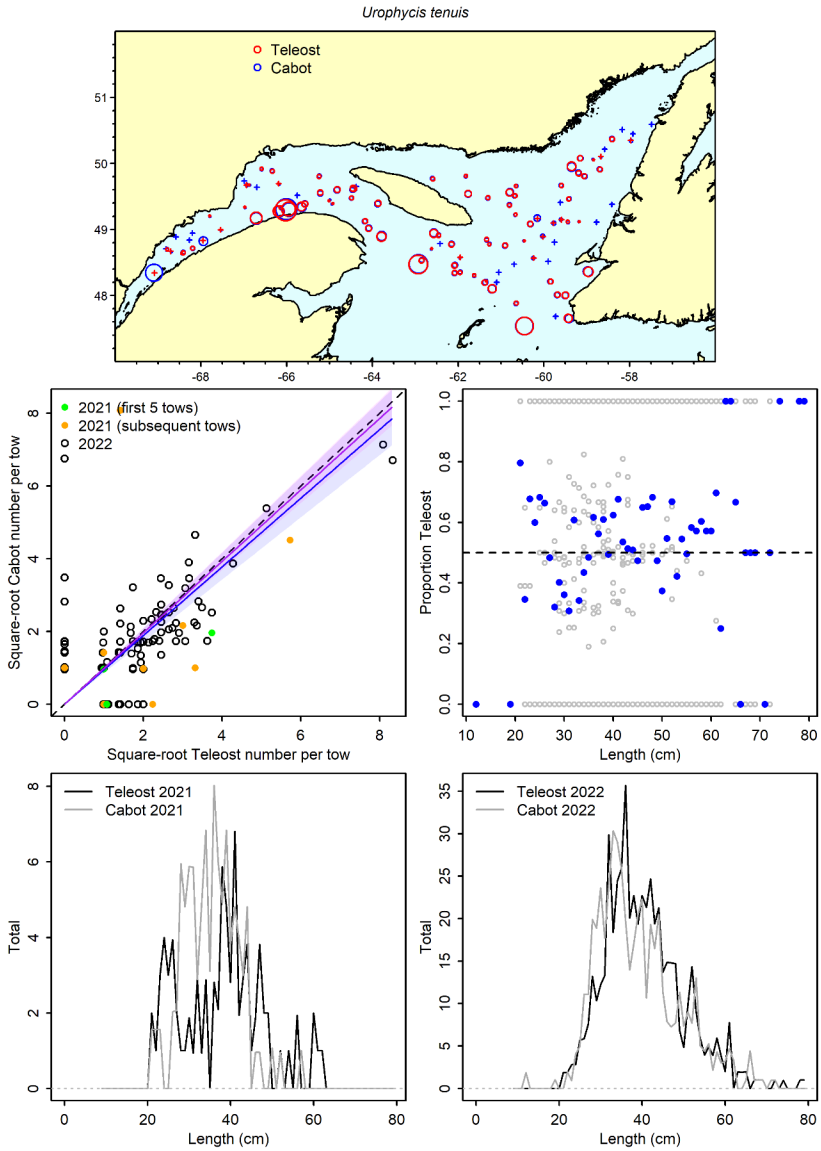

Figure 17a. Visualisation of comparative fishing data and size-aggregated model predictions for Urophycis tenuis.

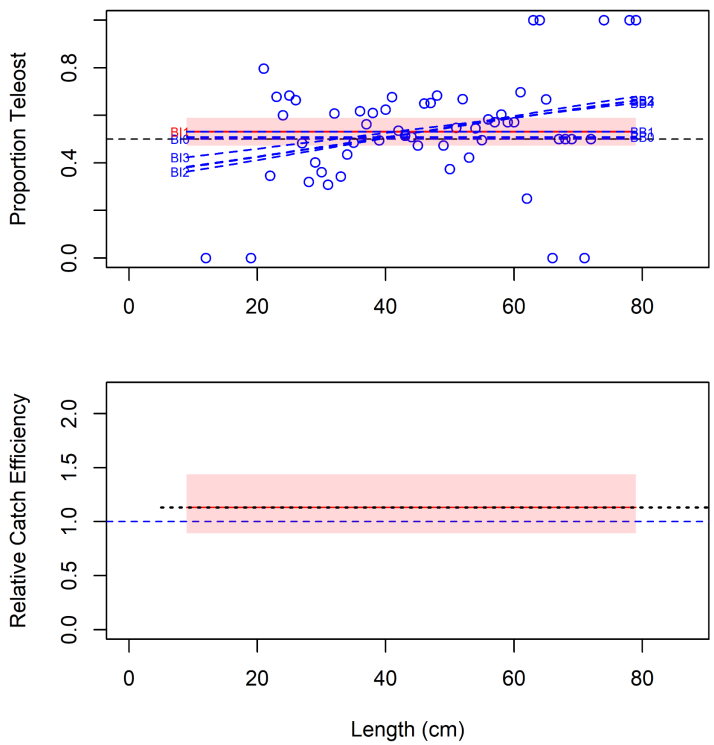

Figure 17b.Model fits and the selected length-based calibration for Urophycis tenuis.

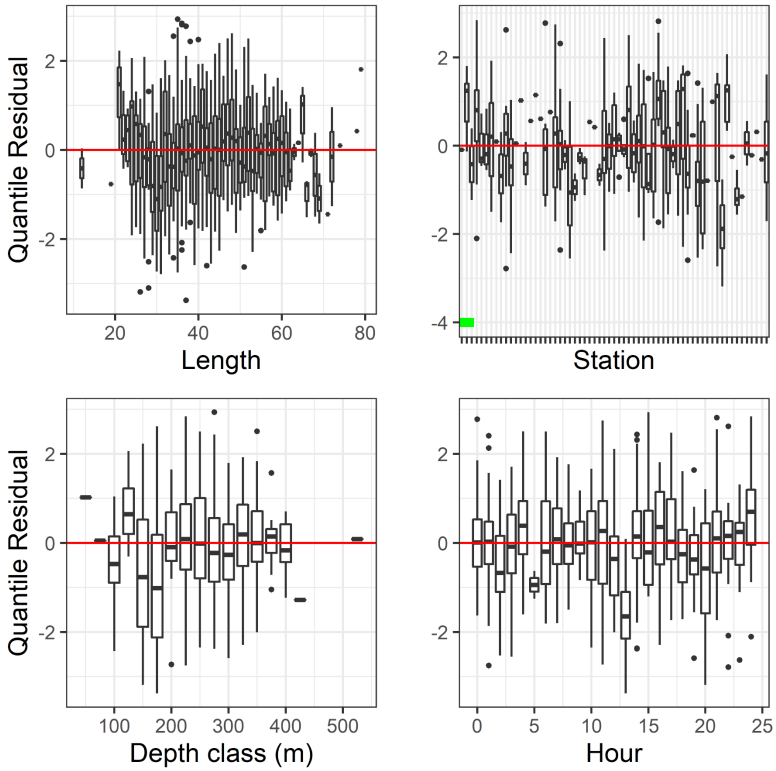

Figure 17c.Normalized quantile residuals for the selected model for Urophycis tenuis.

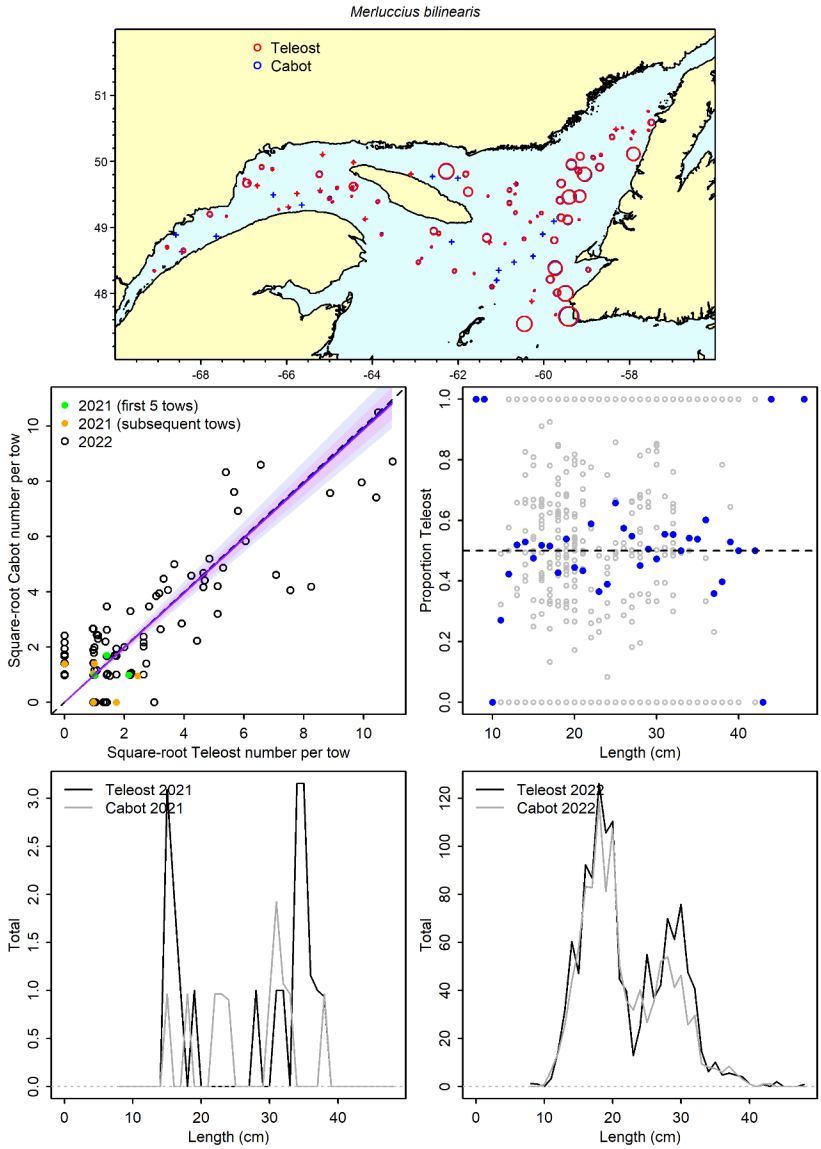

Figure 18a. Visualisation of comparative fishing data and size-aggregated model predictions for Merluccius bilinearis.

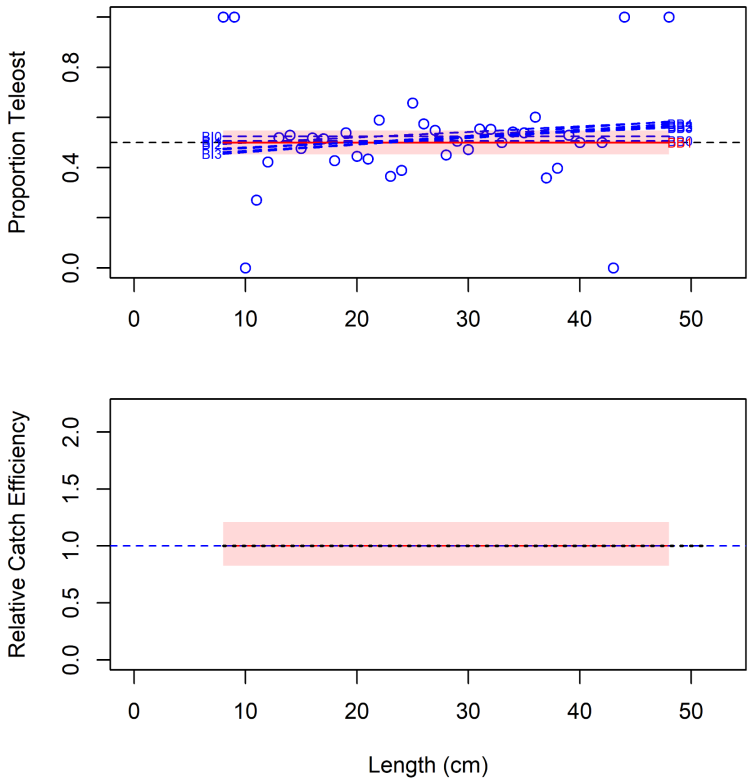

Figure 18b.Model fits and the selected length-based calibration for Merluccius bilinearis.

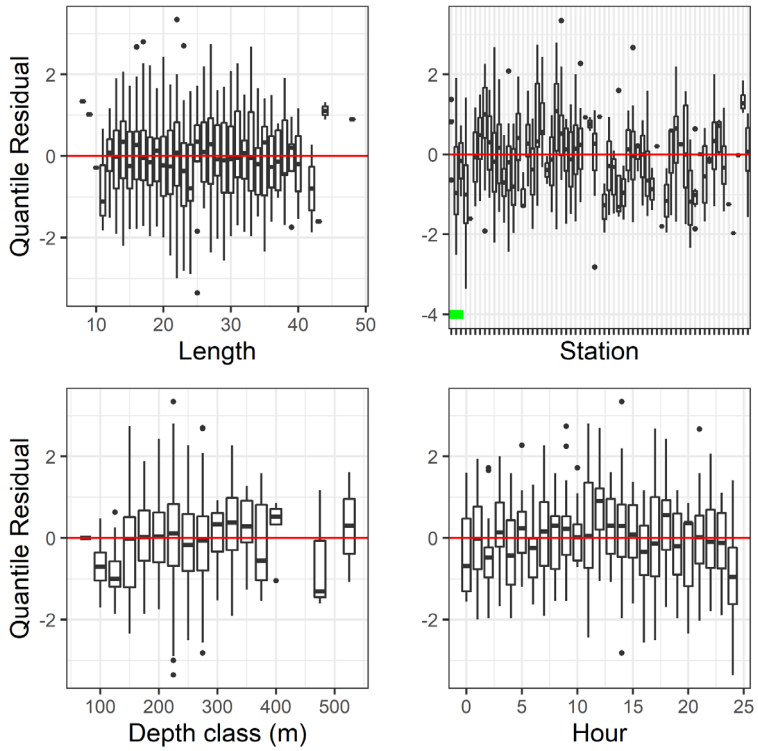

Figure 18c.Normalized quantile residuals for the selected model for Merluccius bilinearis.

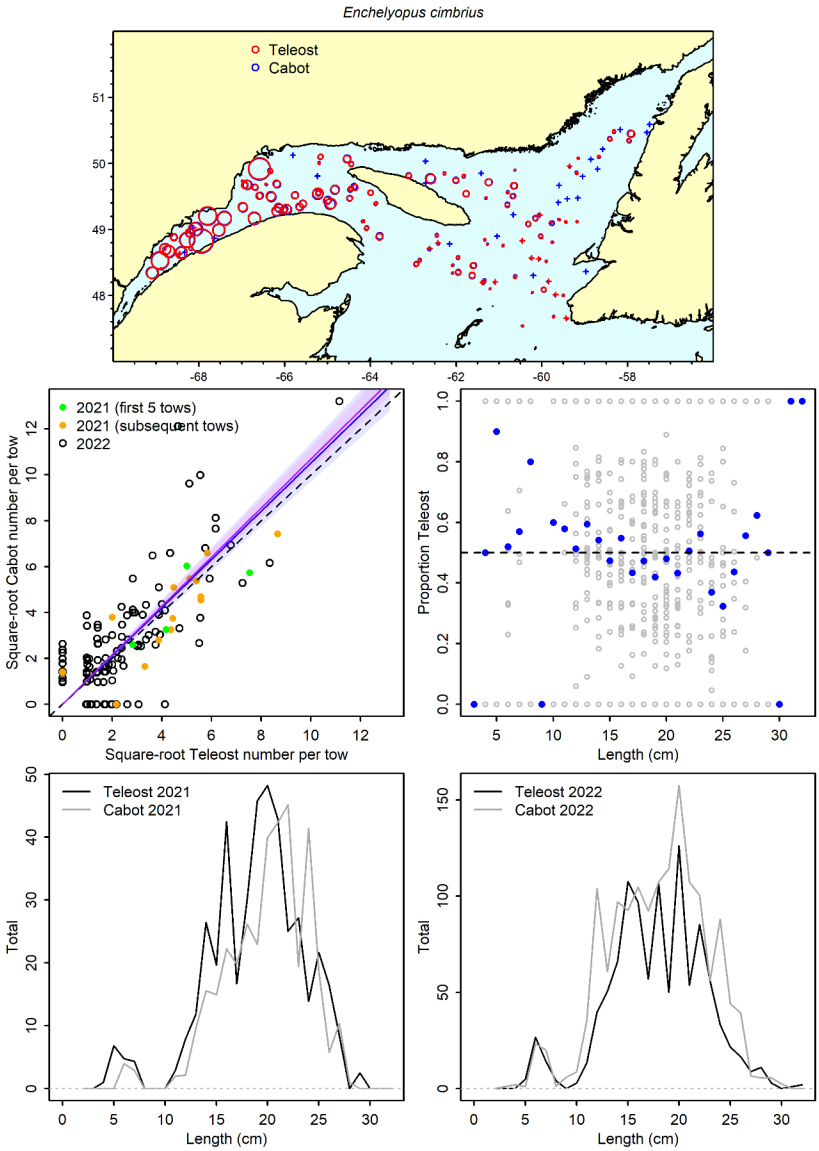

Figure 19a.Visualisation of comparative fishing data and size-aggregated model predictions for Enchelyopus cimbrius.

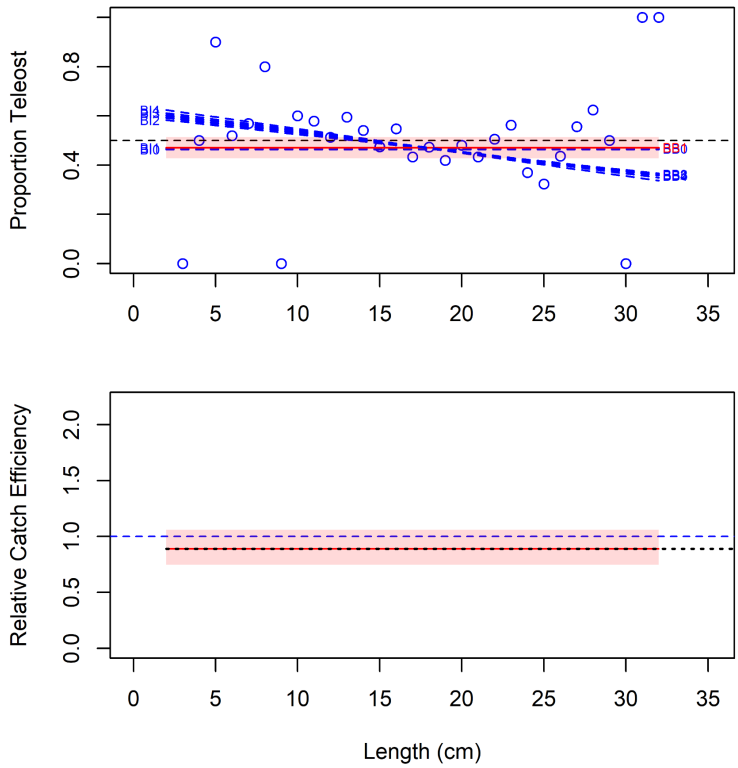

Figure 19b.Model fits and the selected length-based calibration for Enchelyopus cimbrius.

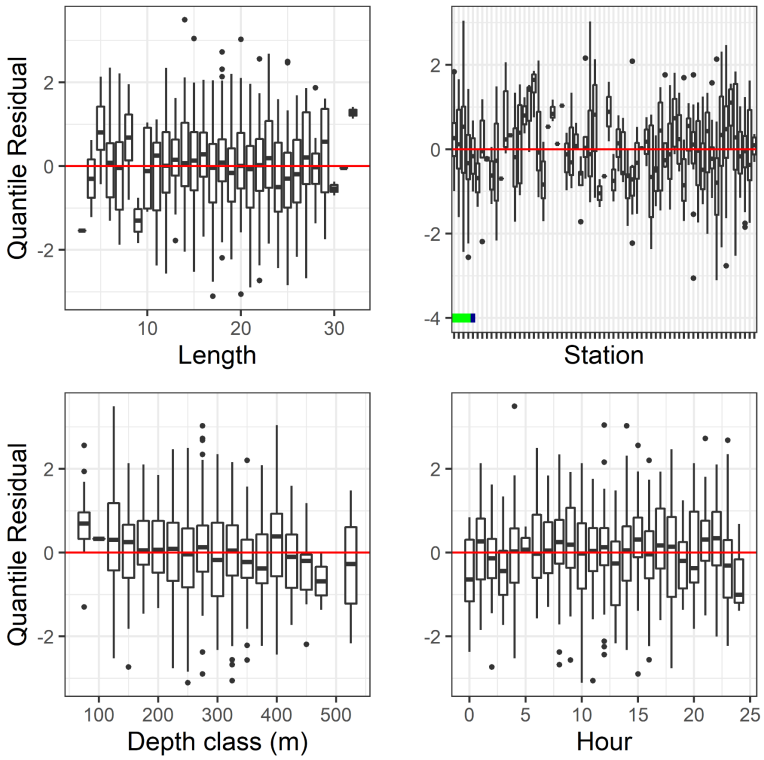

Figure 19c.Normalized quantile residuals for the selected model for Enchelyopus cimbrius.

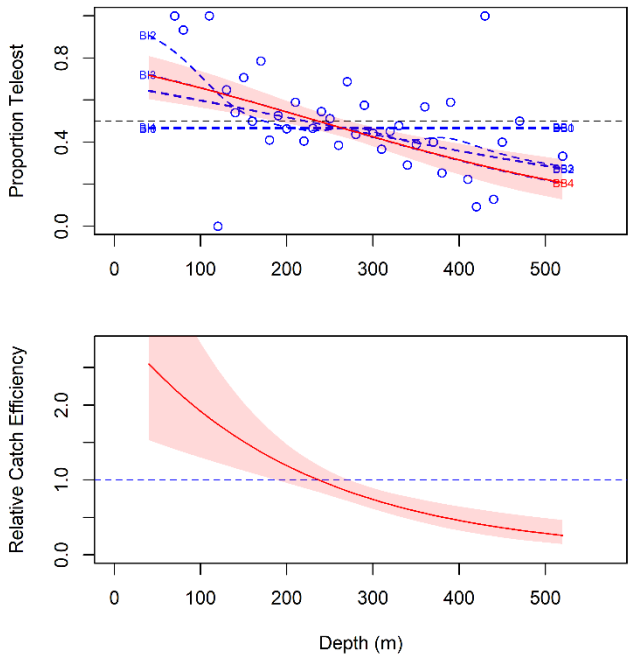

Figure 19d.Model fits and the selected depth-based calibration for Enchelyopus cimbrius.

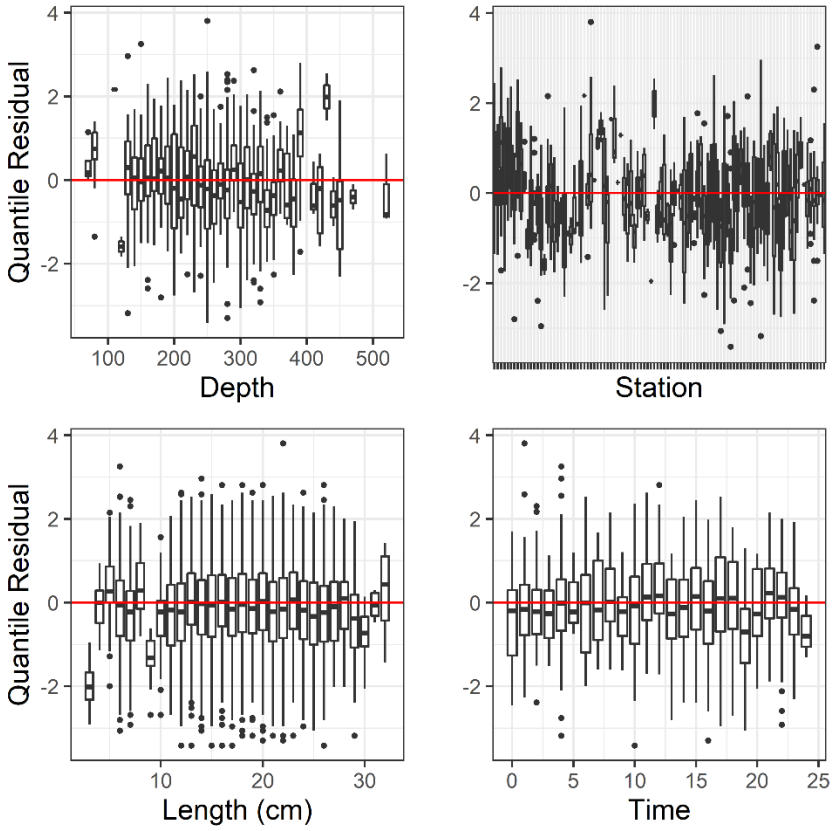

Figure 19e. Normalized quantile residuals for the selected depth-dependent model for Enchelyopus cimbrius.

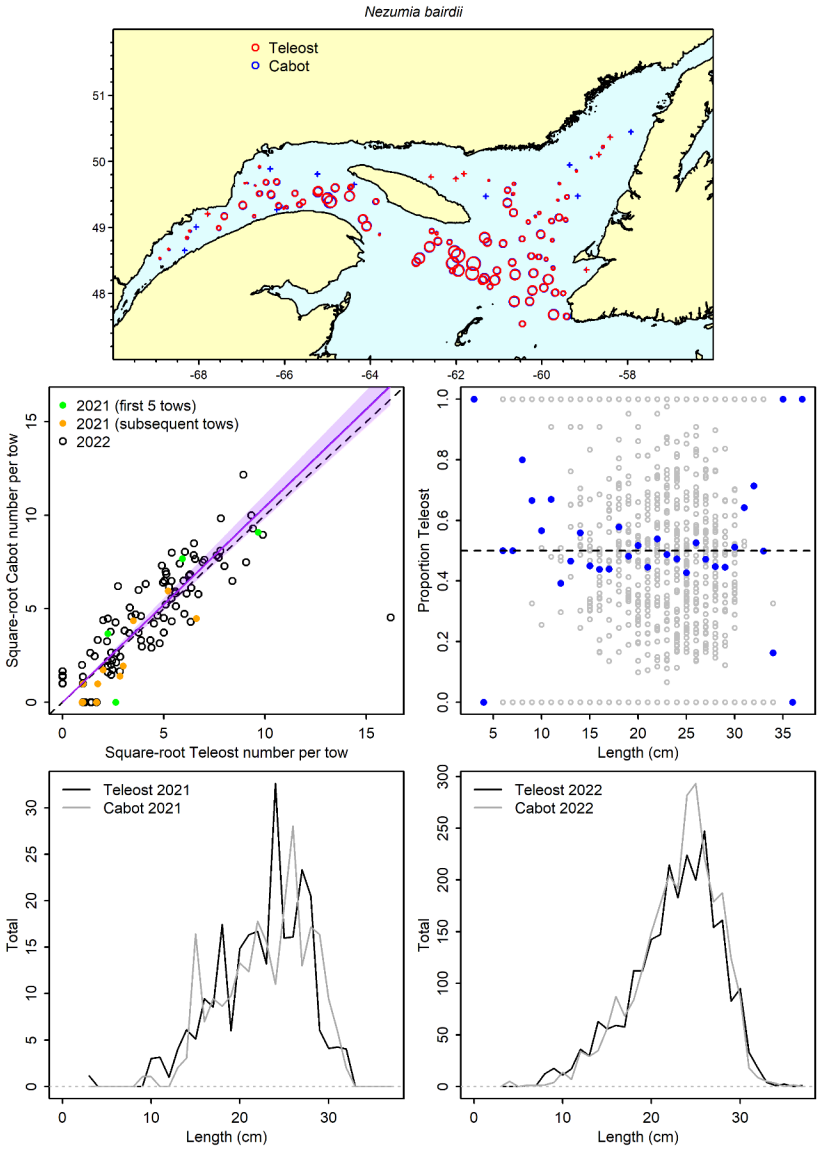

Figure 20a. Visualisation of comparative fishing data and size-aggregated model predictions for Nezumia bairdii.

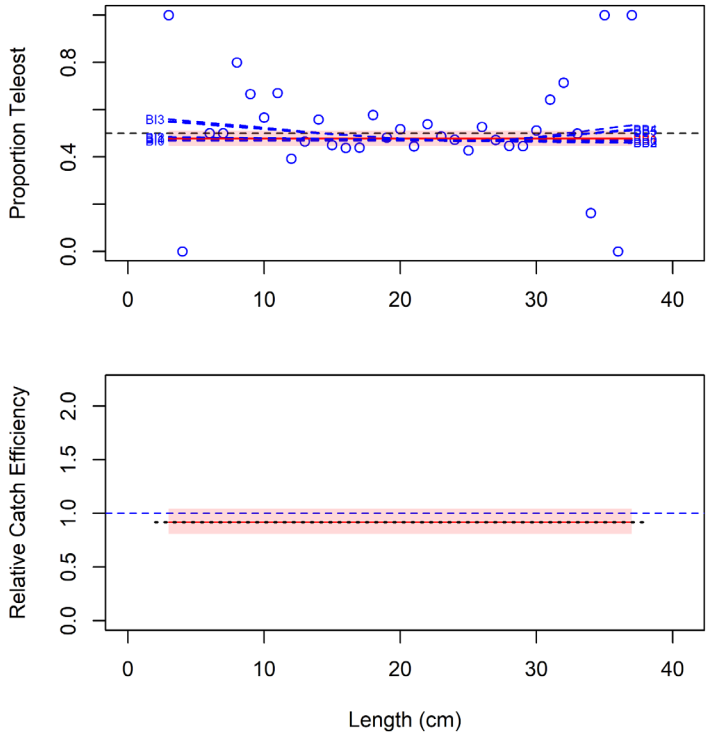

Figure 20b.Model fits and the selected length-based calibration for Nezumia bairdii.

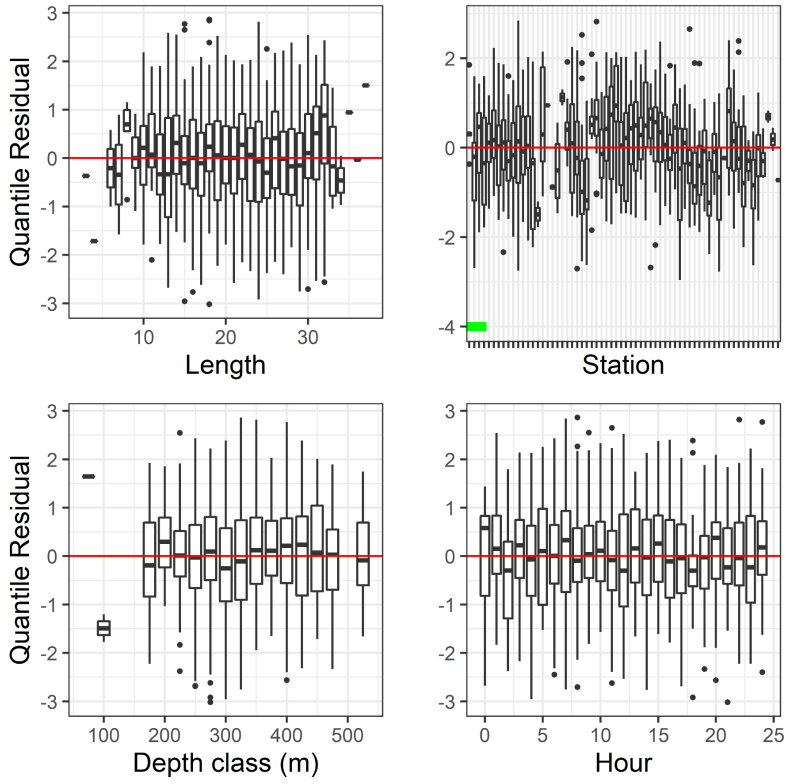

Figure 20c.Normalized quantile residuals for the selected model for Nezumia bairdii.

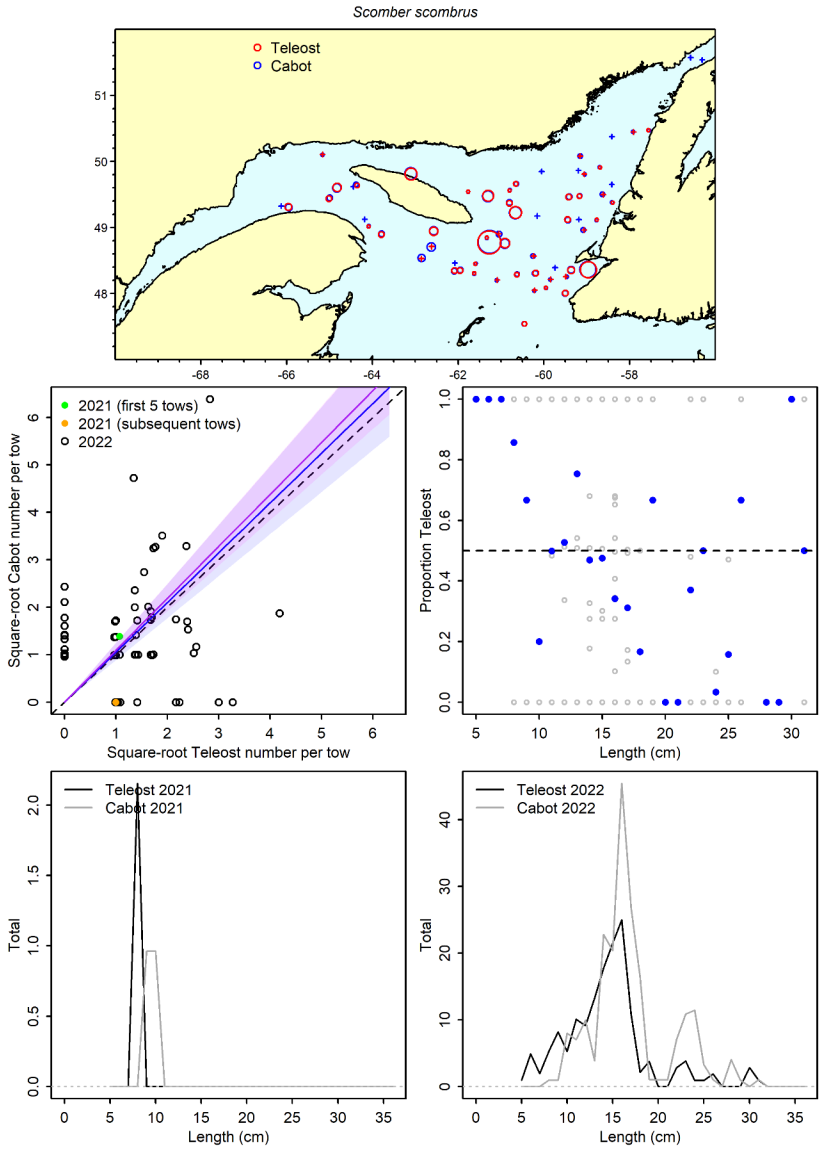

Figure 21a. Visualisation of comparative fishing data and size-aggregated model predictions for Scomber scombrus.

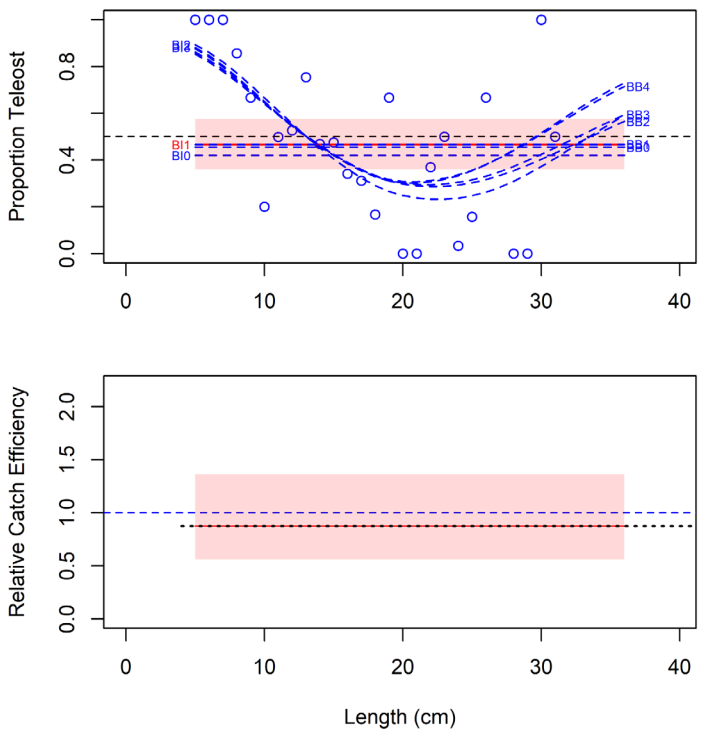

Figure 21b.Model fits and the selected length-based calibration for Scomber scombrus.

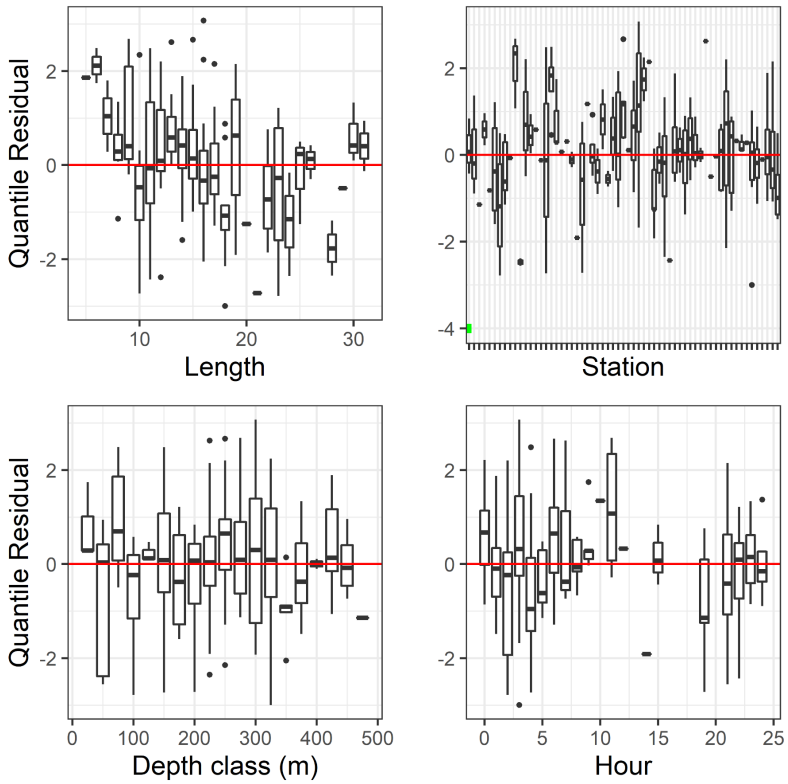

Figure 21c.Normalized quantile residuals for the selected model for Scomber scombrus.

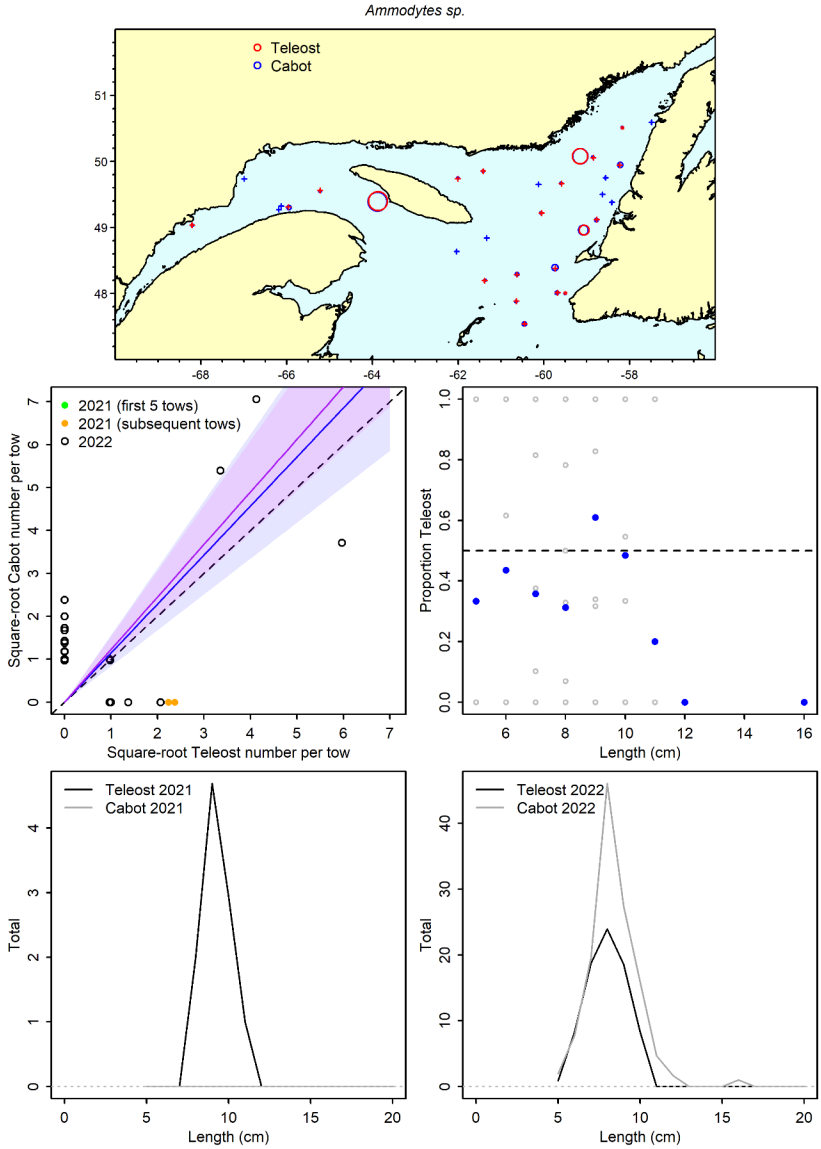

Figure 22a. Visualisation of comparative fishing data and size-aggregated model predictions for Ammodytes sp.

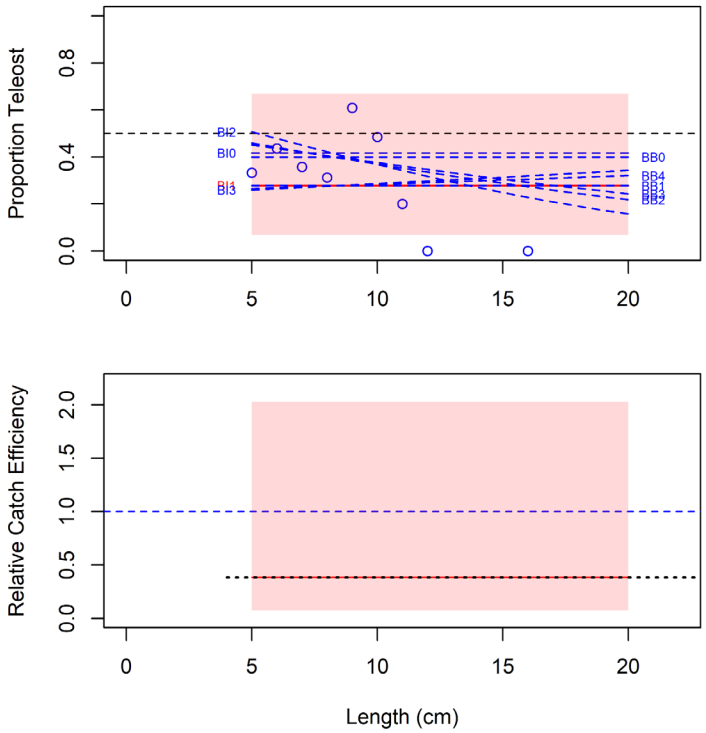

Figure 22b.Model fits and the selected length-based calibration for Ammodytes sp.

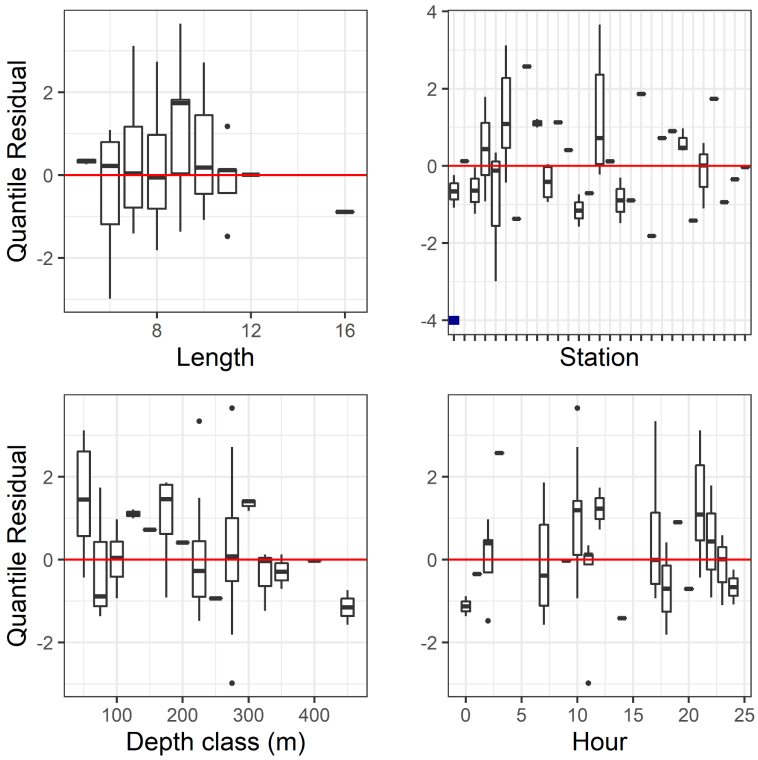

Figure 22c.Normalized quantile residuals for the selected model for Ammodytes sp.

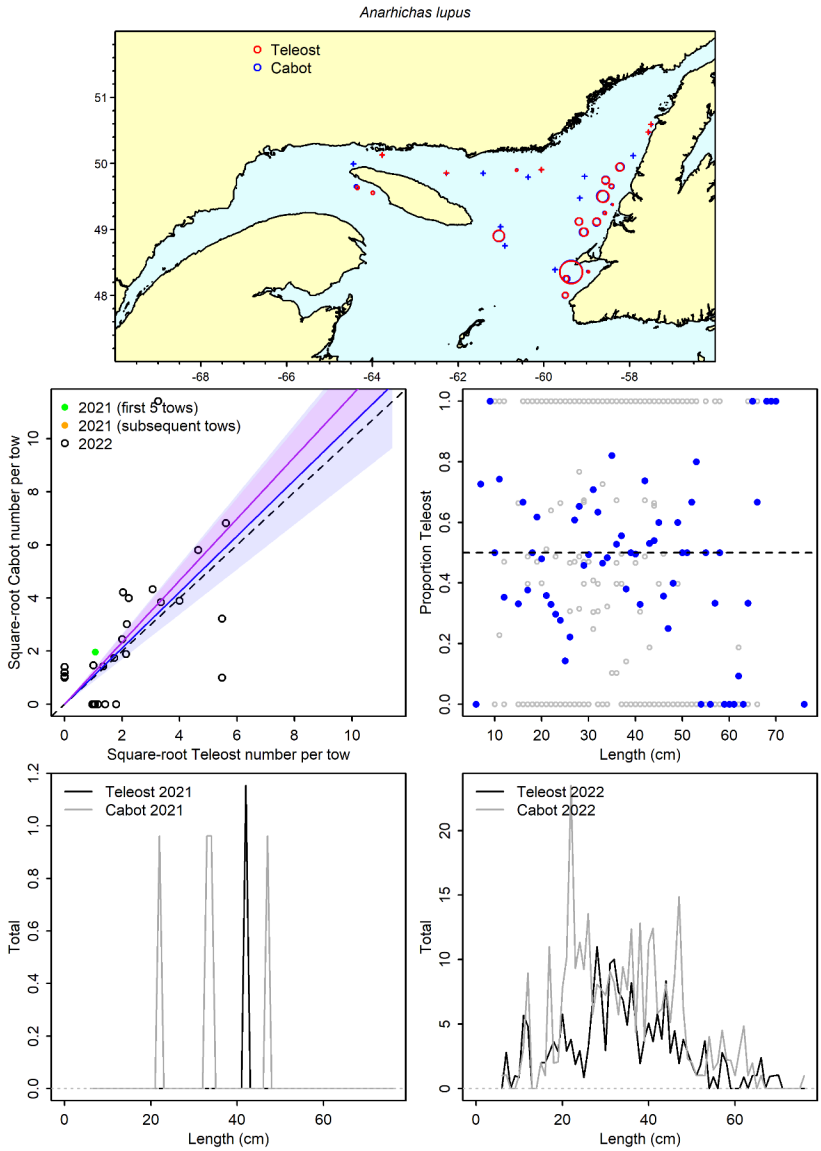

Figure 23a. Visualisation of comparative fishing data and size-aggregated model predictions for Anarhichas lupus.

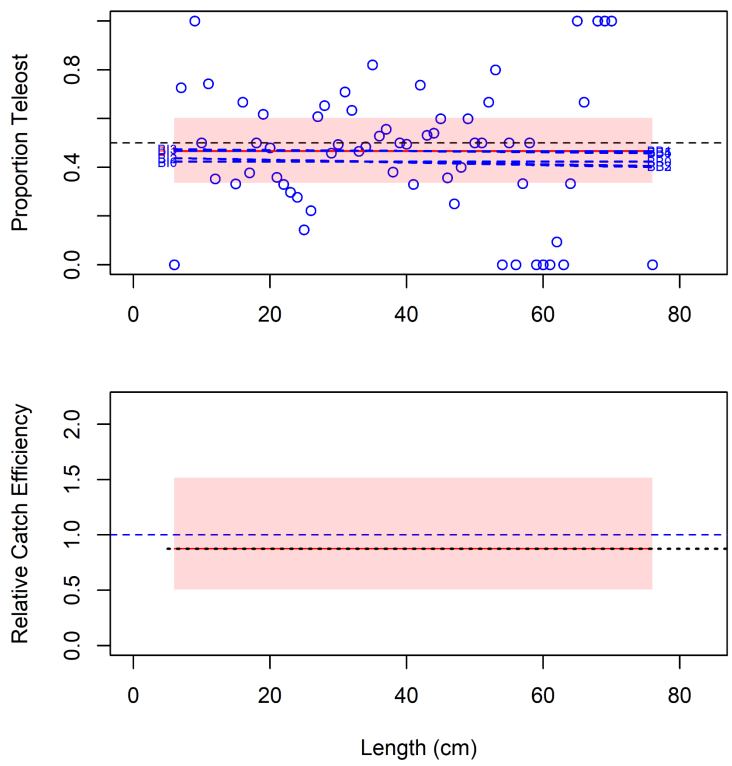

Figure 23b.Model fits and the selected length-based calibration for Anarhichas lupus.

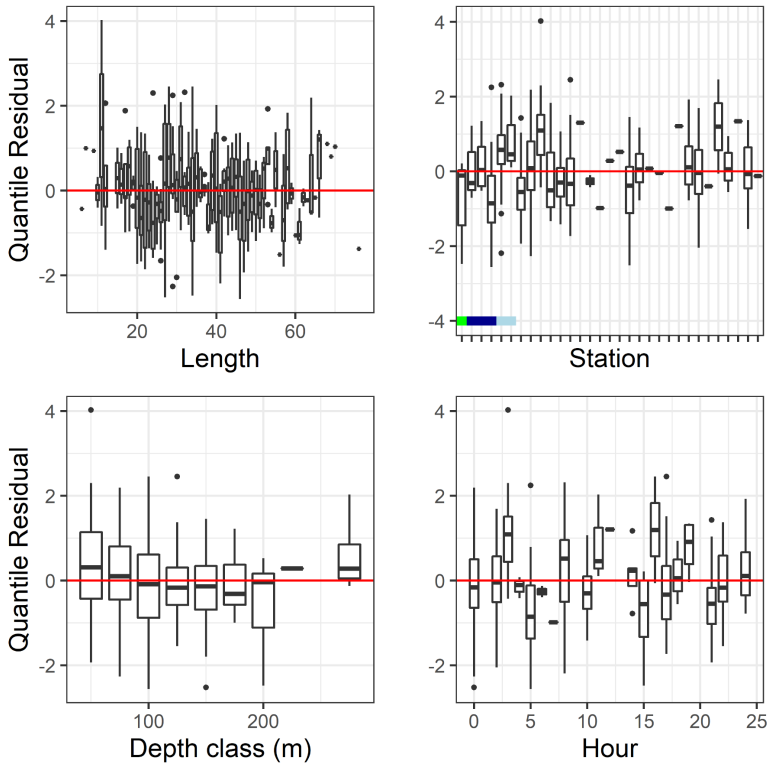

Figure 23c.Normalized quantile residuals for the selected model for Anarhichas lupus.

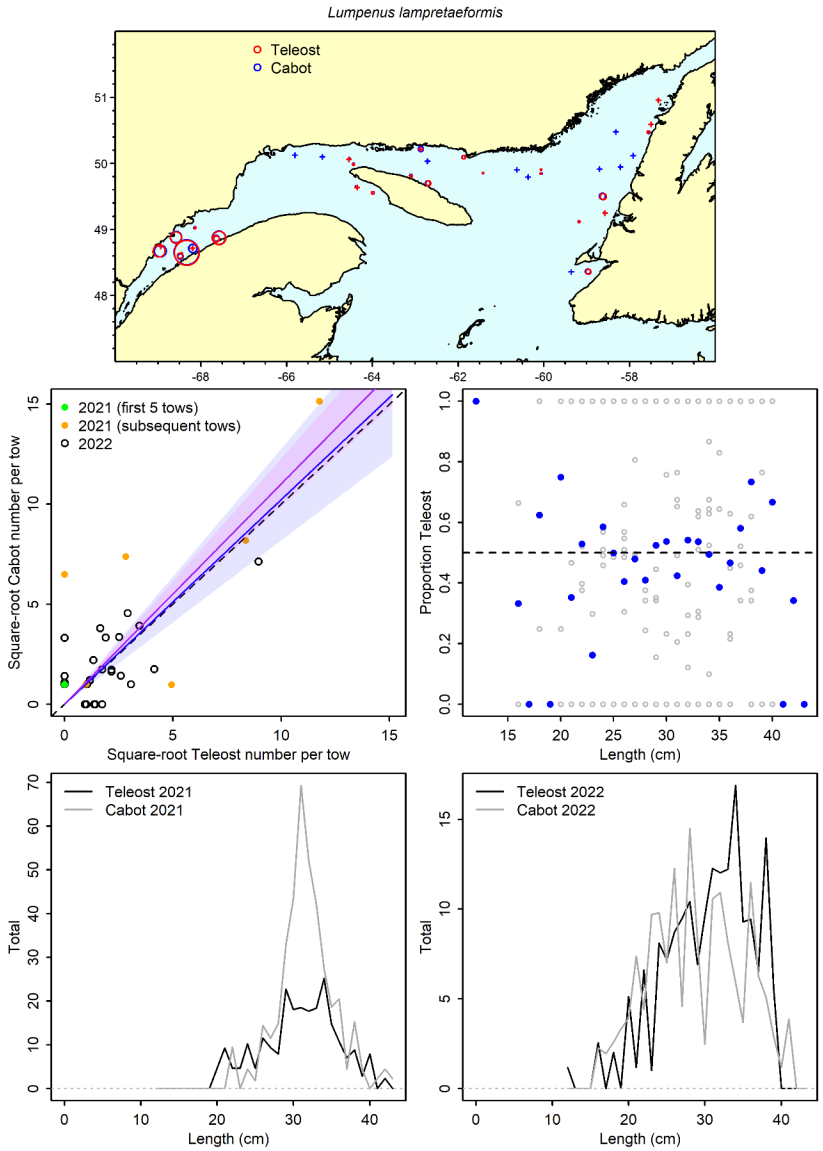

Figure 24a. Visualisation of comparative fishing data and size-aggregated model predictions for Lumpenus lampretaeformis.

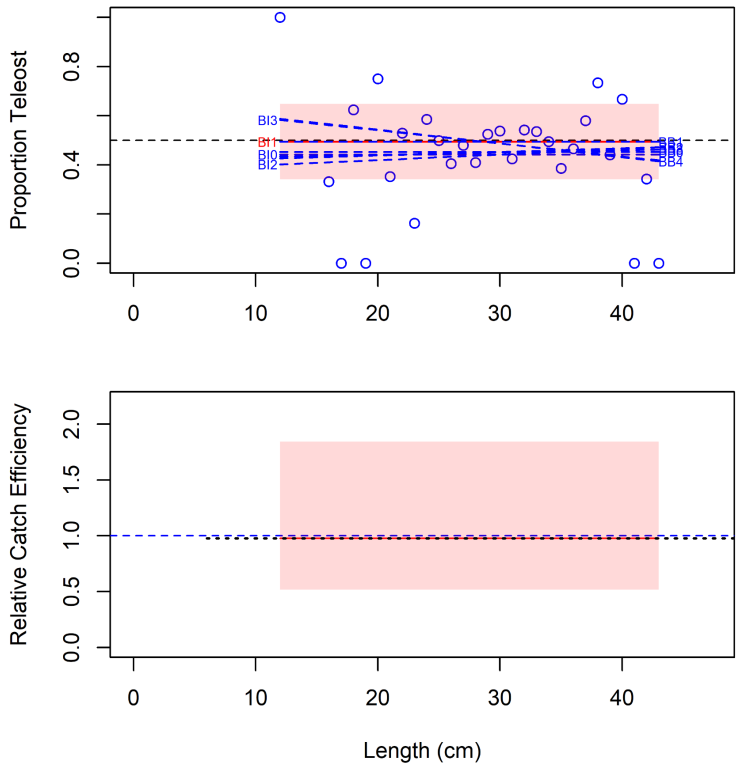

Figure 24b.Model fits and the selected length-based calibration for Lumpenus lampretaeformis.

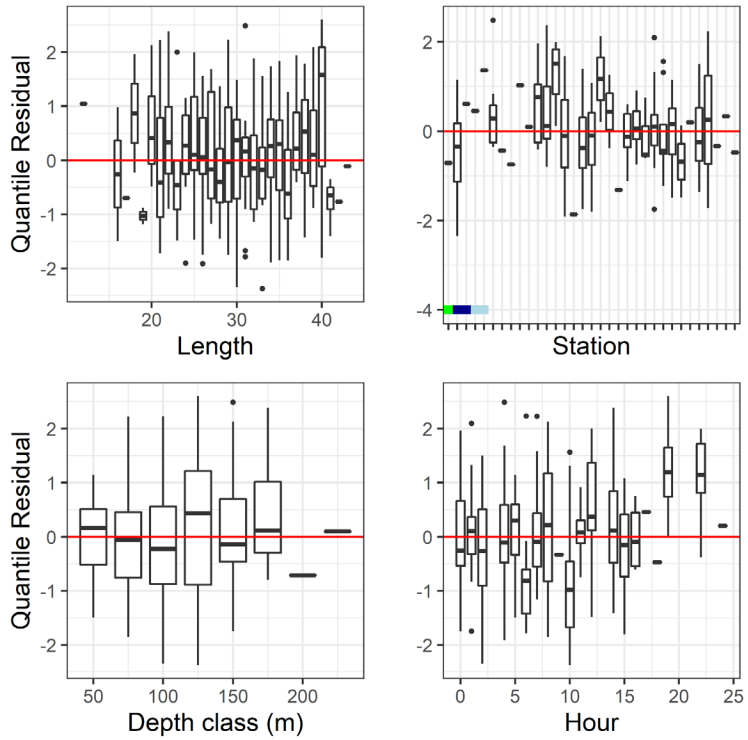

Figure 24c.Normalized quantile residuals for the selected model for Lumpenus lampretaeformis.

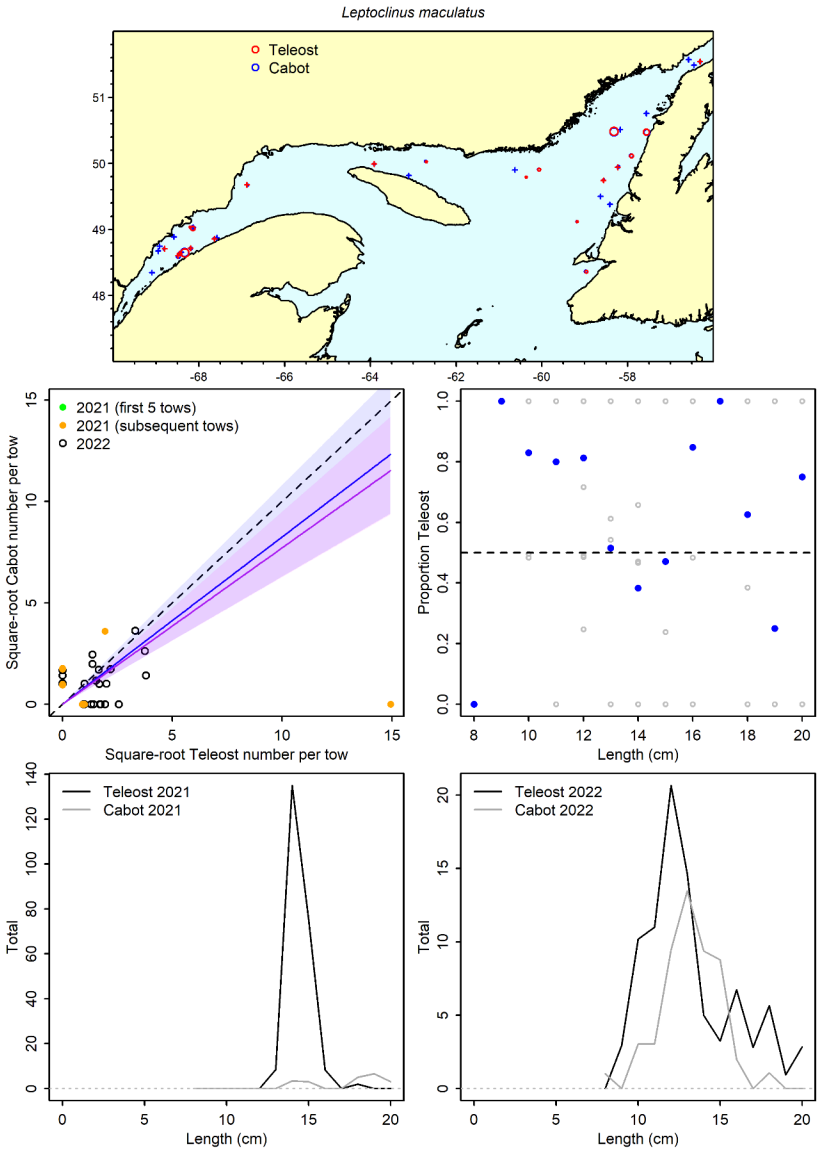

Figure 25a. Visualisation of comparative fishing data and size-aggregated model predictions for Leptoclinus maculatus.

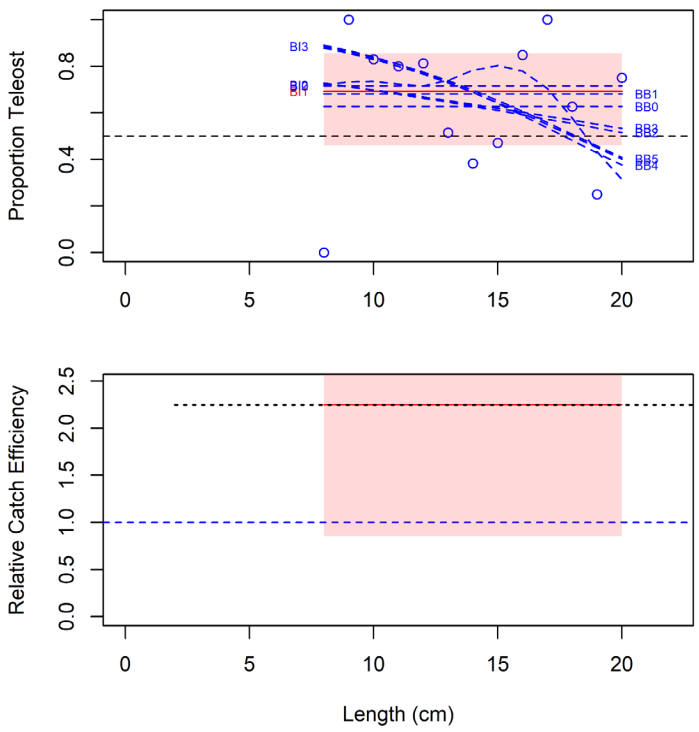

Figure 25b.Model fits and the selected length-based calibration for Leptoclinus maculatus.

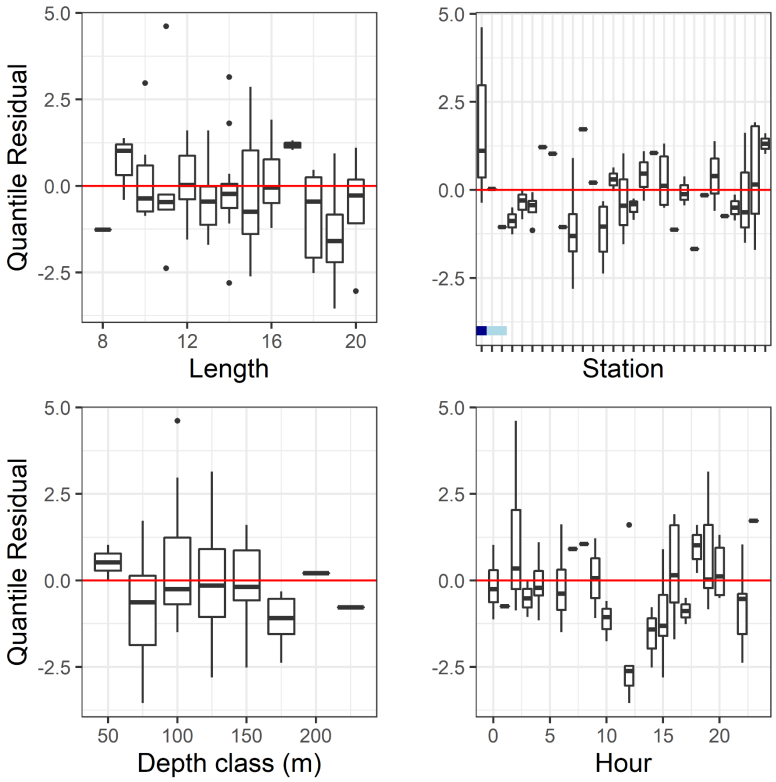

Figure 25c.Normalized quantile residuals for the selected model for Leptoclinus maculatus.

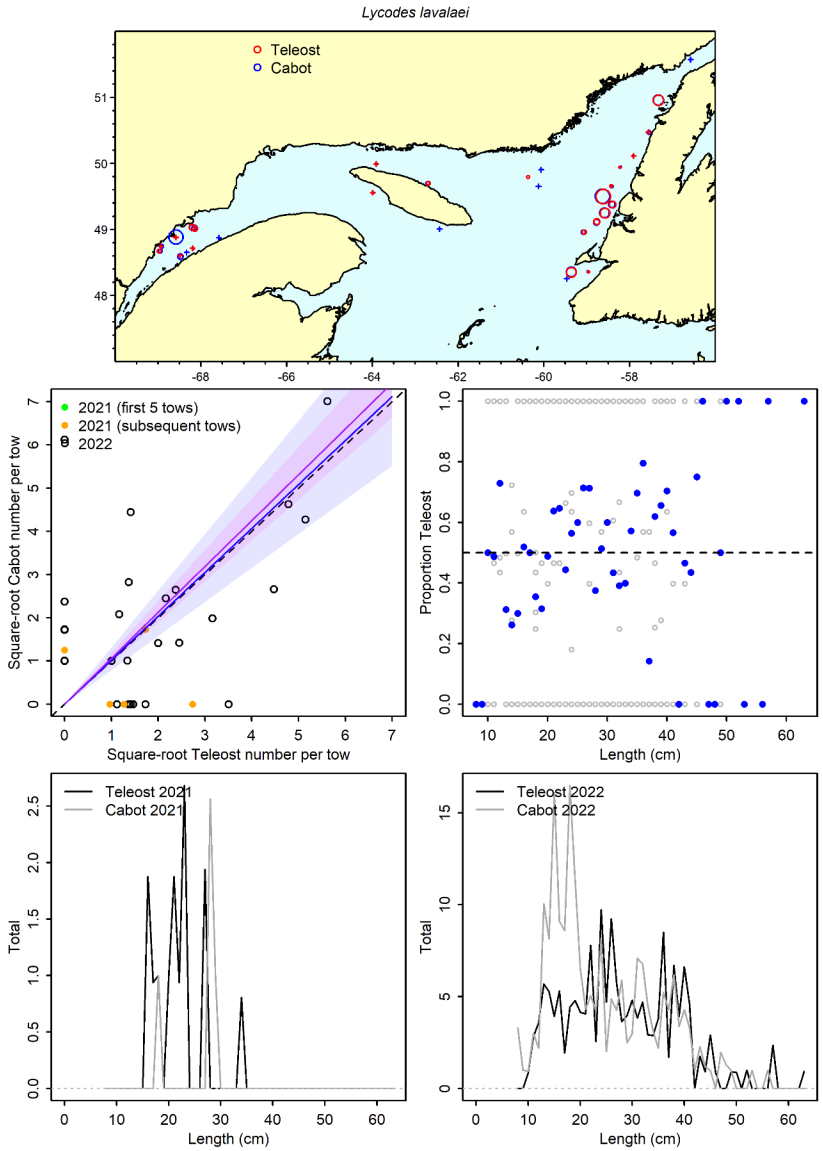

Figure 26a. Visualisation of comparative fishing data and size-aggregated model predictions for Lycodes lavalaei.

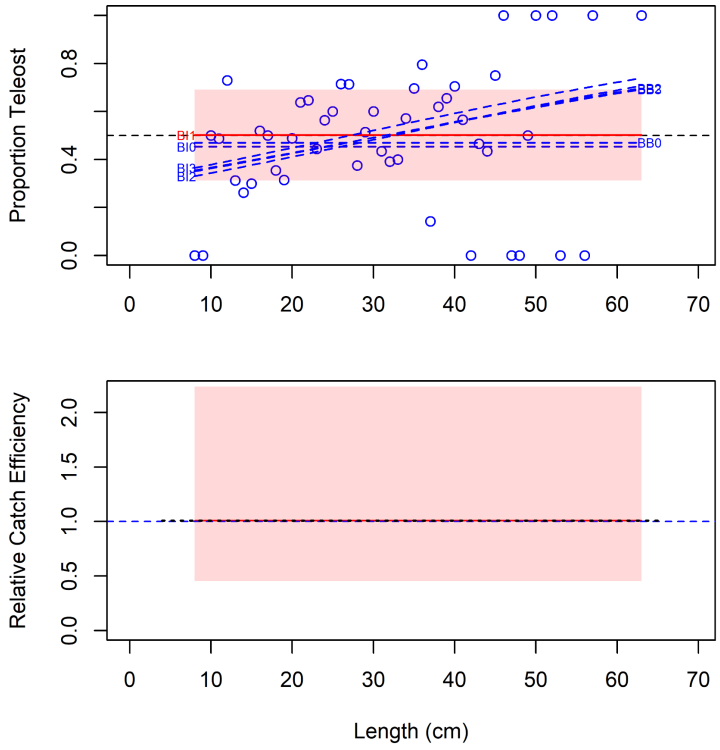

Figure 26b.Model fits and the selected length-based calibration for Lycodes lavalaei.

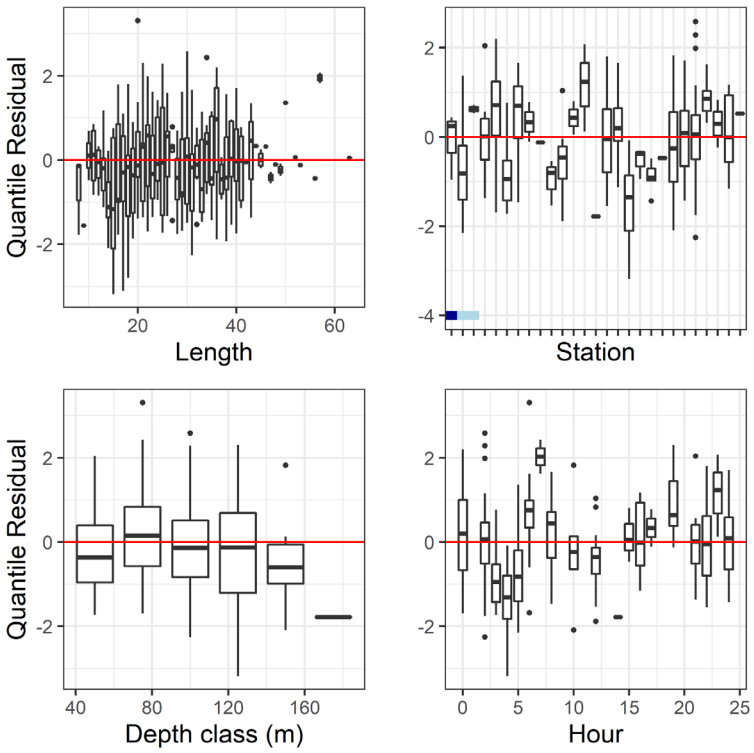

Figure 26c.Normalized quantile residuals for the selected model for Lycodes lavalaei.

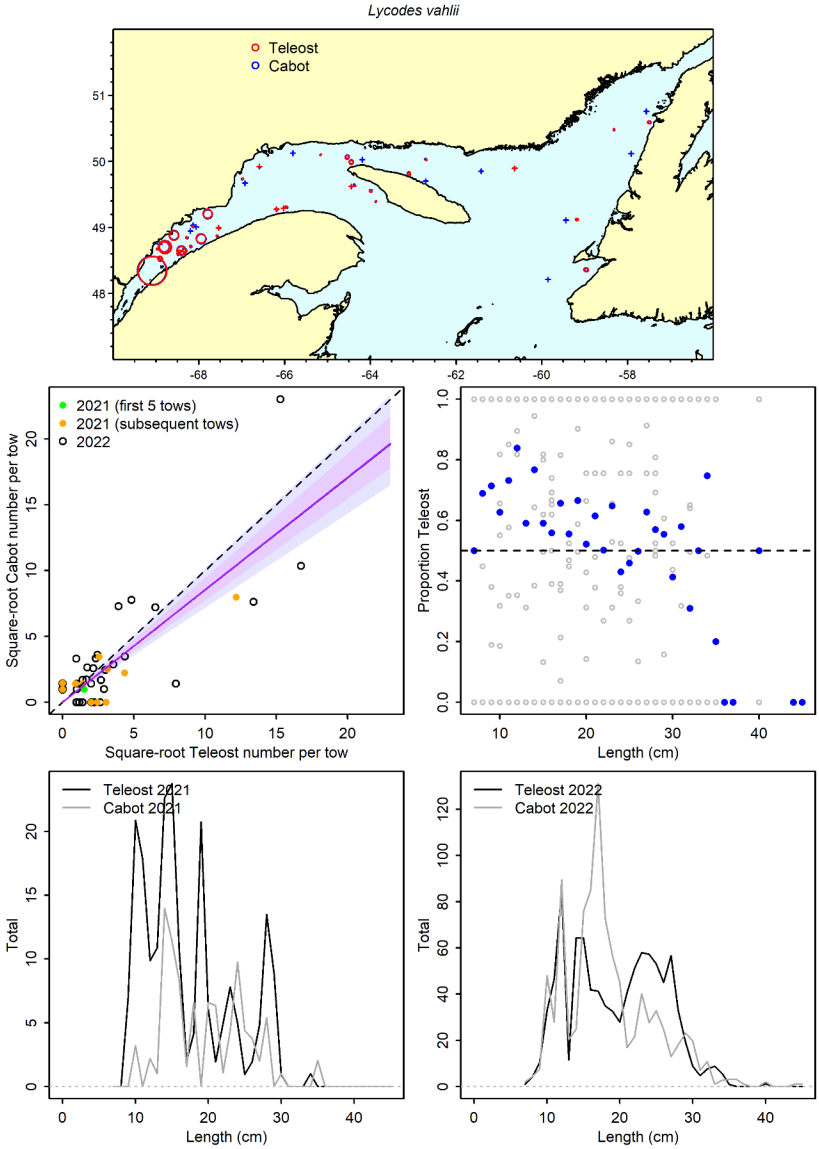

Figure 27a. Visualisation of comparative fishing data and size-aggregated model predictions for Lycodes vahlii.

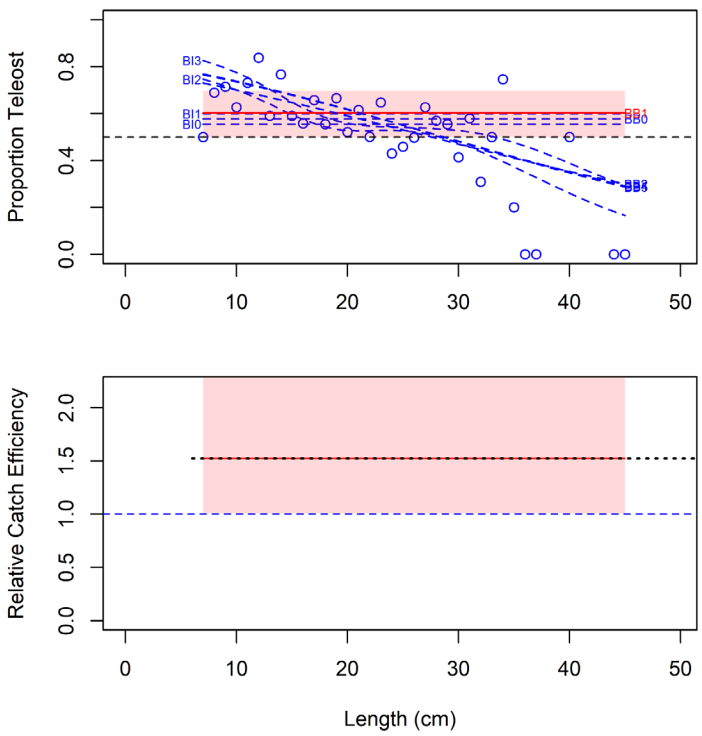

Figure 27b.Model fits and the selected length-based calibration for Lycodes vahlii.

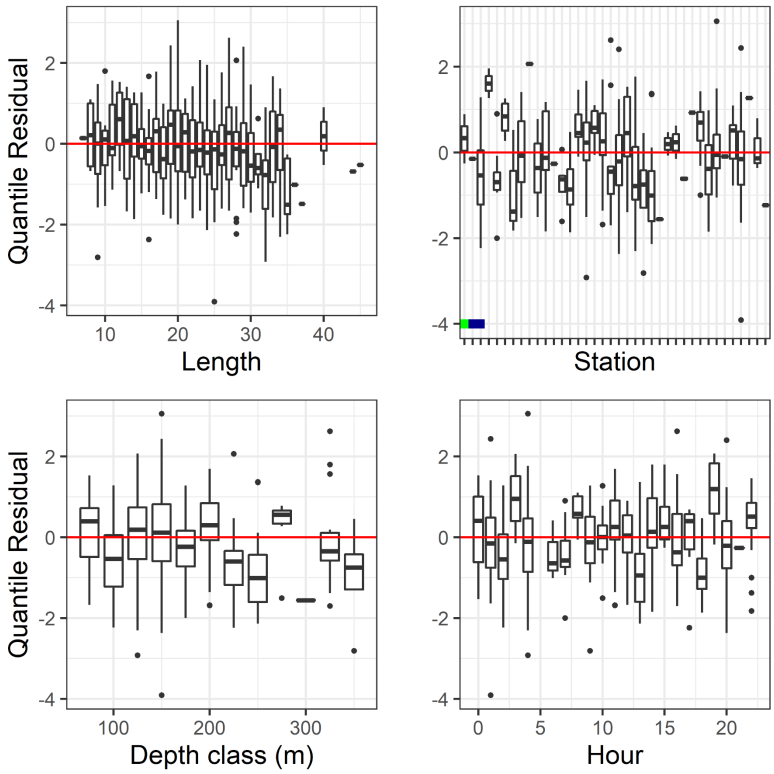

Figure 27c.Normalized quantile residuals for the selected model for Lycodes vahlii.

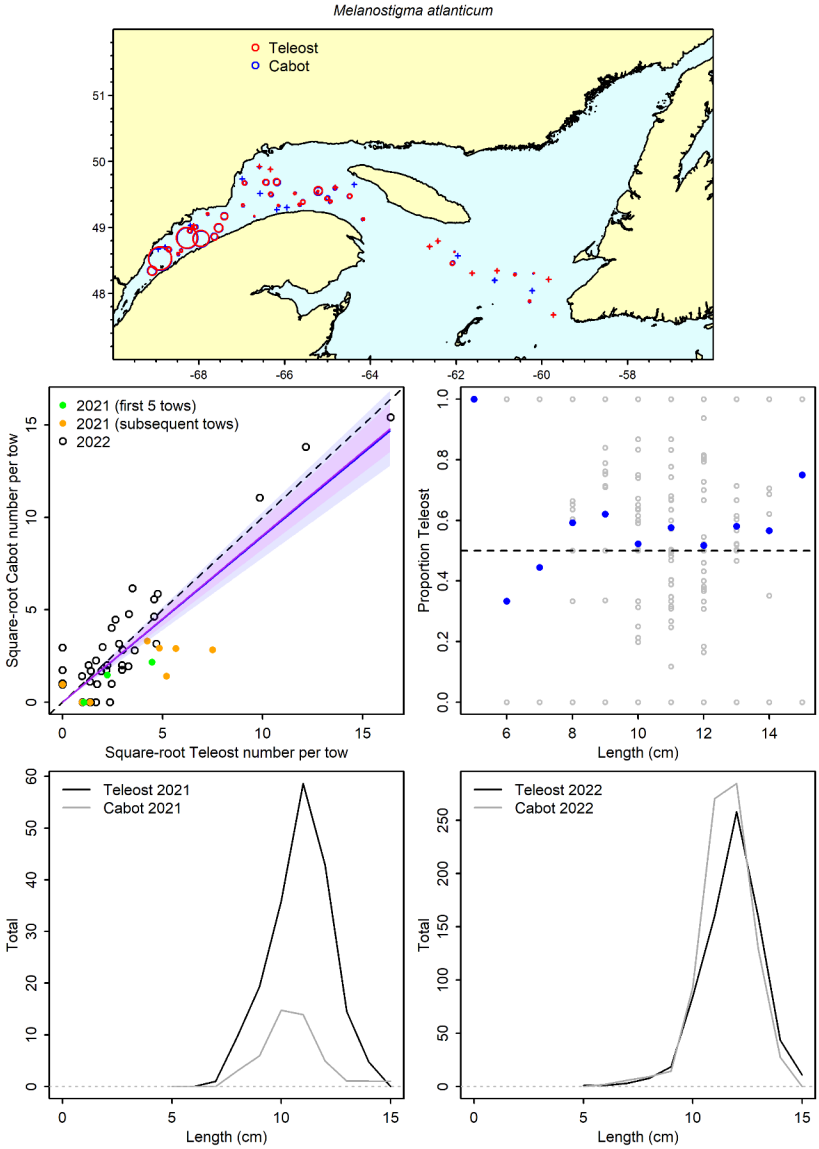

Figure 28a. Visualisation of comparative fishing data and size-aggregated model predictions for Melanostigma atlanticum.

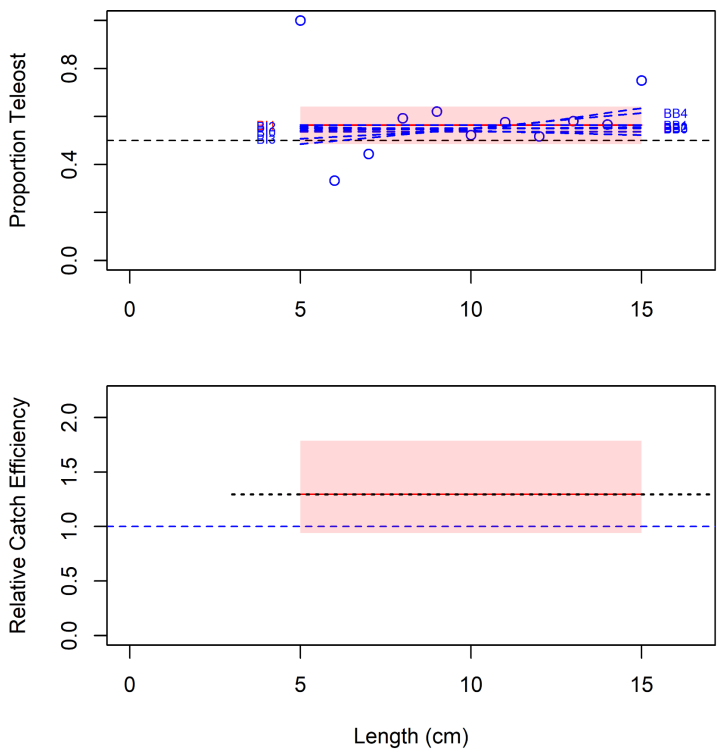

Figure 28b.Model fits and the selected length-based calibration for Melanostigma atlanticum.

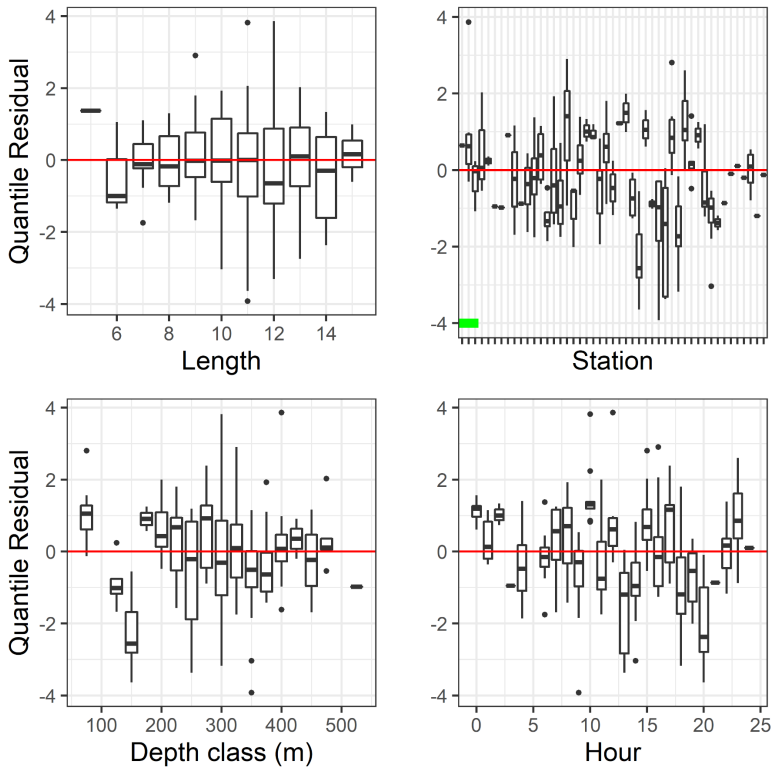

Figure 28c.Normalized quantile residuals for the selected model for Melanostigma atlanticum.

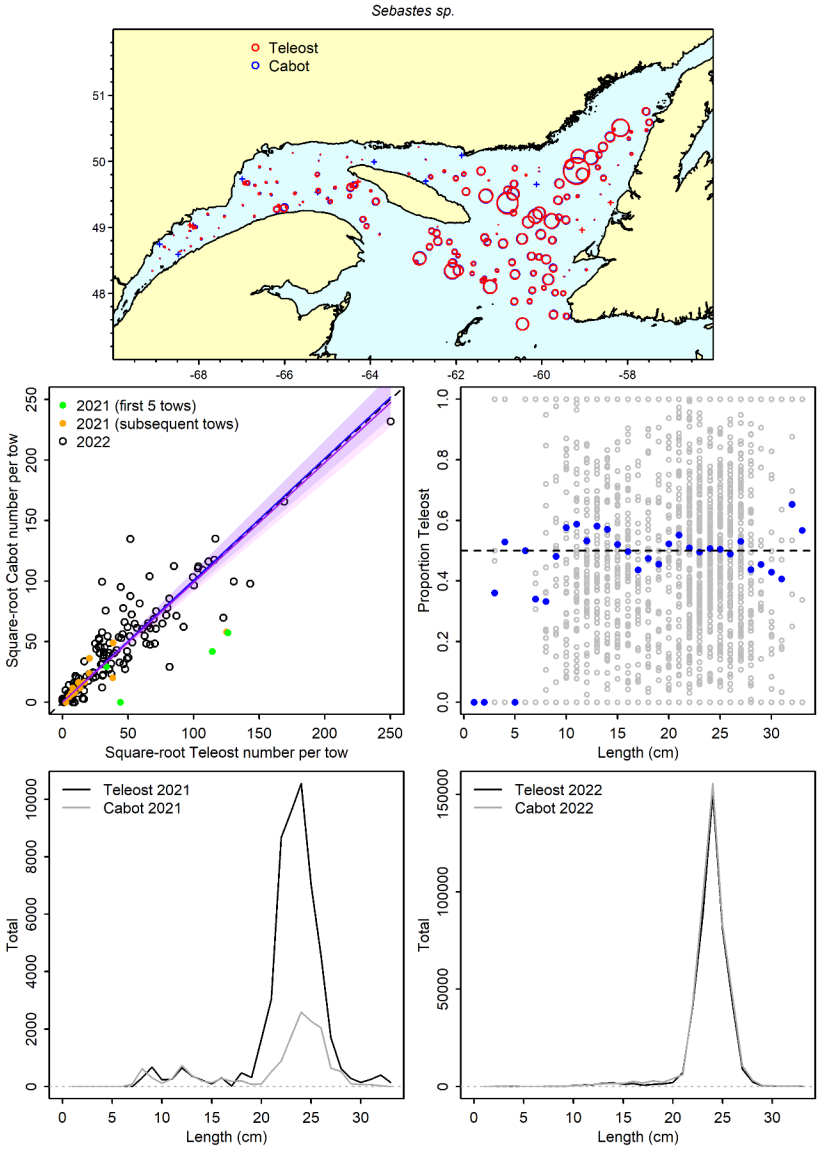

Figure 29a. Visualisation of comparative fishing data and size-aggregated model predictions for Sebastes sp..

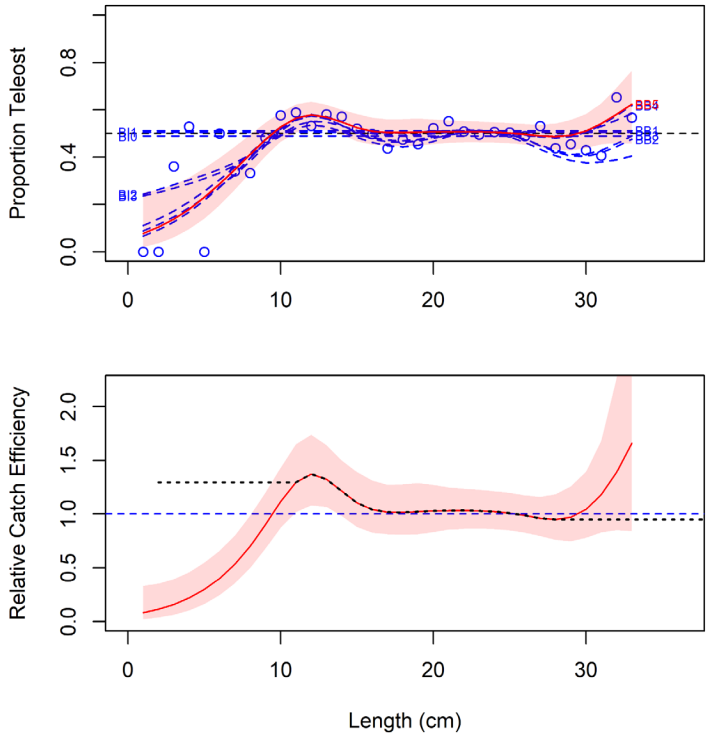

Figure 29b.Model fits and the selected length-based calibration for Sebastes sp.

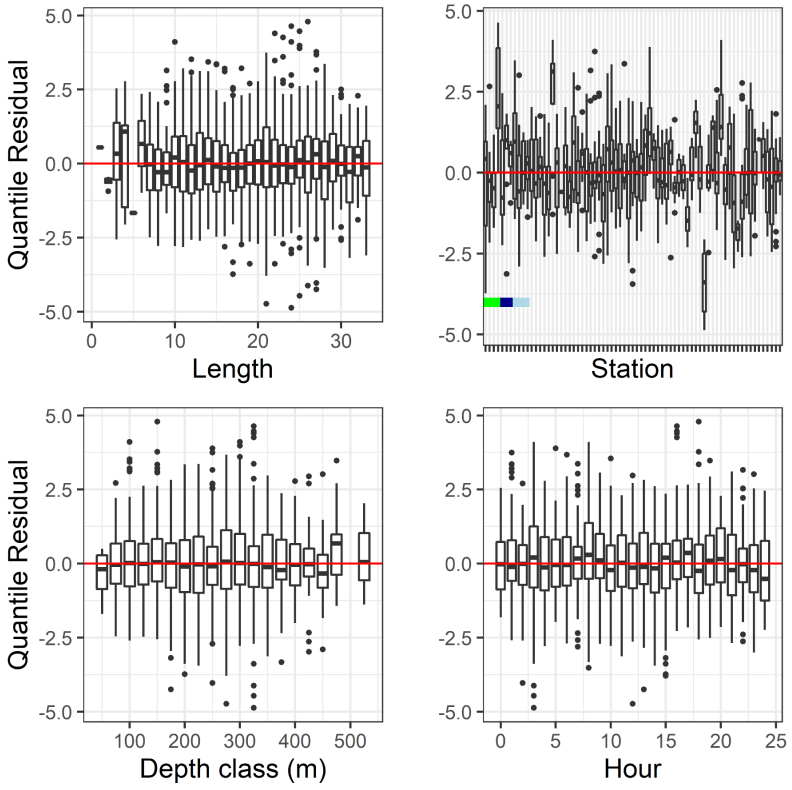

Figure 29c.Normalized quantile residuals for the selected model for Sebastes sp.

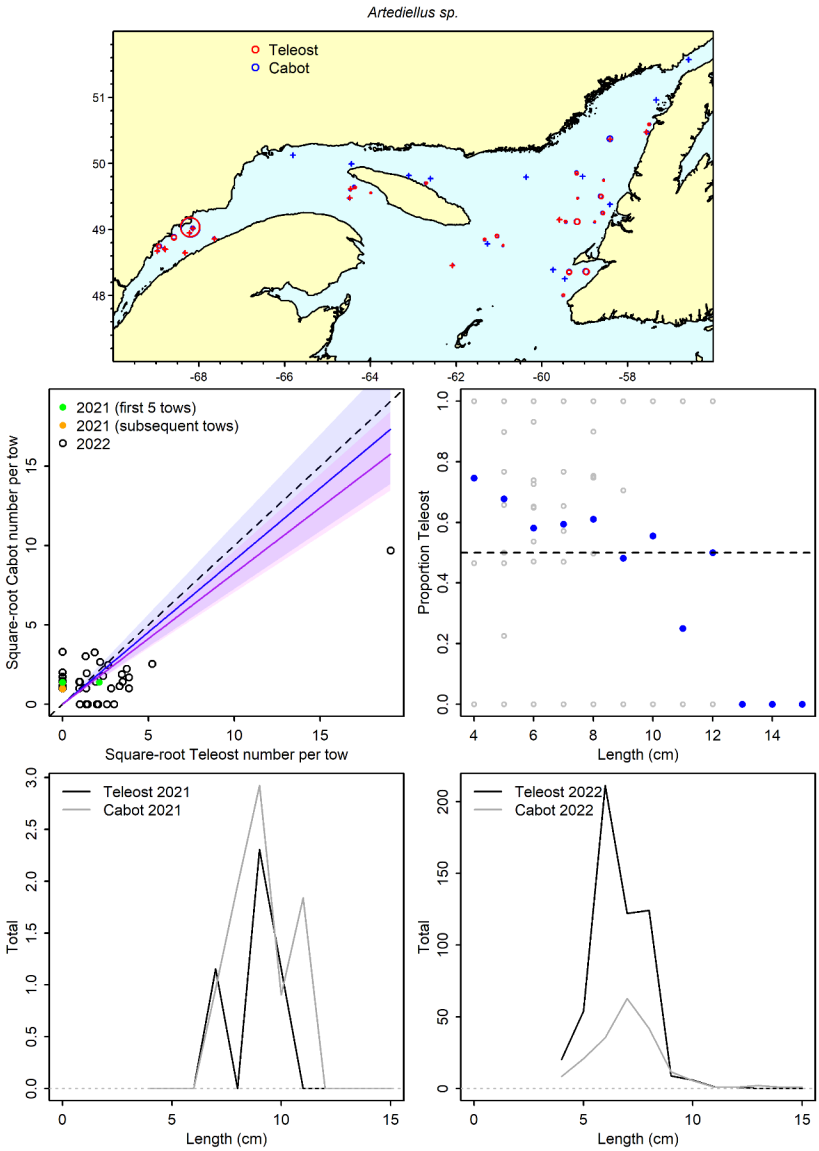

Figure 30a. Visualisation of comparative fishing data and size-aggregated model predictions for Artediellus sp.

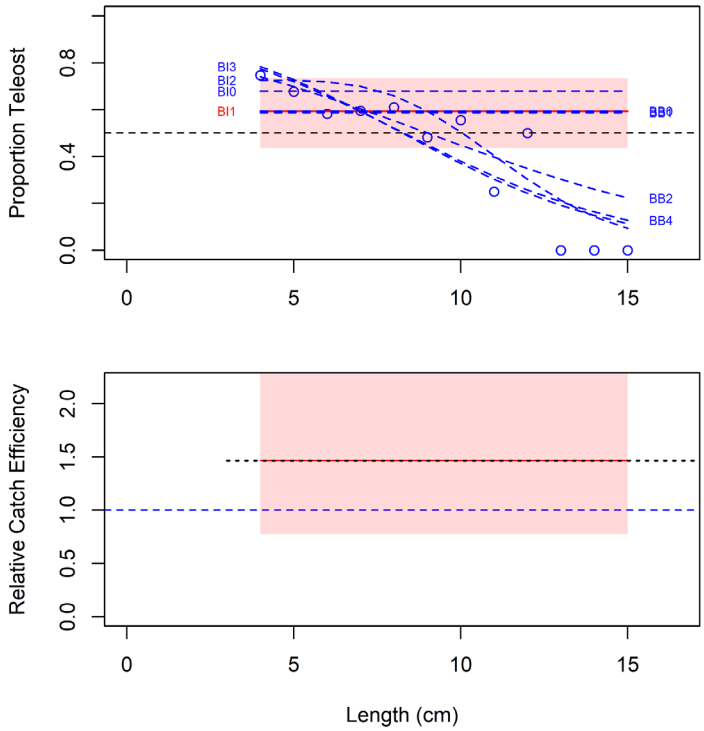

Figure 30b.Model fits and the selected length-based calibration for Artediellus sp.

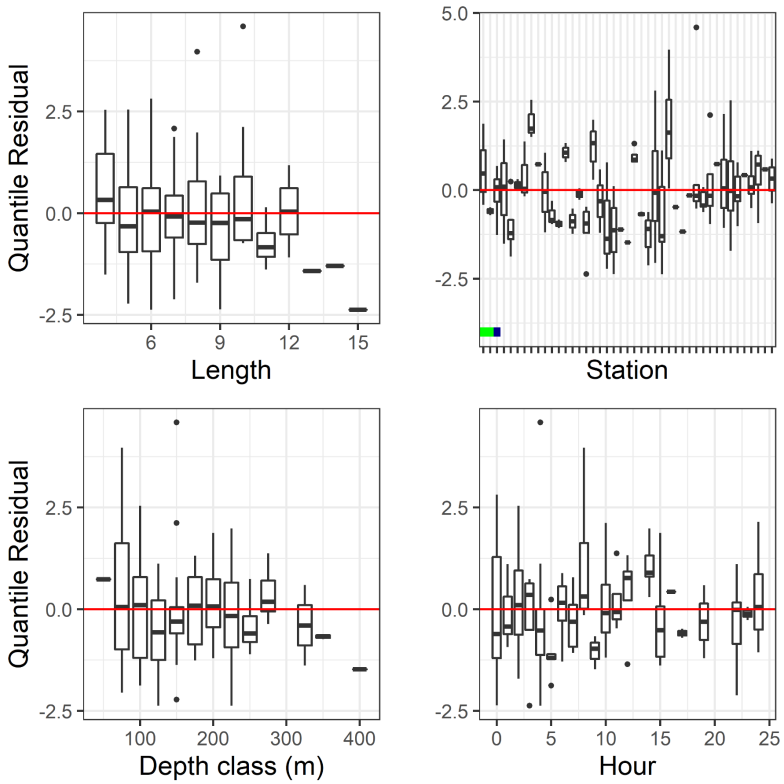

Figure 30c.Normalized quantile residuals for the selected model for Artediellus sp.

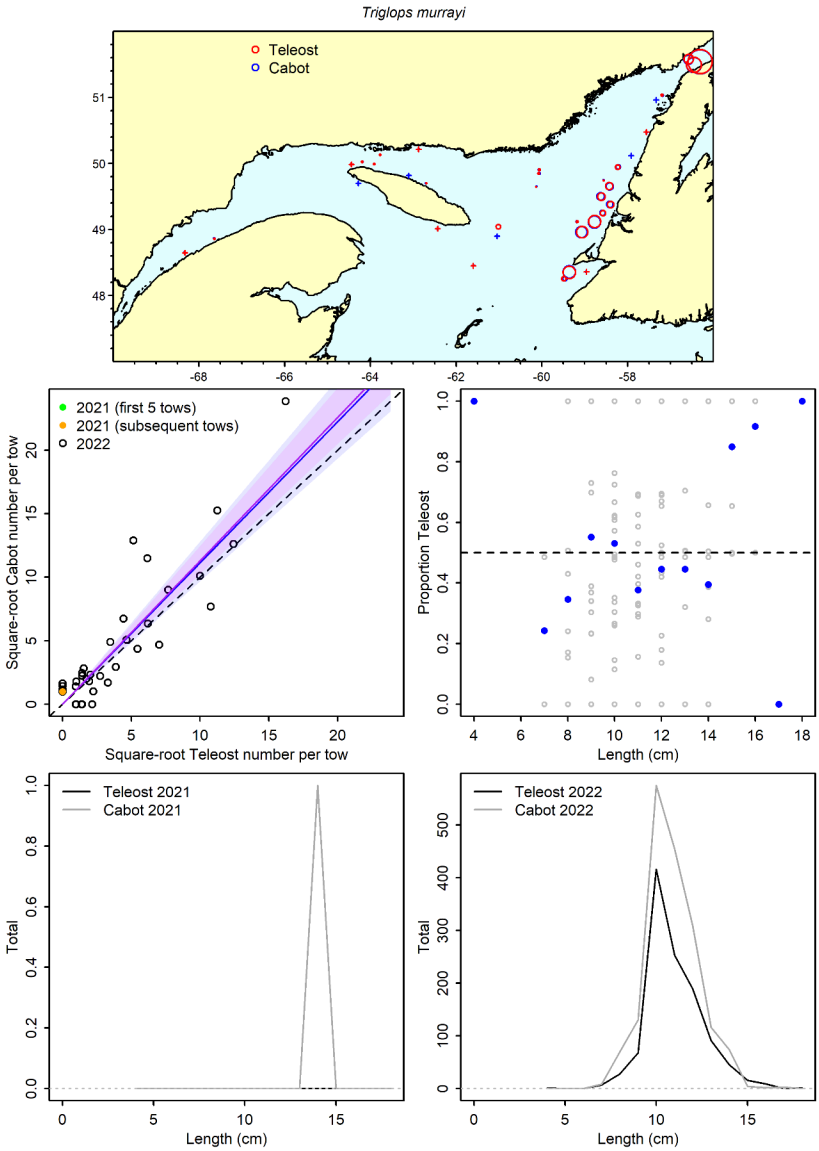

Figure 31a. Visualisation of comparative fishing data and size-aggregated model predictions for Triglops murrayi.

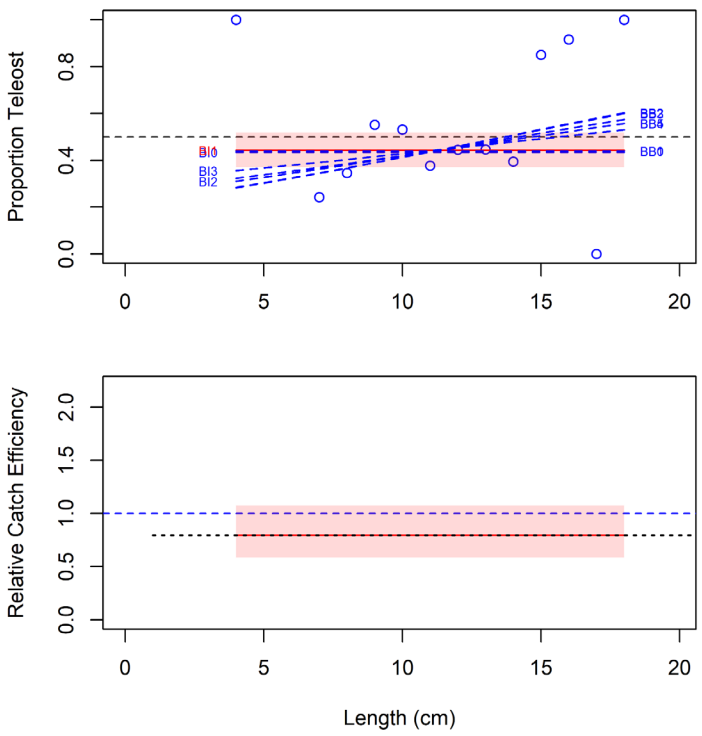

Figure 31b.Model fits and the selected length-based calibration for Triglops murrayi.

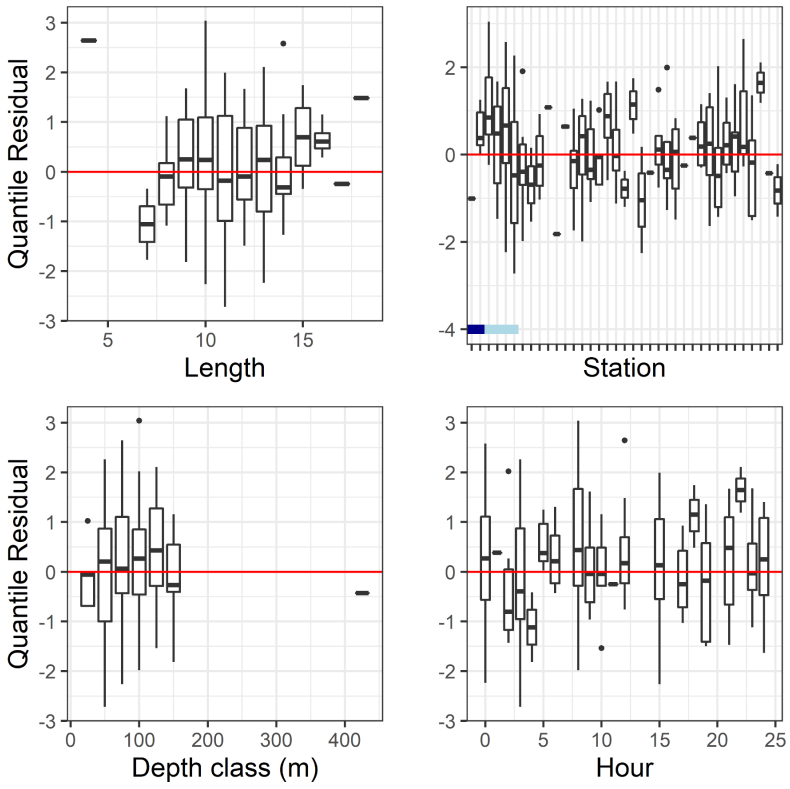

Figure 31c.Normalized quantile residuals for the selected model for Triglops murrayi.

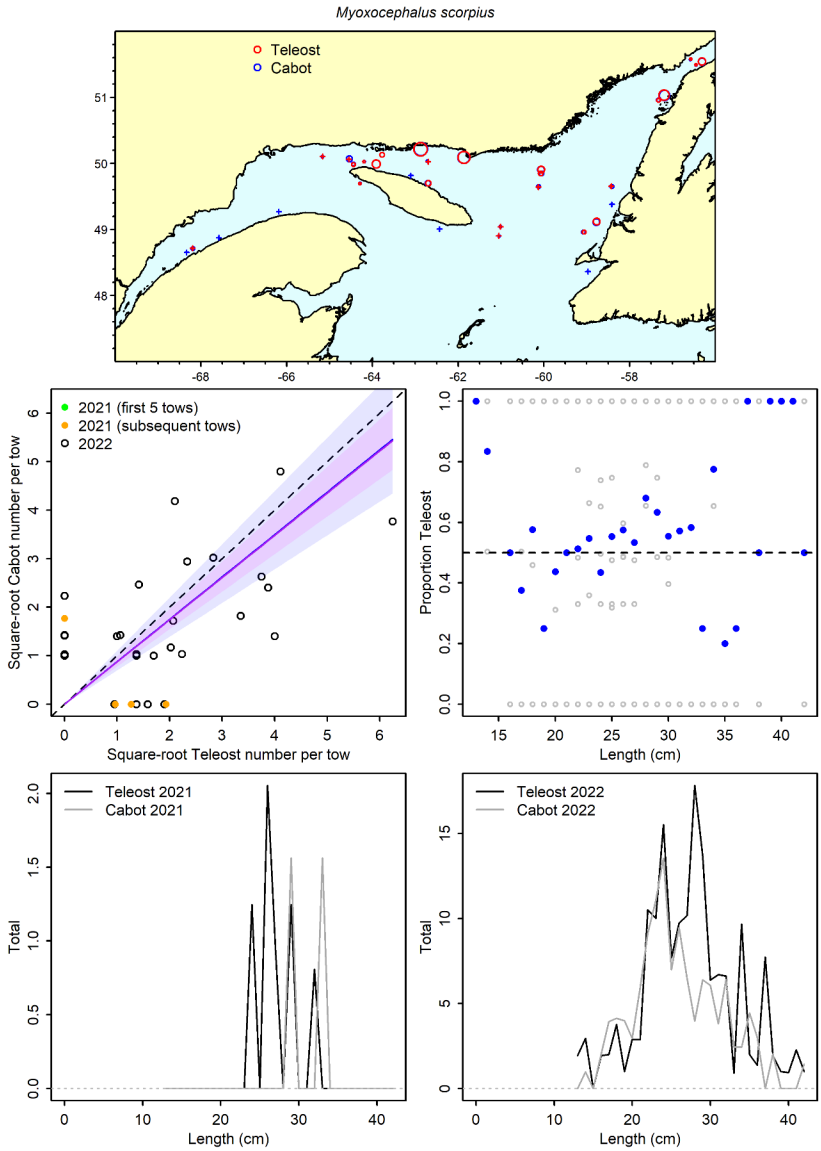

Figure 32a. Visualisation of comparative fishing data and size-aggregated model predictions for Myoxocephalus scorpius.

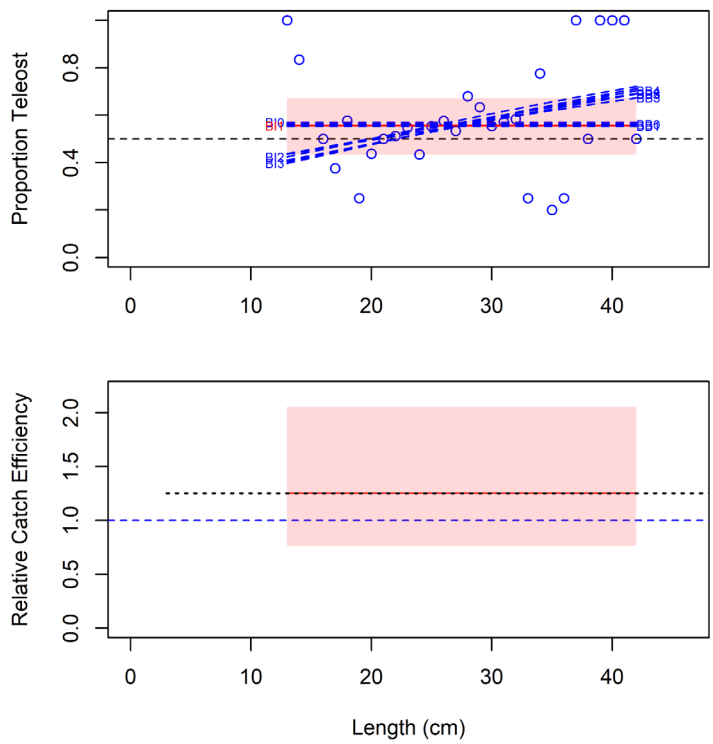

Figure 32b.Model fits and the selected length-based calibration for Myoxocephalus scorpius.

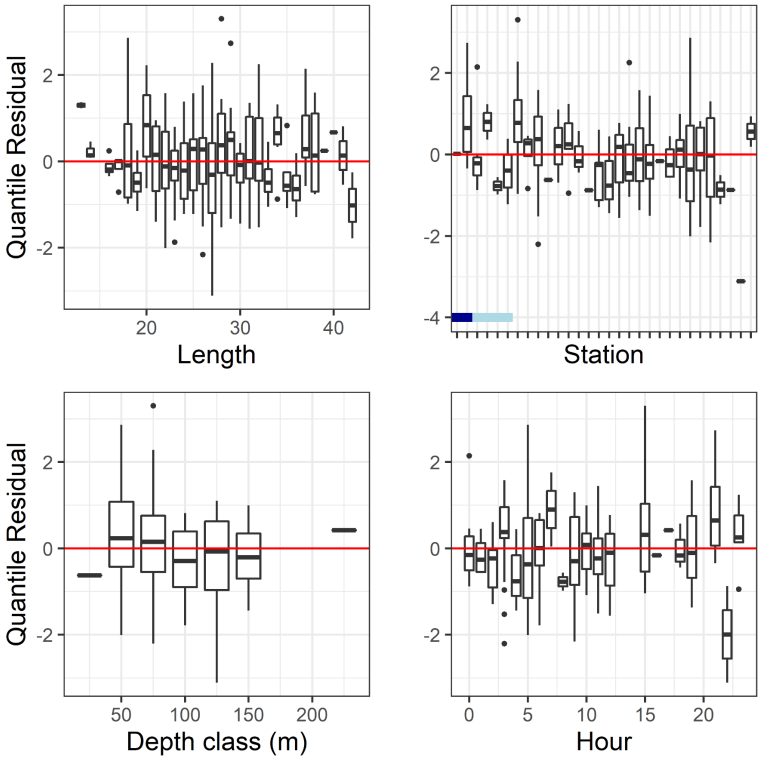

Figure 32c.Normalized quantile residuals for the selected model for Myoxocephalus scorpius.

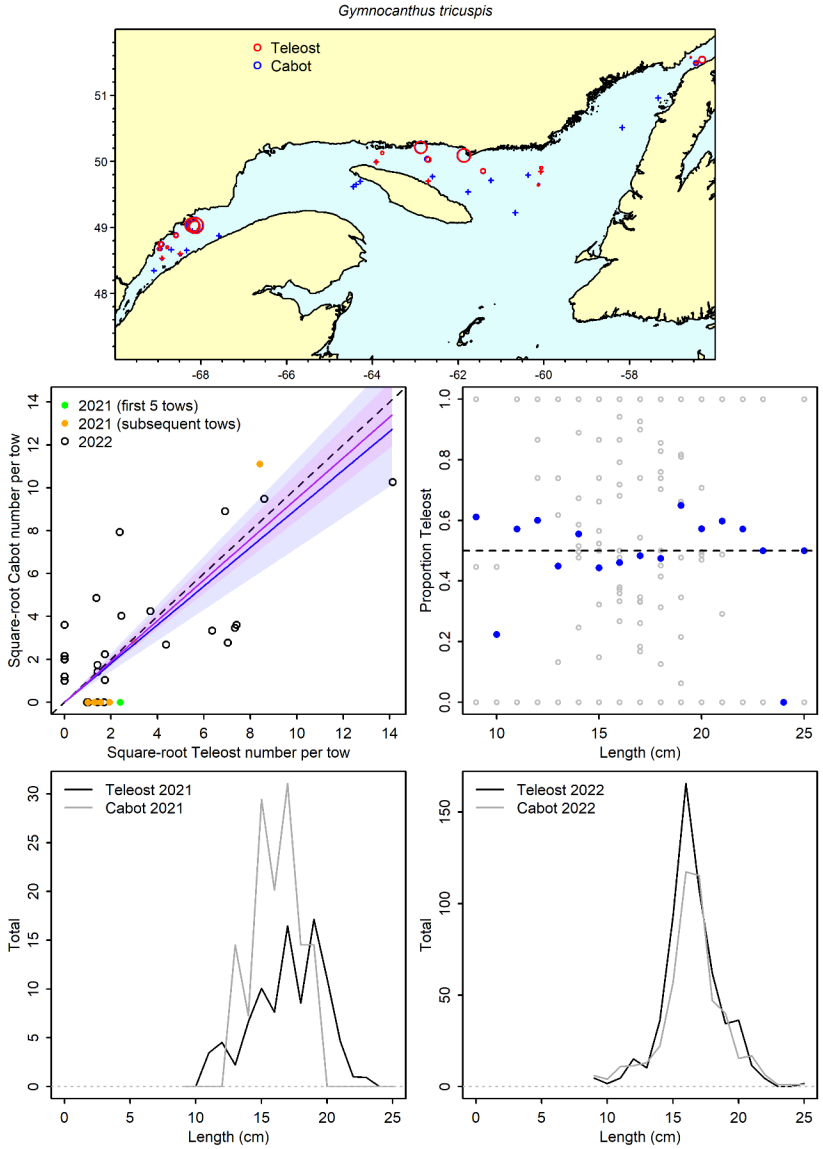

Figure 33a. Visualisation of comparative fishing data and size-aggregated model predictions for Gymnocanthus tricuspis.

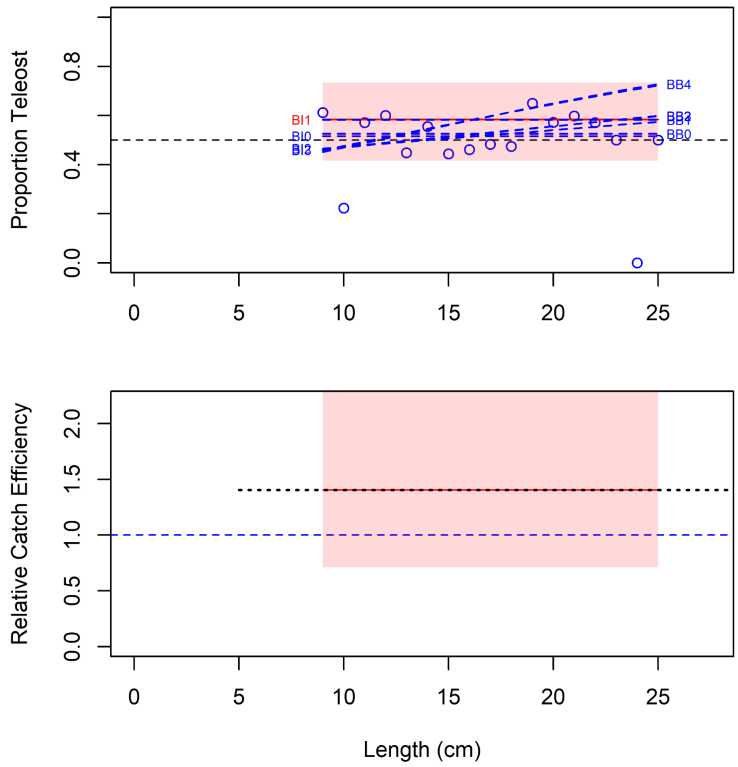

Figure 33b.Model fits and the selected length-based calibration for Gymnocanthus tricuspis.

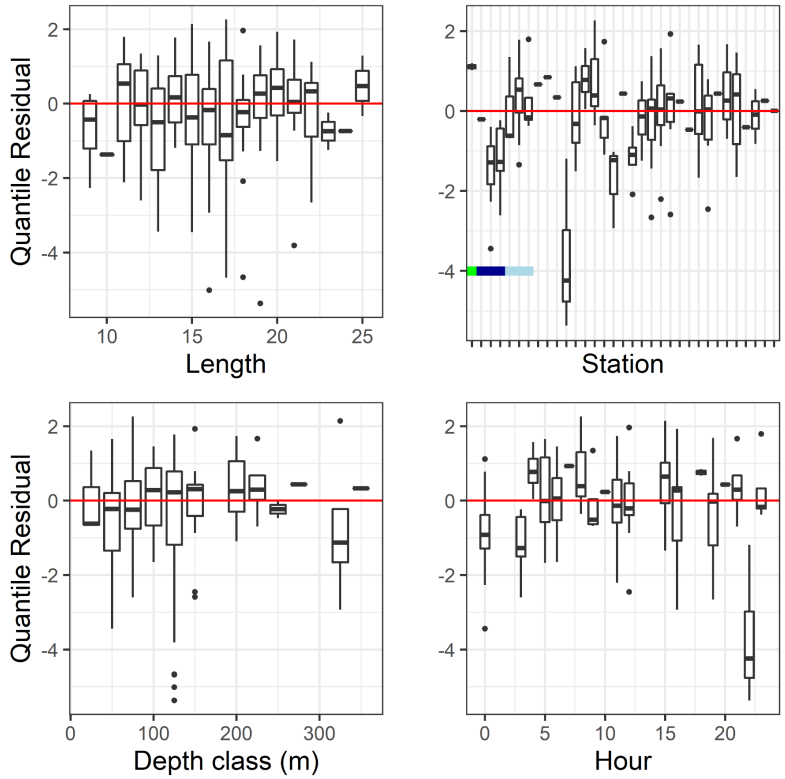

Figure 33c.Normalized quantile residuals for the selected model for Gymnocanthus tricuspis.

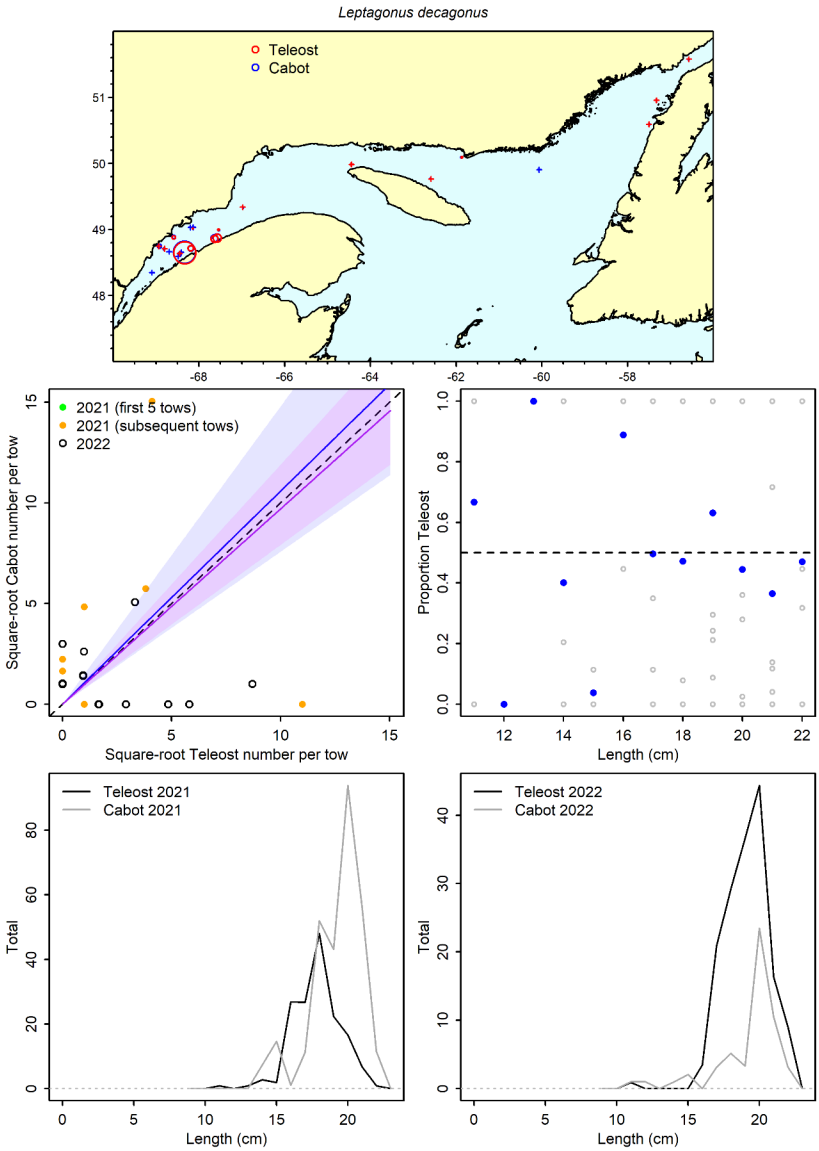

Figure 34a. Visualisation of comparative fishing data and size-aggregated model predictions for Leptagonus decagonus.

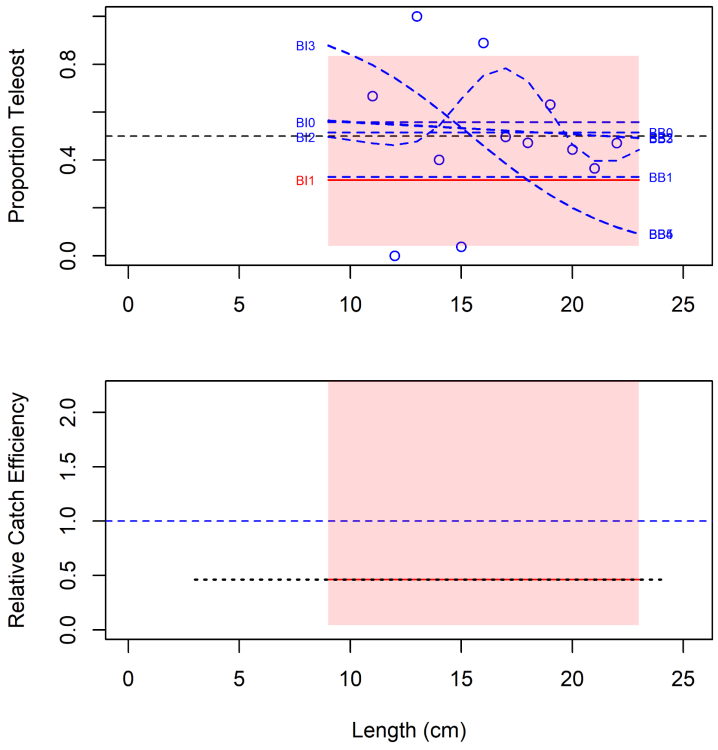

Figure 34b.Model fits and the selected length-based calibration for Leptagonus decagonus.

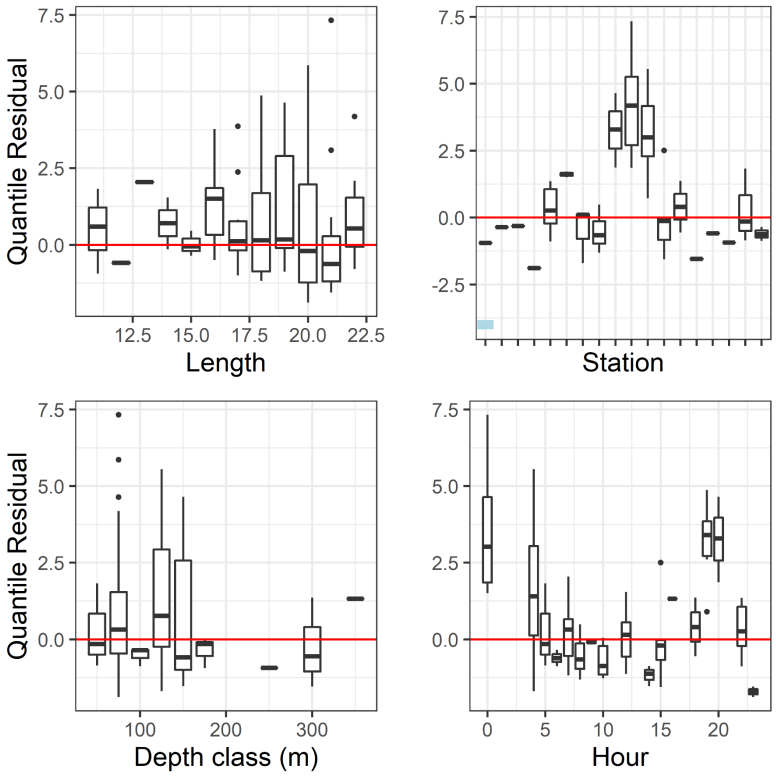

Figure 34c.Normalized quantile residuals for the selected model for Leptagonus decagonus.

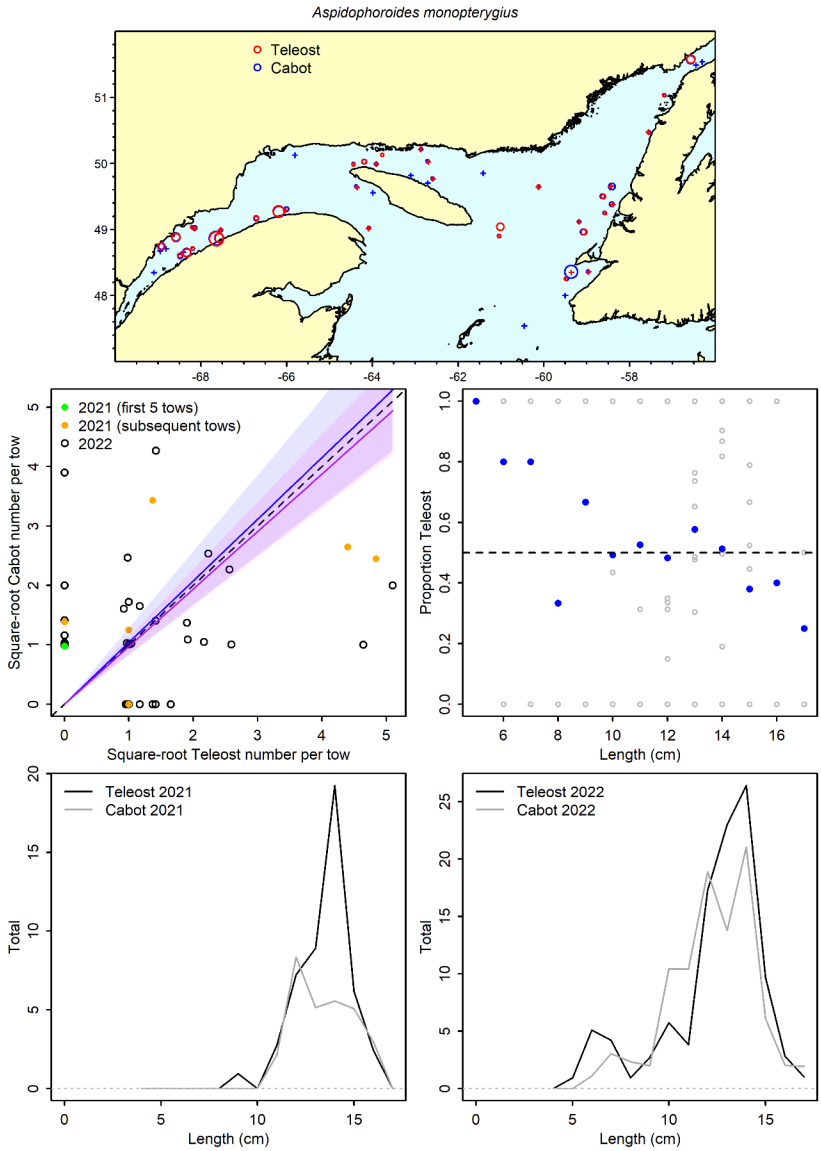

Figure 35a. Visualisation of comparative fishing data and size-aggregated model predictions for Aspidophoroides monopterygius.

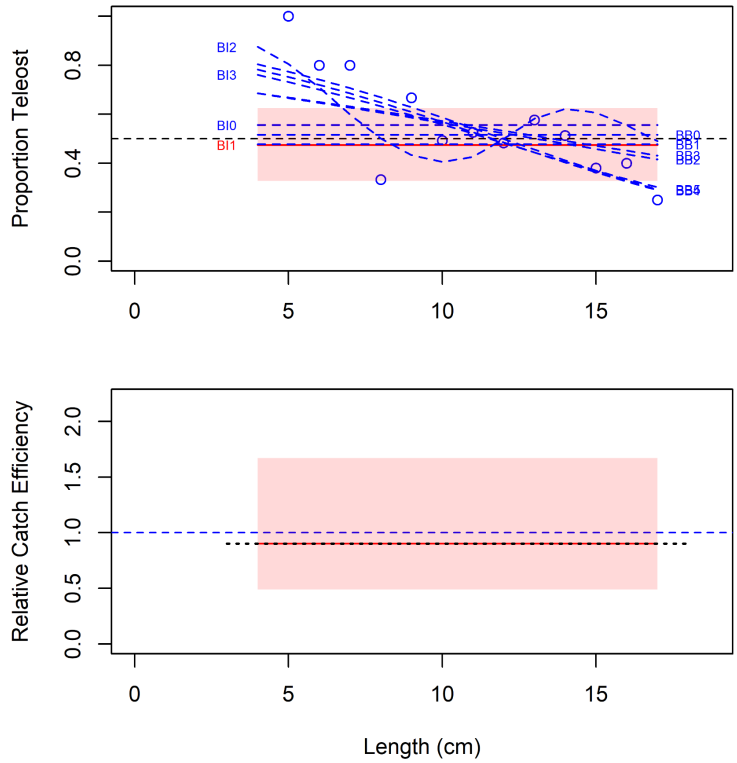

Figure 35b.Model fits and the selected length-based calibration for Aspidophoroides monopterygius.

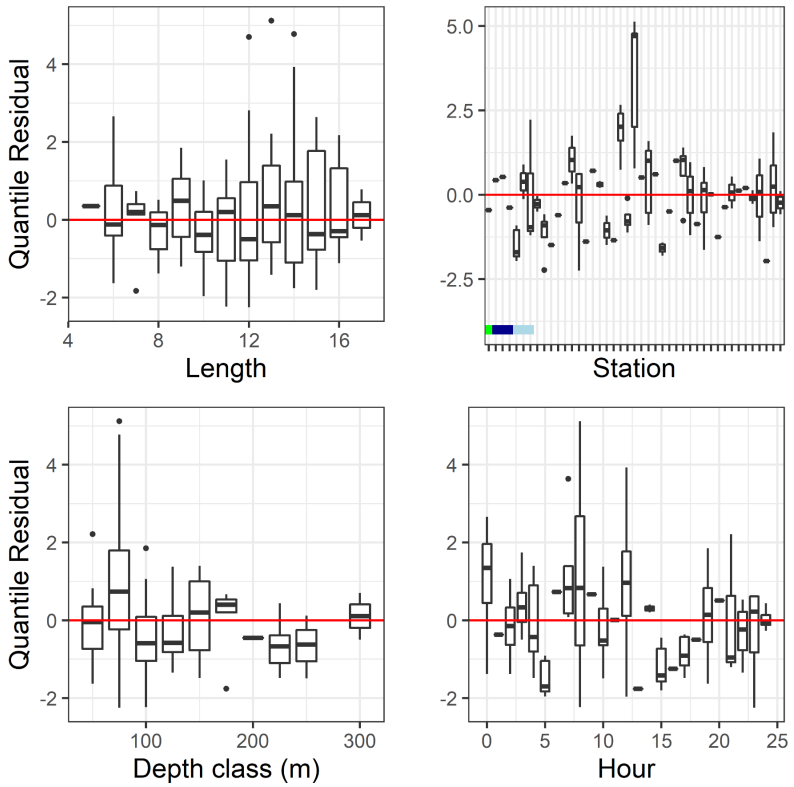

Figure 35c.Normalized quantile residuals for the selected model for Aspidophoroides monopterygius.

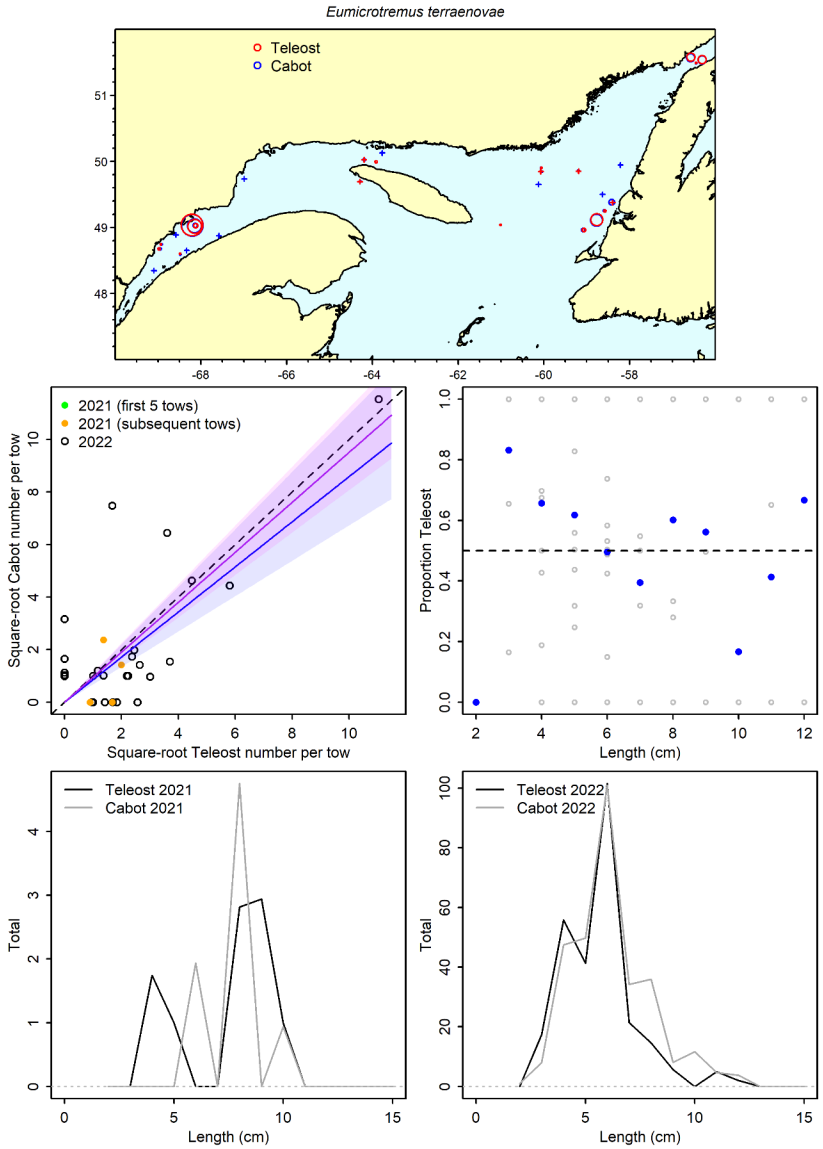

Figure 36a. Visualisation of comparative fishing data and size-aggregated model predictions for Eumicrotremus terraenovae.

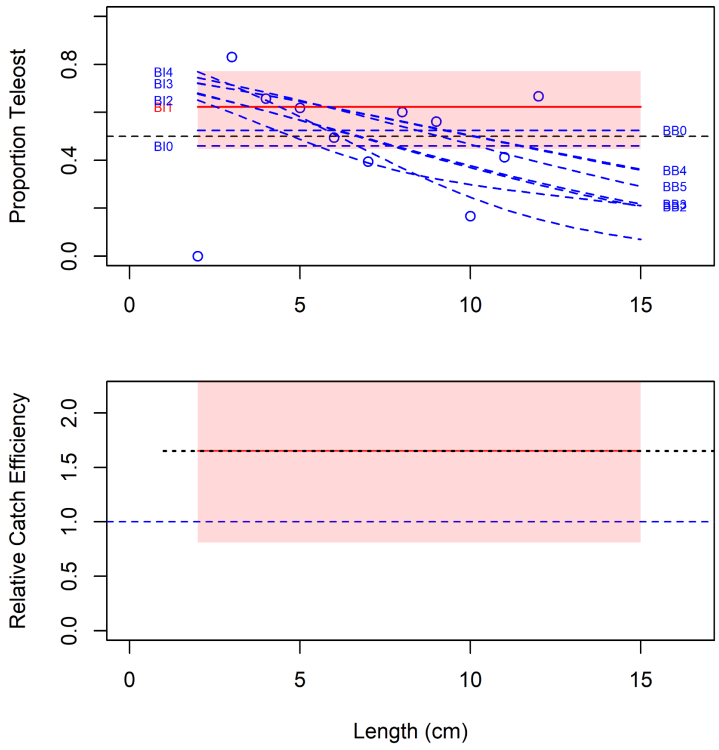

Figure 36b.Model fits and the selected length-based calibration for Eumicrotremus terraenovae.

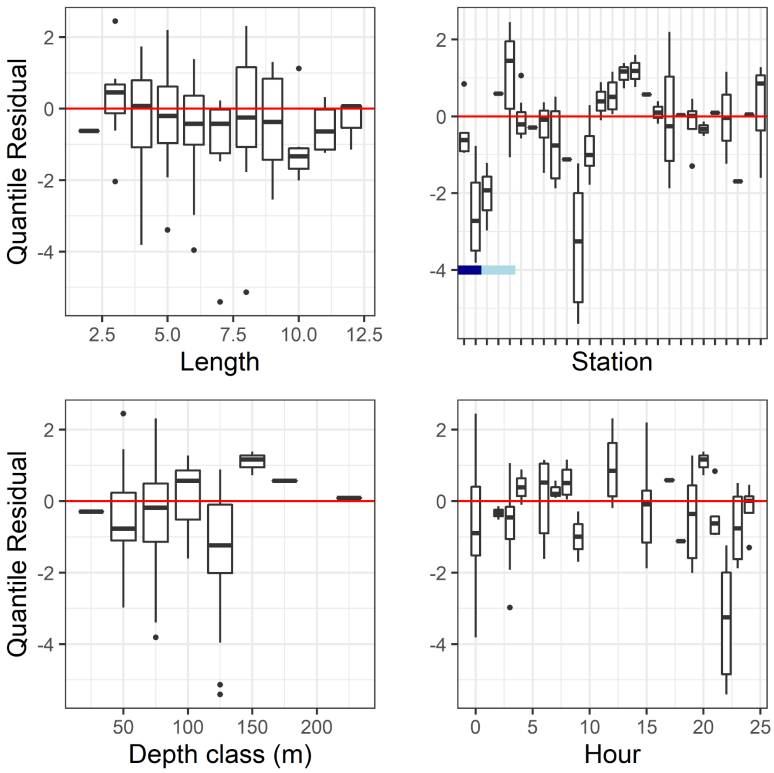

Figure 36c.Normalized quantile residuals for the selected model for Eumicrotremus terraenovae.

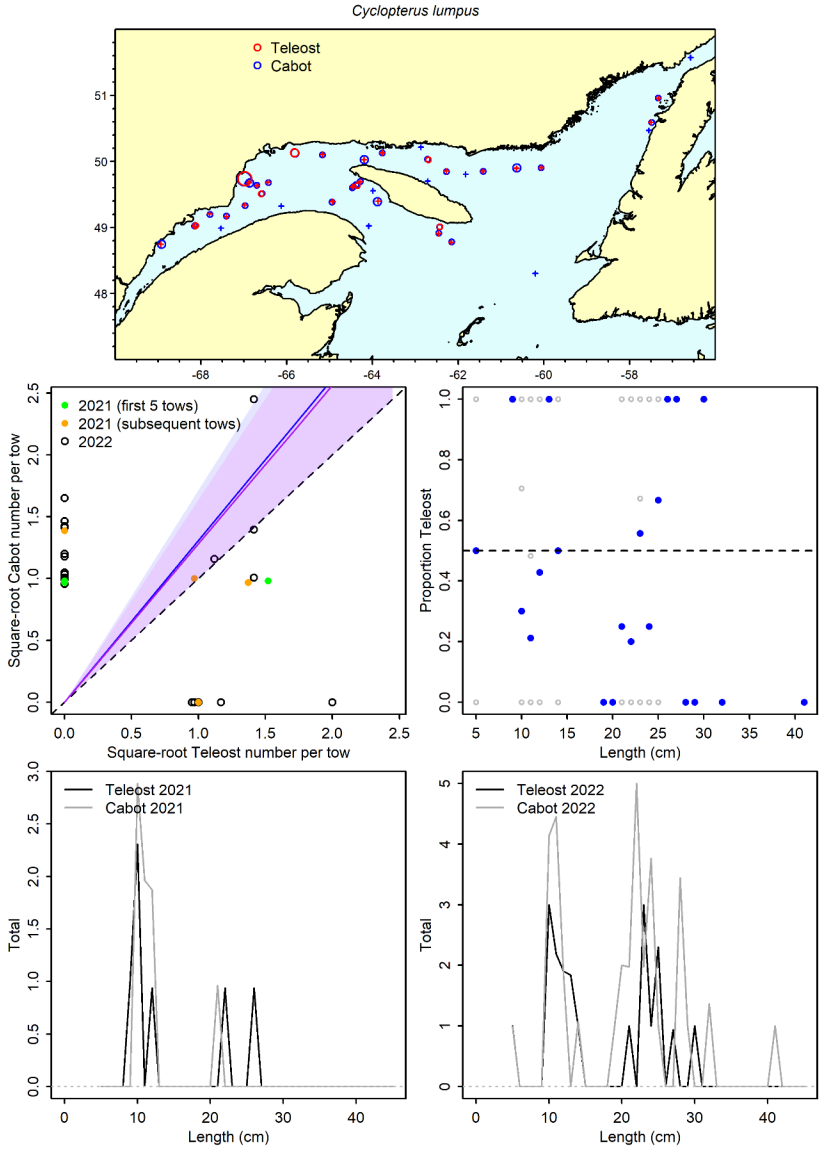

Figure 37a. Visualisation of comparative fishing data and size-aggregated model predictions for Cyclopterus lumpus.

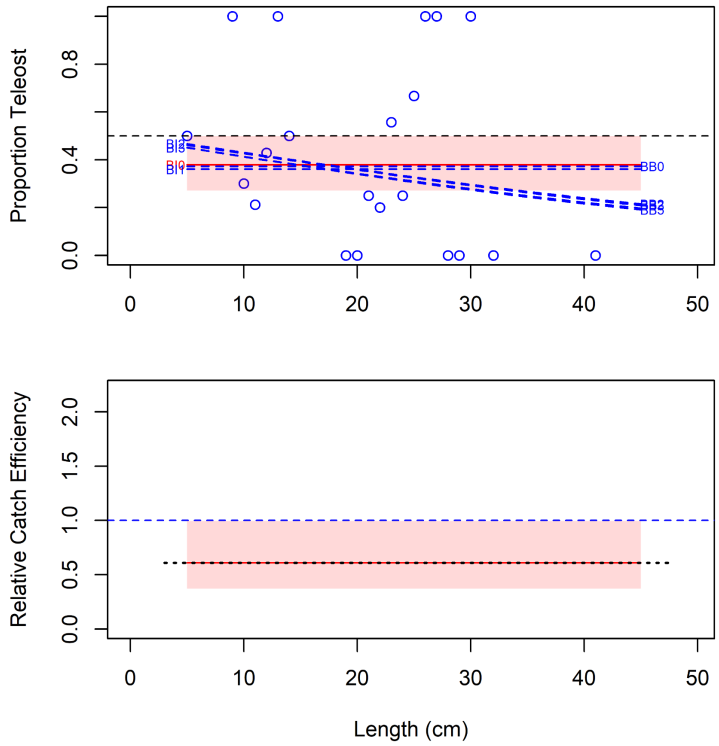

Figure 37b.Model fits and the selected length-based calibration for Cyclopterus lumpus.

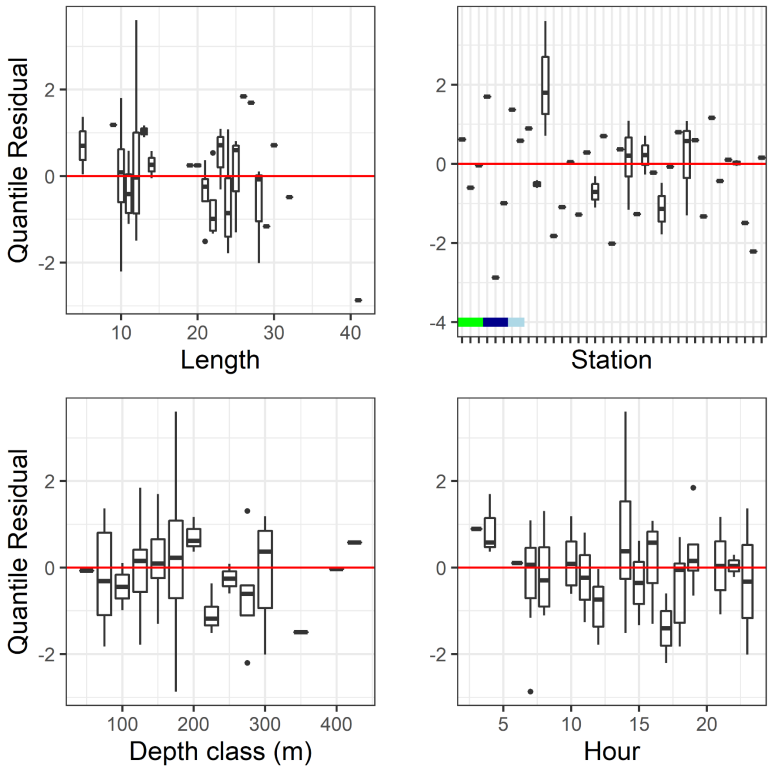

Figure 37c.Normalized quantile residuals for the selected model for Cyclopterus lumpus.

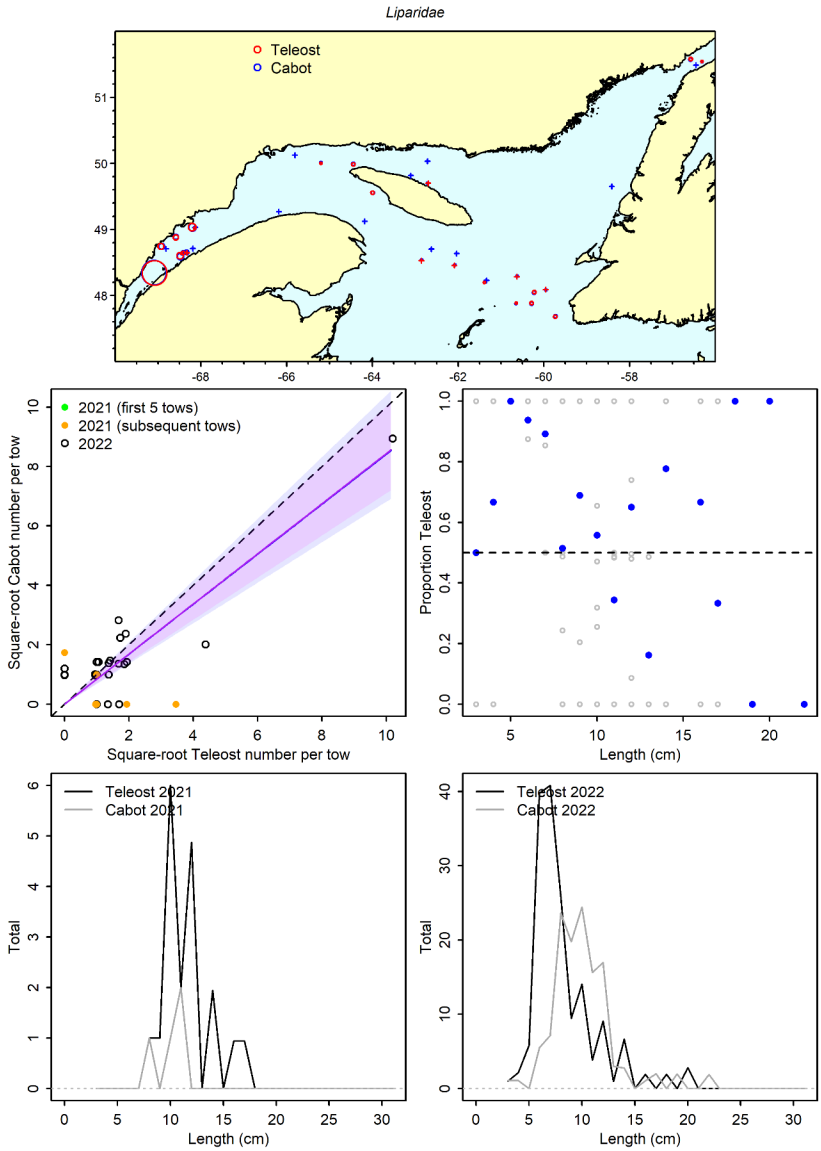

Figure 38a. Visualisation of comparative fishing data and size-aggregated model predictions for Liparidae.

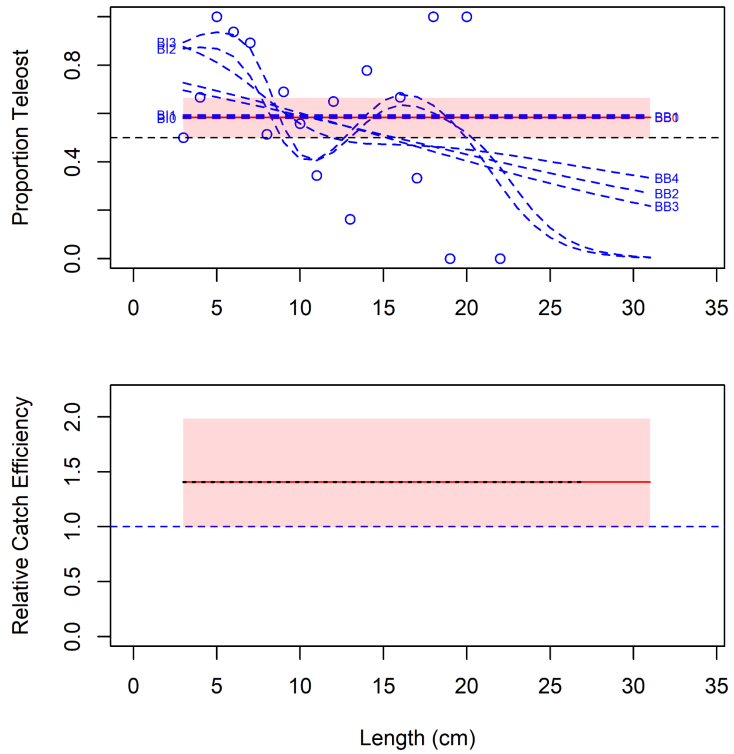

Figure 38b.Model fits and the selected length-based calibration for Liparidae.

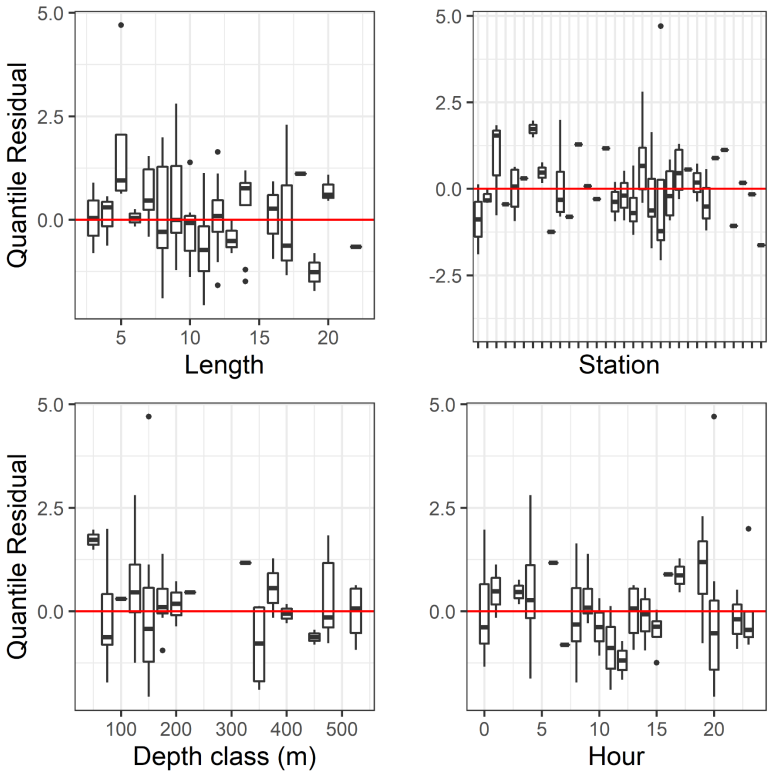

Figure 38c.Normalized quantile residuals for the selected model for Liparidae.

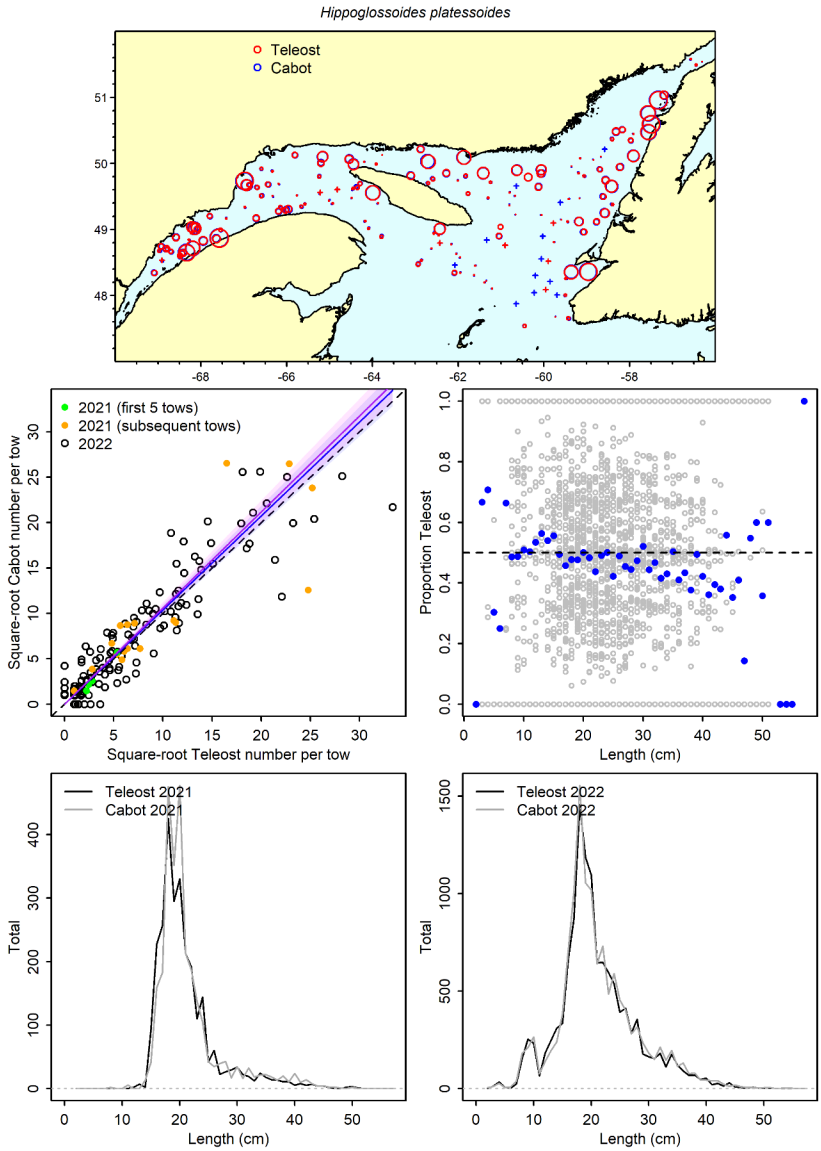

Figure 39a.Visualisation of comparative fishing data and size-aggregated model predictions for Hippoglossoides platessoides.

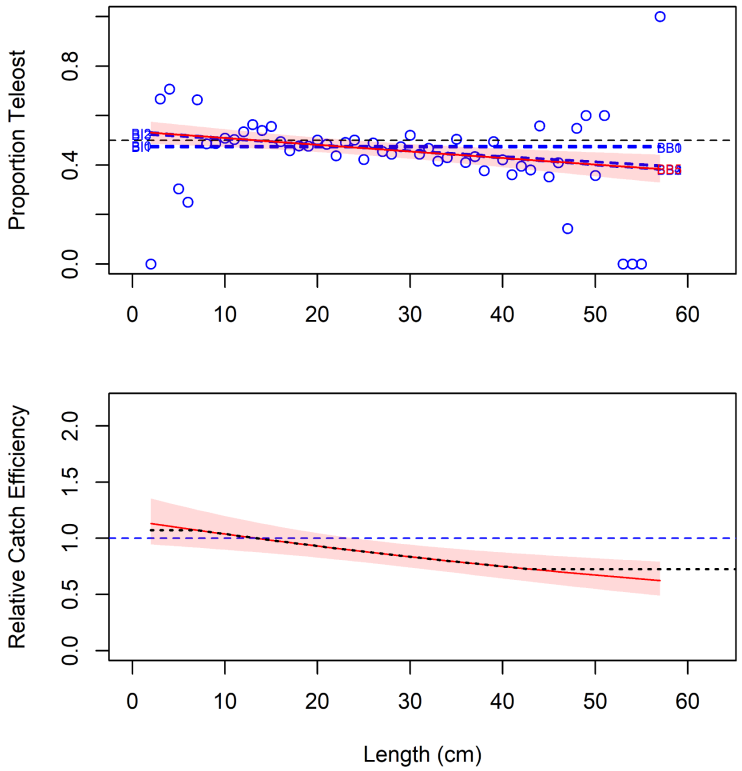

Figure 39b.Model fits and the selected length-based calibration for Hippoglossoides platessoides.

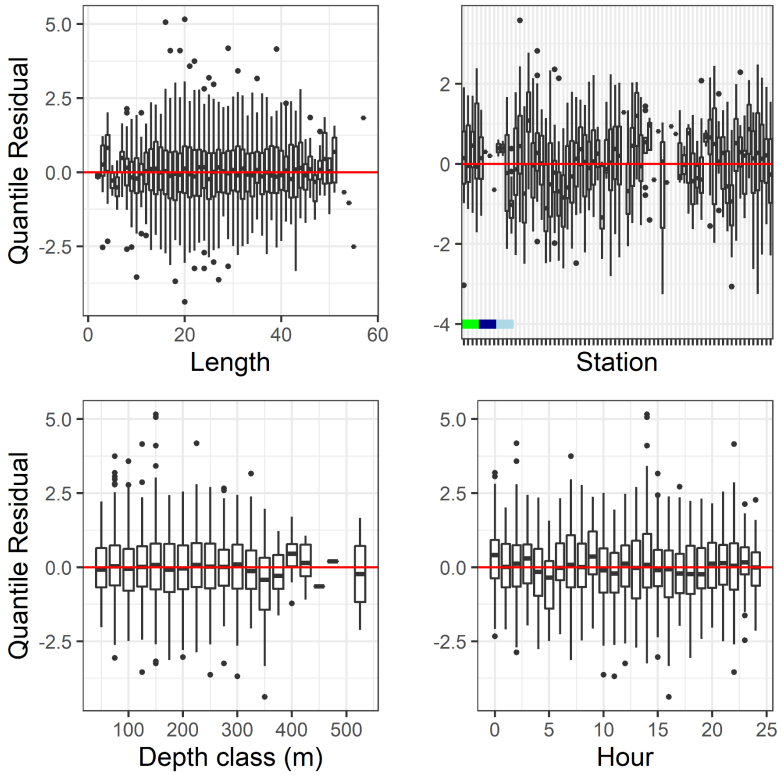

Figure 39c.Normalized quantile residuals for the selected model for Hippoglossoides platessoides.

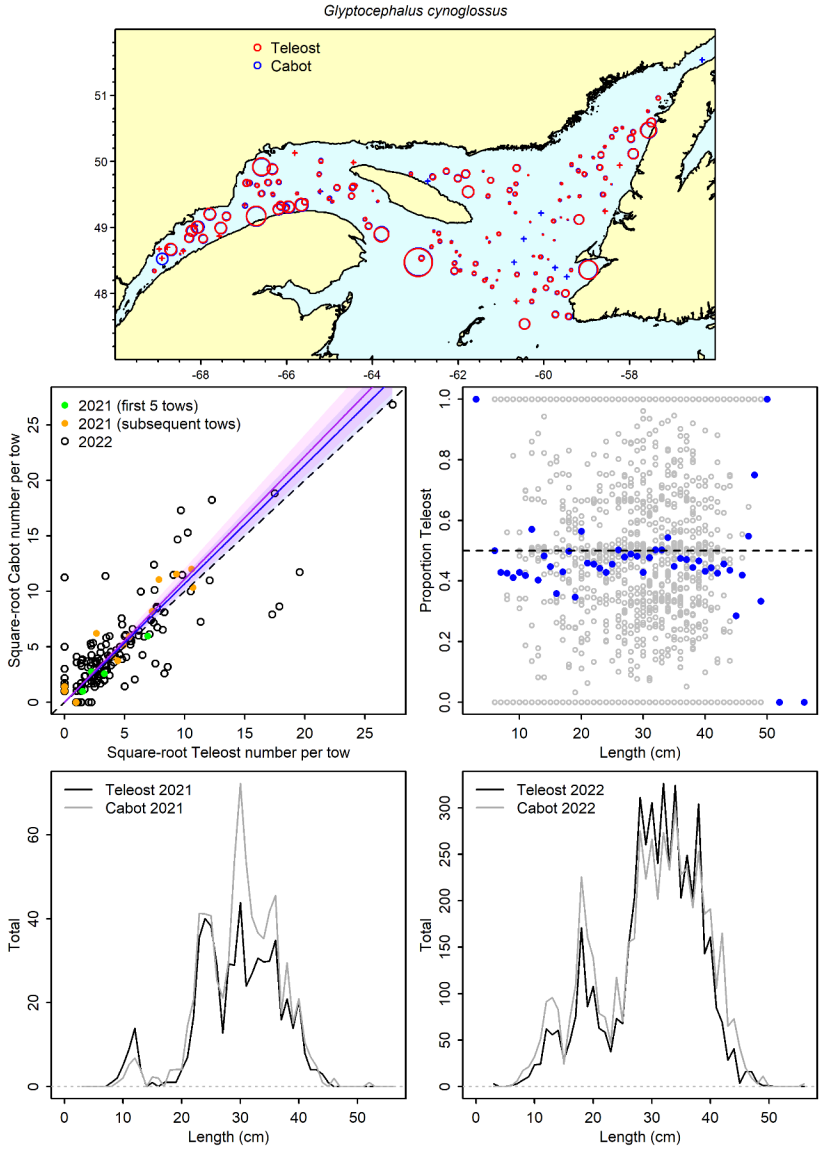

Figure 40a. Visualisation of comparative fishing data and size-aggregated model predictions for Glyptocephalus cynoglossus.

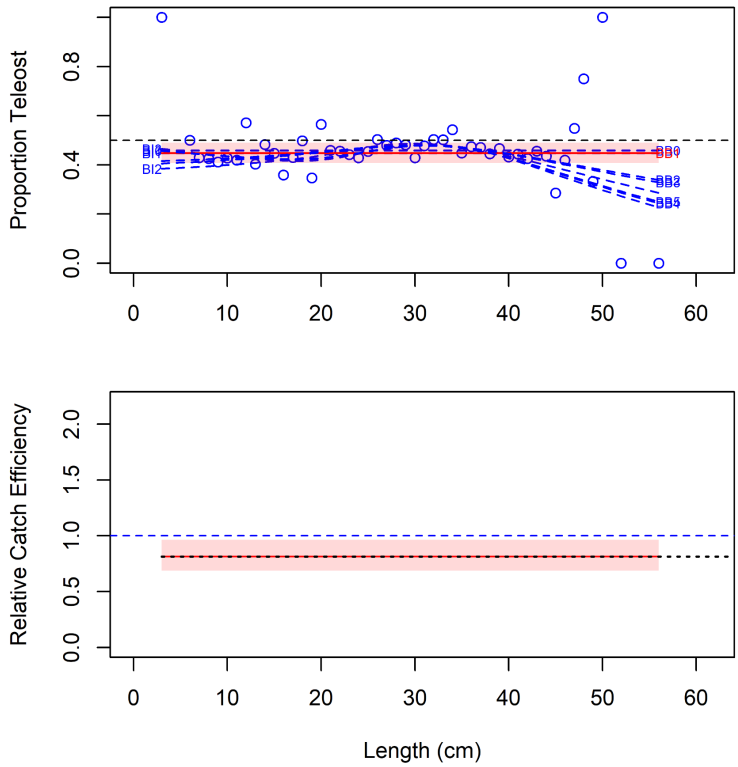

Figure 40b.Model fits and the selected length-based calibration for Glyptocephalus cynoglossus.

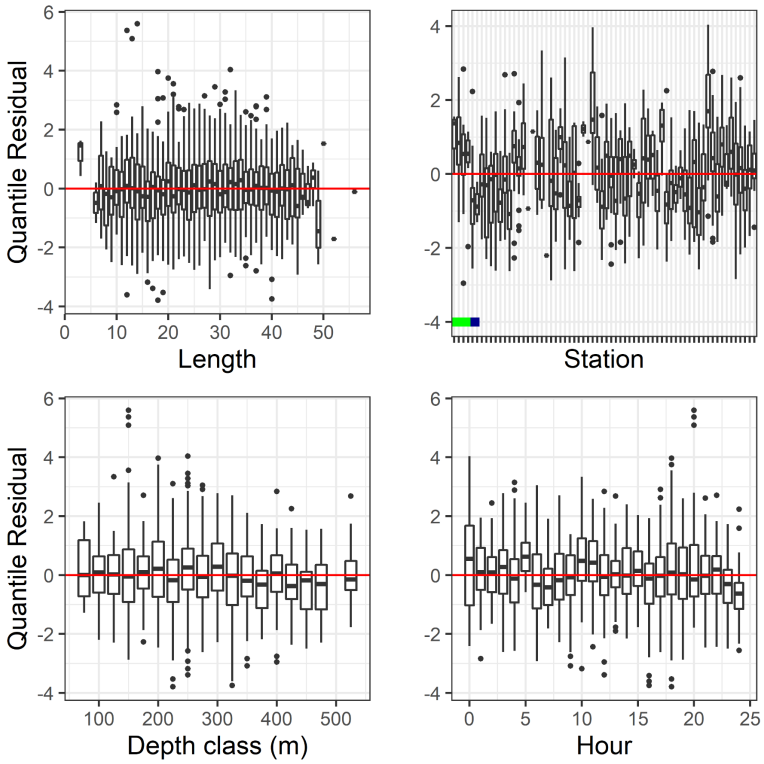

Figure 40c.Normalized quantile residuals for the selected model for Glyptocephalus cynoglossus.

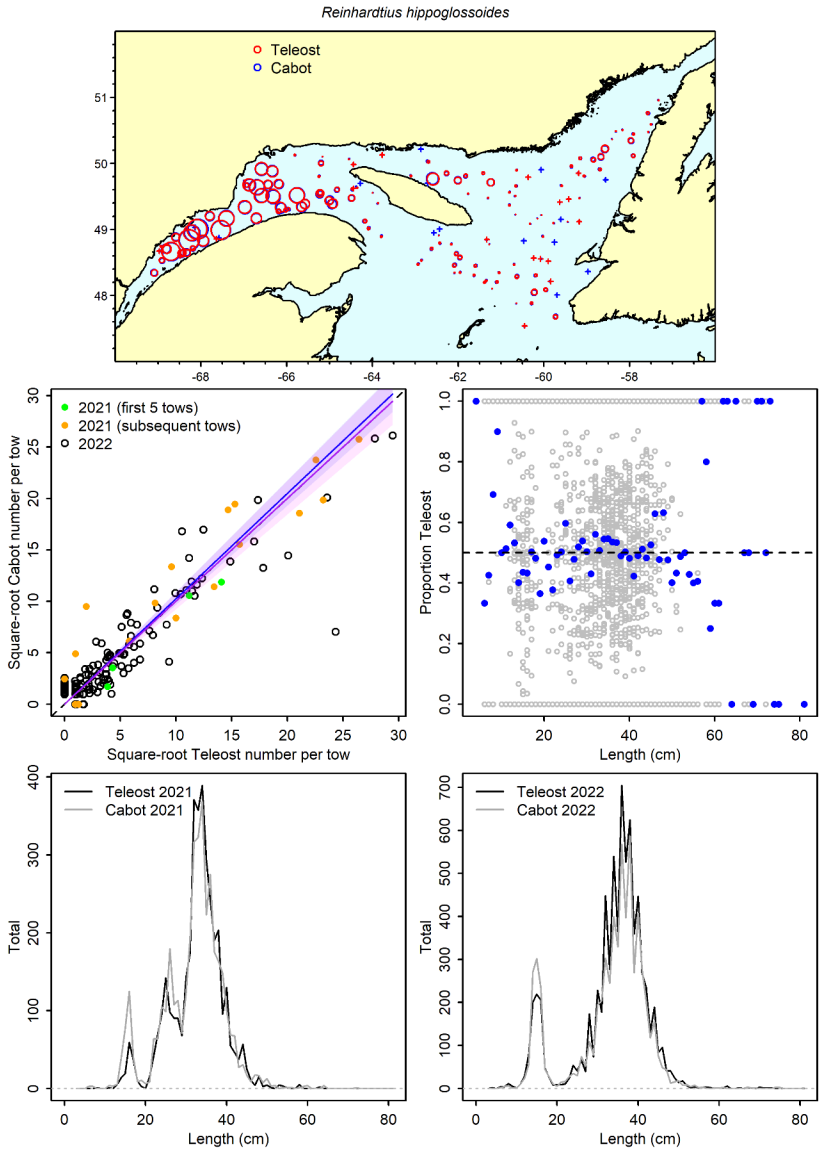

Figure 41a.Visualisation of comparative fishing data and size-aggregated model predictions for Reinhardtius hippoglossoides.

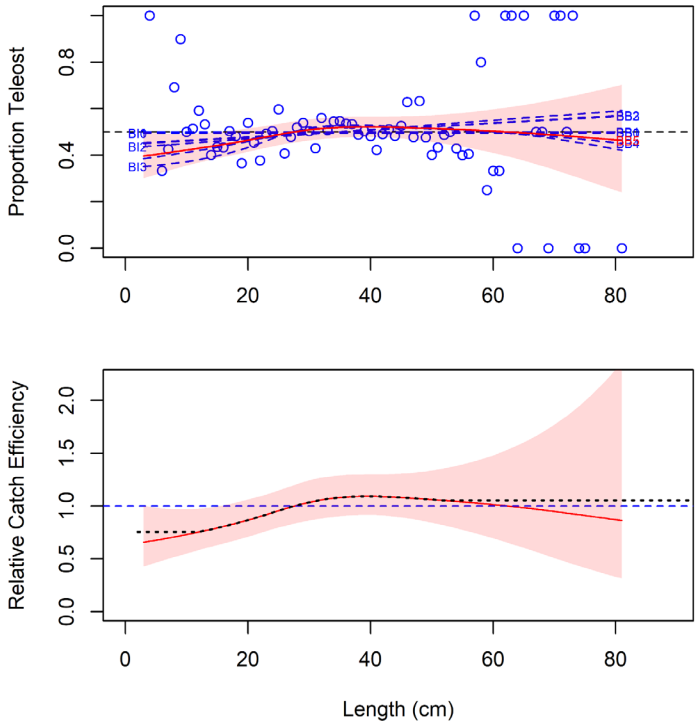

Figure 41b.Model fits and the selected length-based calibration for Reinhardtius hippoglossoides.

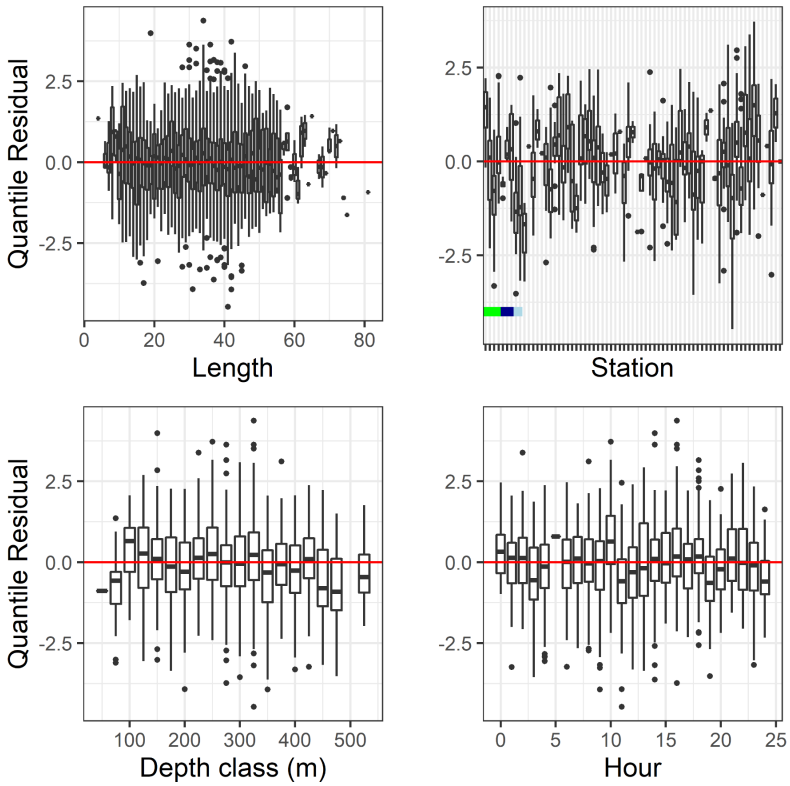

Figure 41c.Normalized quantile residuals for the selected model for Reinhardtius hippoglossoides.

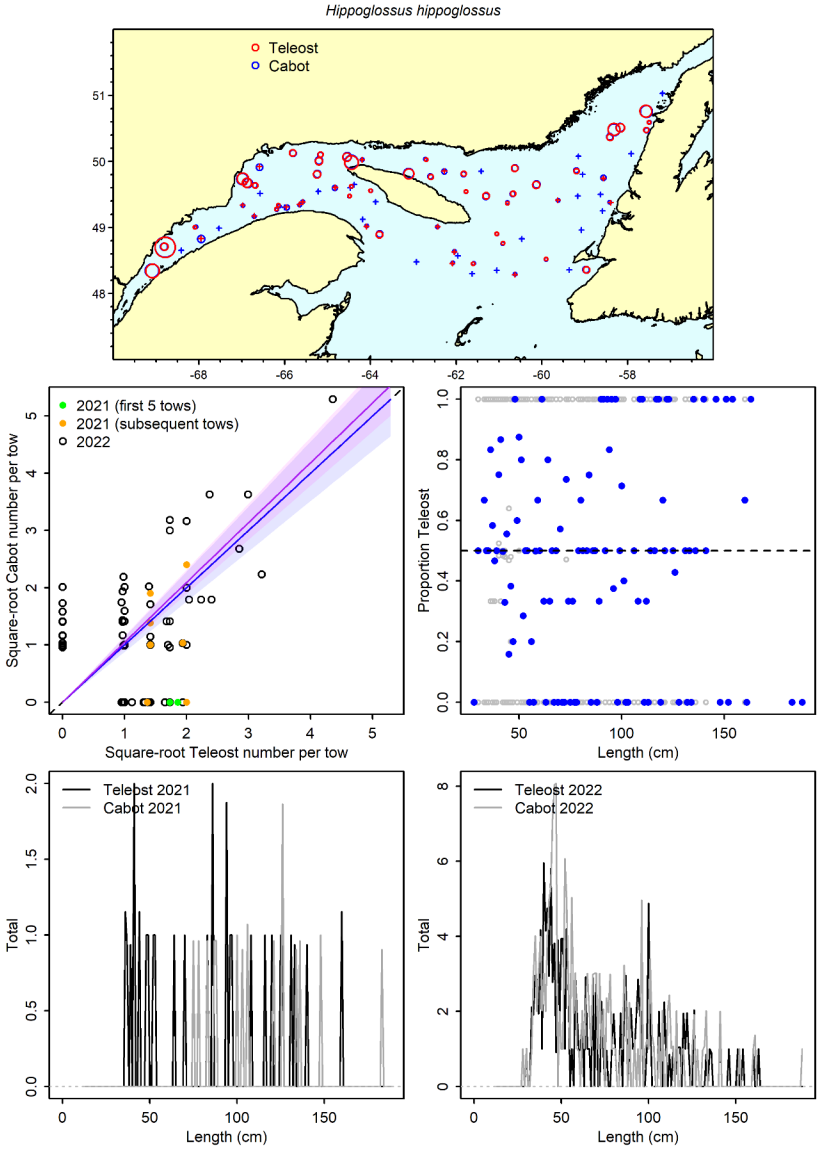

Figure 42a. Visualisation of comparative fishing data and size-aggregated model predictions for Hippoglossus hippoglossus.

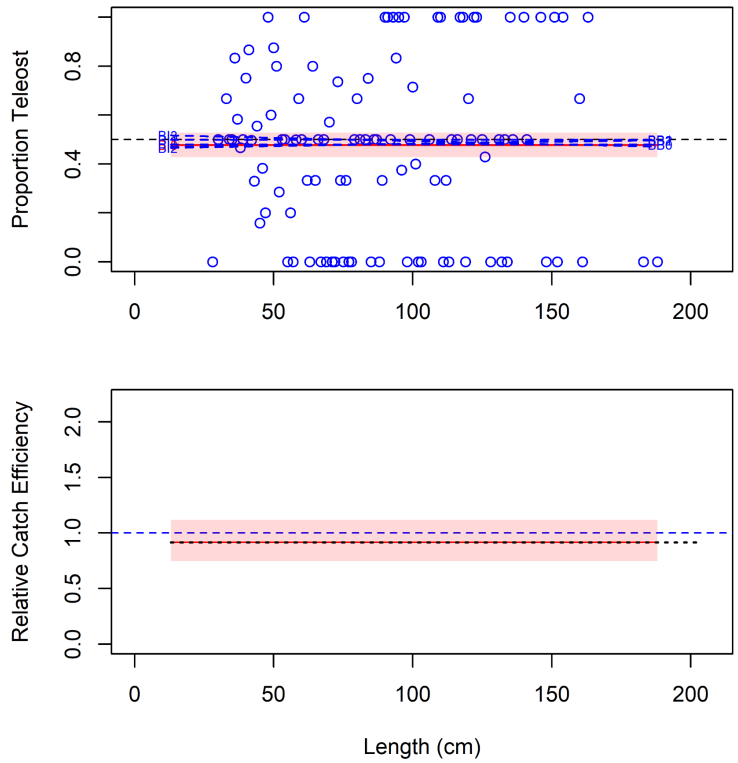

Figure 42b.Model fits and the selected length-based calibration for Hippoglossus hippoglossus.

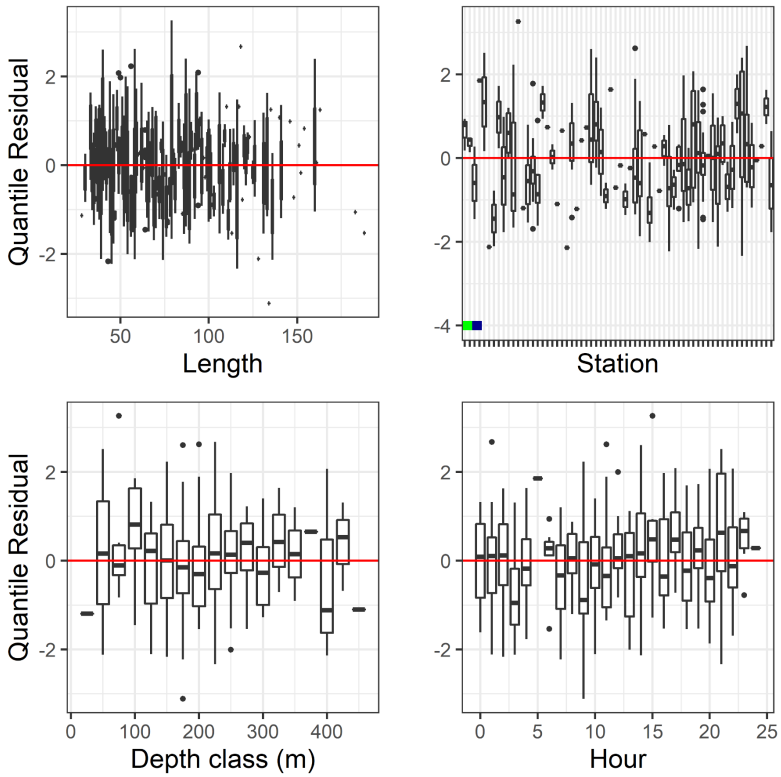

Figure 42c.Normalized quantile residuals for the selected model for Hippoglossus hippoglossus.

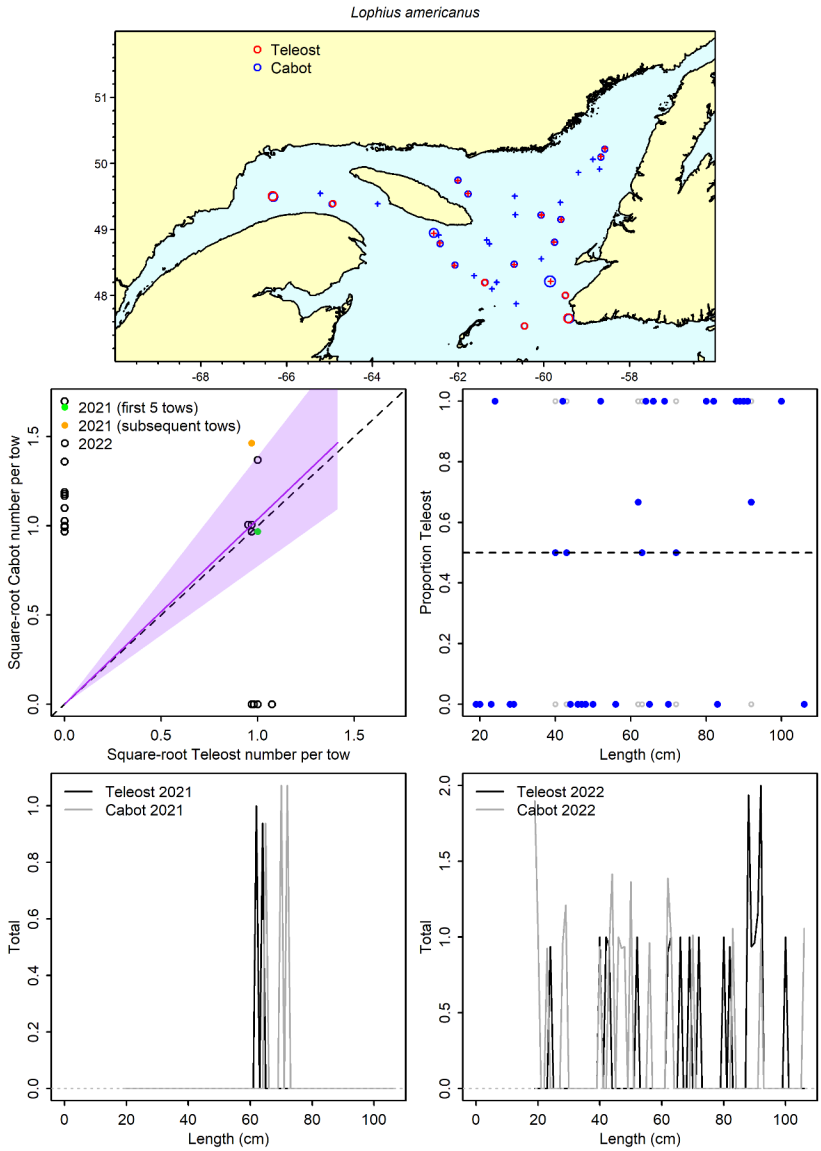

Figure 43a. Visualisation of comparative fishing data and size-aggregated model predictions for Lophius americanus.

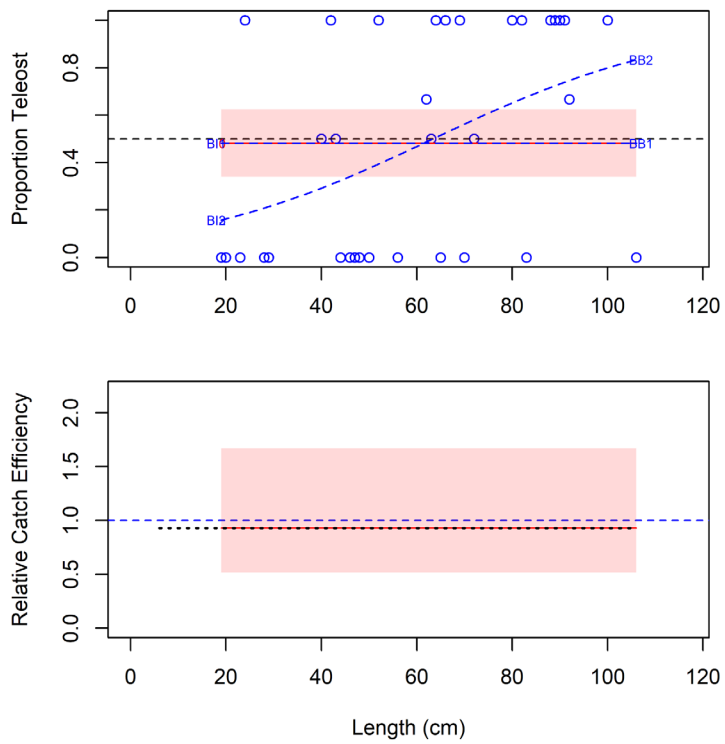

Figure 43b.Model fits and the selected length-based calibration for Lophius americanus.

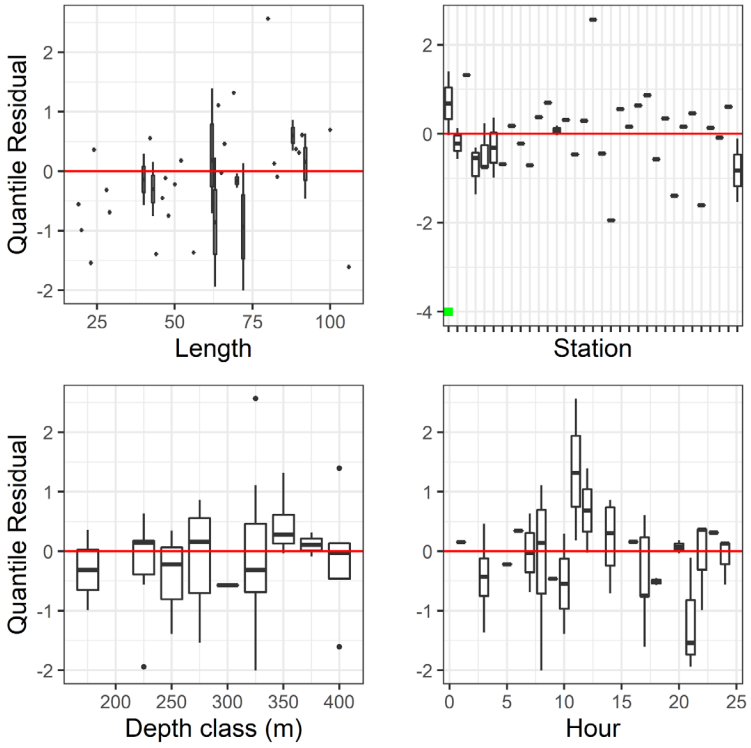

Figure 43c.Normalized quantile residuals for the selected model for Lophius americanus.

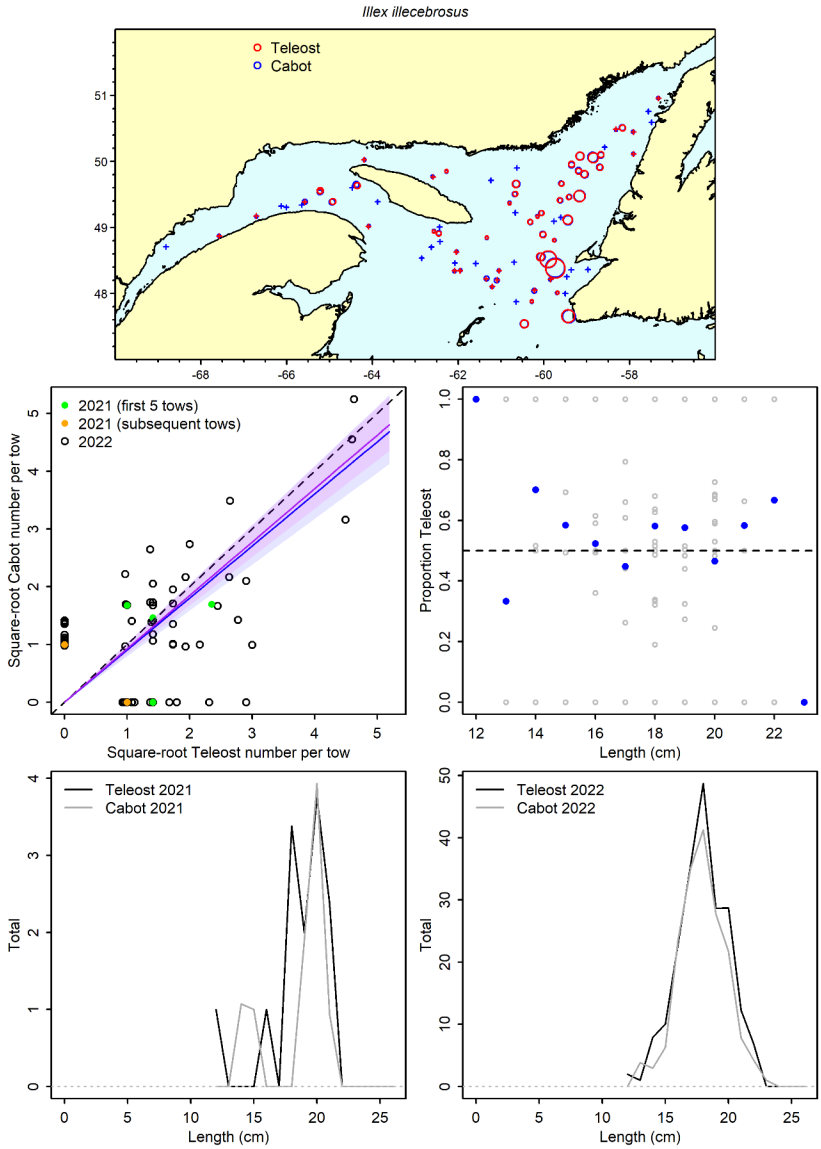

Figure 44a.Visualisation of comparative fishing data and size-aggregated model predictions for Illex illecebrosus.

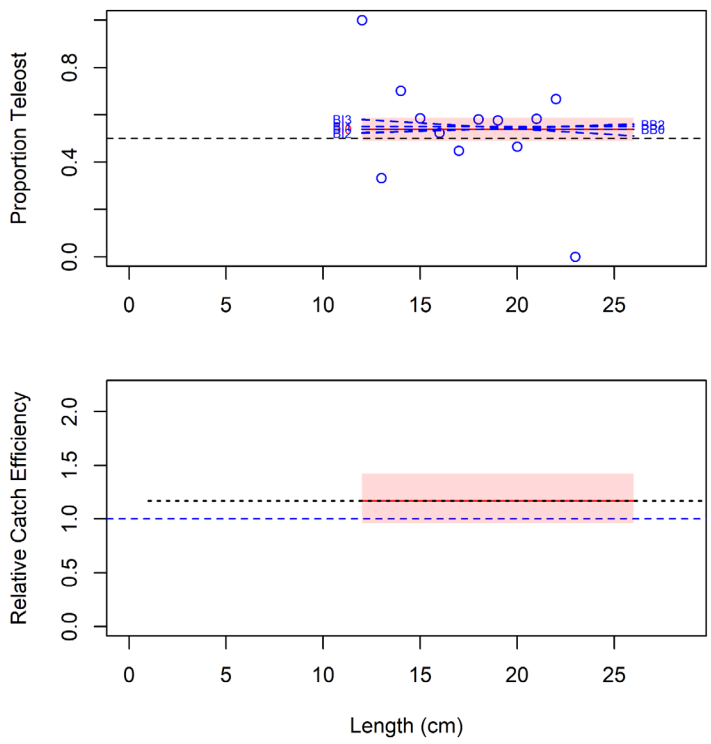

Figure 44b.Model fits and the selected length-based calibration for Illex illecebrosus.

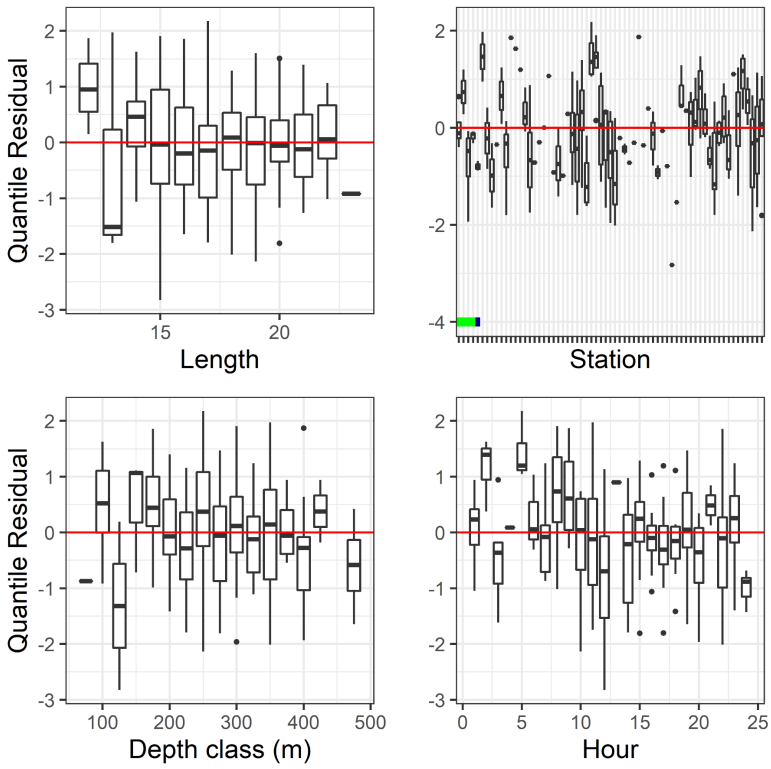

Figure 44c.Normalized quantile residuals for the selected model for Illex illecebrosus.

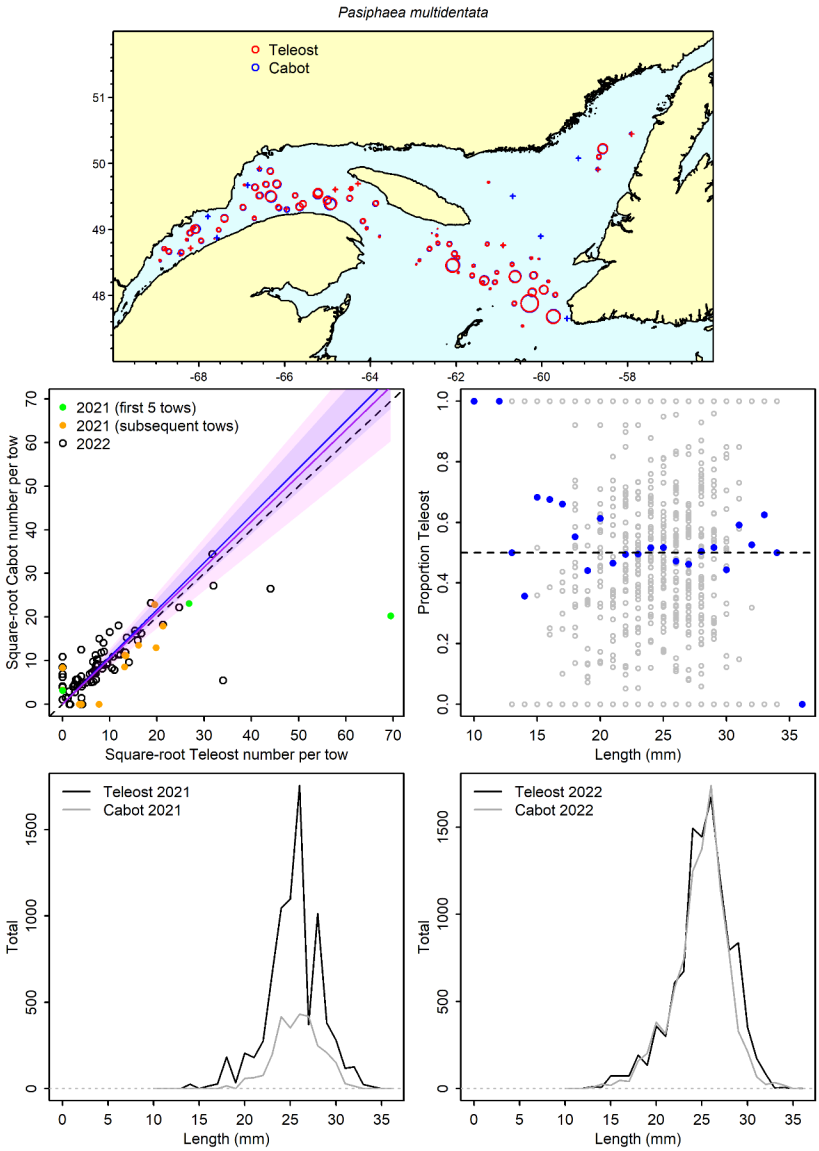

Figure 45a. Visualisation of comparative fishing data and size-aggregated model predictions for Pasiphaea multidentata.

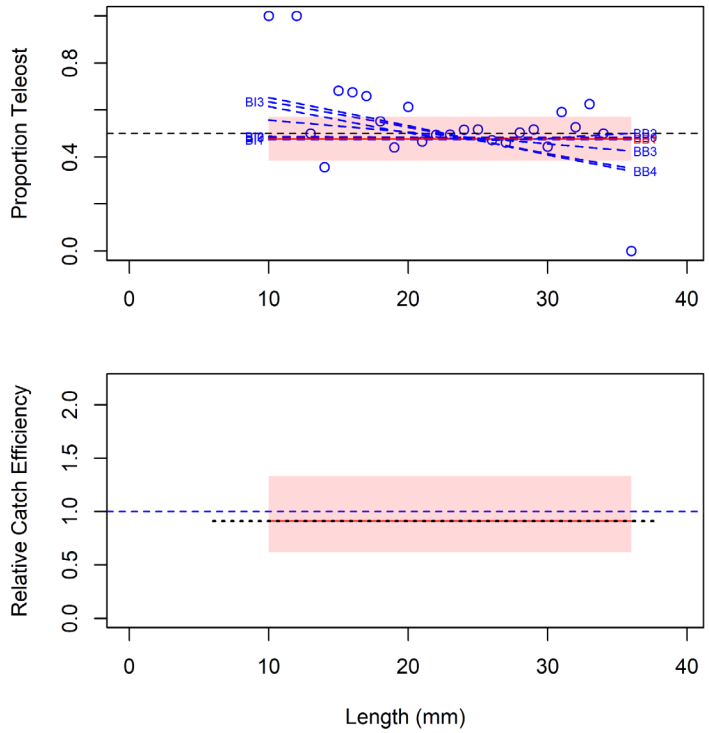

Figure 45b.Model fits and the selected length-based calibration for Pasiphaea multidentata.

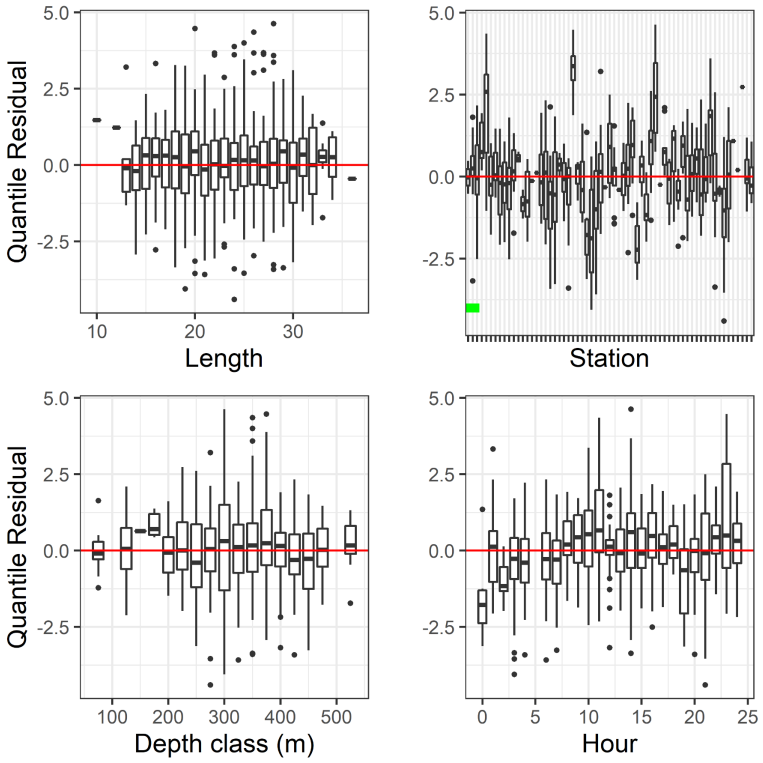

Figure 45c.Normalized quantile residuals for the selected model for Pasiphaea multidentata.

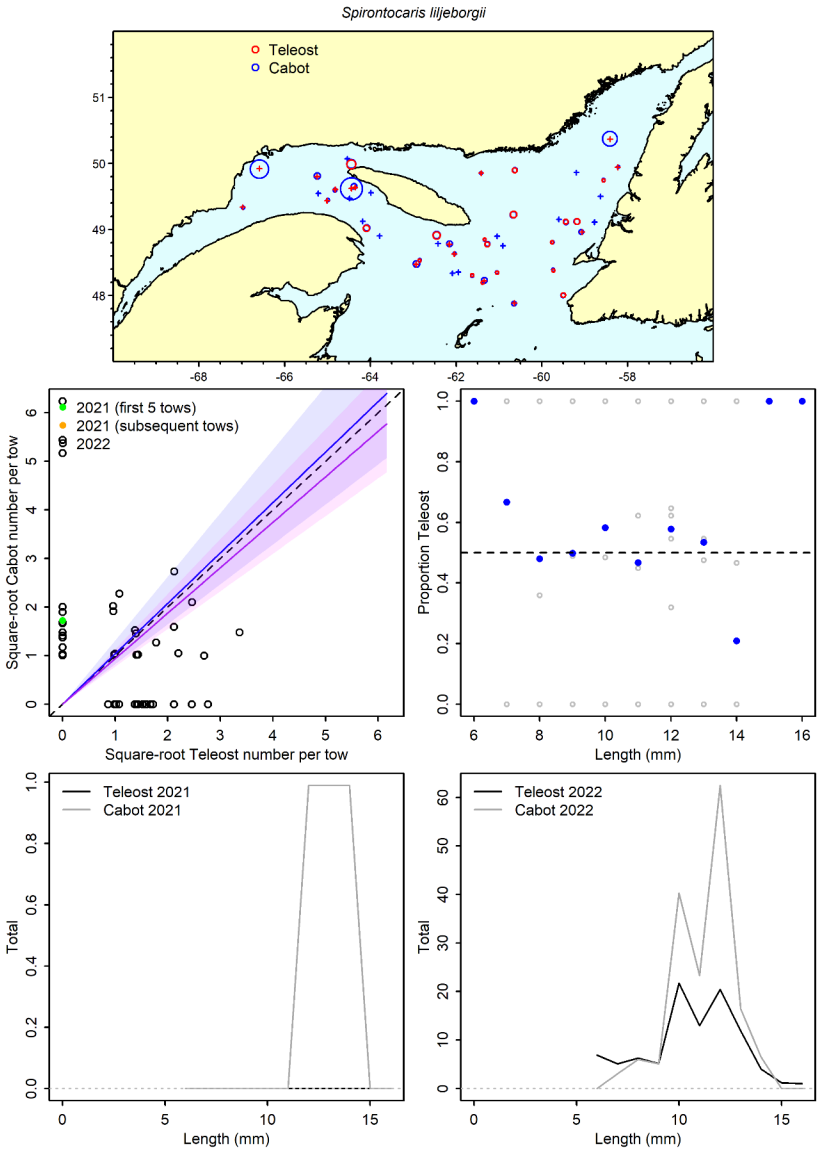

Figure 46a. Visualisation of comparative fishing data and size-aggregated model predictions for Spirontocaris liljeborgii.

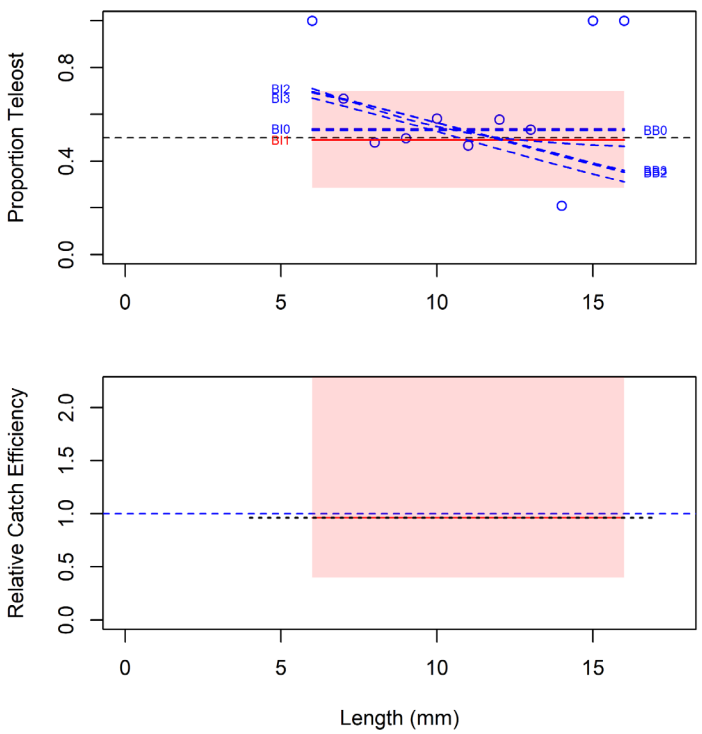

Figure 46b.Model fits and the selected length-based calibration for Spirontocaris liljeborgii.

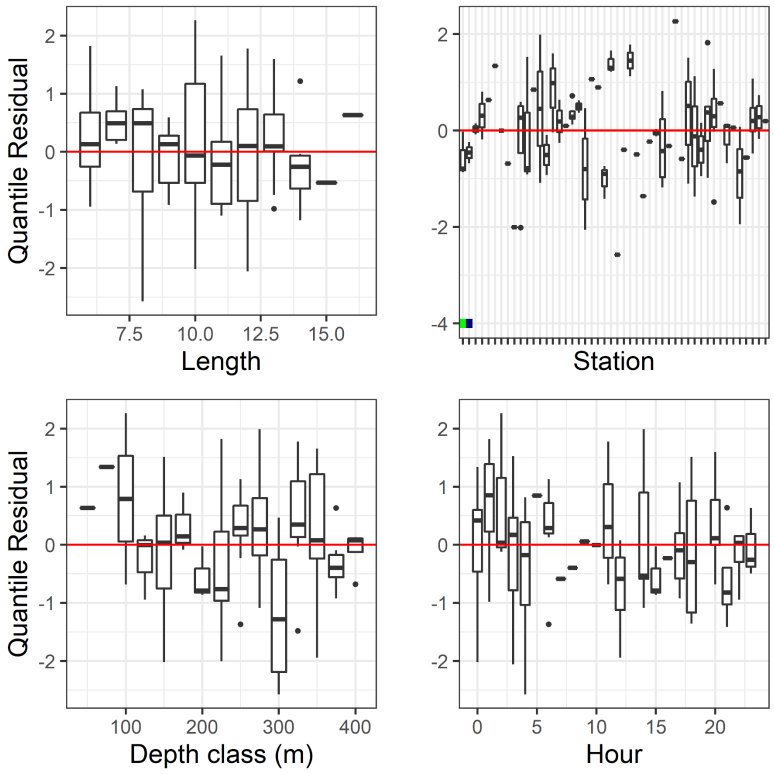

Figure 46c.Normalized quantile residuals for the selected model for Spirontocaris liljeborgii.

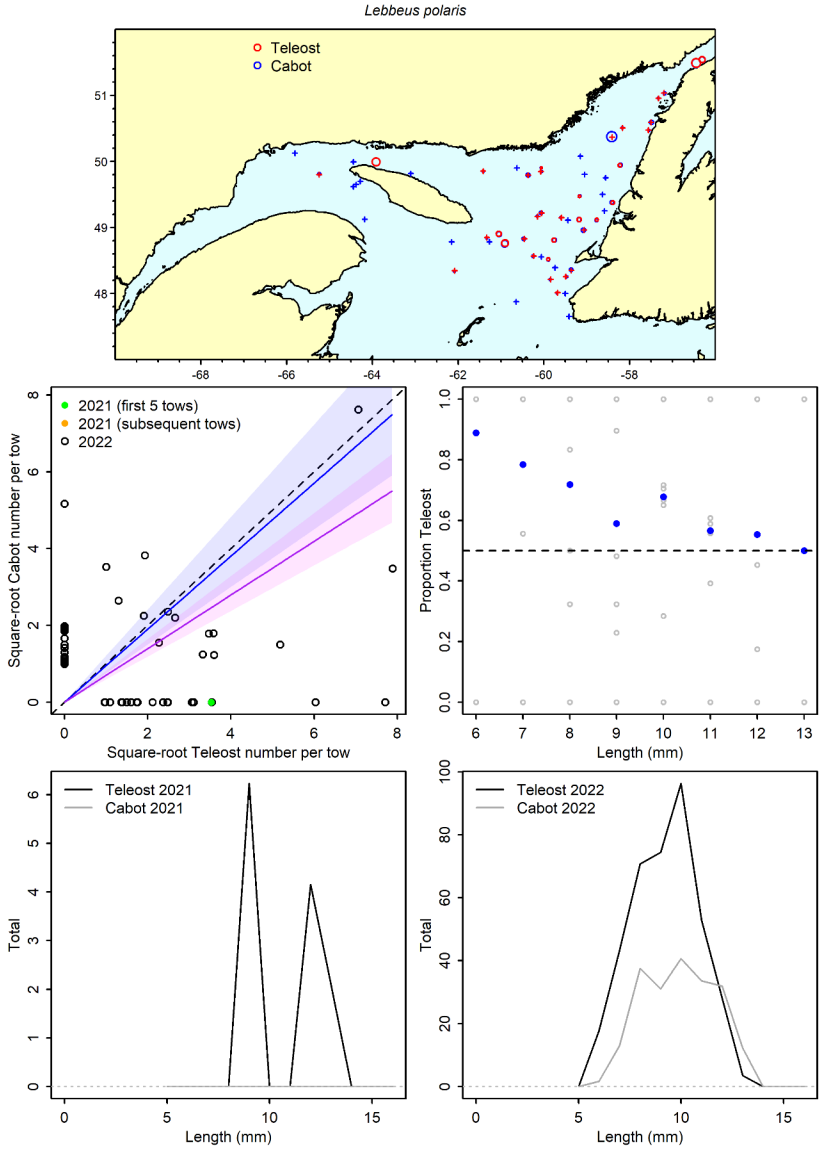

Figure 47a. Visualisation of comparative fishing data and size-aggregated model predictions for Lebbeus polaris.

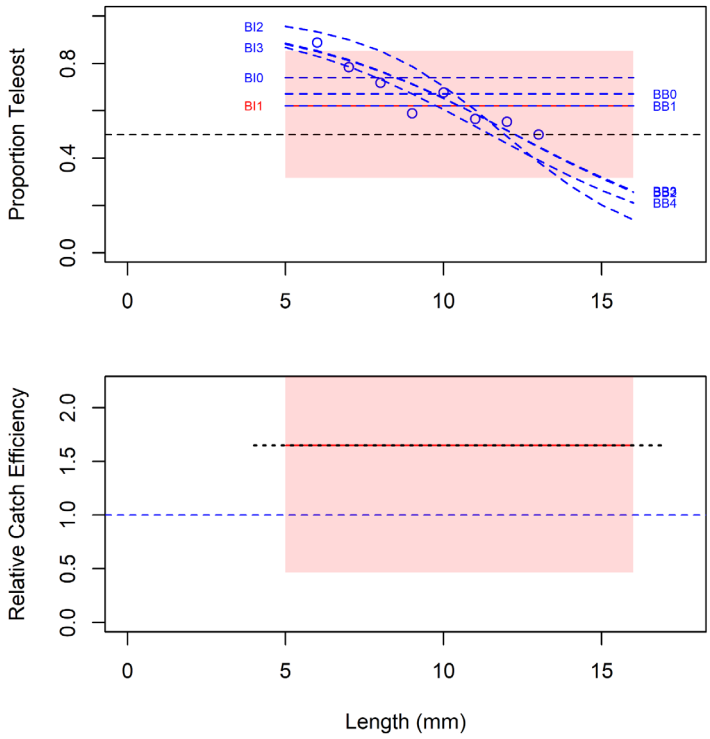

Figure 47b.Model fits and the selected length-based calibration for Lebbeus polaris.

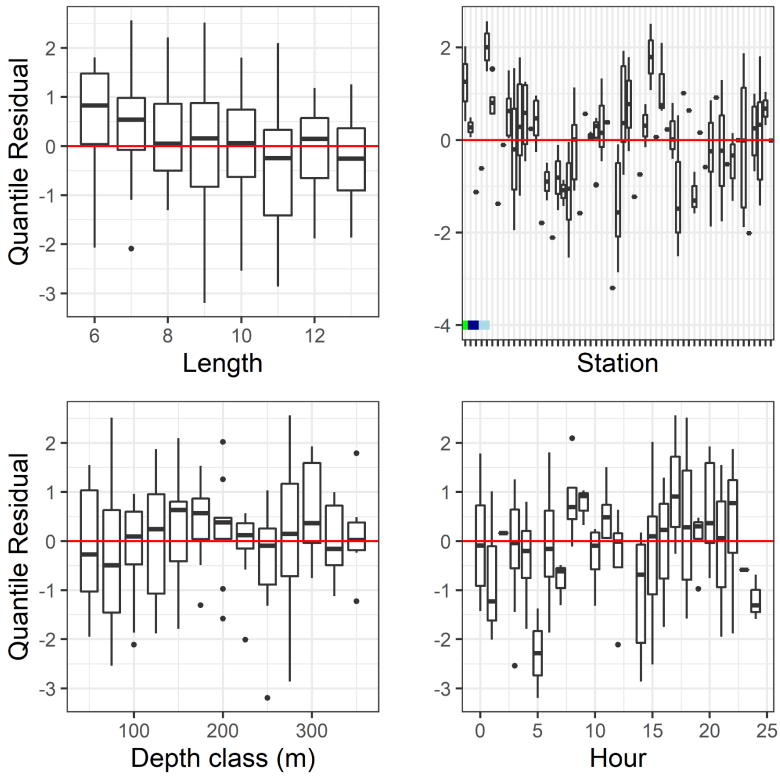

Figure 47c.Normalized quantile residuals for the selected model for Lebbeus polaris.

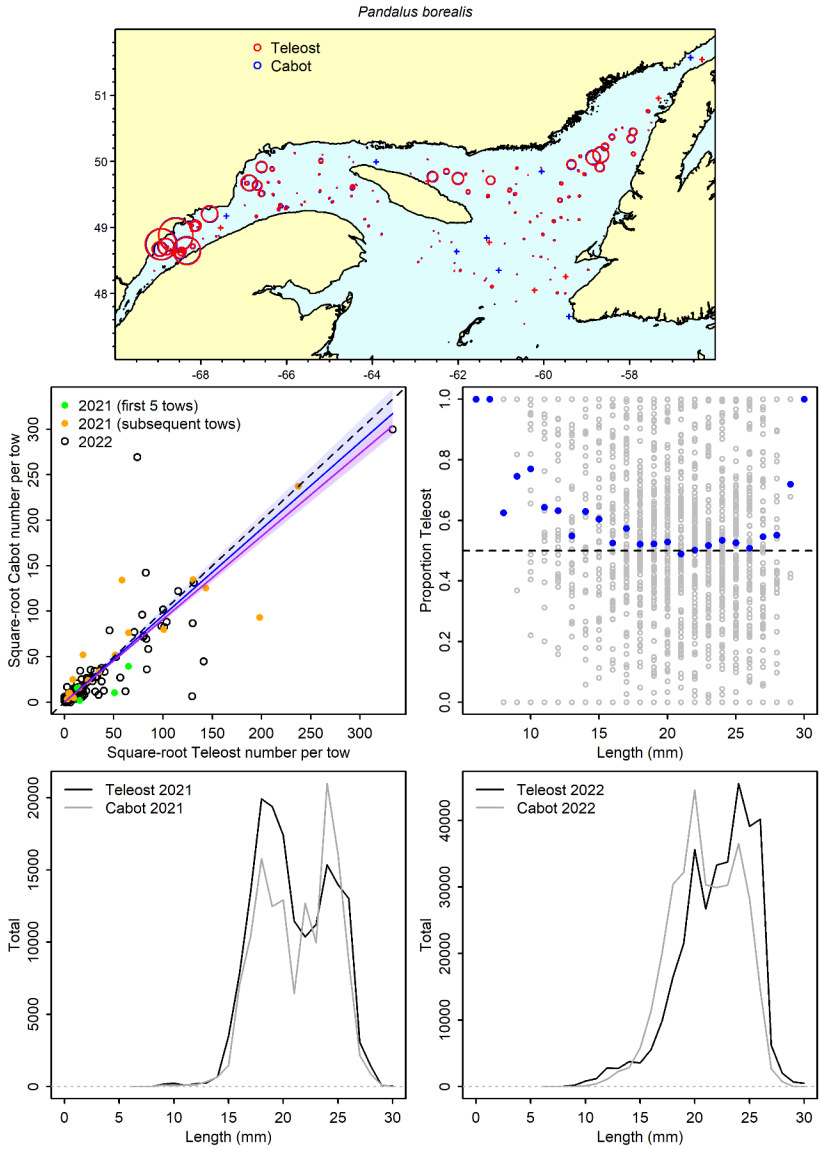

Figure 48a. Visualisation of comparative fishing data and size-aggregated model predictions for Pandalus borealis.

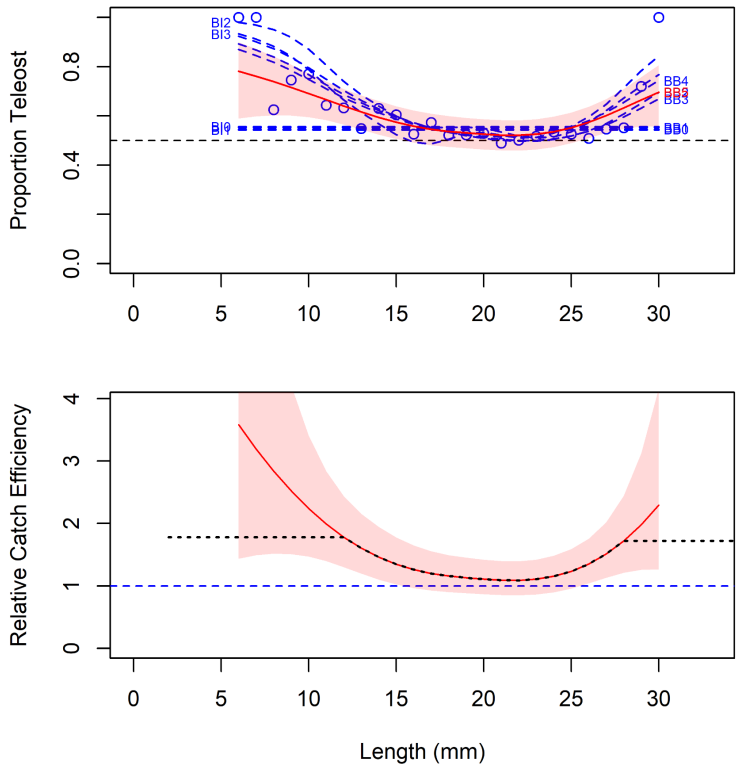

Figure 48b.Model fits and the selected length-based calibration for Pandalus borealis.

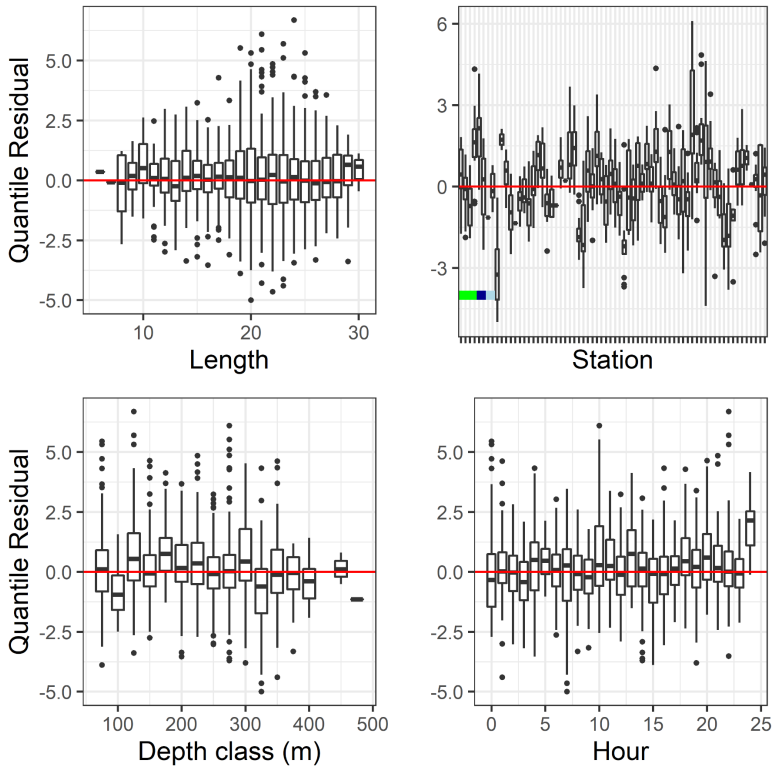

Figure 48c.Normalized quantile residuals for the selected model for Pandalus borealis.

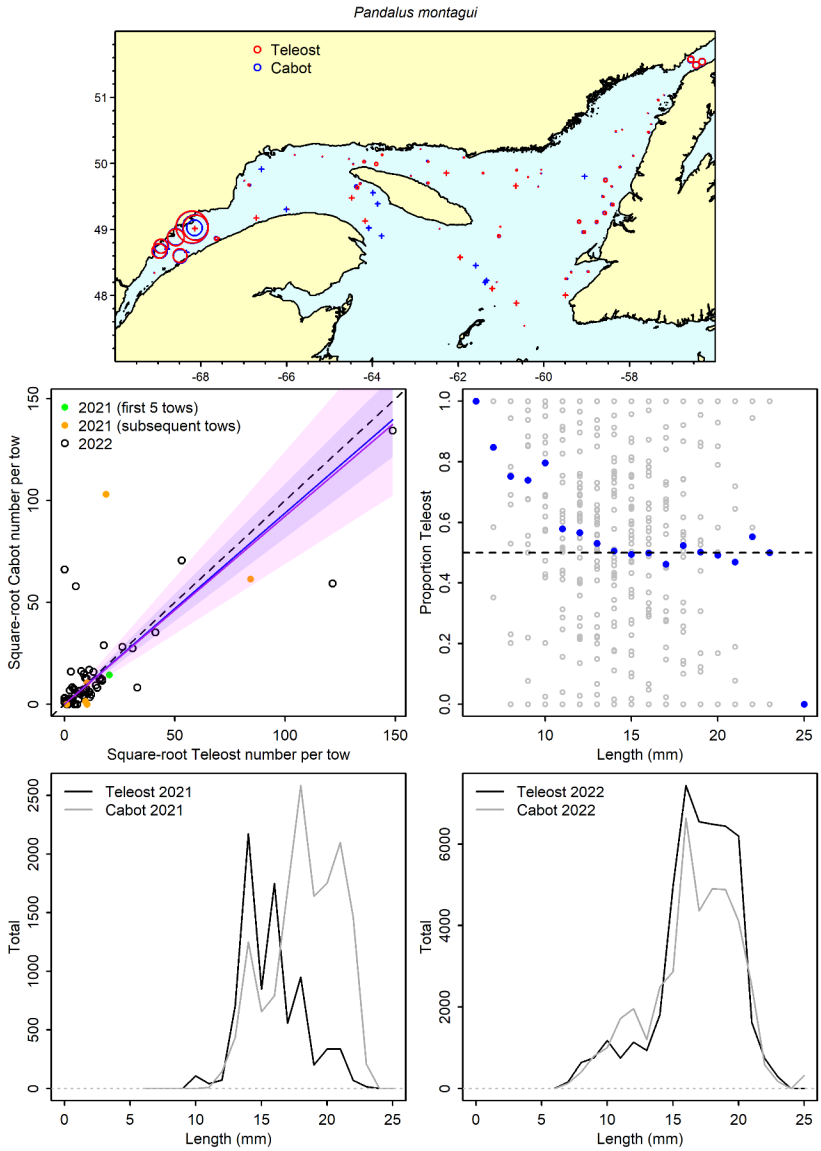

Figure 49a. Visualisation of comparative fishing data and size-aggregated model predictions for Pandalus montagui.

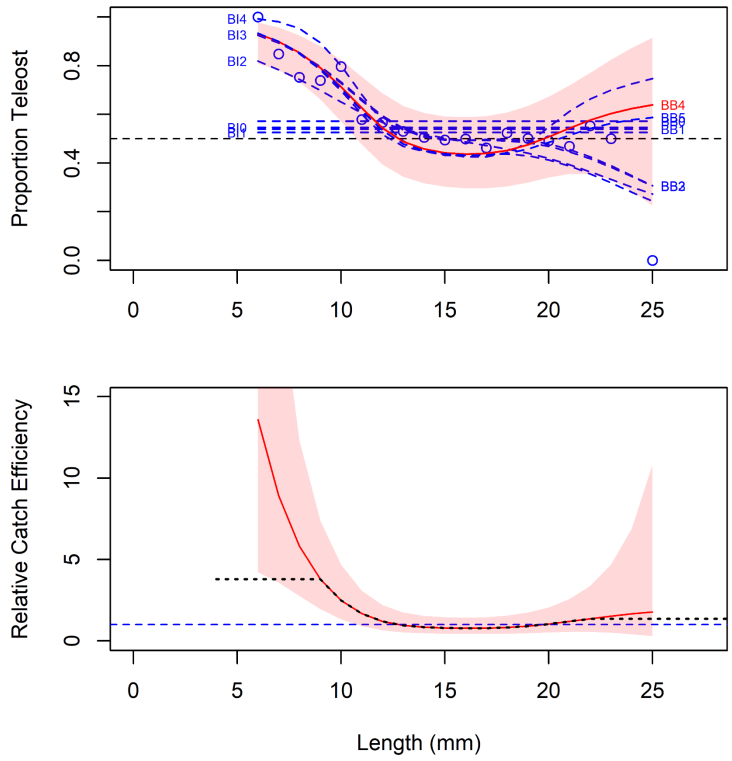

Figure 49b.Model fits and the selected length-based calibration for Pandalus montagui.

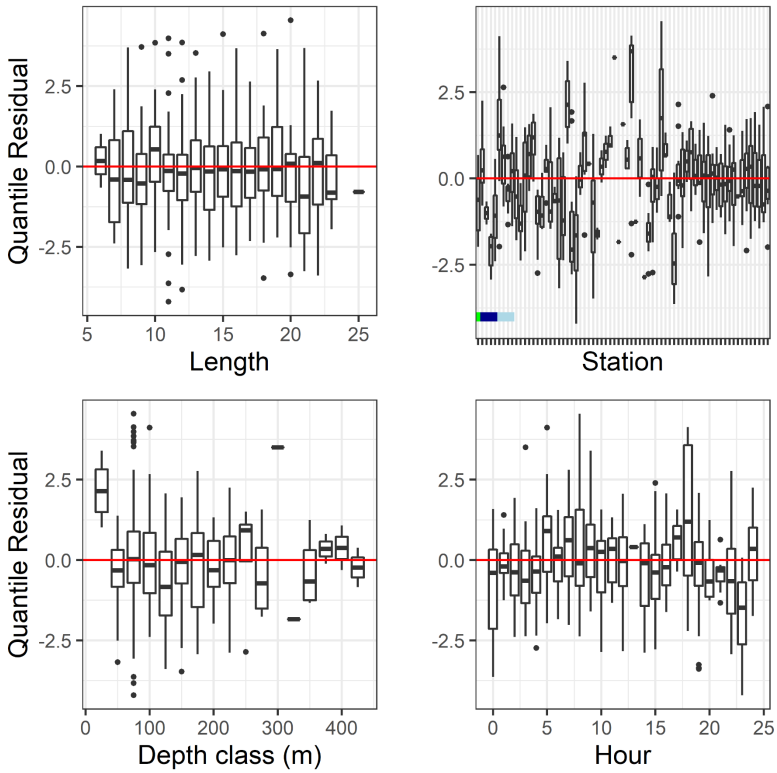

Figure 49c.Normalized quantile residuals for the selected model for Pandalus montagui.

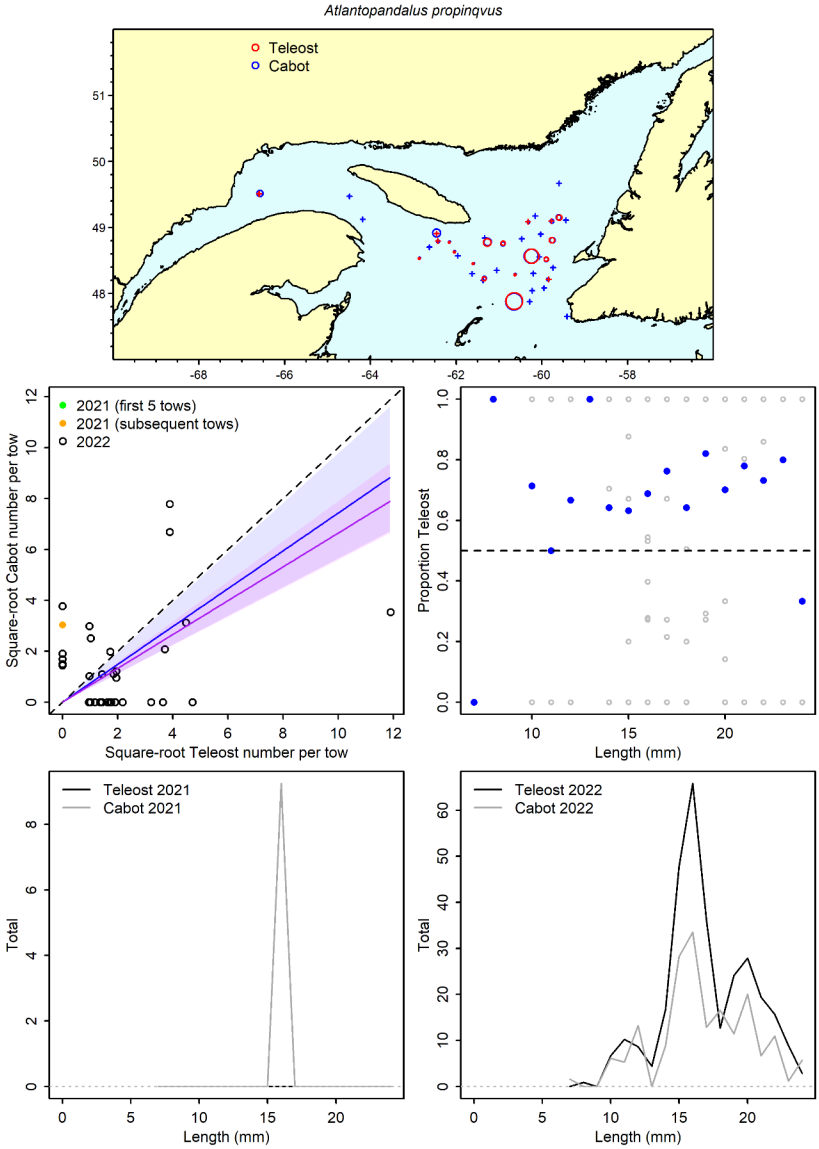

Figure 50a. Visualisation of comparative fishing data and size-aggregated model predictions for Atlantopandalus propinqvus.

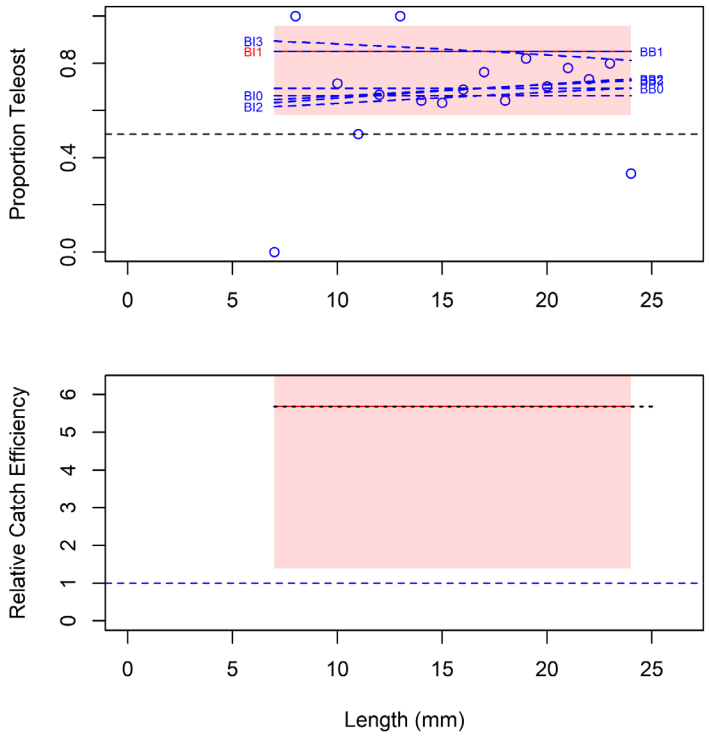

Figure 50b.Model fits and the selected length-based calibration for Atlantopandalus propinqvus.

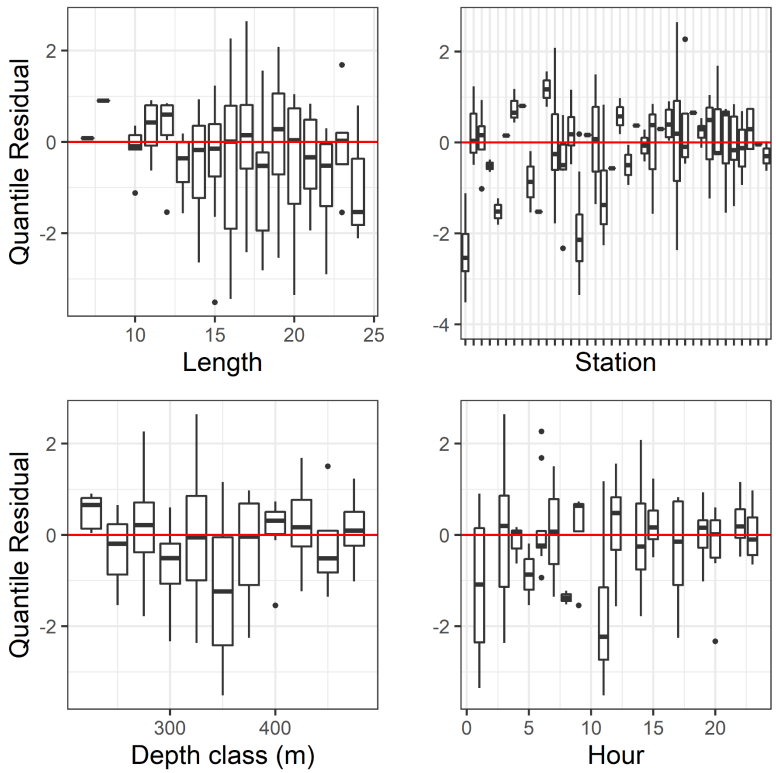

Figure 50c.Normalized quantile residuals for the selected model for Atlantopandalus propinqvus.

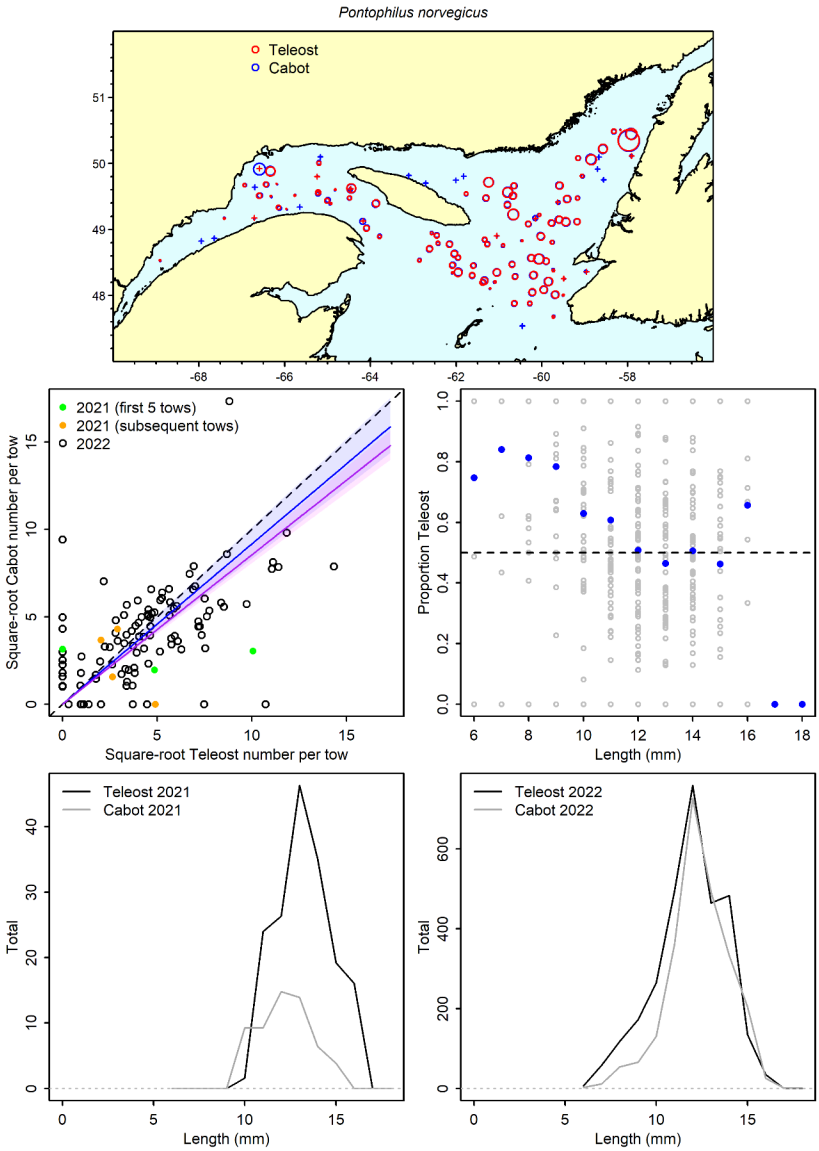

Figure 51a.Visualisation of comparative fishing data and size-aggregated model predictions for Pontophilus norvegicus.

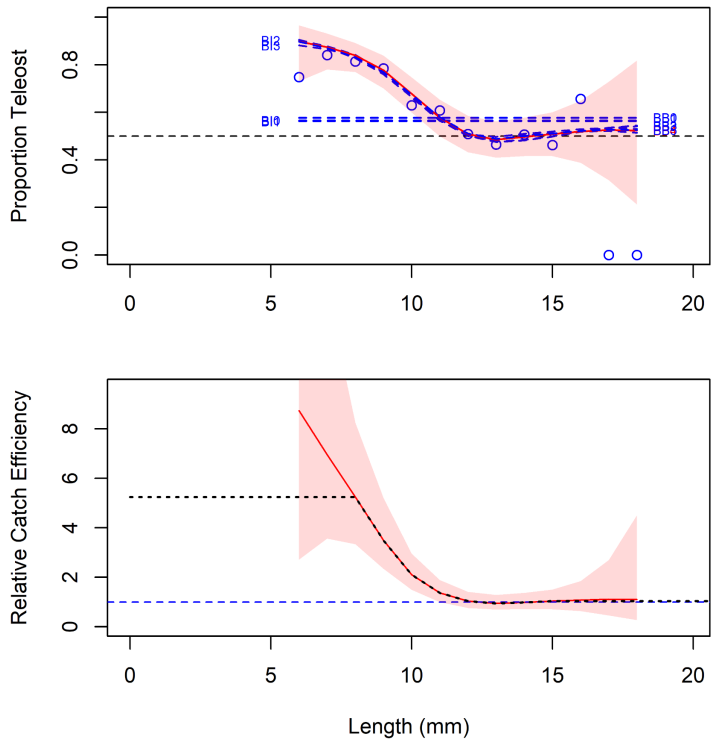

Figure 51b.Model fits and the selected length-based calibration for Pontophilus norvegicus.

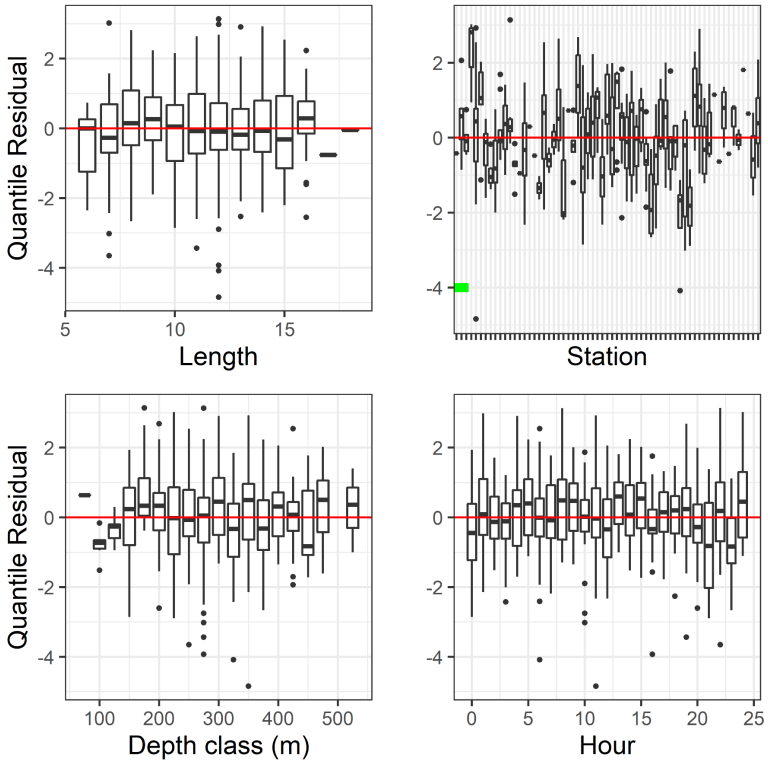

Figure 51c.Normalized quantile residuals for the selected model for Pontophilus norvegicus.

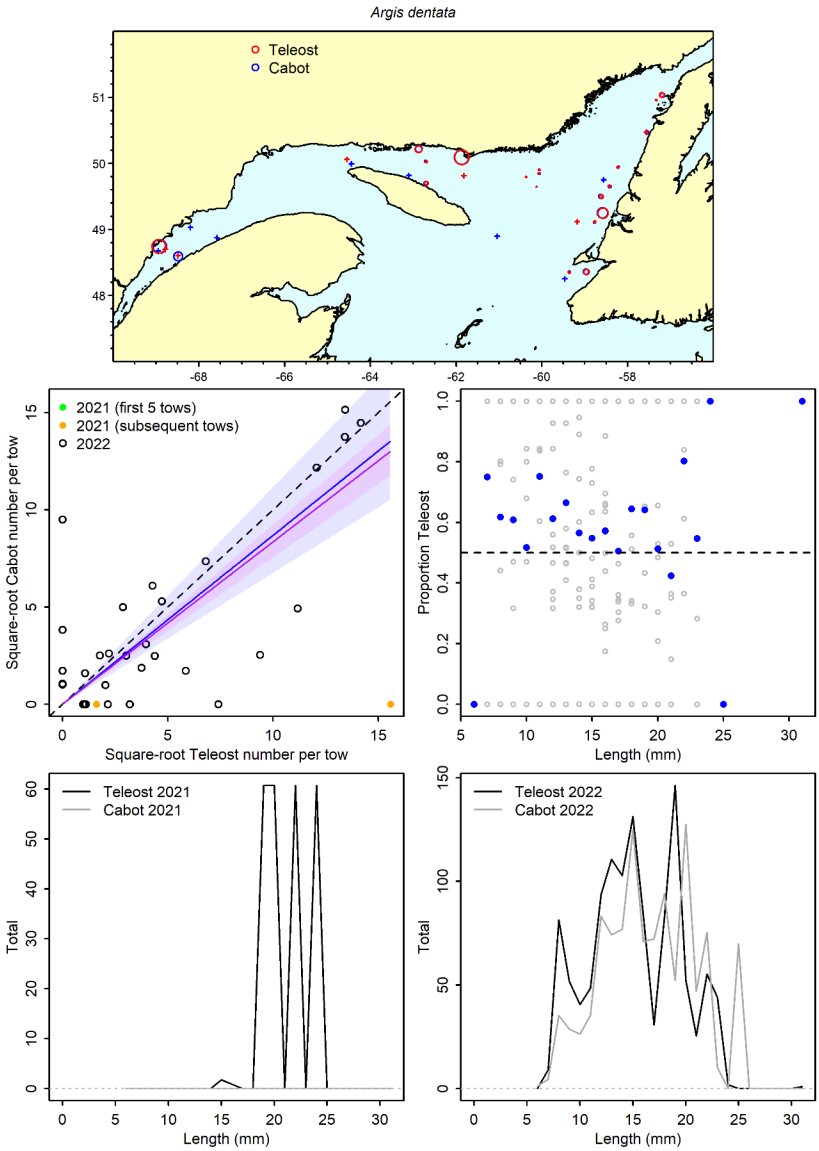

Figure 52a. Visualisation of comparative fishing data and size-aggregated model predictions for Argis dentata.

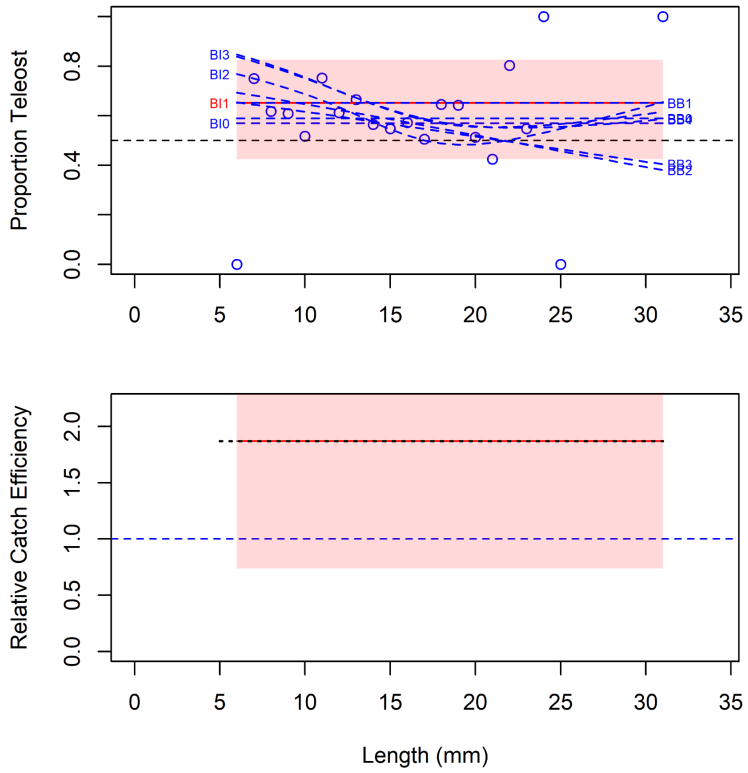

Figure 52b.Model fits and the selected length-based calibration for Argis dentata.

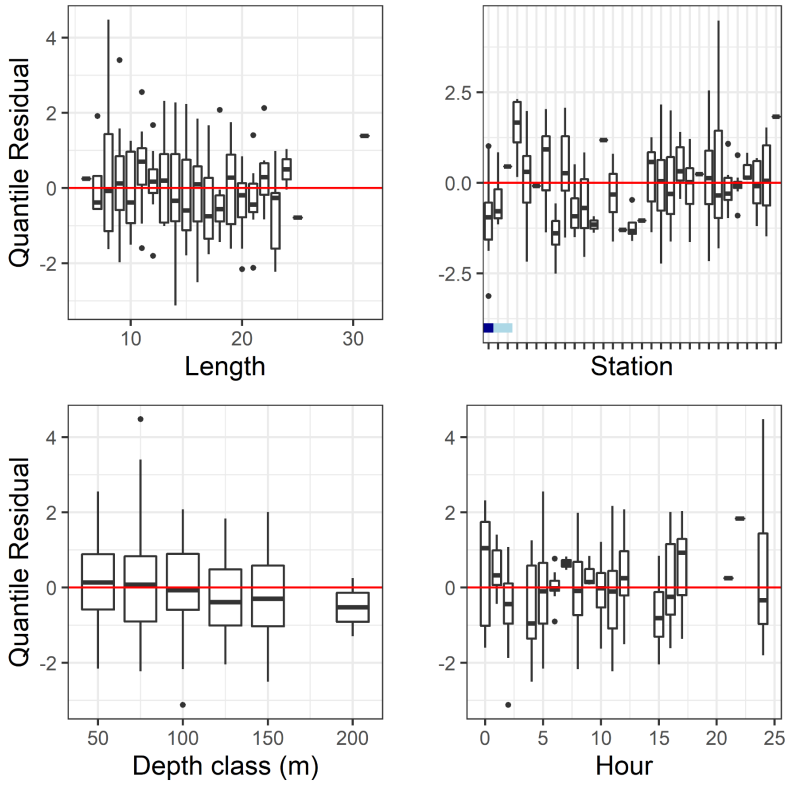

Figure 52c.Normalized quantile residuals for the selected model for Argis dentata.

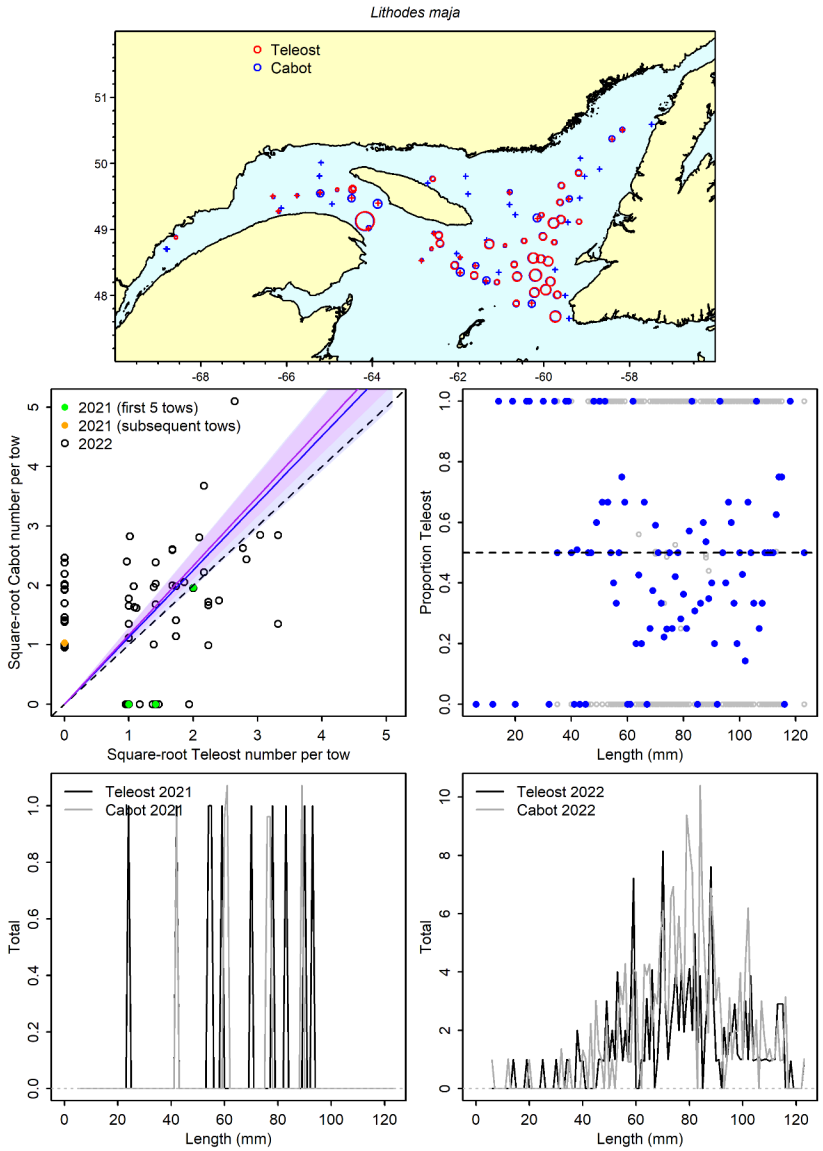

Figure 53a. Visualisation of comparative fishing data and size-aggregated model predictions for Lithodes maja.

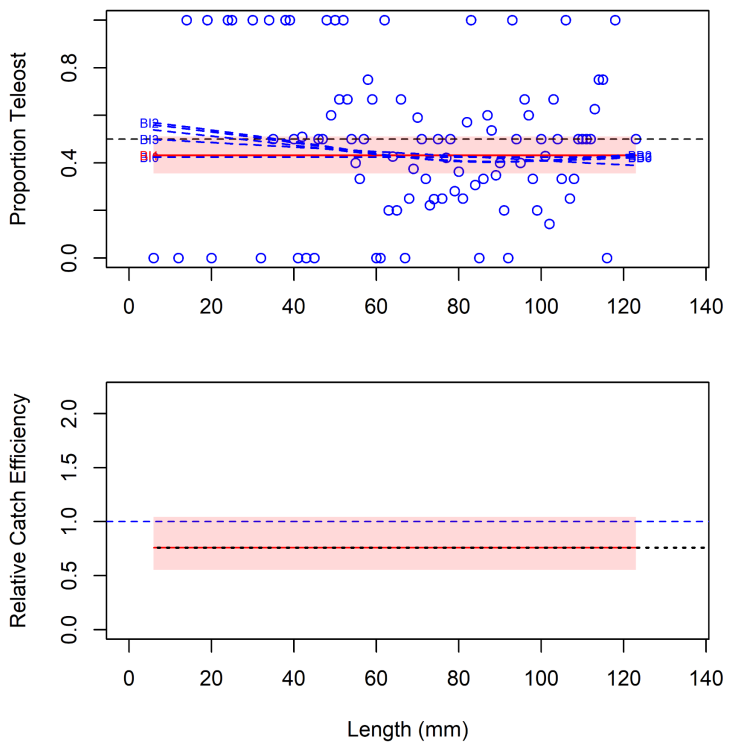

Figure 53b.Model fits and the selected length-based calibration for Lithodes maja.

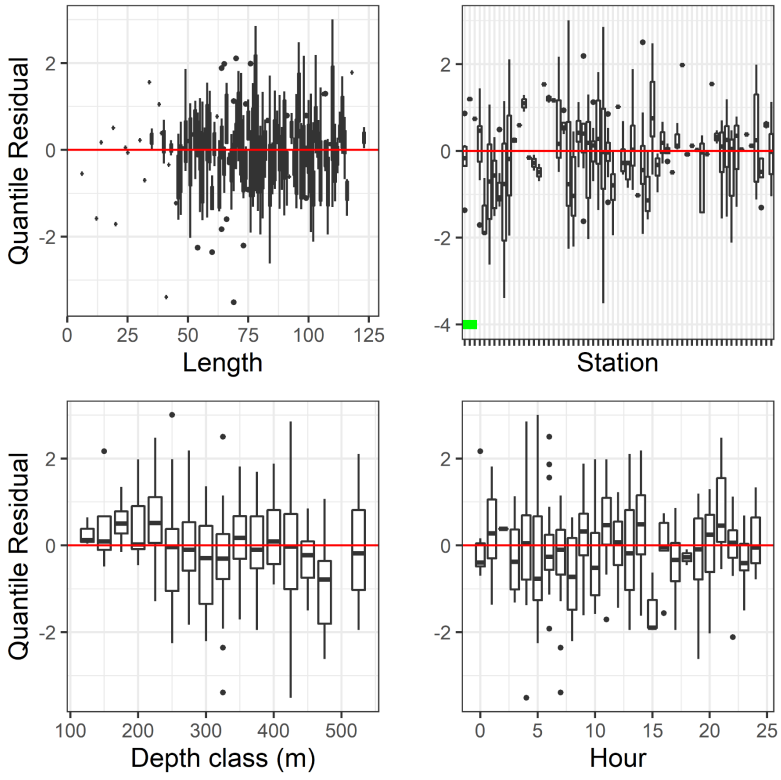

Figure 53c.Normalized quantile residuals for the selected model for Lithodes maja.

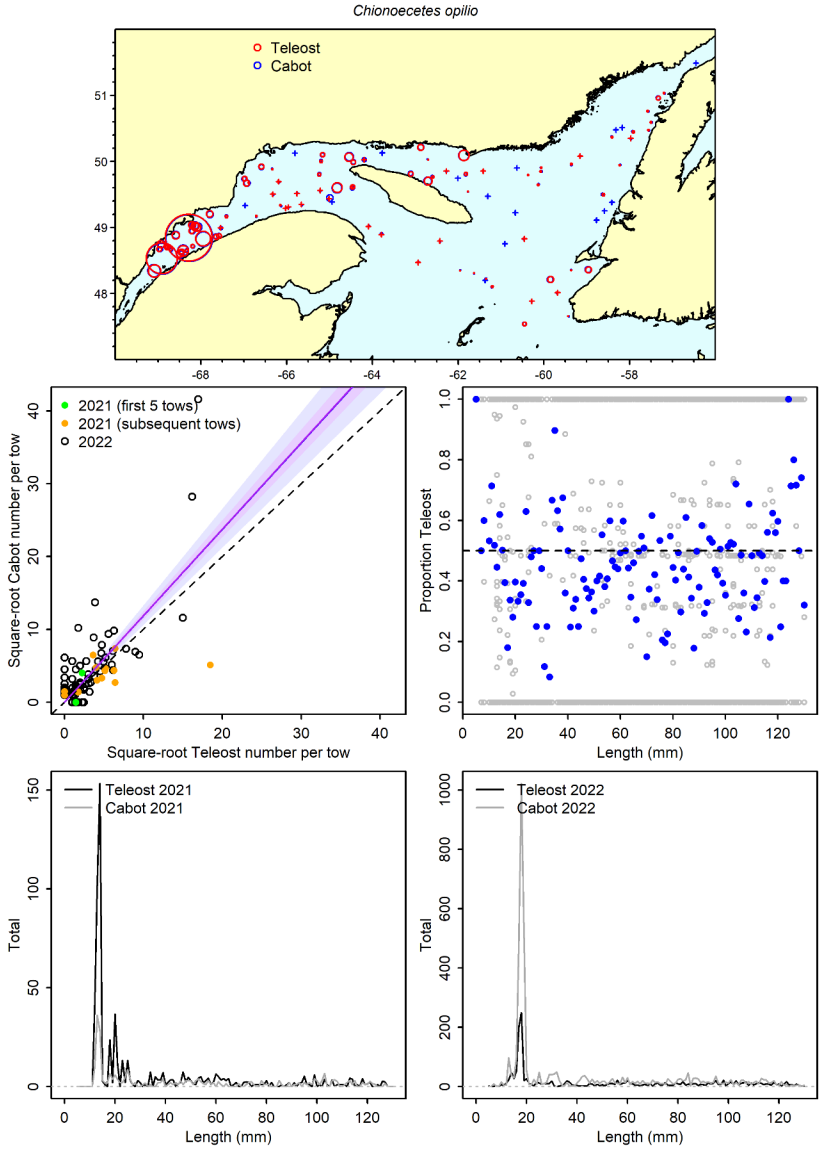

Figure 54a. Visualisation of comparative fishing data and size-aggregated model predictions for Chionoecetes opilio.

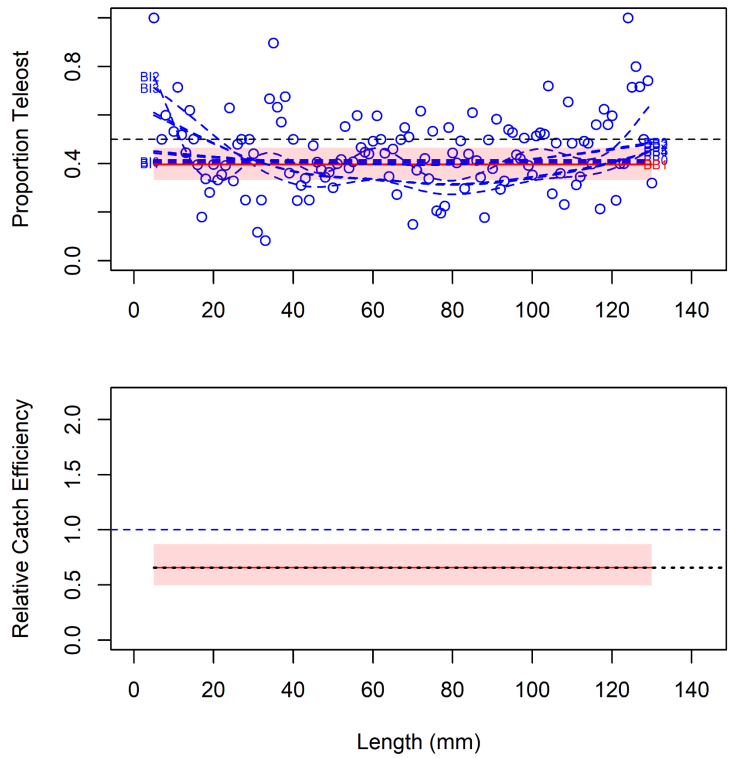

Figure 54b.Model fits and the selected length-based calibration for Chionoecetes opilio.

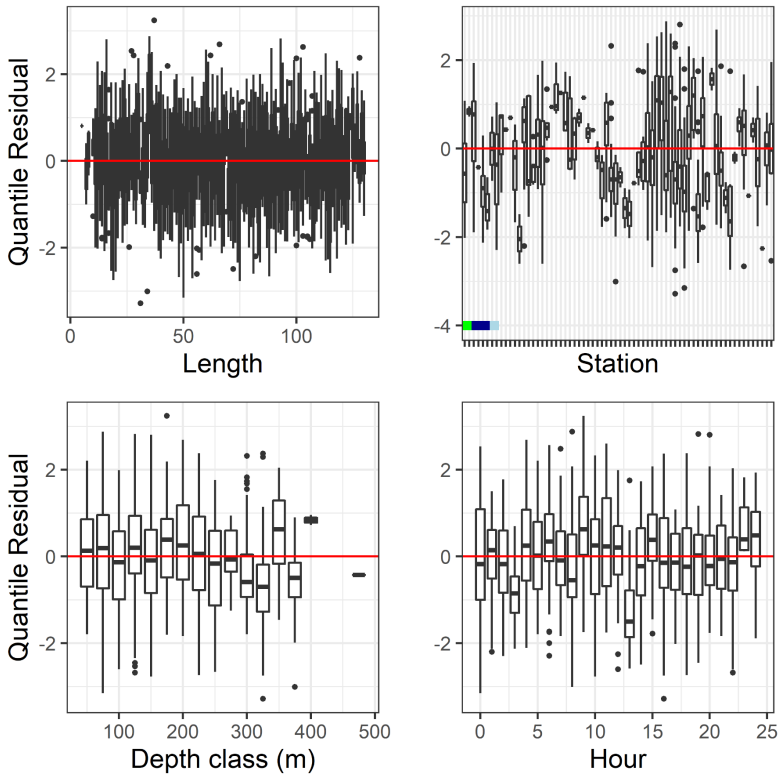

Figure 54c.Normalized quantile residuals for the selected model for Chionoecetes opilio.

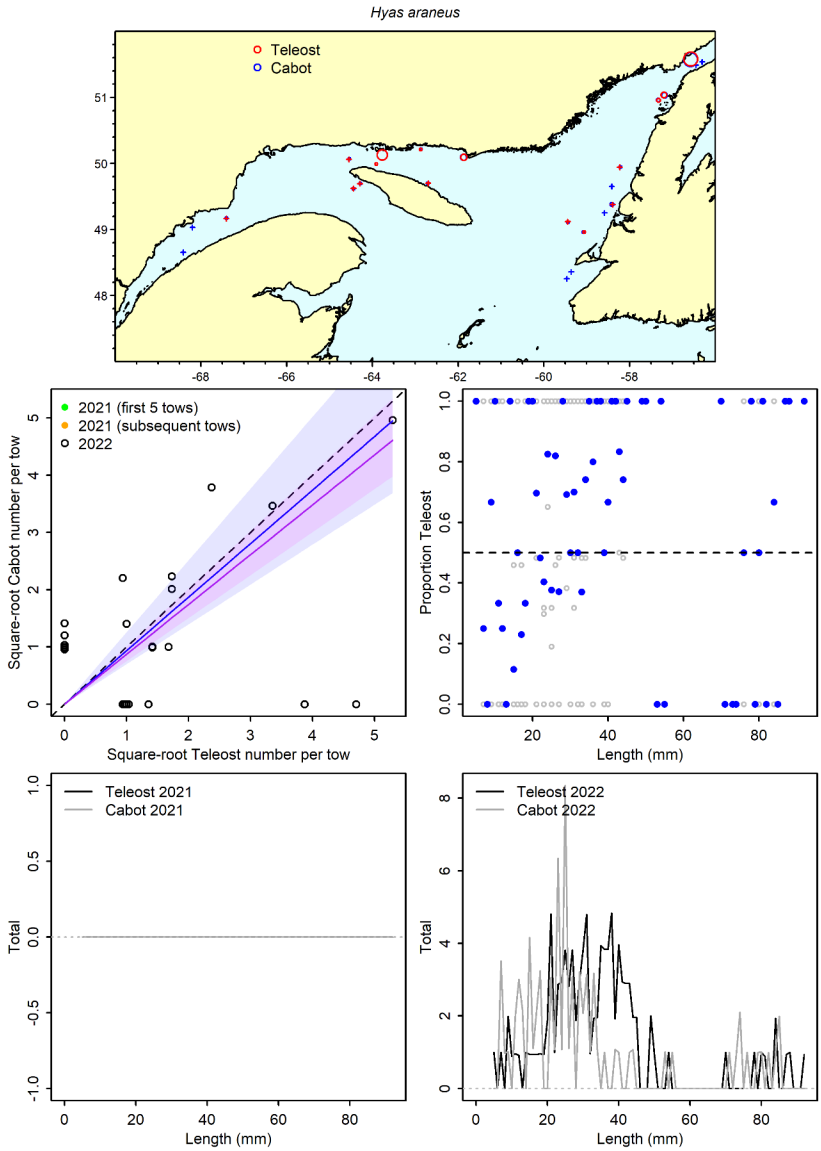

Figure 55a. Visualisation of comparative fishing data and size-aggregated model predictions for Hyas araneus.

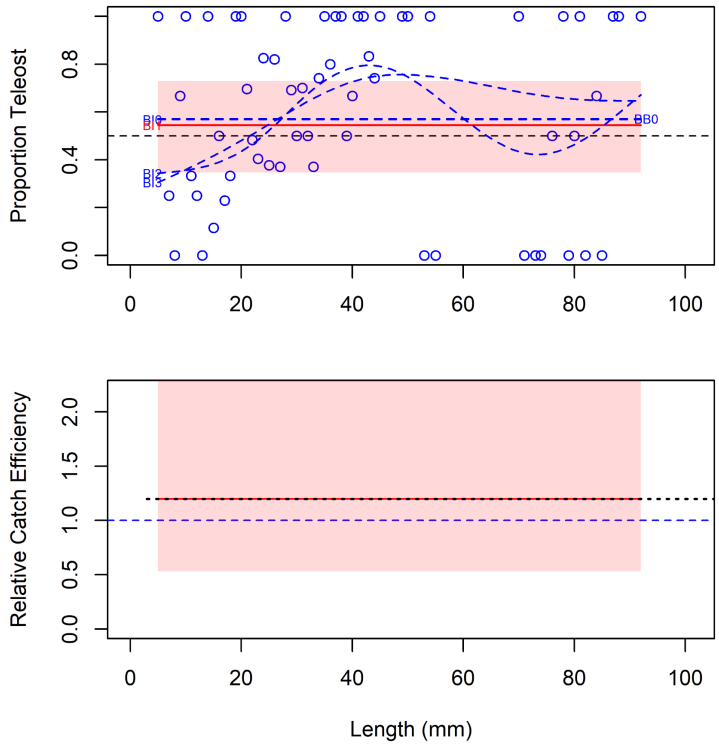

Figure 55b.Model fits and the selected length-based calibration for Hyas araneus.

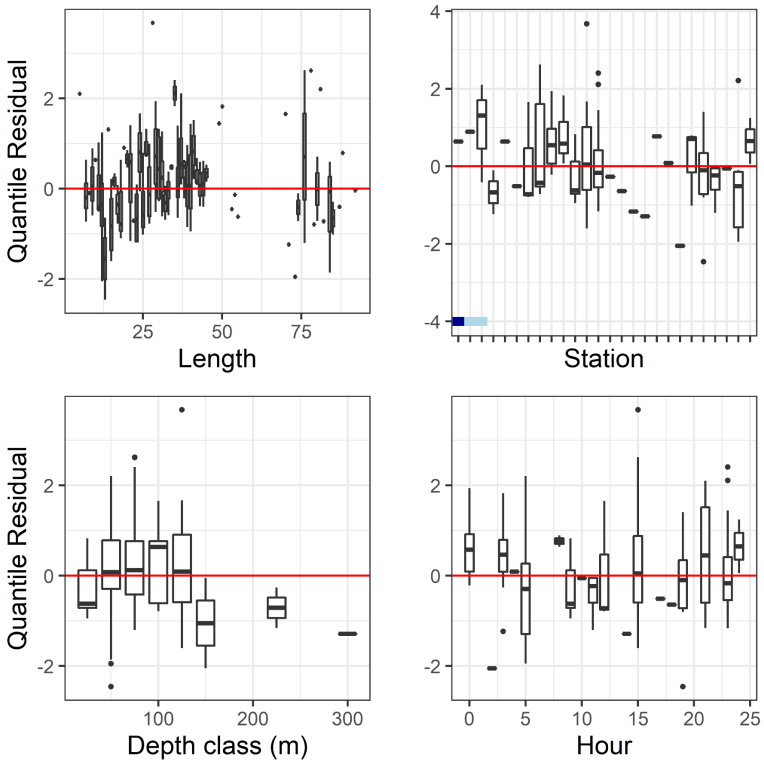

Figure 55c.Normalized quantile residuals for the selected model for Hyas araneus.

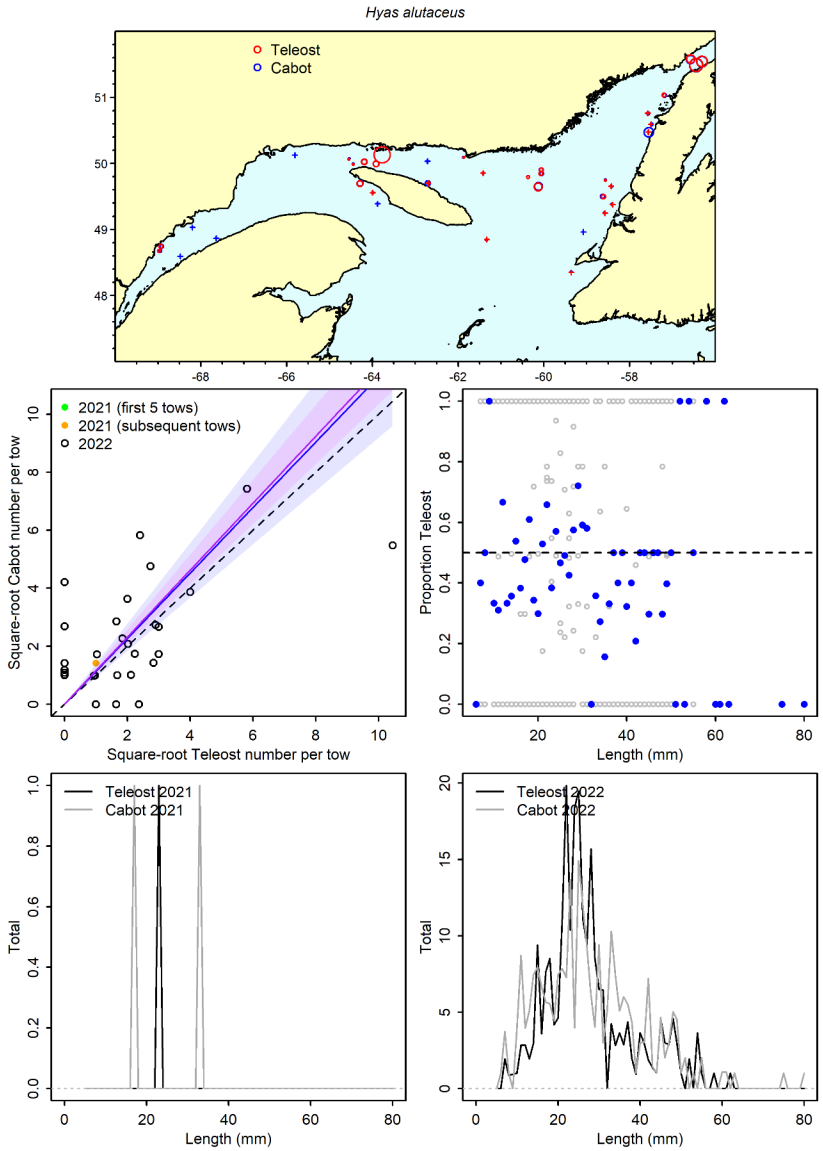

Figure 56a. Visualisation of comparative fishing data and size-aggregated model predictions for Hyas alutaceus.

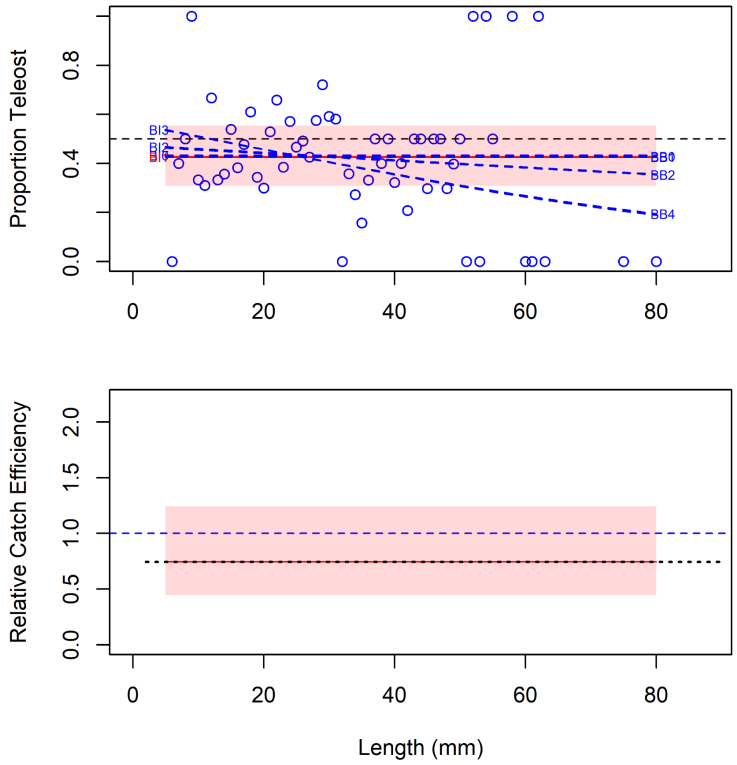

Figure 56b.Model fits and the selected length-based calibration for Hyas alutaceus.

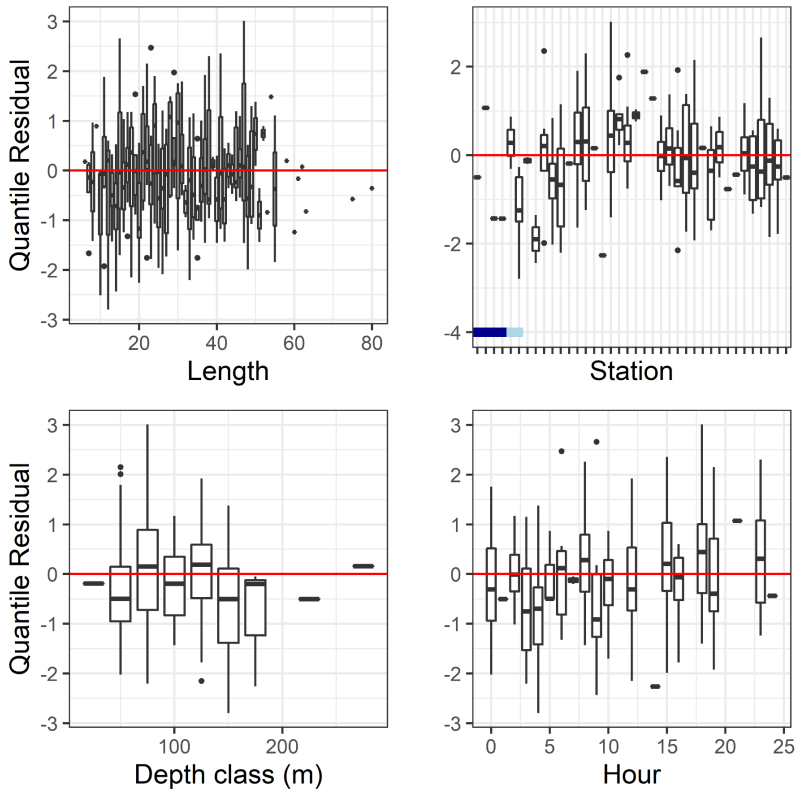

Figure 56c.Normalized quantile residuals for the selected model for Hyas alutaceus.

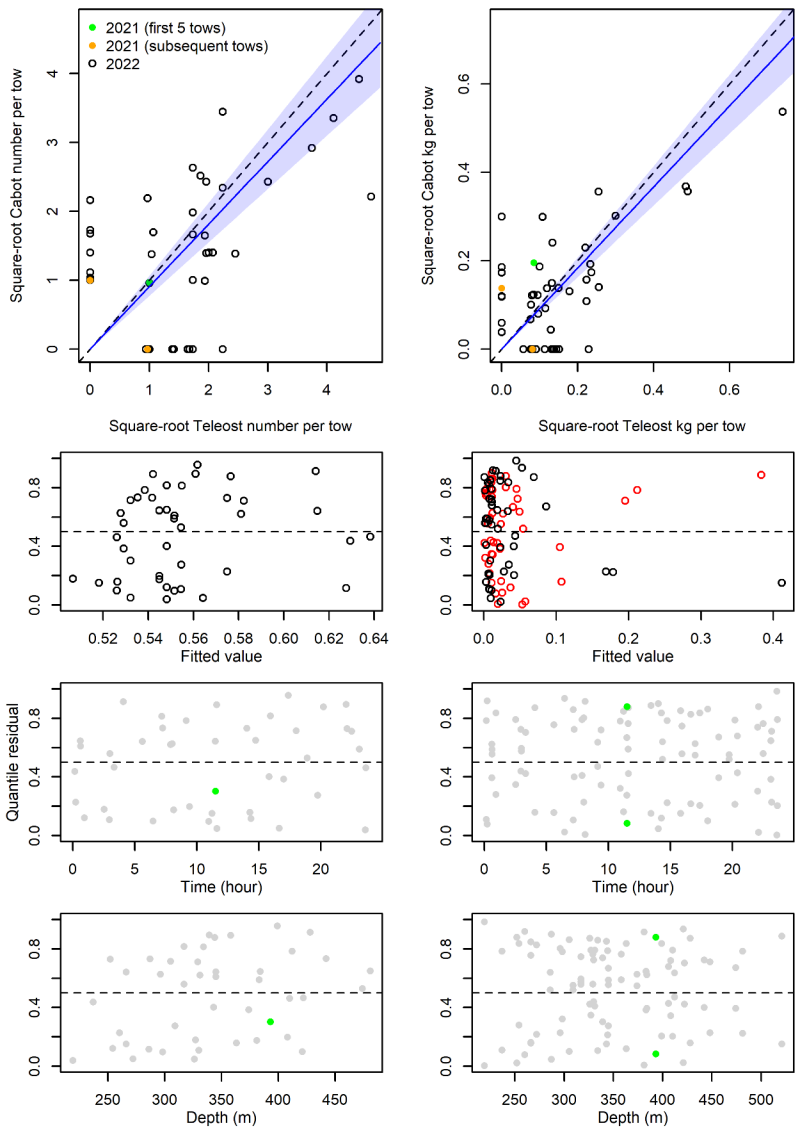

Figure 57.Visualisation of comparative fishing data, size-aggregated model predictions and residual plots for Myctophiformes.

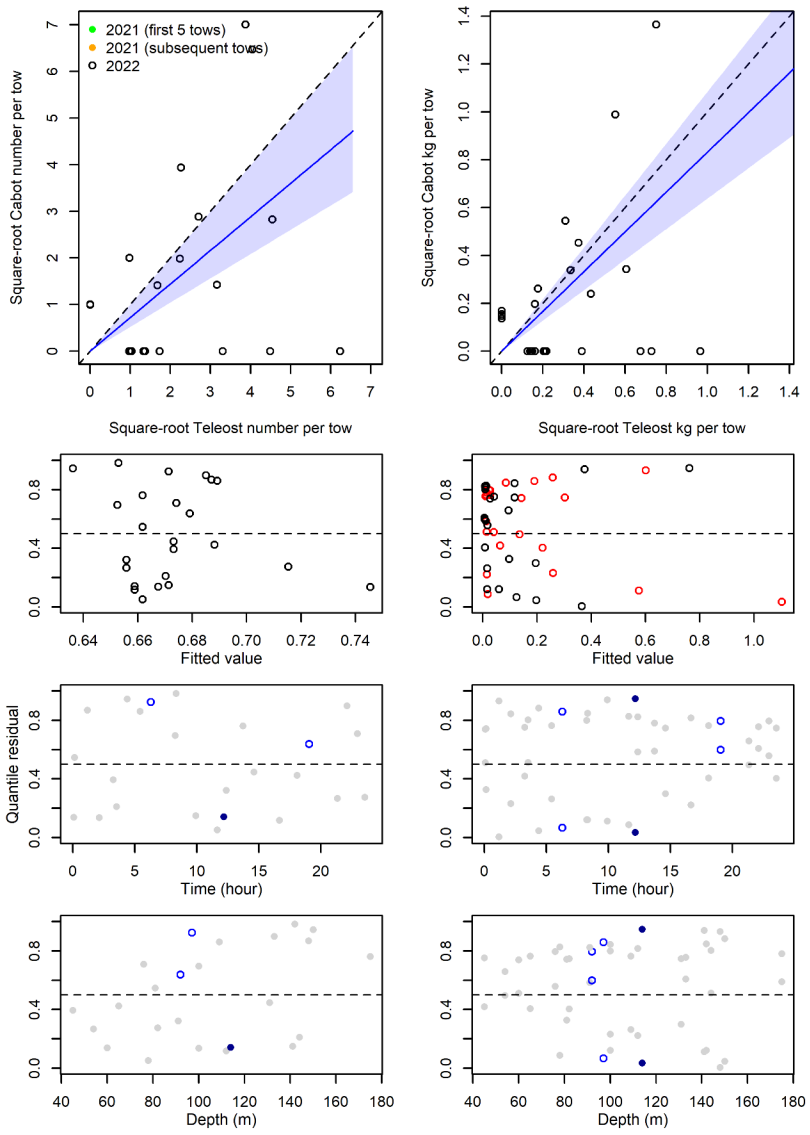

Figure 58.Visualisation of comparative fishing data, size-aggregated model predictions and residual plots for Eumesogrammus praecisus.

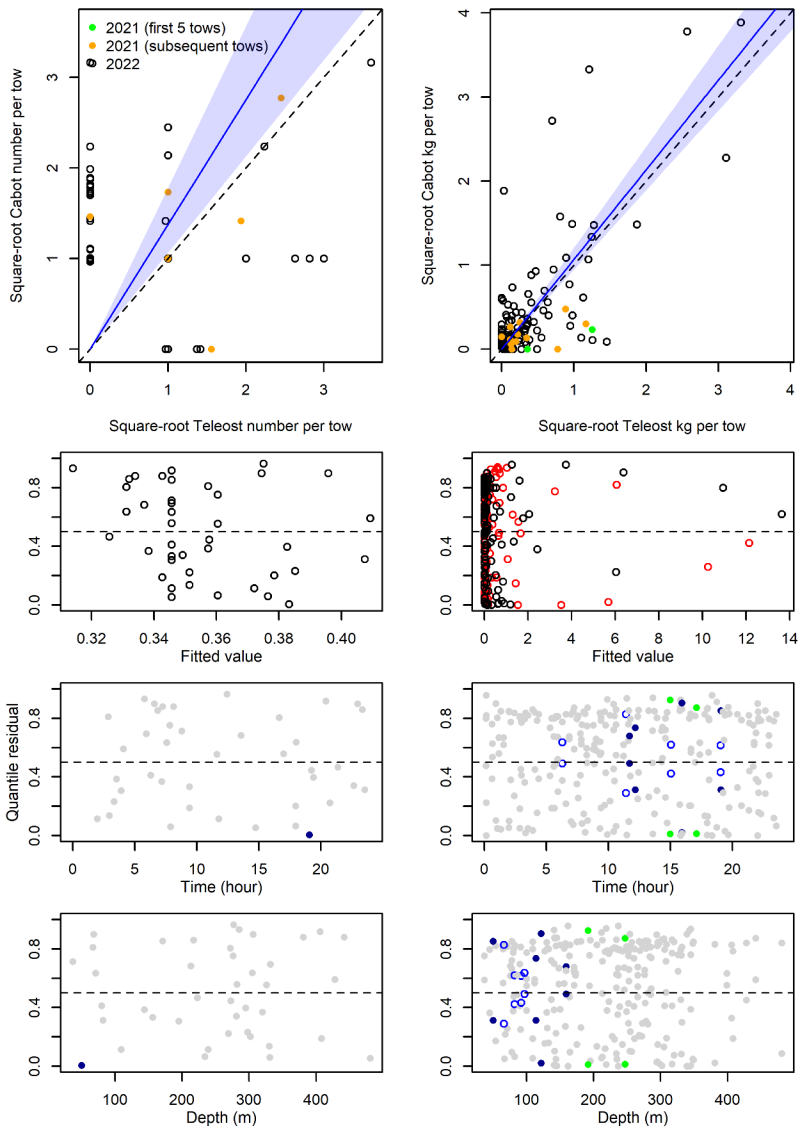

Figure 59.Visualisation of comparative fishing data, size-aggregated model predictions and residual plots for Porifera.

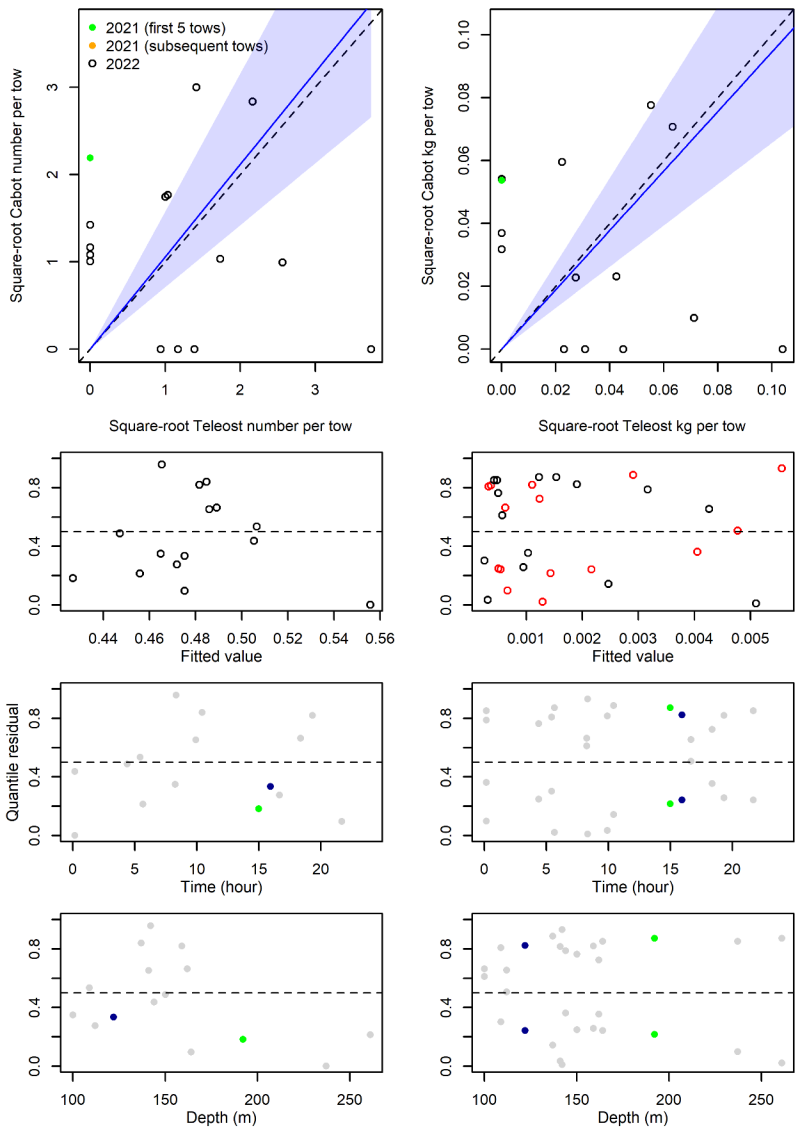

Figure 60.Visualisation of comparative fishing data, size-aggregated model predictions and residual plots for Tentorium semisuberites.

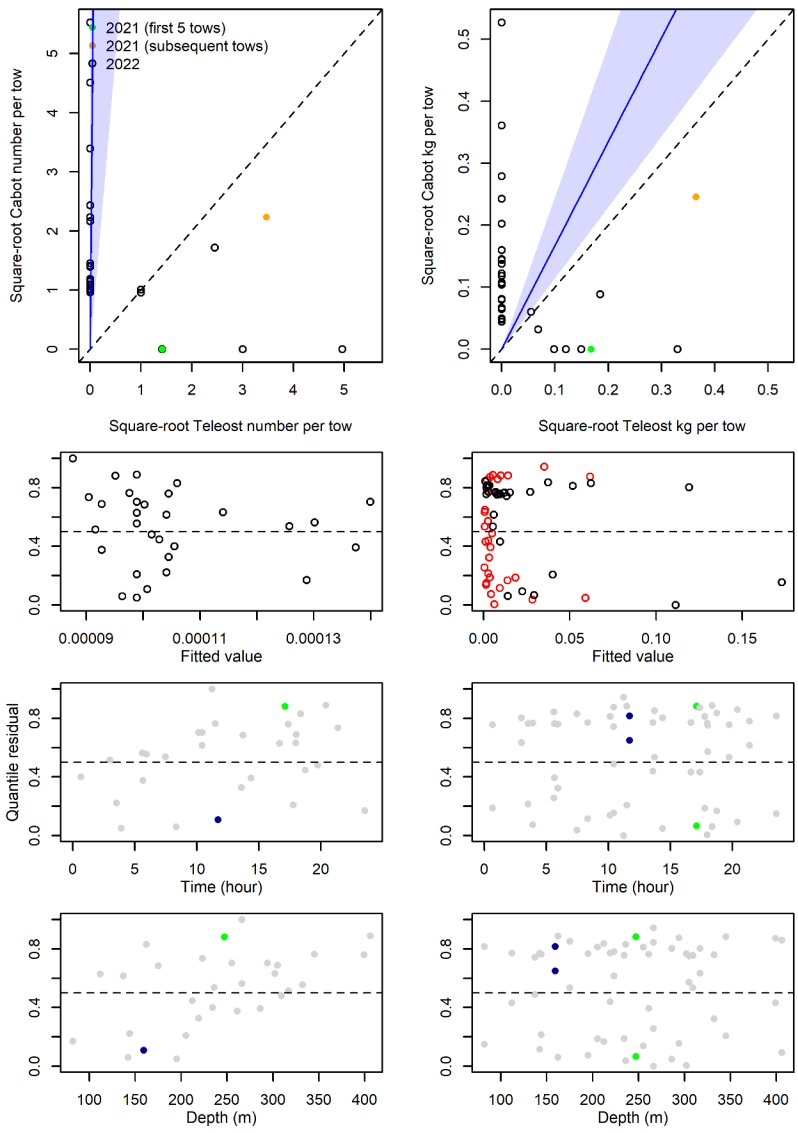

Figure 61.Visualisation of comparative fishing data, size-aggregated model predictions and residual plots for Polymastia sp.

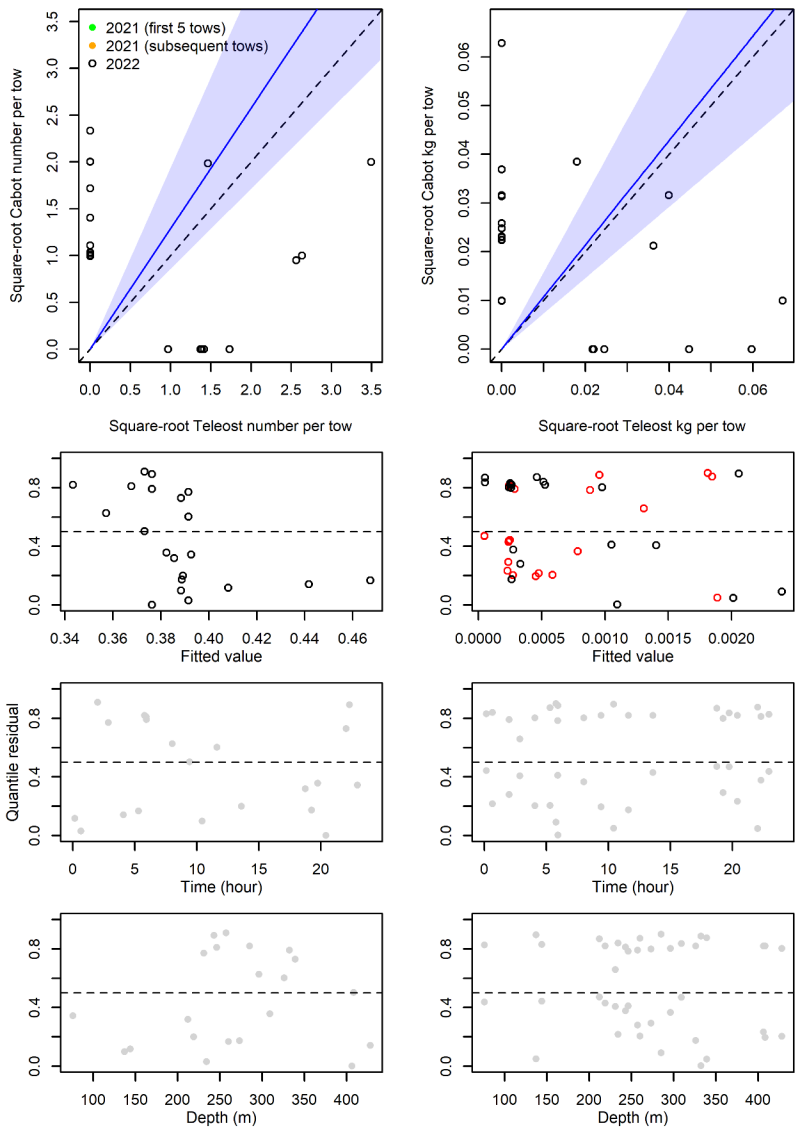

Figure 62.Visualisation of comparative fishing data, size-aggregated model predictions and residual plots for Stylocordyla borealis.

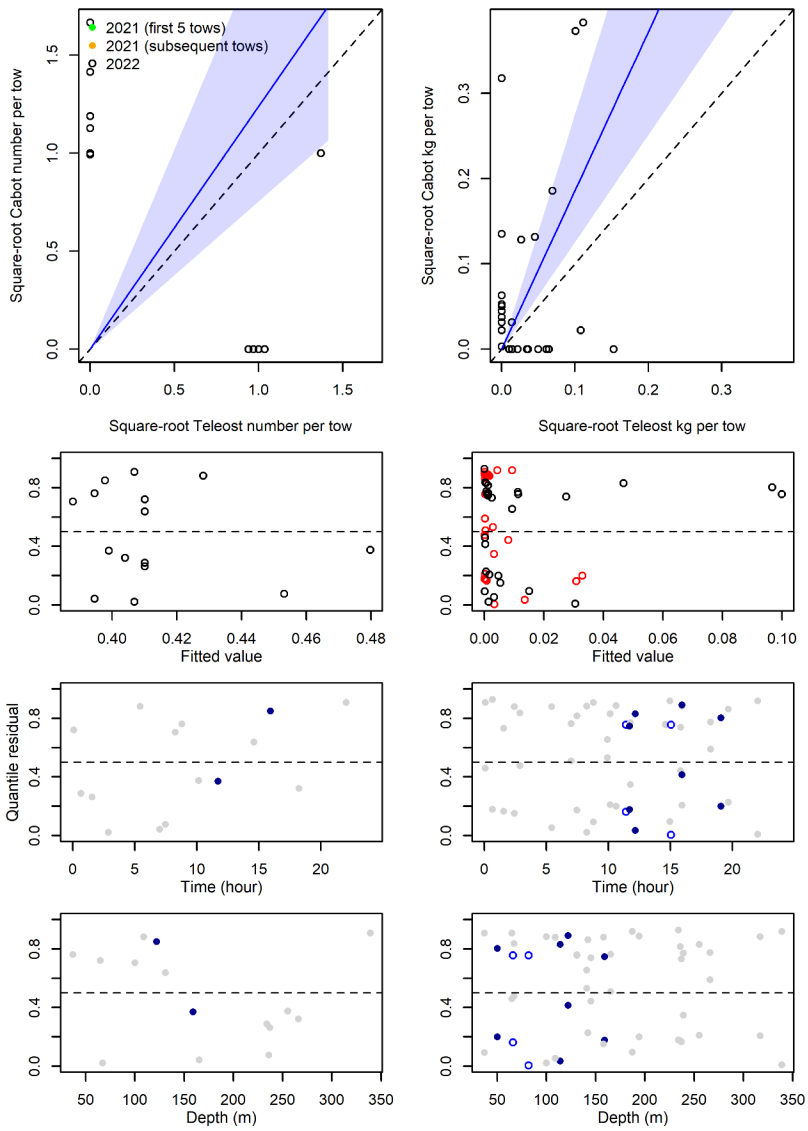

Figure 63.Visualisation of comparative fishing data, size-aggregated model predictions and residual plots for Hydrozoa.

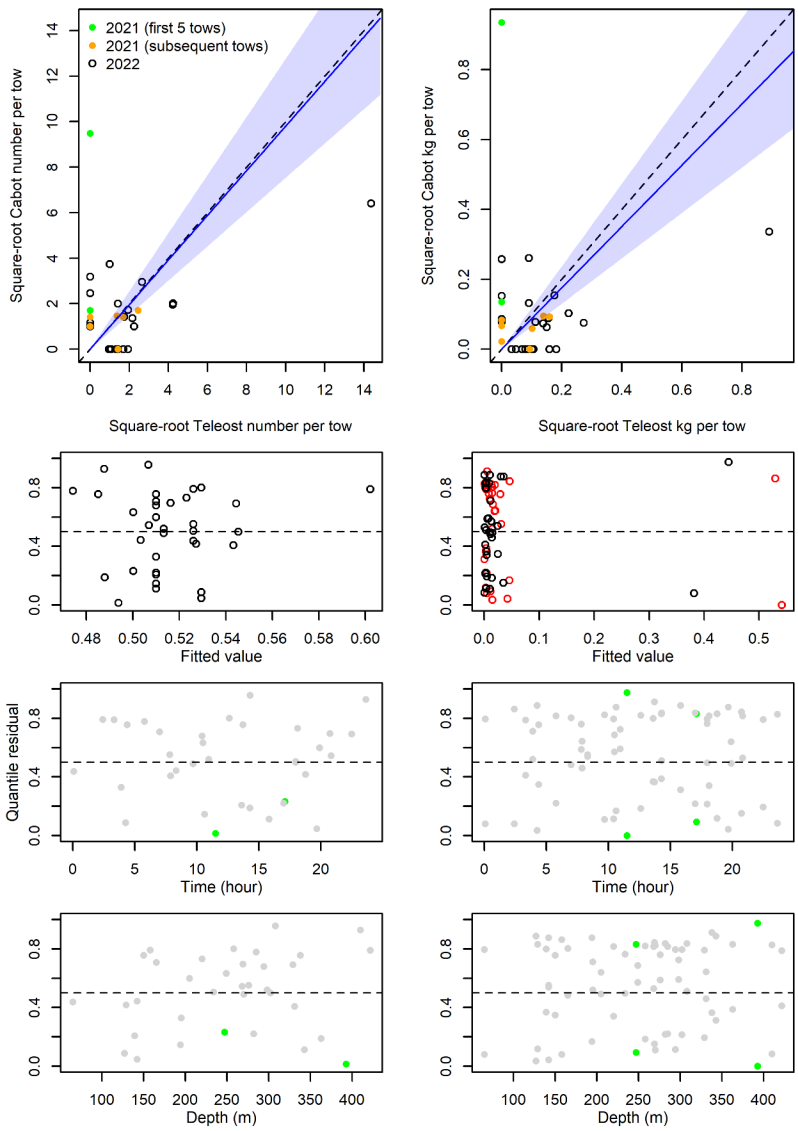

Figure 64.Visualisation of comparative fishing data, size-aggregated model predictions and residual plots for Ptychogena lactea.

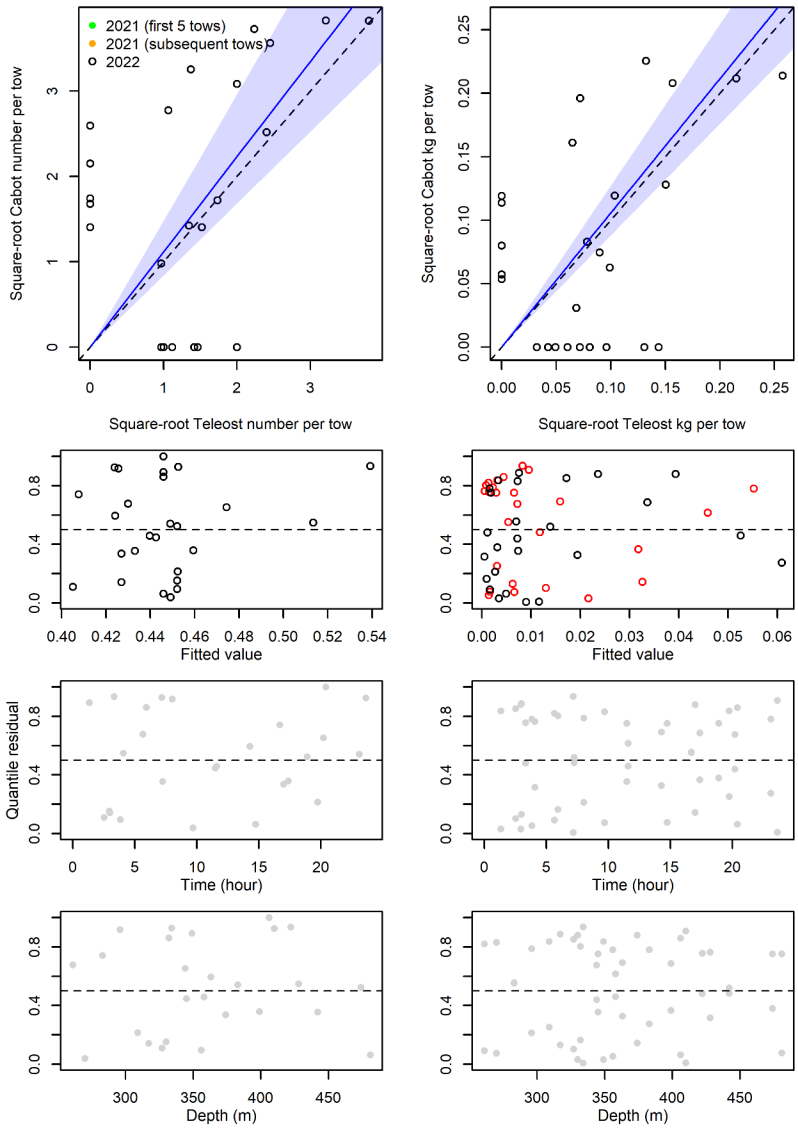

Figure 65.Visualisation of comparative fishing data, size-aggregated model predictions and residual plots for Rhodaliidae.

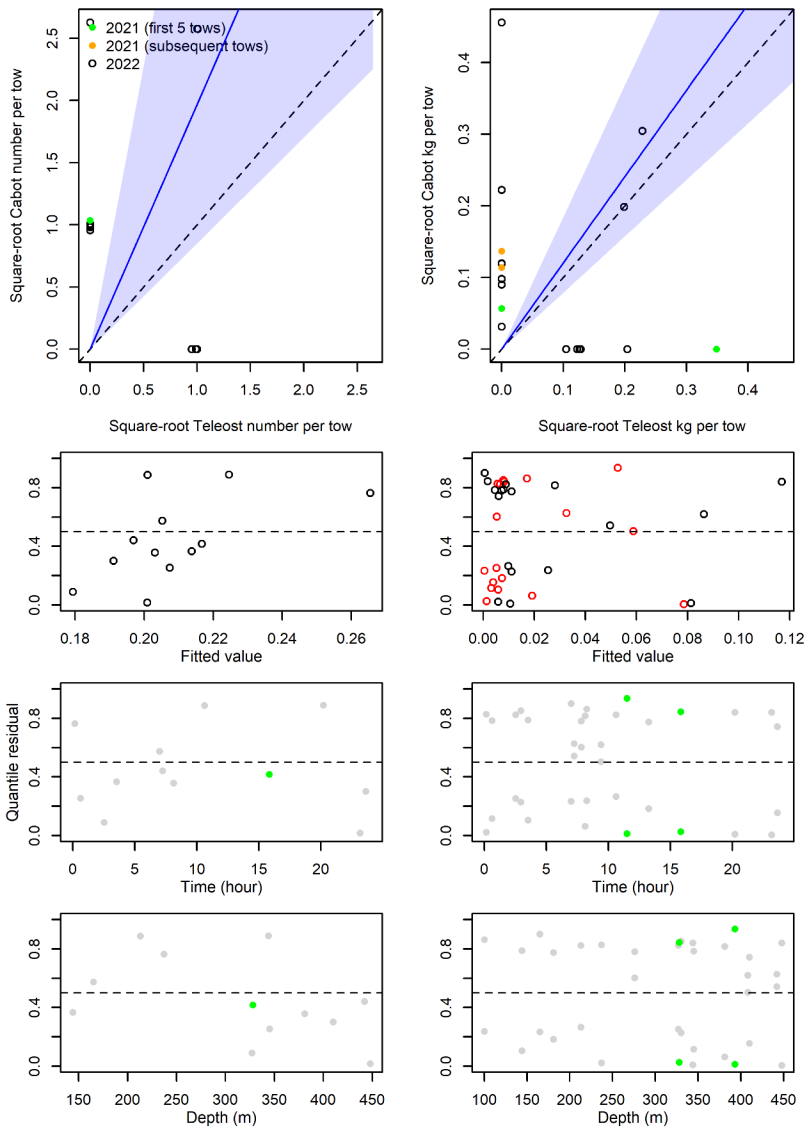

Figure 66.Visualisation of comparative fishing data, size-aggregated model predictions and residual plots for Scyphozoa.

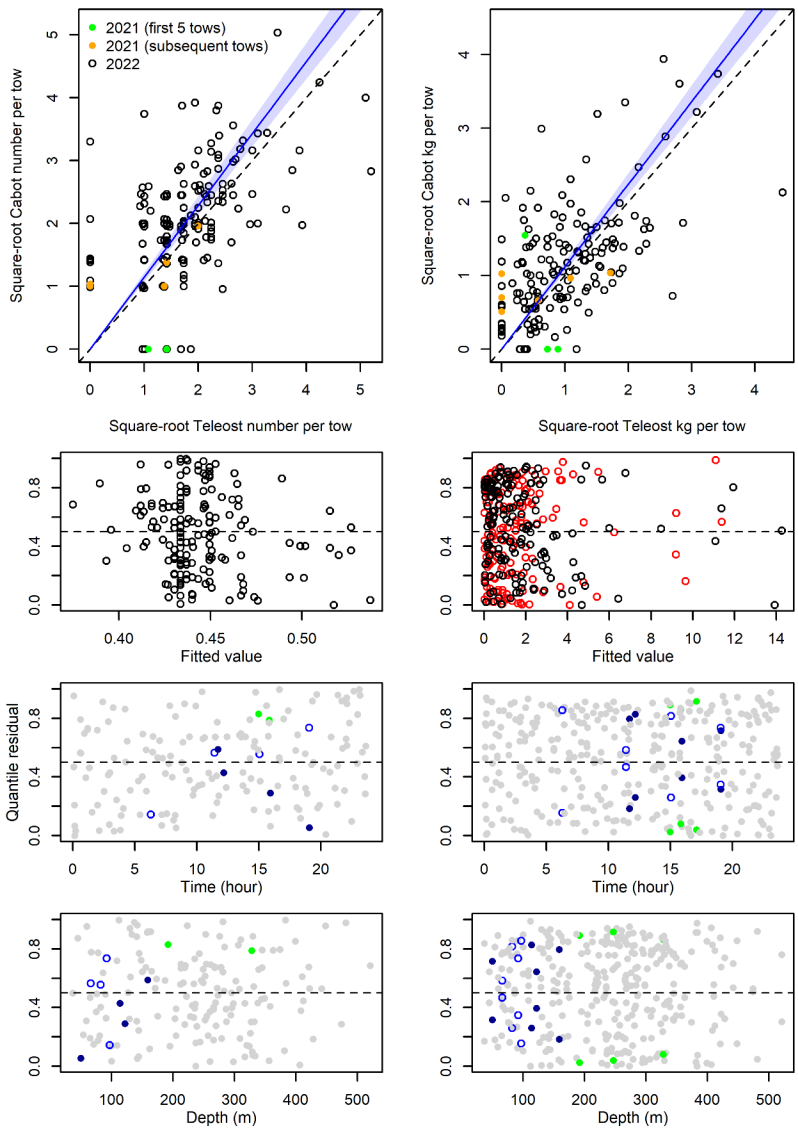

Figure 67.Visualisation of comparative fishing data, size-aggregated model predictions and residual plots for Cyanea capillata.

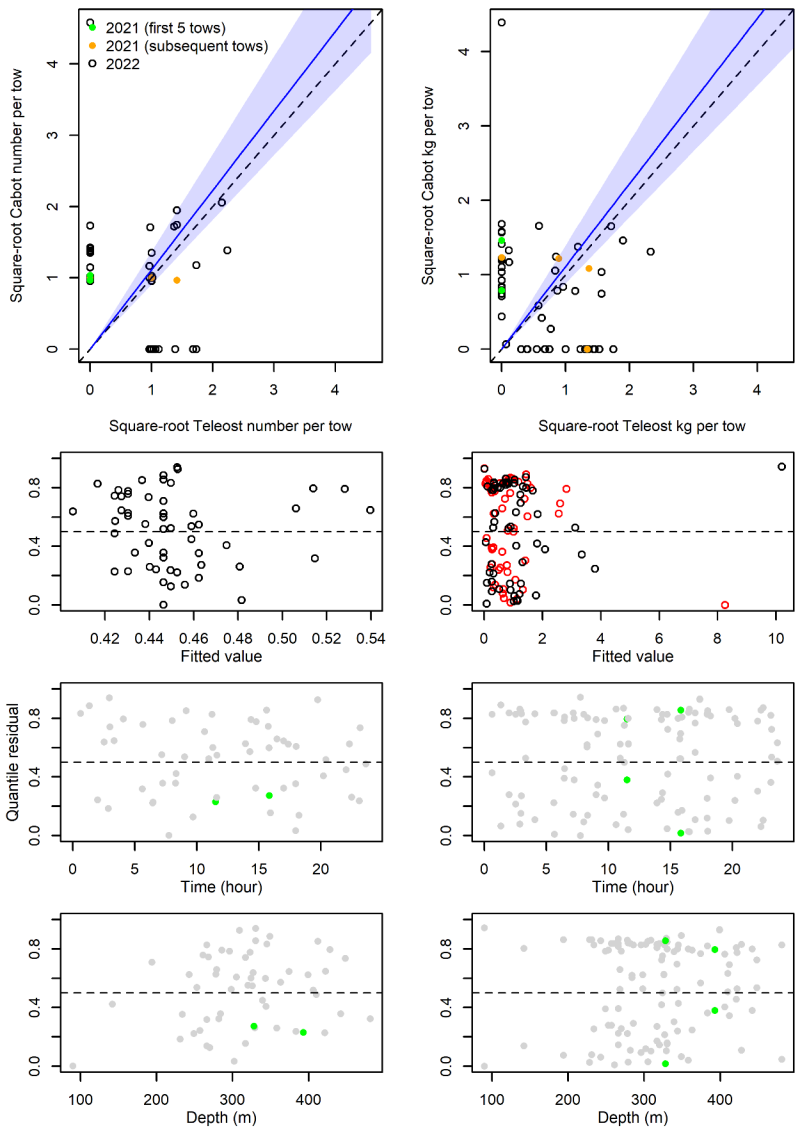

Figure 68.Visualisation of comparative fishing data, size-aggregated model predictions and residual plots for Periphylla periphylla.

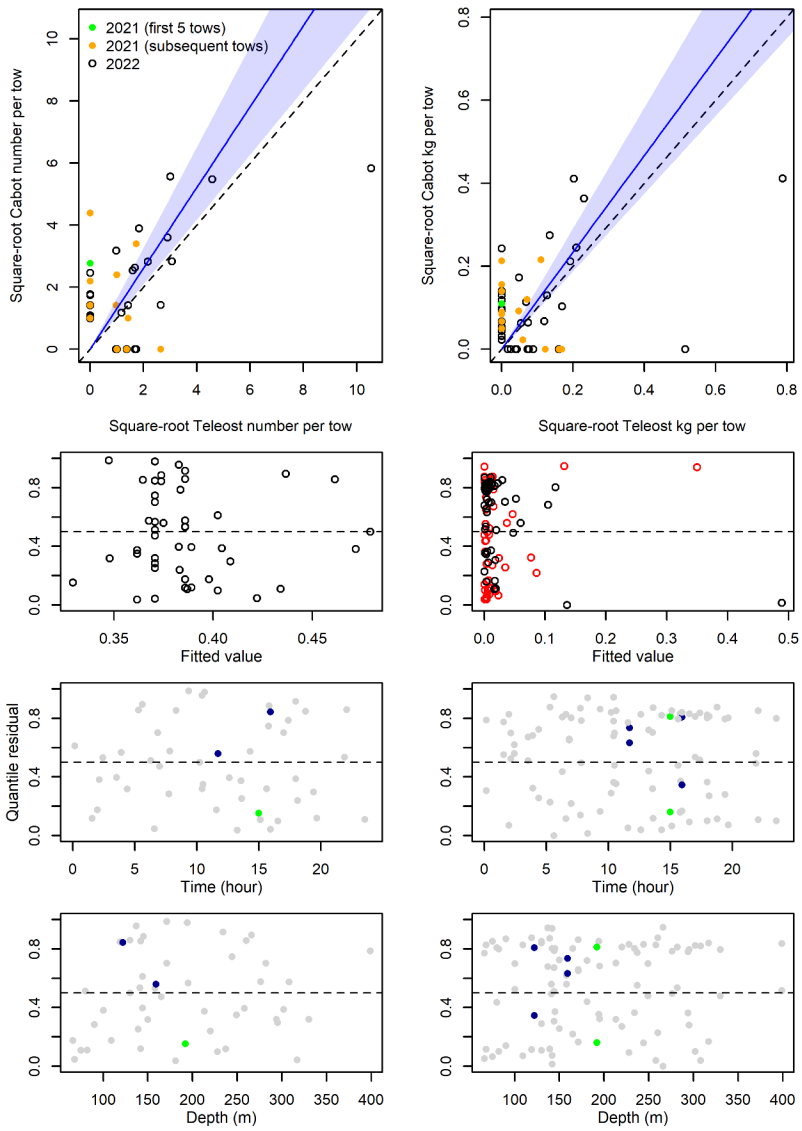

Figure 69.Visualisation of comparative fishing data, size-aggregated model predictions and residual plots for Hormathia digitata.

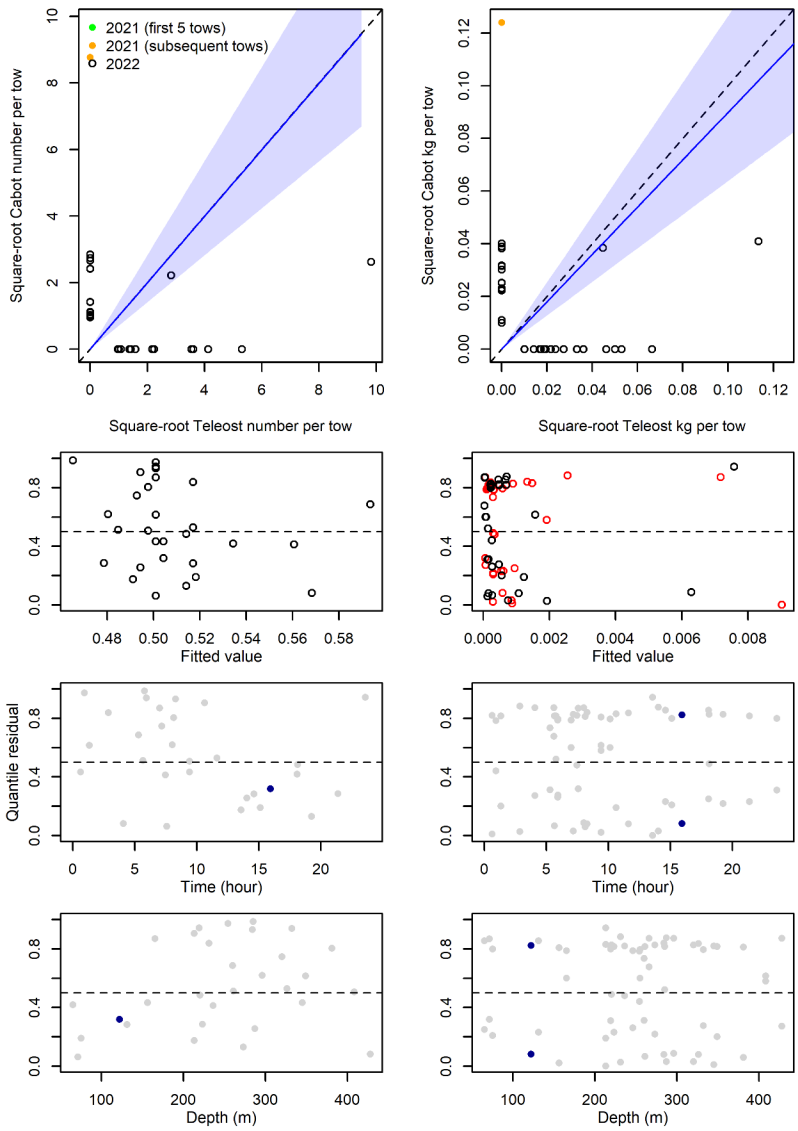

Figure 70.Visualisation of comparative fishing data, size-aggregated model predictions and residual plots for Epizoanthus erdmanni.

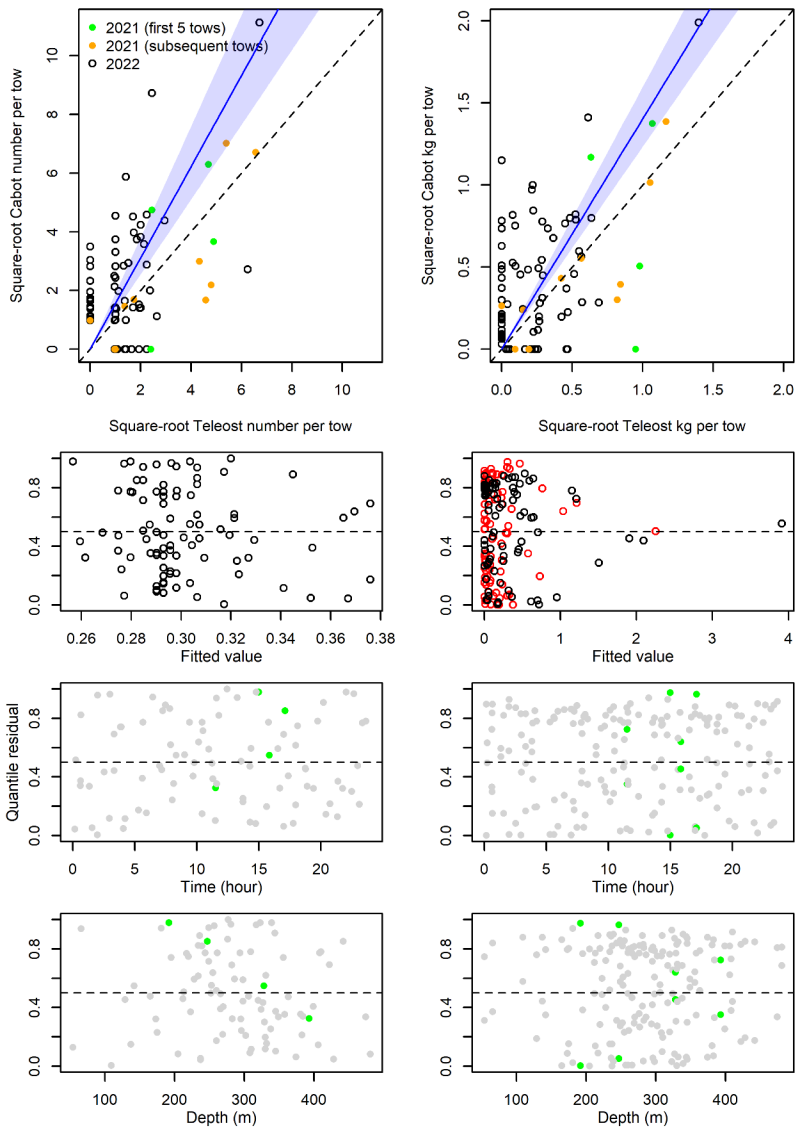

Figure 71.Visualisation of comparative fishing data, size-aggregated model predictions and residual plots for Bolocera tuediae.

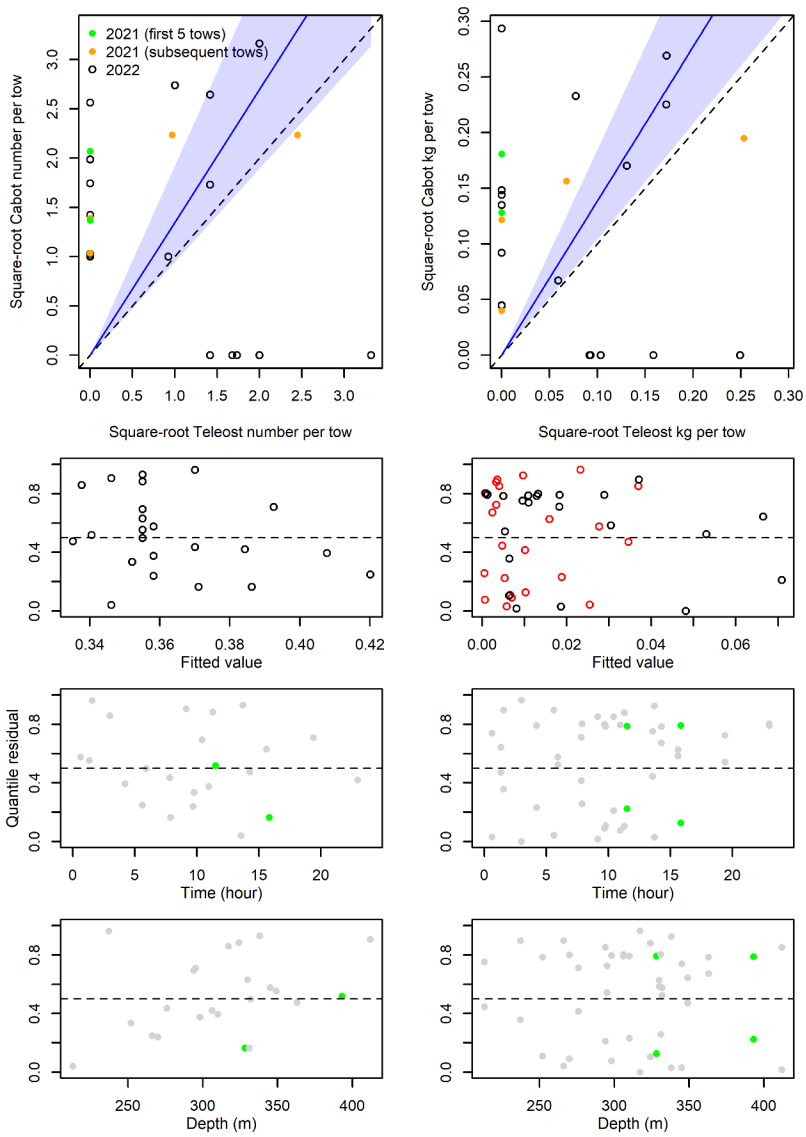

Figure 72.Visualisation of comparative fishing data, size-aggregated model predictions and residual plots for Stephanauge nexilis.

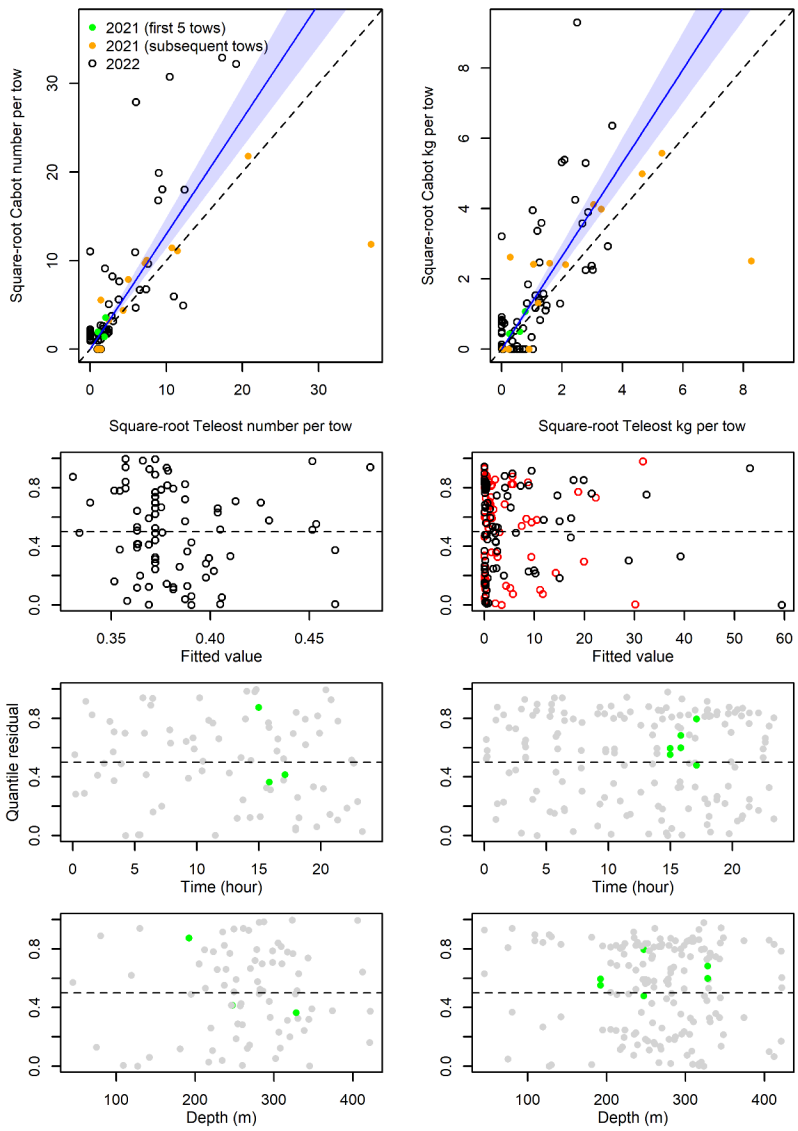

Figure 73.Visualisation of comparative fishing data, size-aggregated model predictions and residual plots for Actinostola callosa.

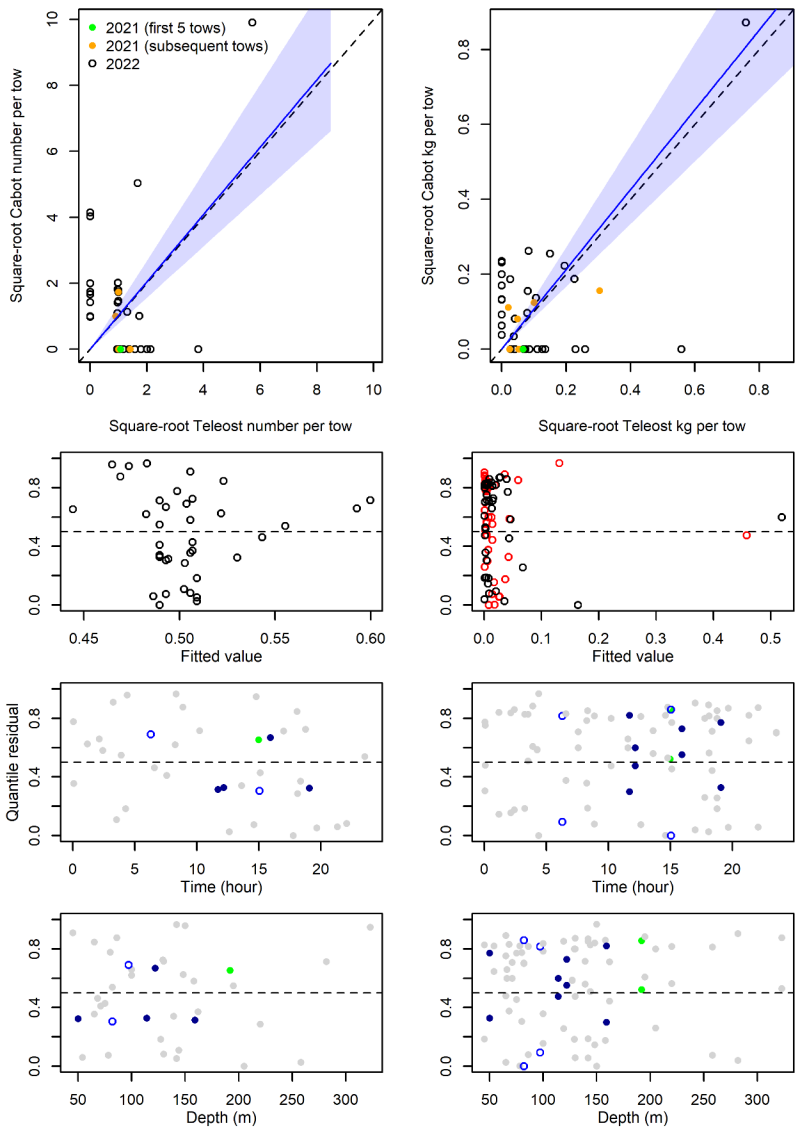

Figure 74.Visualisation of comparative fishing data, size-aggregated model predictions and residual plots for Stomphia coccinea.

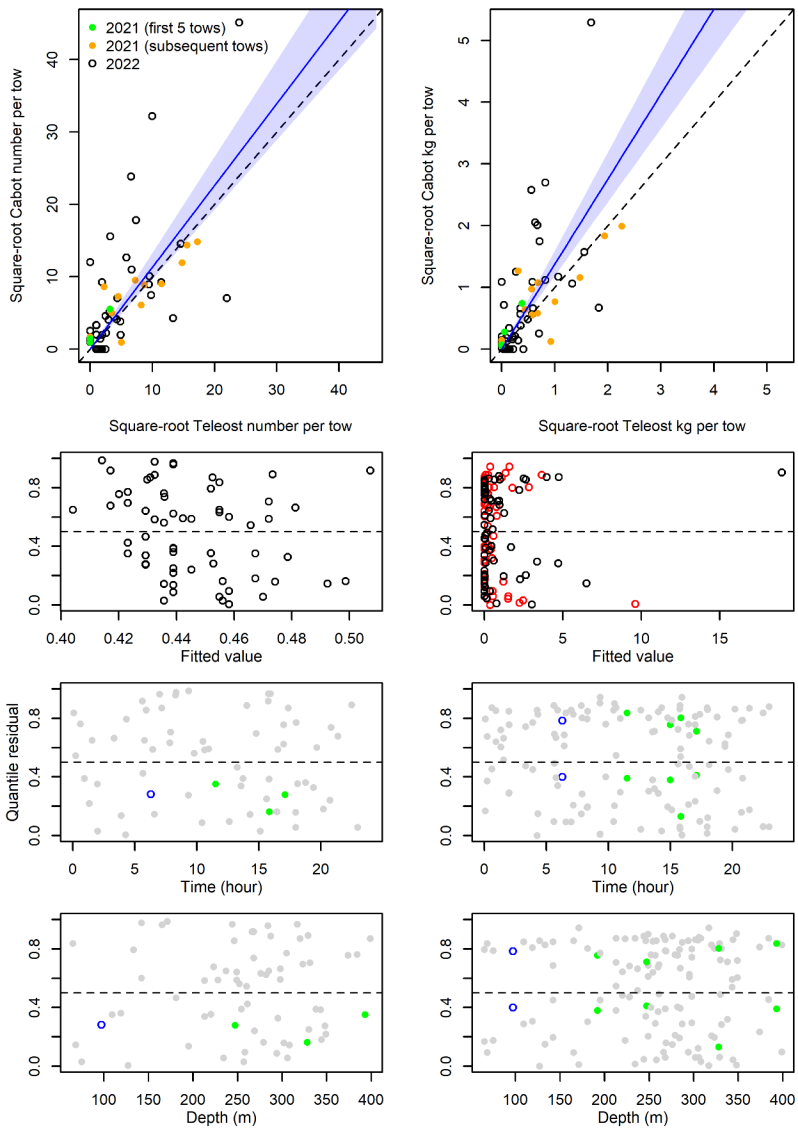

Figure 75.Visualisation of comparative fishing data, size-aggregated model predictions and residual plots for Actinauge cristata.

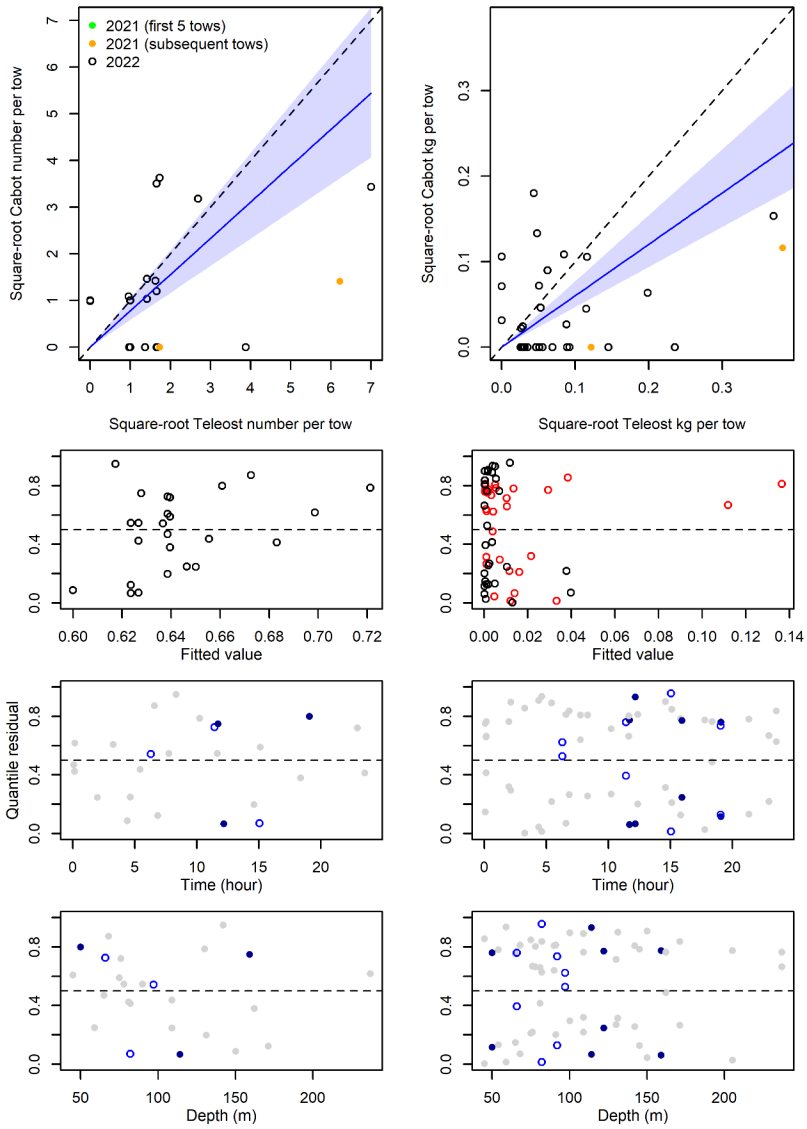

Figure 76.Visualisation of comparative fishing data, size-aggregated model predictions and residual plots for Gersemia rubiformis.

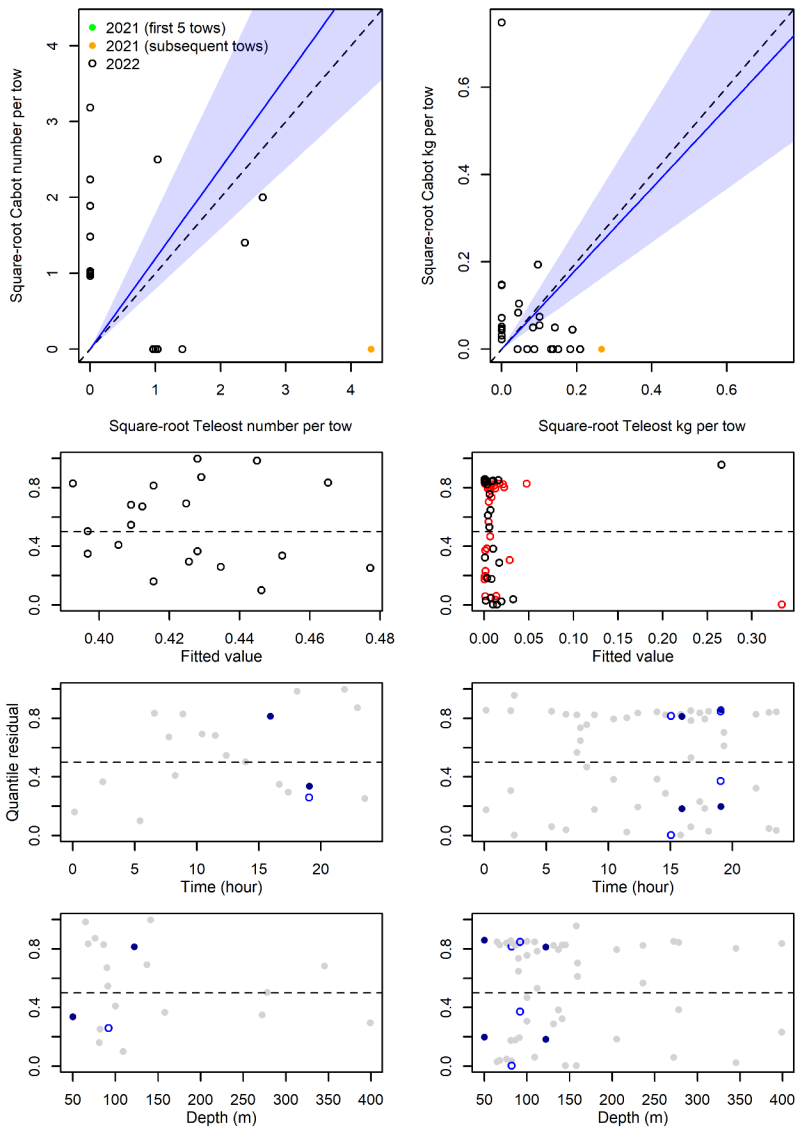

Figure 77.Visualisation of comparative fishing data, size-aggregated model predictions and residual plots for Drifa glomerata.

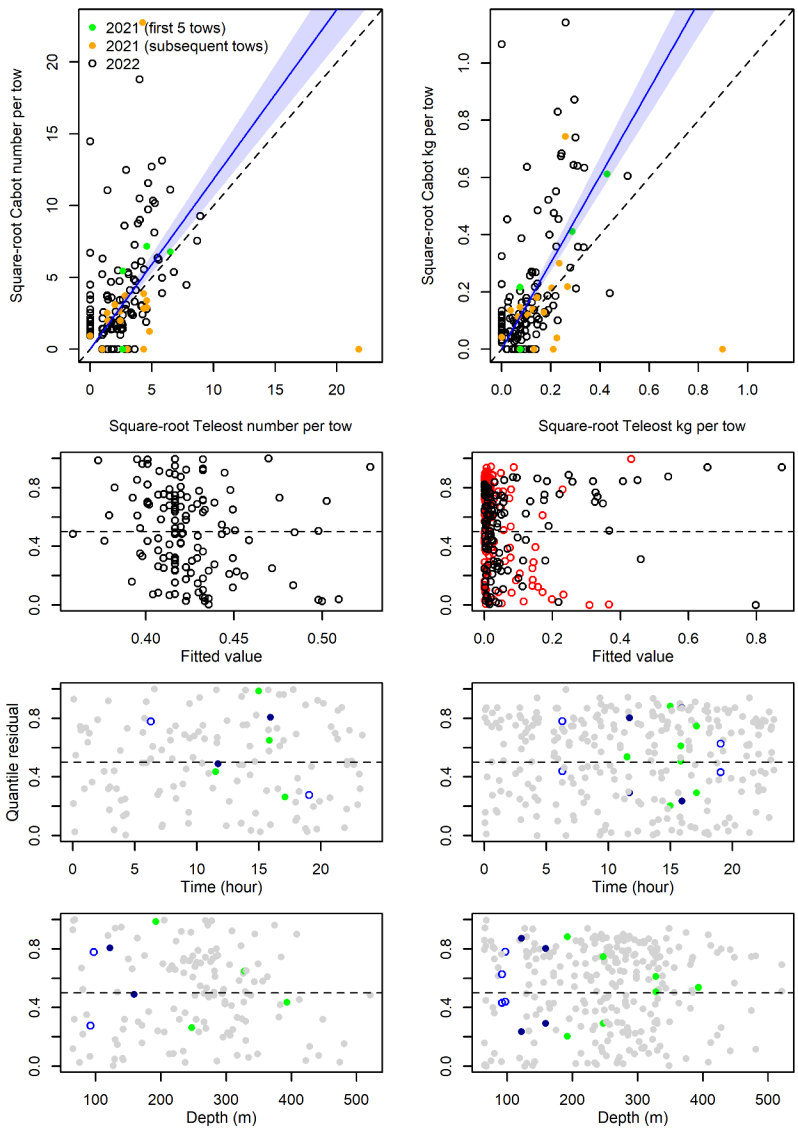

Figure 78.Visualisation of comparative fishing data, size-aggregated model predictions and residual plots for Pennatula aculeata.

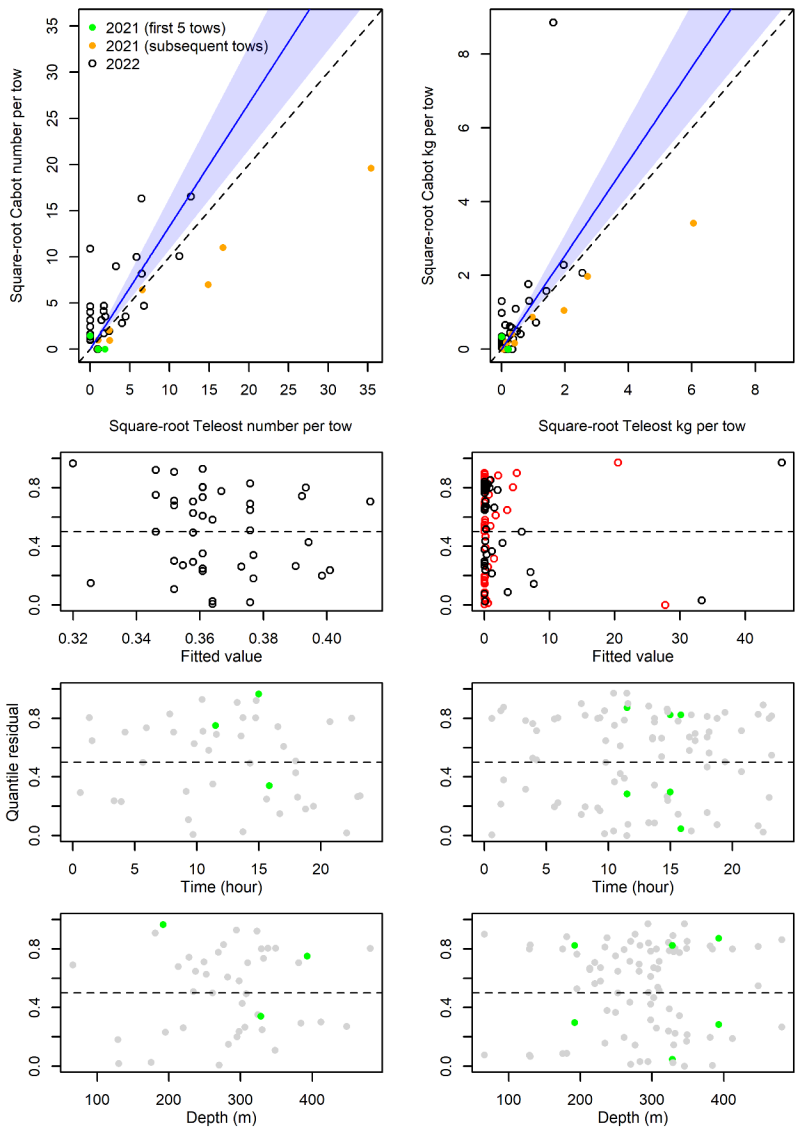

Figure 79. Visualisation of comparative fishing data, size-aggregated model predictions and residual plots for Ptilella grandis.

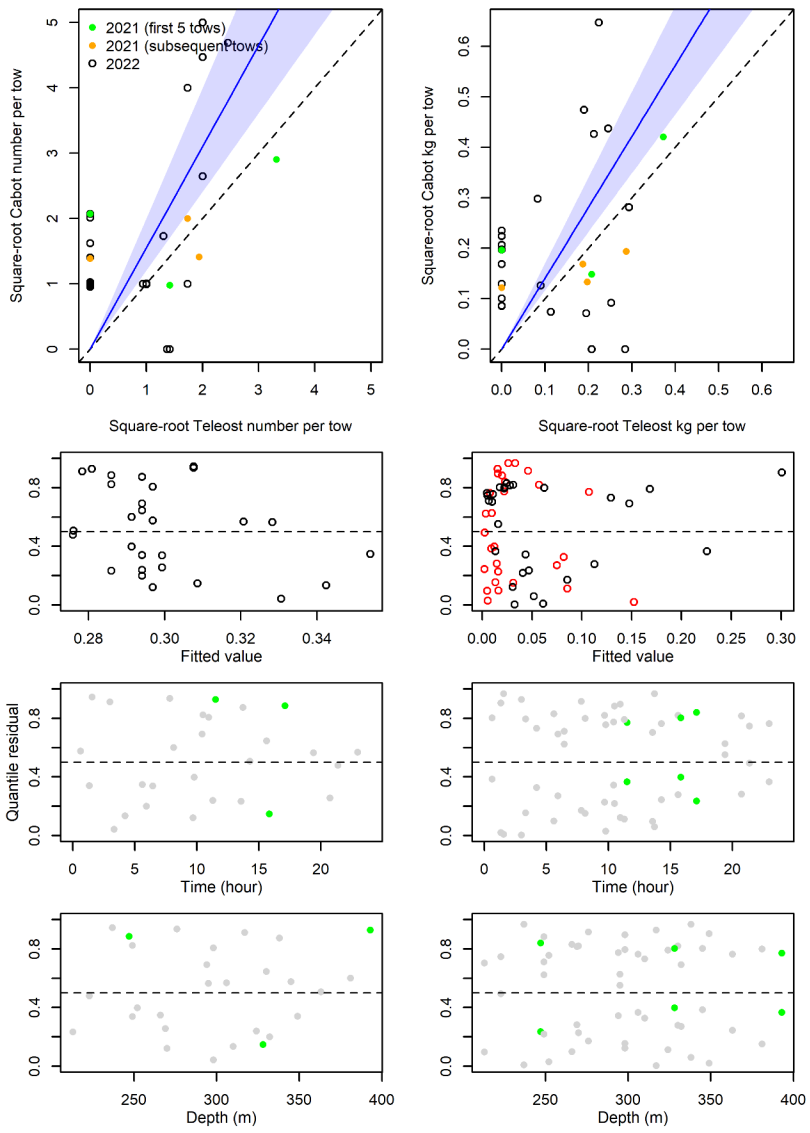

Figure 80.Visualisation of comparative fishing data, size-aggregated model predictions and residual plots for Halipteris finmarchica.

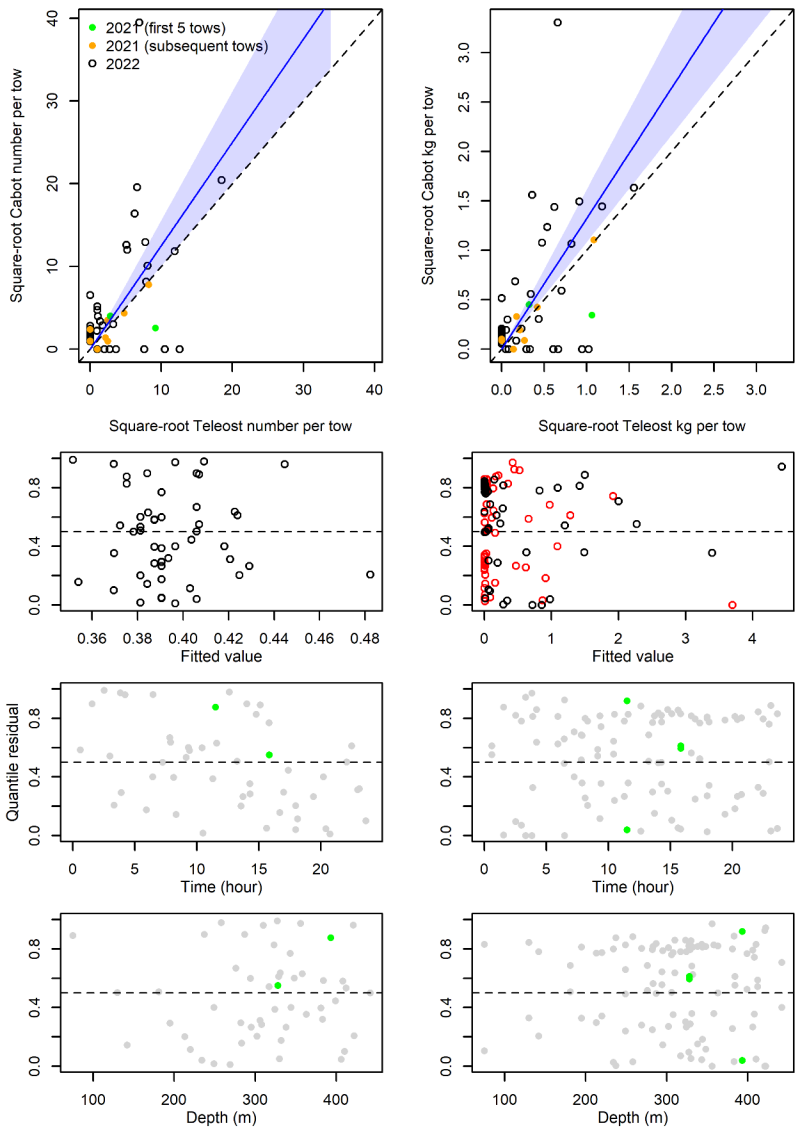

Figure 81.Visualisation of comparative fishing data, size-aggregated model predictions and residual plots for Anthoptilum grandiflorum.

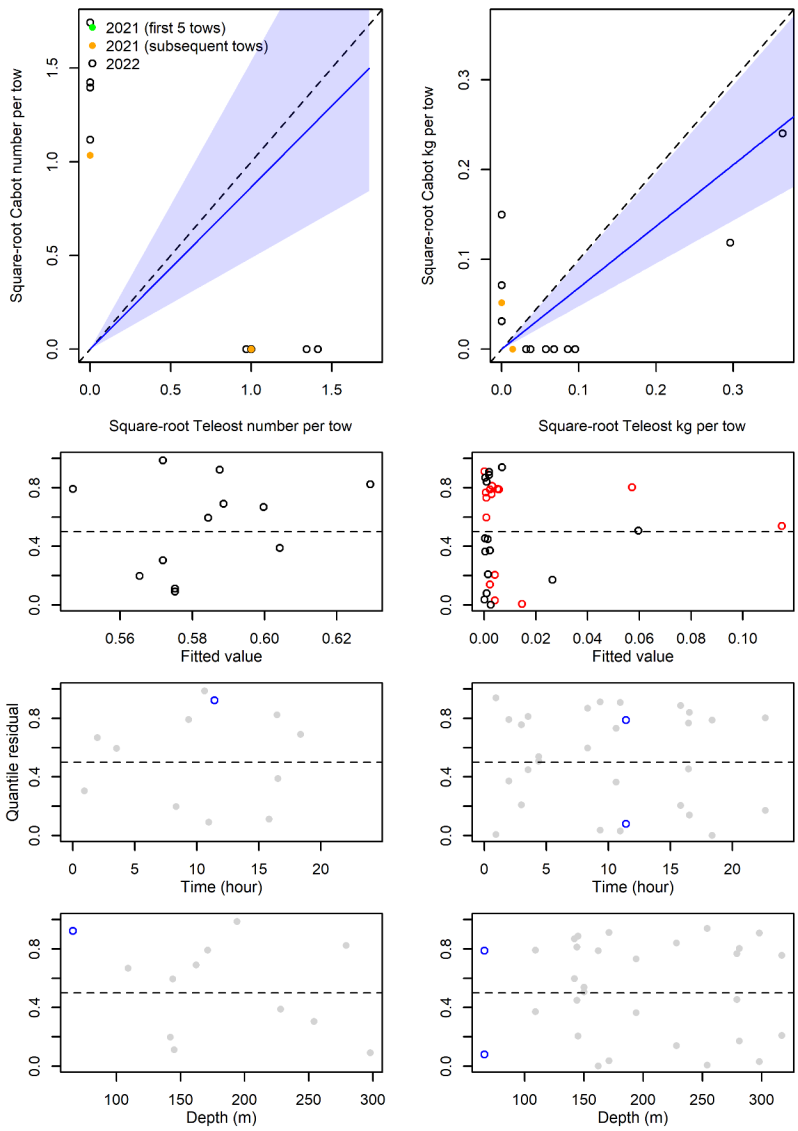

Figure 82.Visualisation of comparative fishing data, size-aggregated model predictions and residual plots for Nephtheidae.

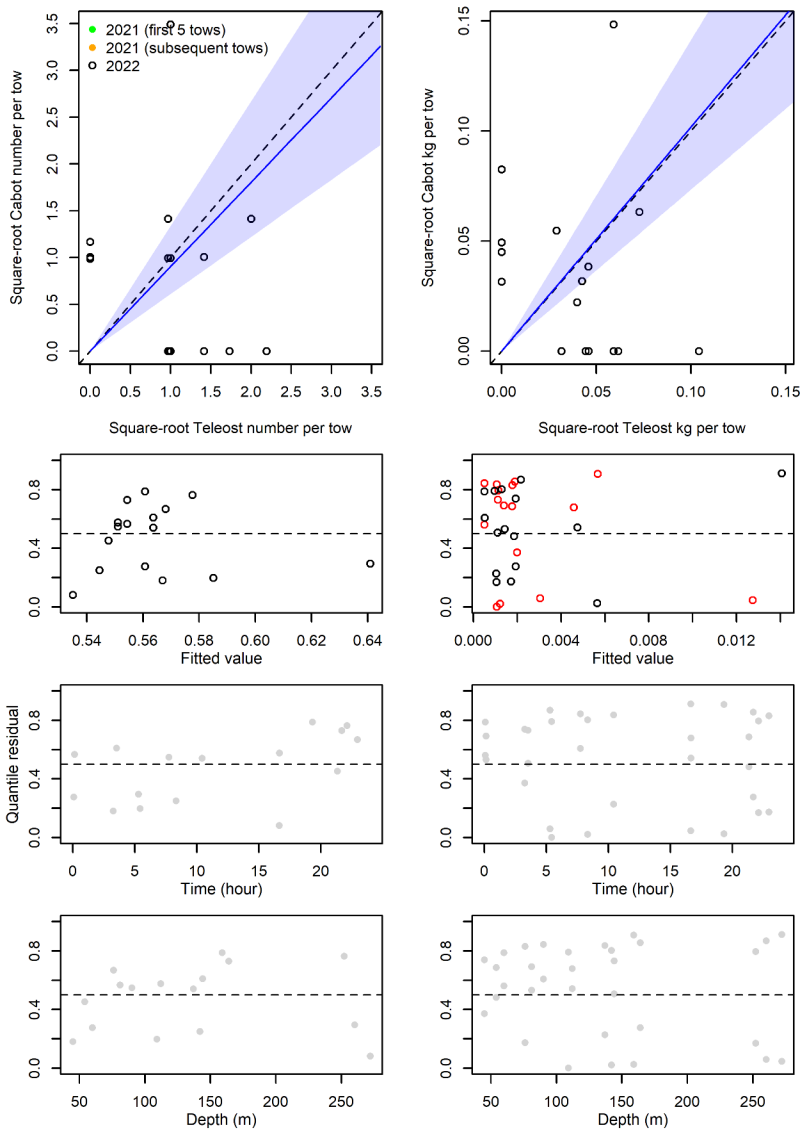

Figure 83.Visualisation of comparative fishing data, size-aggregated model predictions and residual plots for Pleurobrachia pileus.

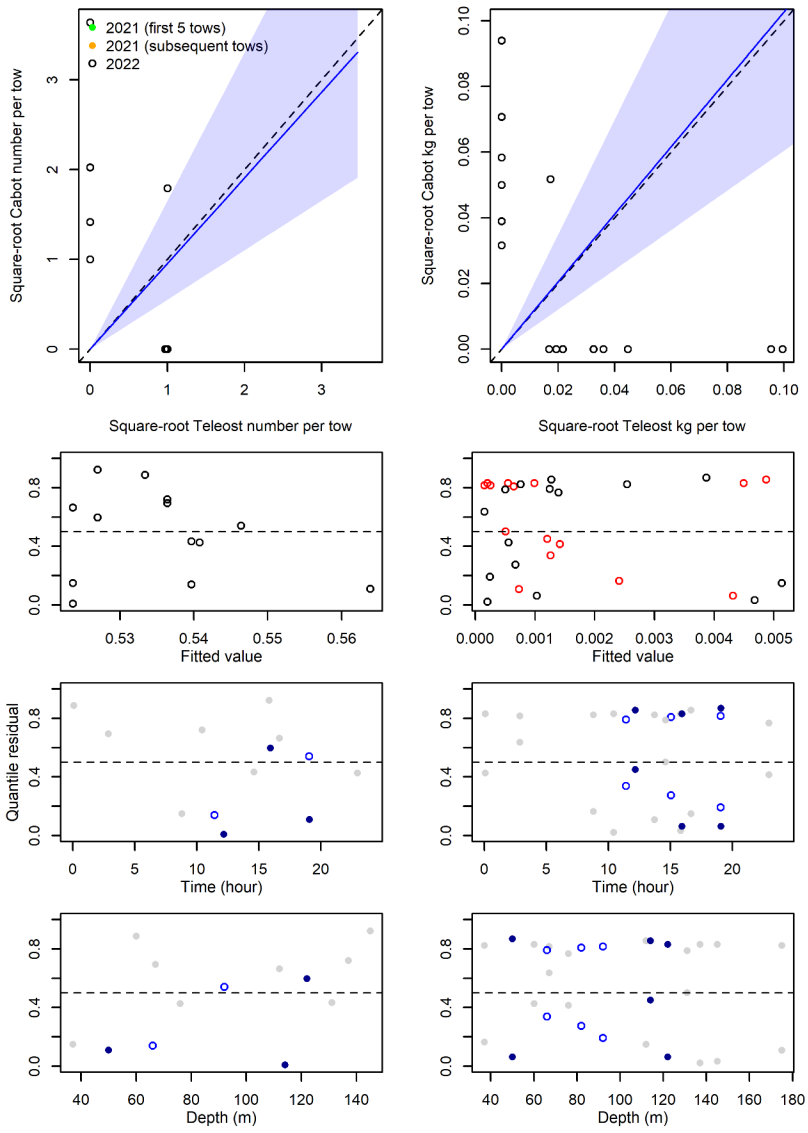

Figure 84.Visualisation of comparative fishing data, size-aggregated model predictions and residual plots for Bryozoa.

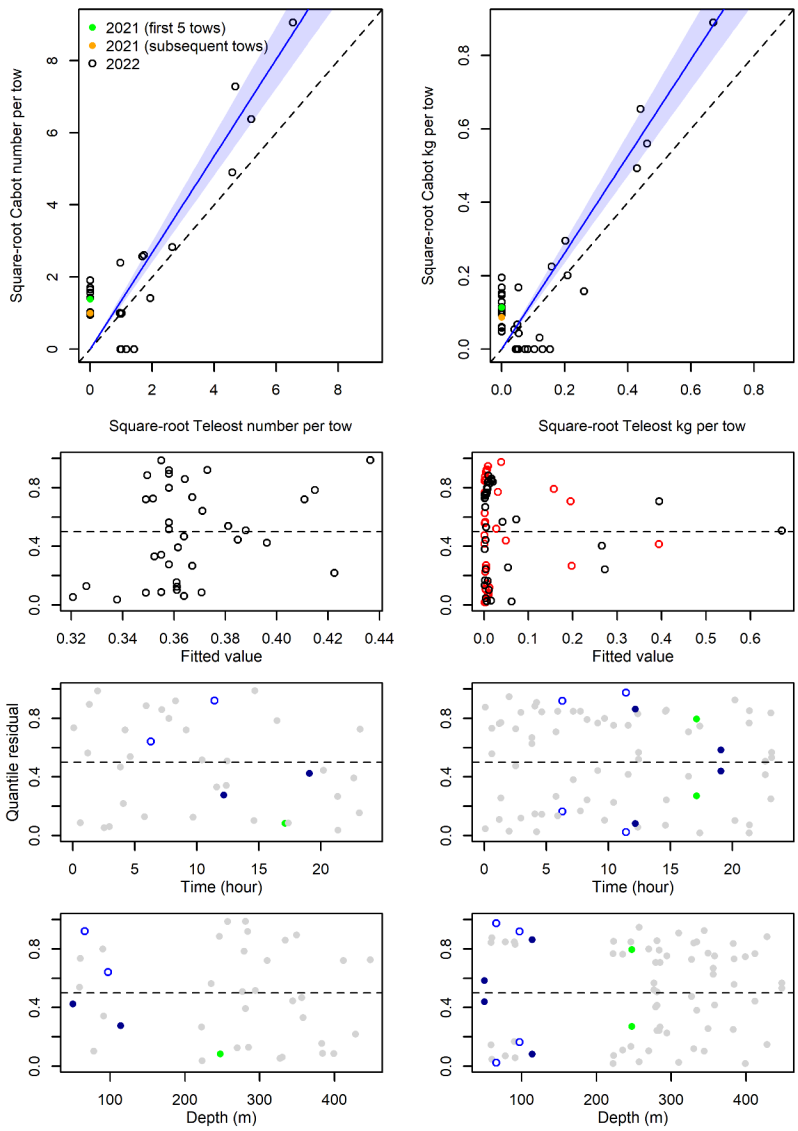

Figure 85.Visualisation of comparative fishing data, size-aggregated model predictions and residual plots for Arrhoges occidentalis.

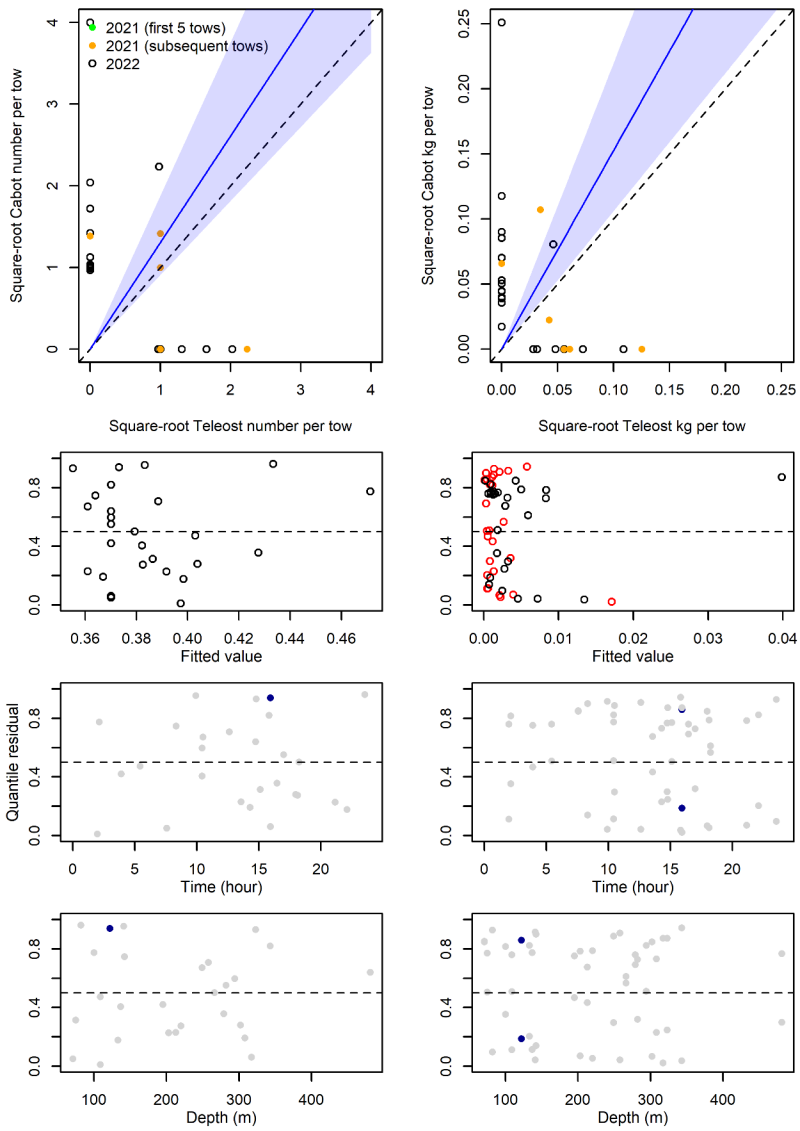

Figure 86.Visualisation of comparative fishing data, size-aggregated model predictions and residual plots for Cryptonatica affinis.

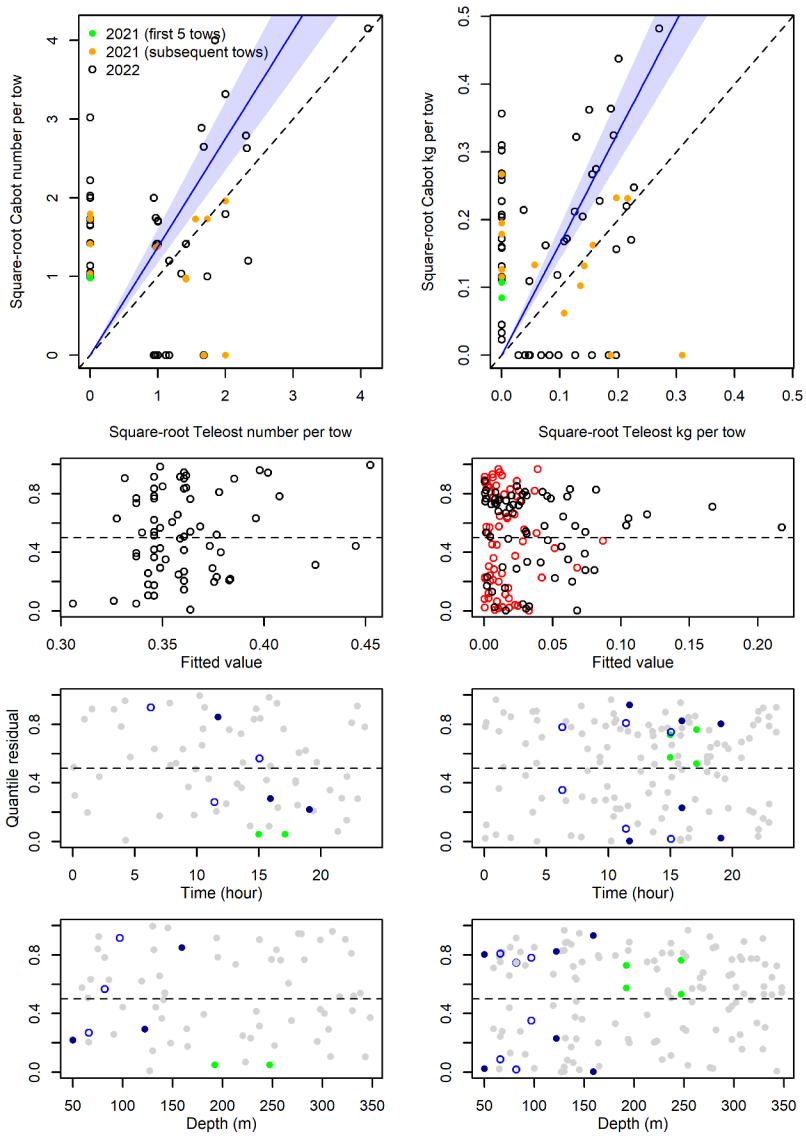

Figure 87.Visualisation of comparative fishing data, size-aggregated model predictions and residual plots for Buccinum sp.

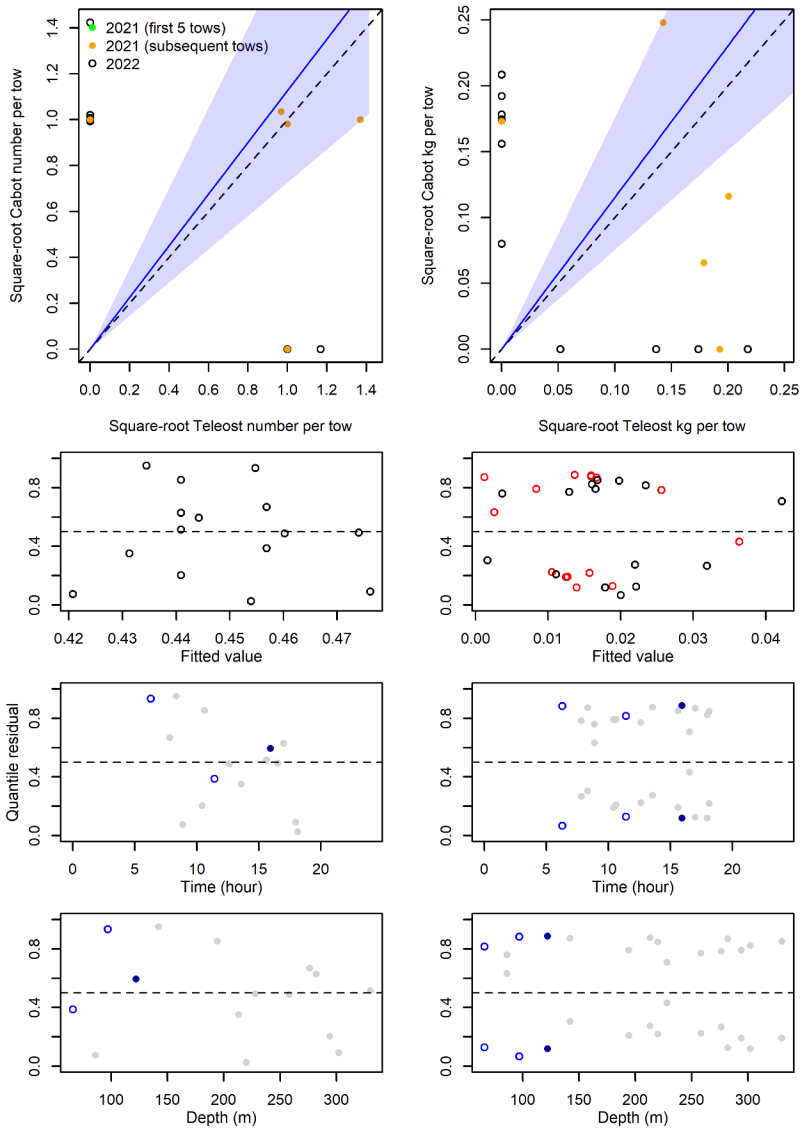

Figure 88.Visualisation of comparative fishing data, size-aggregated model predictions and residual plots for Neptunea despecta.

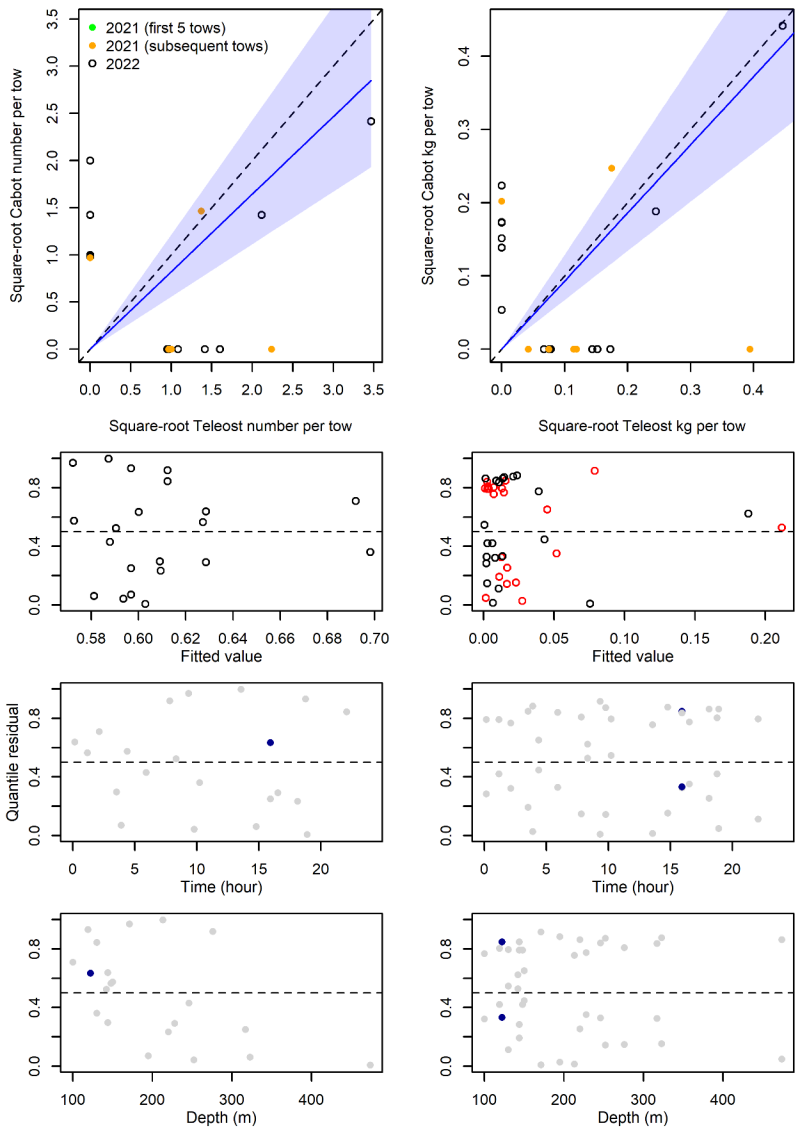

Figure 89.Visualisation of comparative fishing data, size-aggregated model predictions and residual plots for Colus sp.

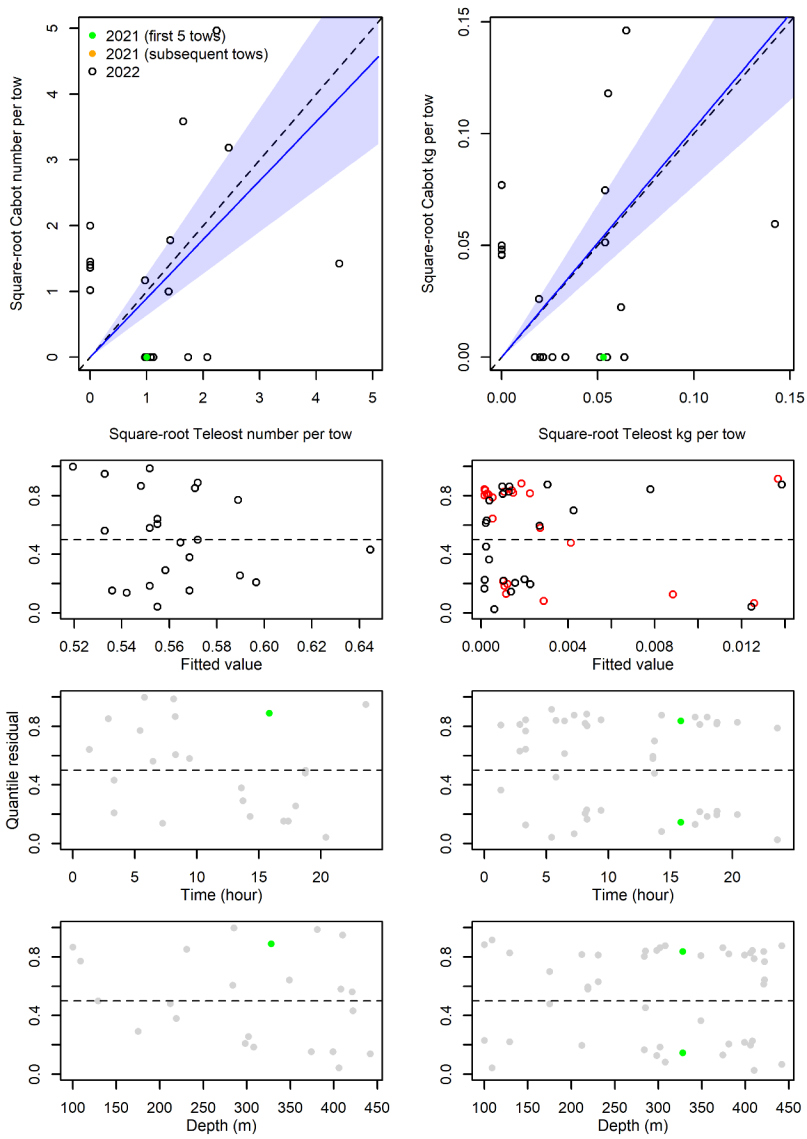

Figure 90.Visualisation of comparative fishing data, size-aggregated model predictions and residual plots for Scaphander punctostriatus.

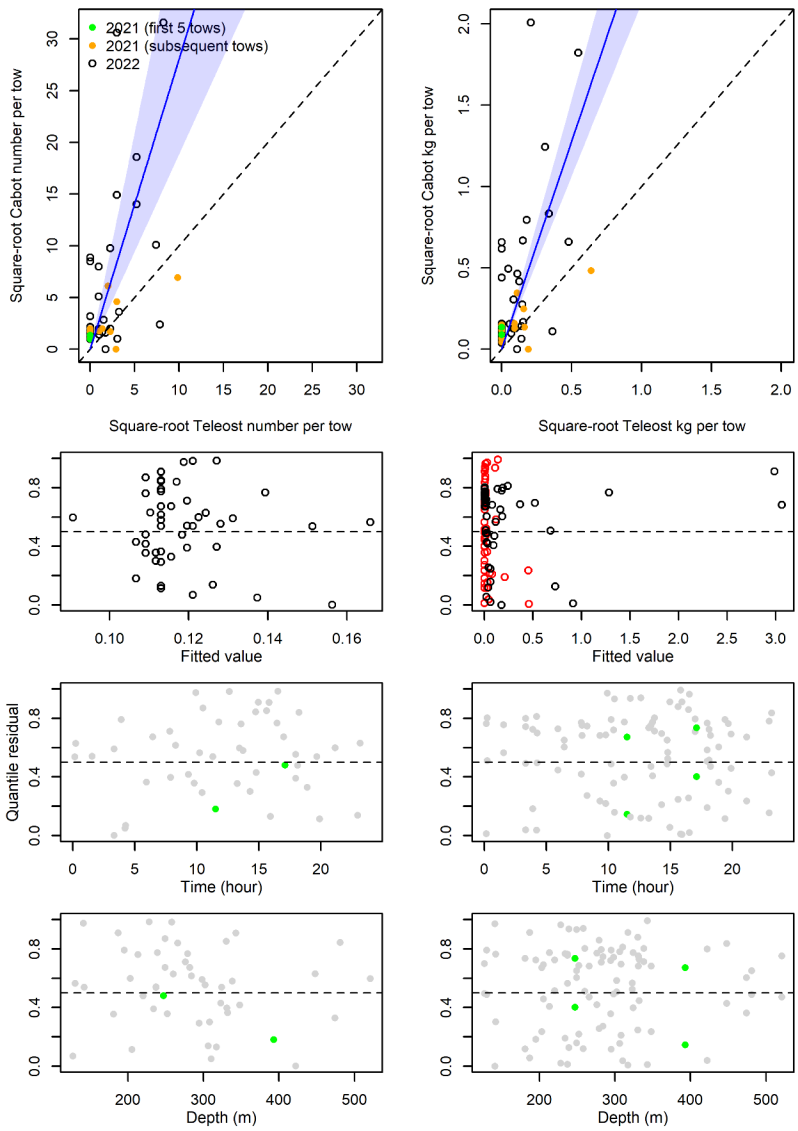

Figure 91.Visualisation of comparative fishing data, size-aggregated model predictions and residual plots for Megayoldia thraciaeformis.

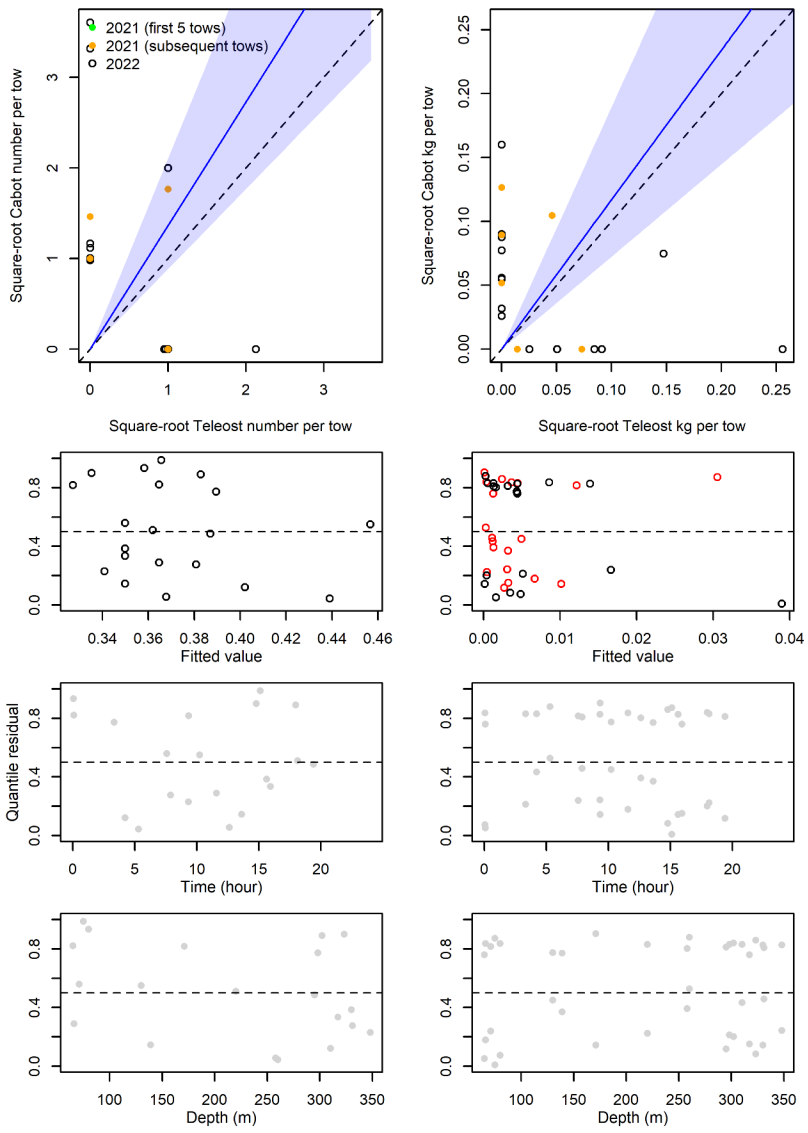

Figure 92.Visualisation of comparative fishing data, size-aggregated model predictions and residual plots for Mytilus sp.

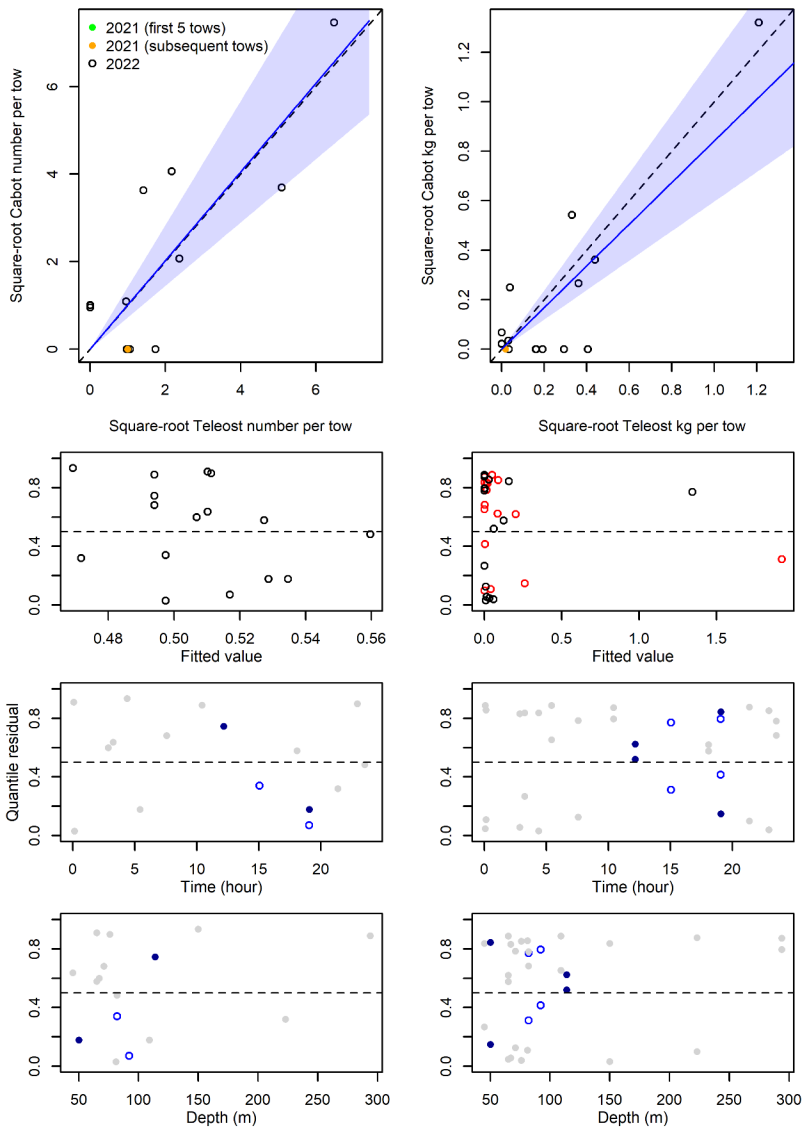

Figure 93.Visualisation of comparative fishing data, size-aggregated model predictions and residual plots for Chlamys islandica.

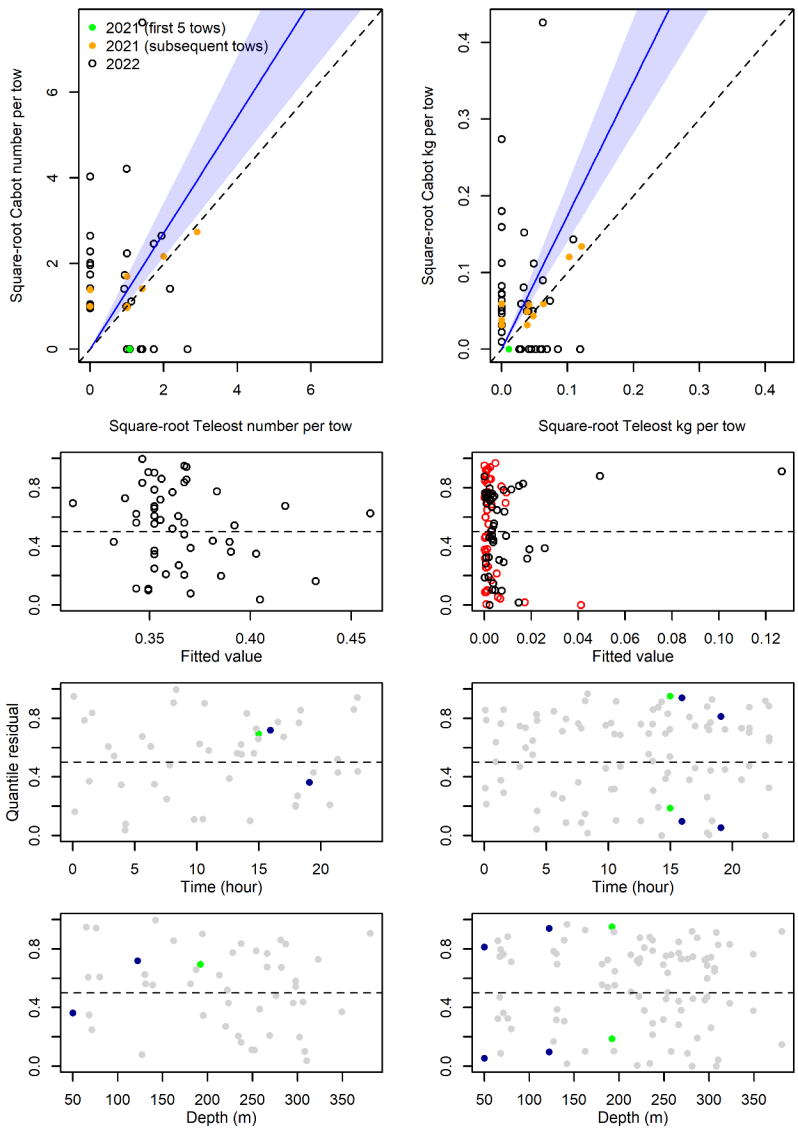

Figure 94.Visualisation of comparative fishing data, size-aggregated model predictions and residual plots for Astarte sp.

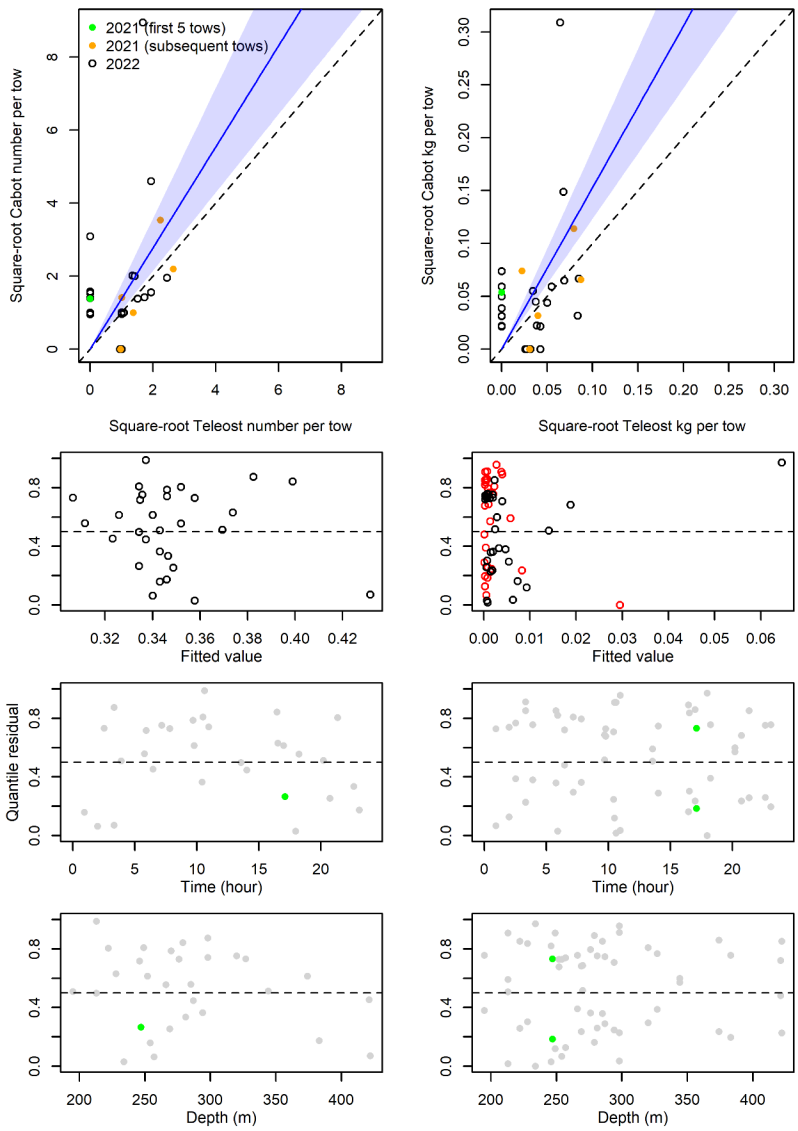

Figure 95.Visualisation of comparative fishing data, size-aggregated model predictions and residual plots for Cuspidaria glacialis.

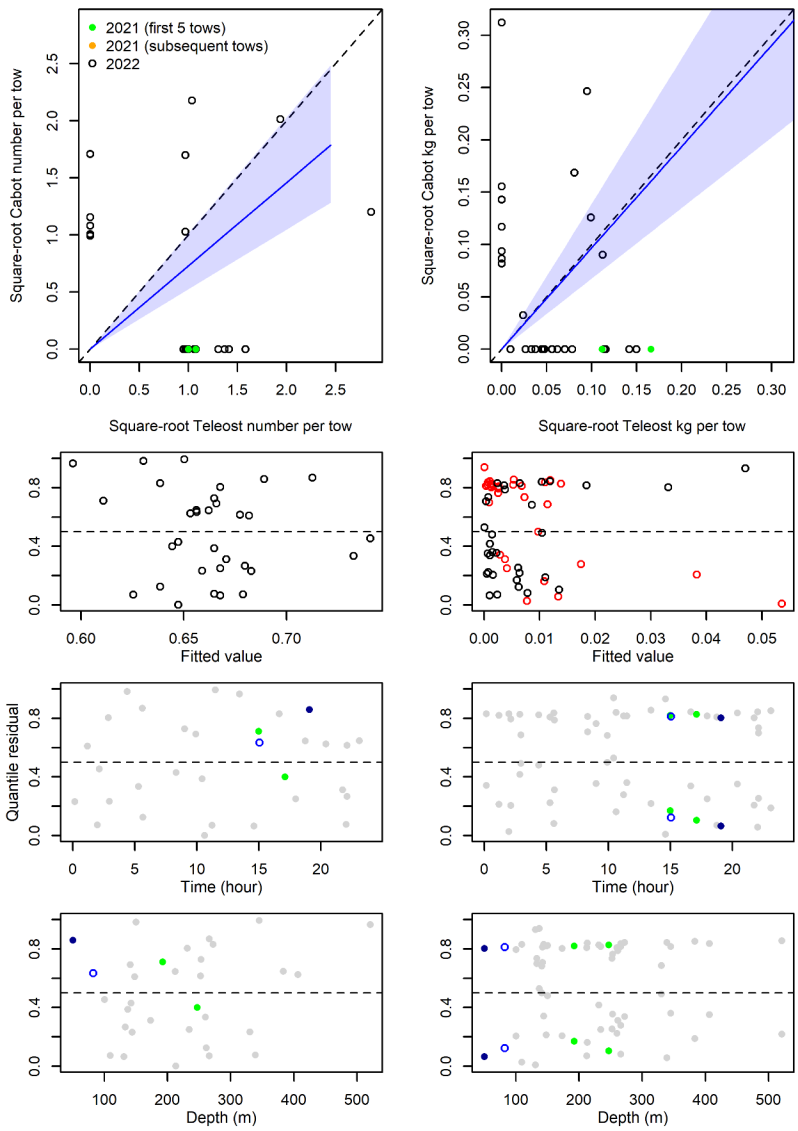

Figure 96.Visualisation of comparative fishing data, size-aggregated model predictions and residual plots for Rossia sp.

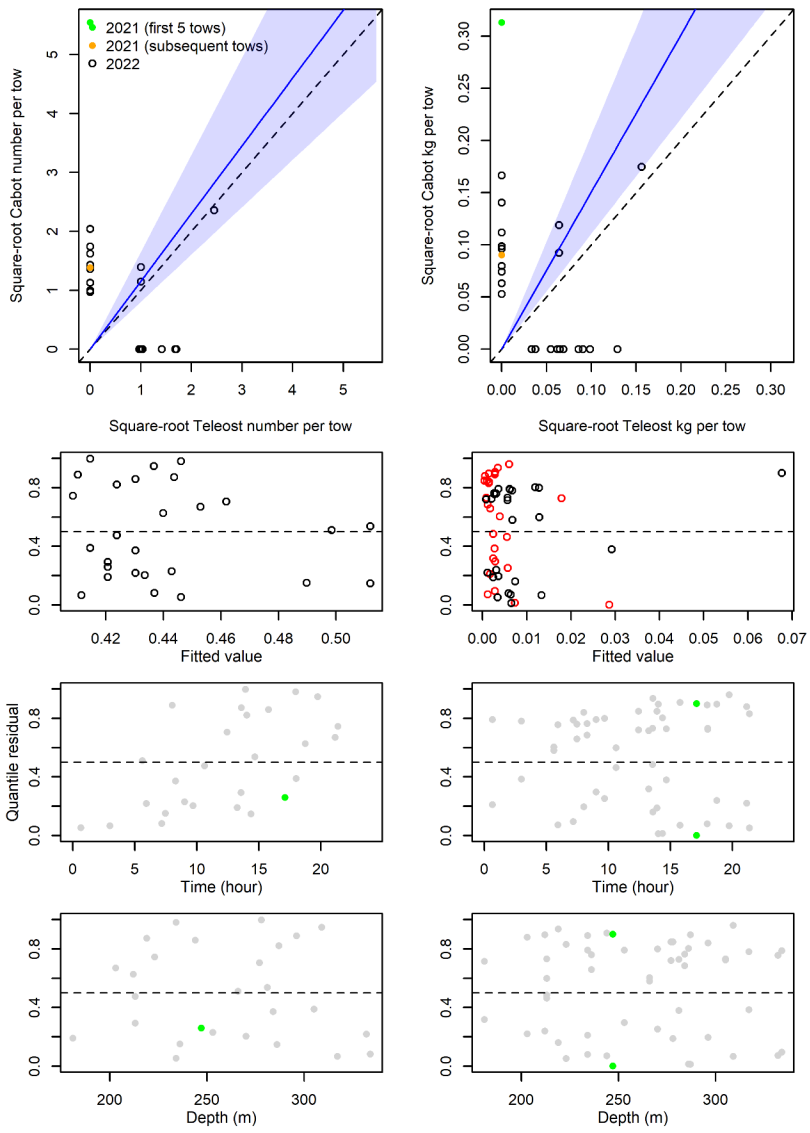

Figure 97.Visualisation of comparative fishing data, size-aggregated model predictions and residual plots for Stoloteuthis leucoptera.

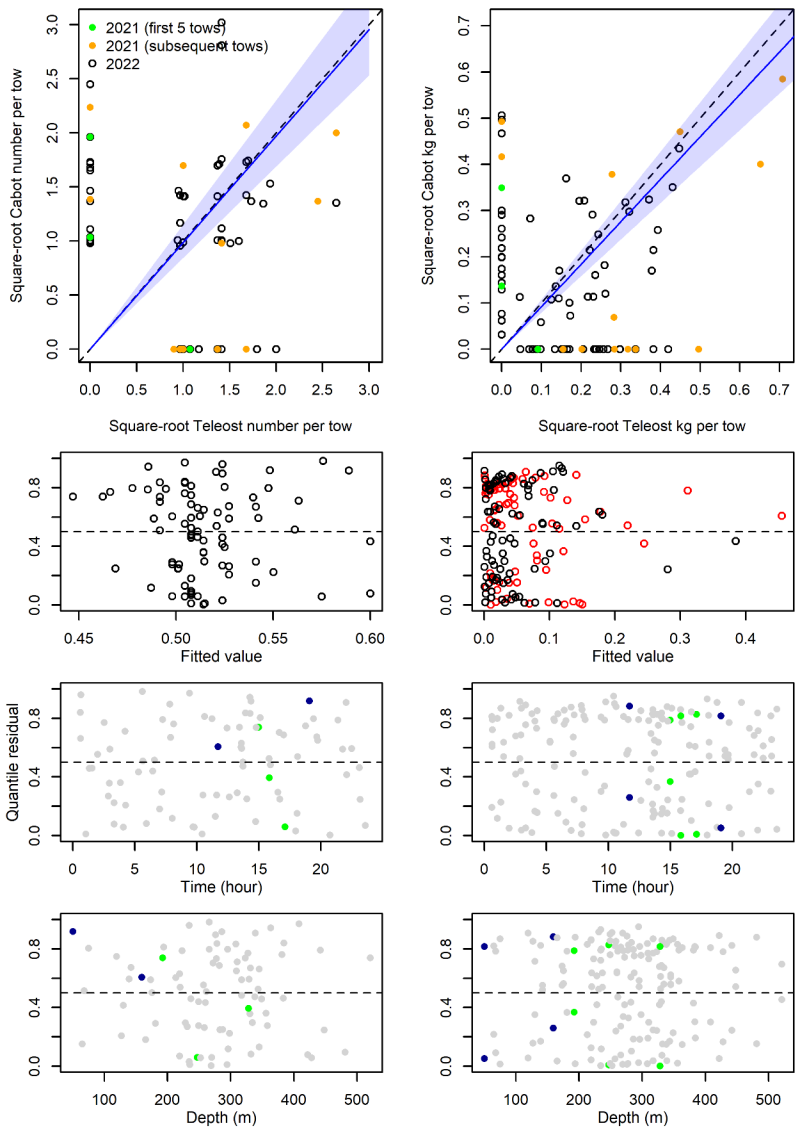

Figure 98.Visualisation of comparative fishing data, size-aggregated model predictions and residual plots for Bathypolypus bairdii.

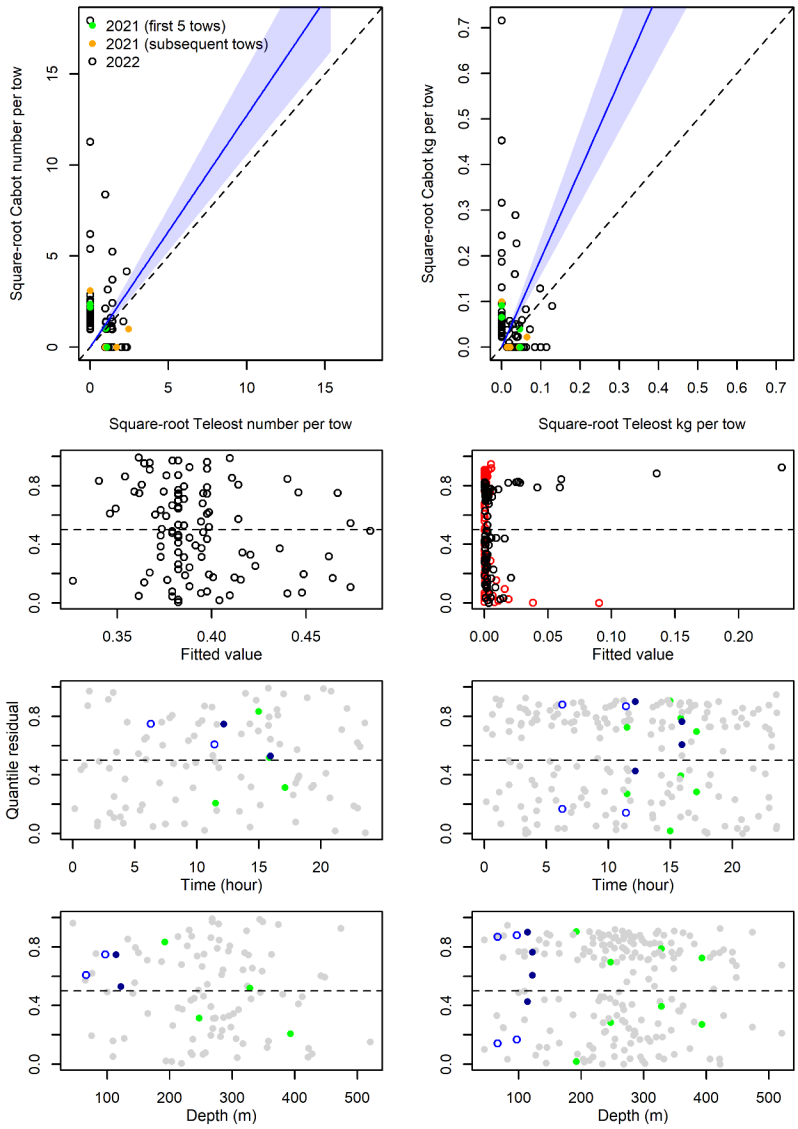

Figure 99.Visualisation of comparative fishing data, size-aggregated model predictions and residual plots for Polychaeta.

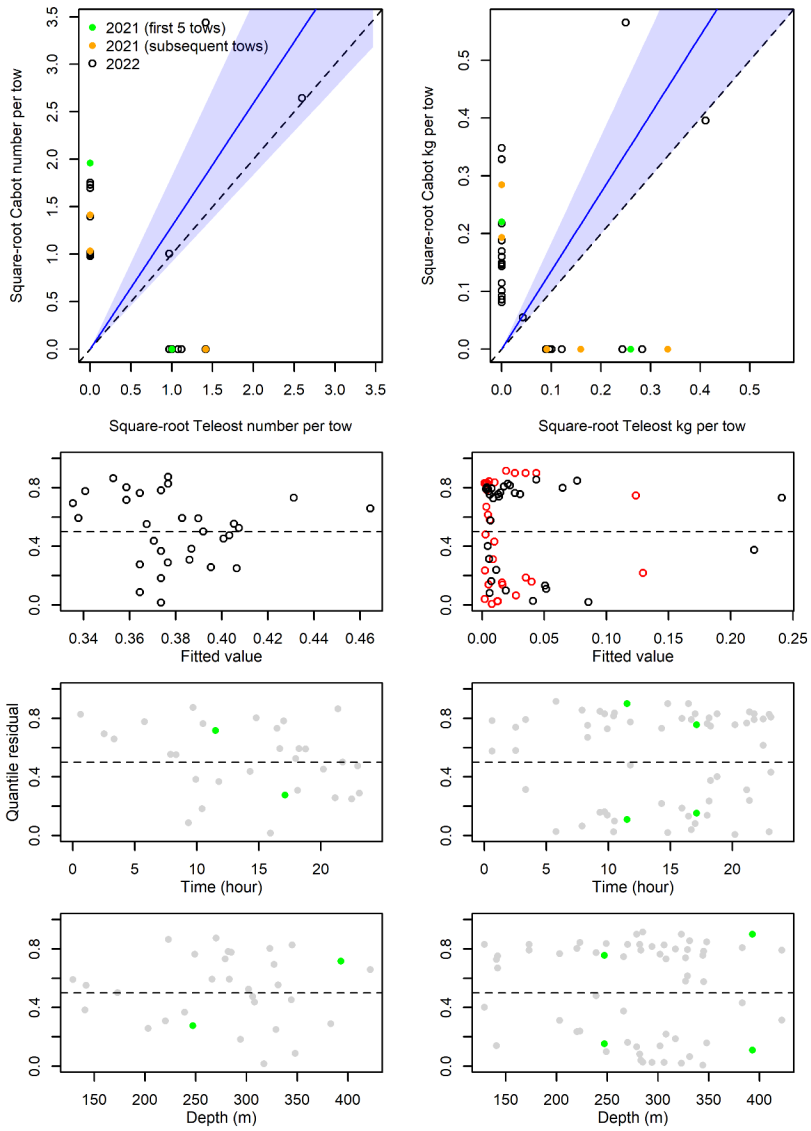

Figure 100.Visualisation of comparative fishing data, size-aggregated model predictions and residual plots for Aphrodita hastata.

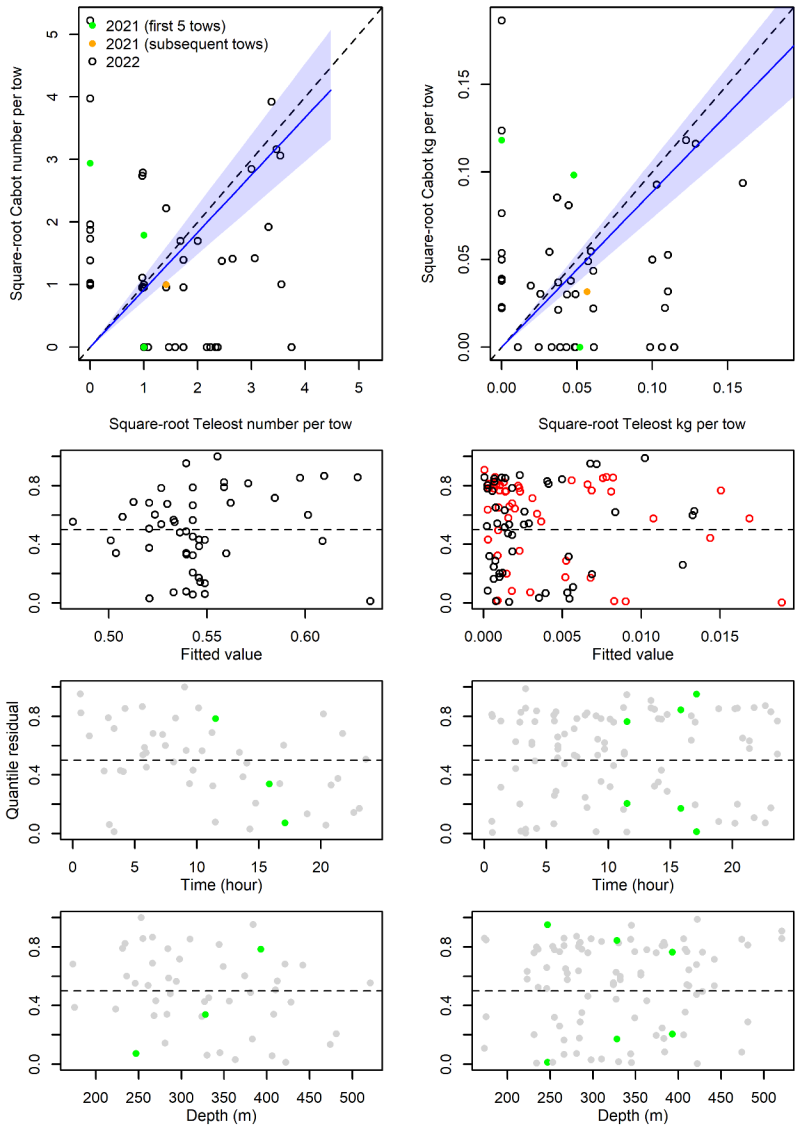

Figure 101.Visualisation of comparative fishing data, size-aggregated model predictions and residual plots for Laetmonice filicornis.

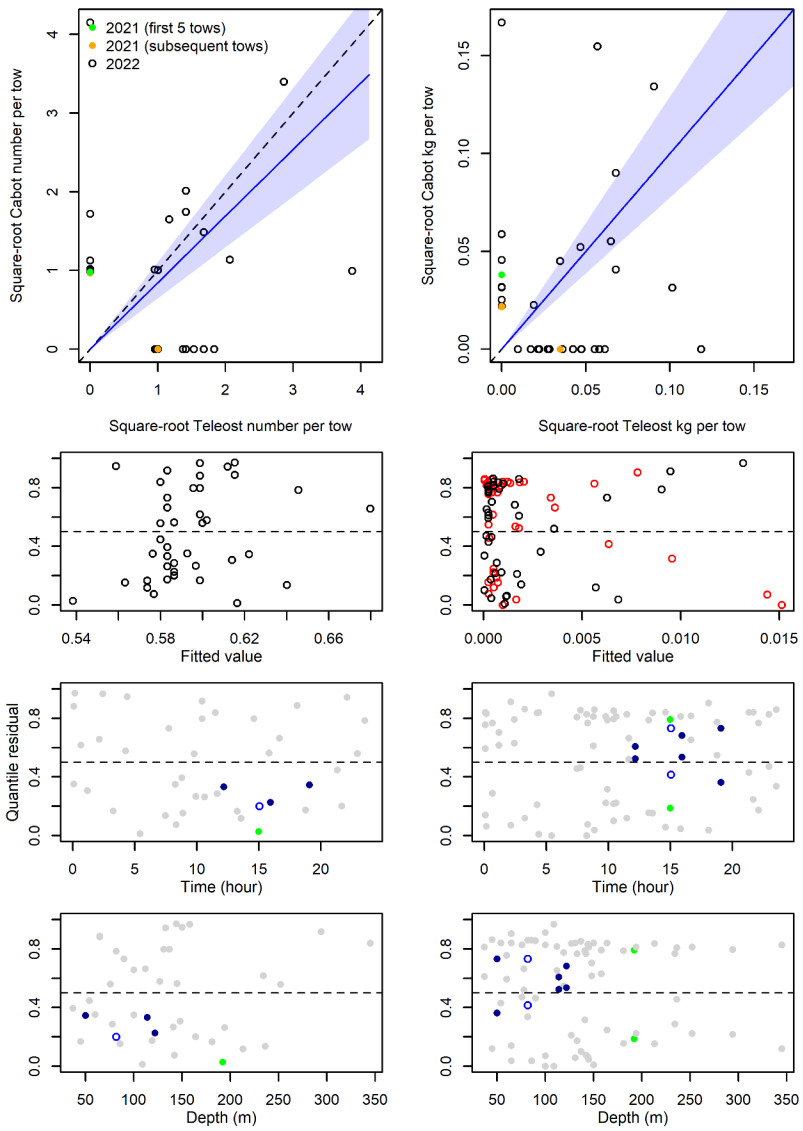

Figure 102.Visualisation of comparative fishing data, size-aggregated model predictions and residual plots for Polynoidae.

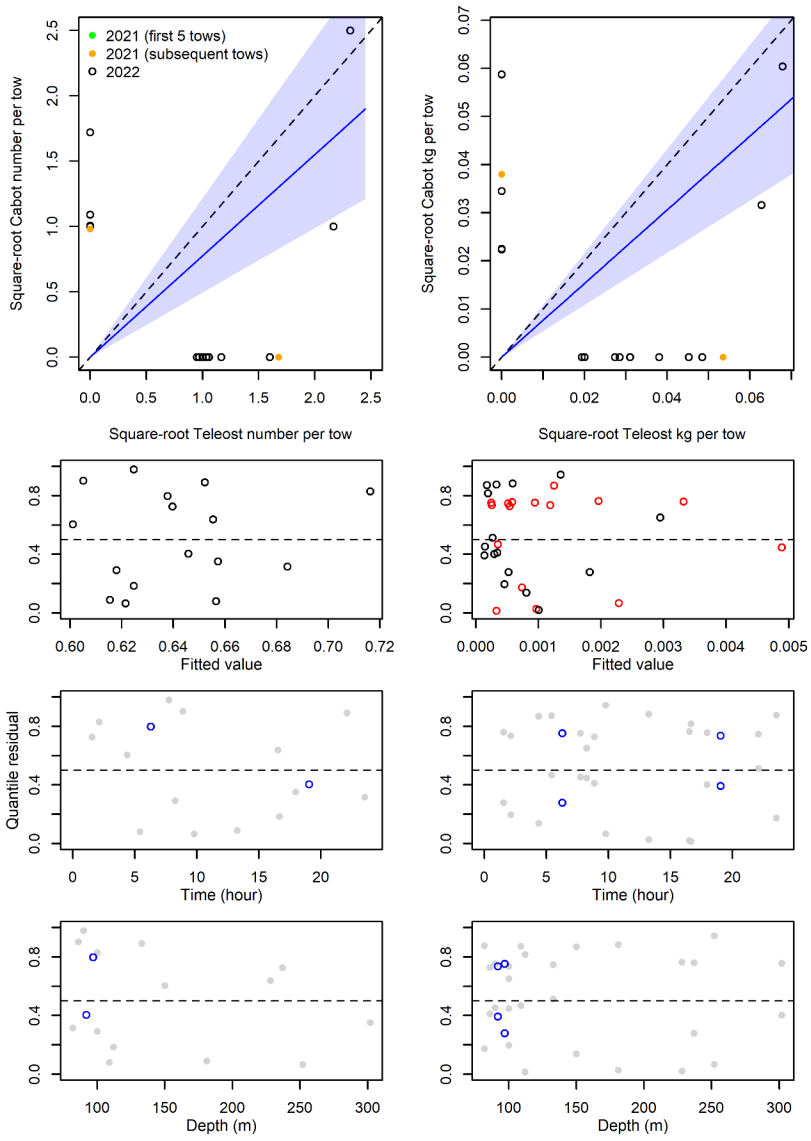

Figure 103.Visualisation of comparative fishing data, size-aggregated model predictions and residual plots for Brada inhabilis.

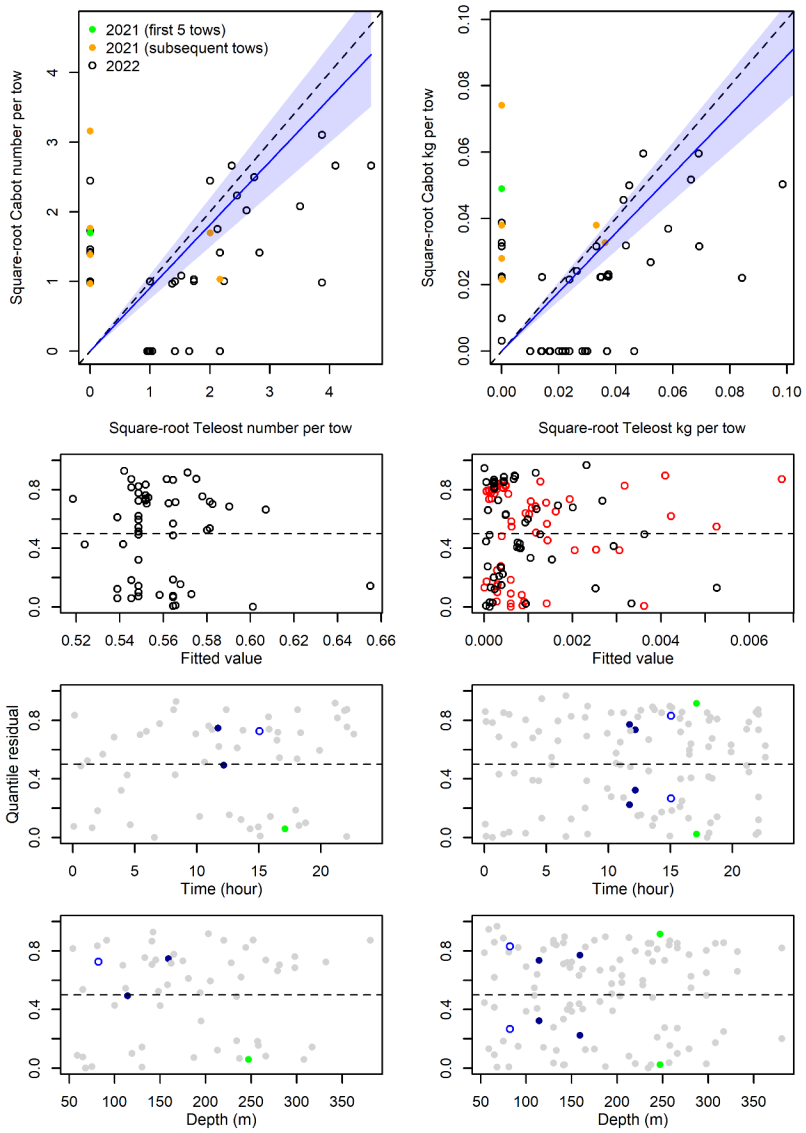

Figure 104.Visualisation of comparative fishing data, size-aggregated model predictions and residual plots for Nymphon sp.

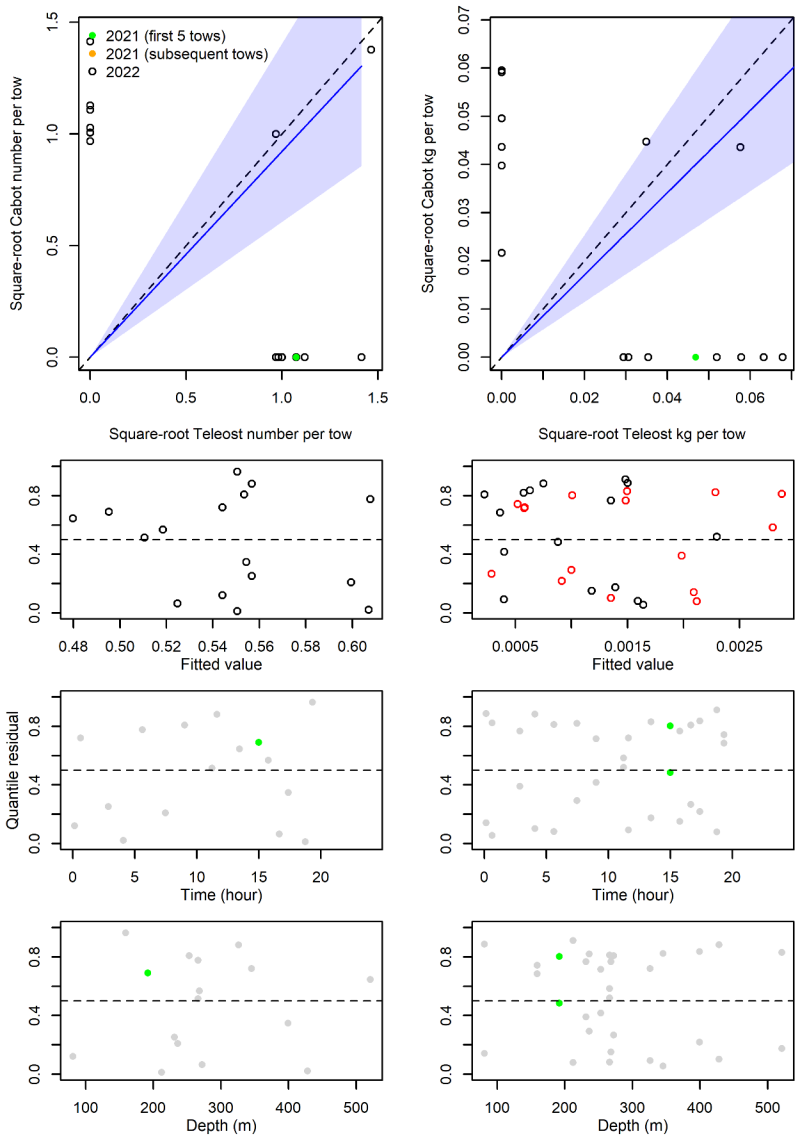

Figure 105.Visualisation of comparative fishing data, size-aggregated model predictions and residual plots for Aega psora.

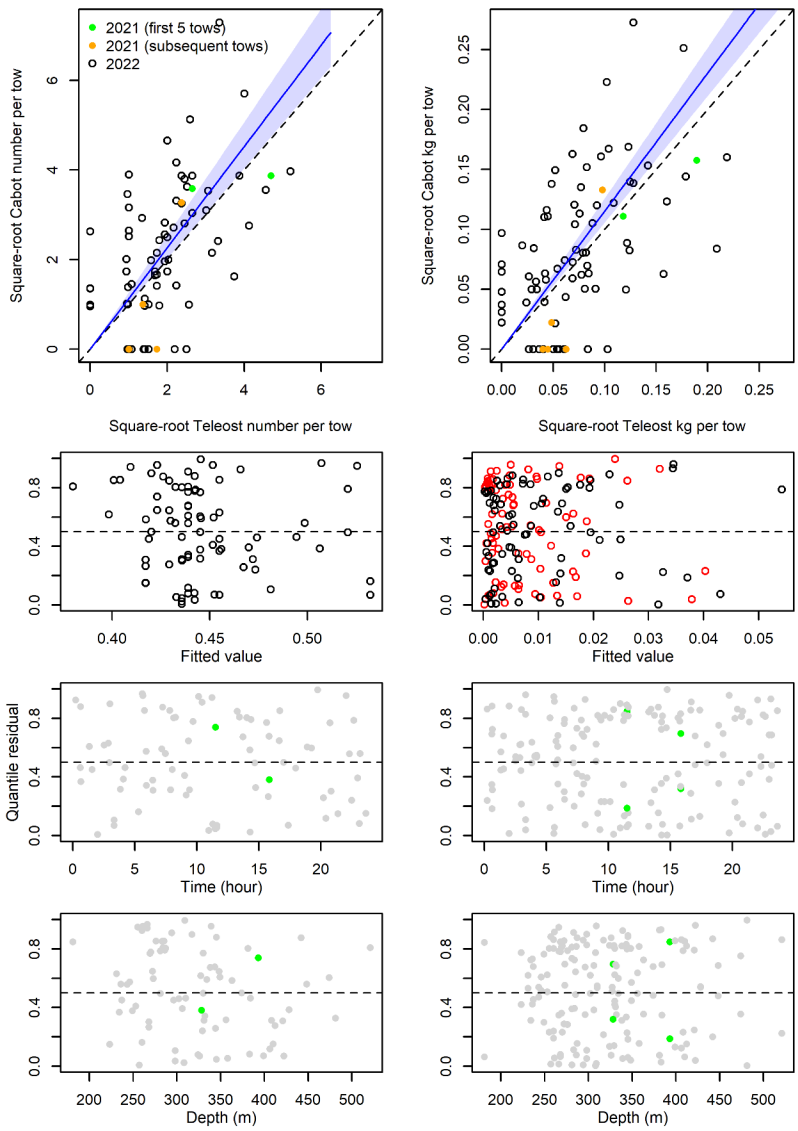

Figure 106.Visualisation of comparative fishing data, size-aggregated model predictions and residual plots for Syscenus infelix.

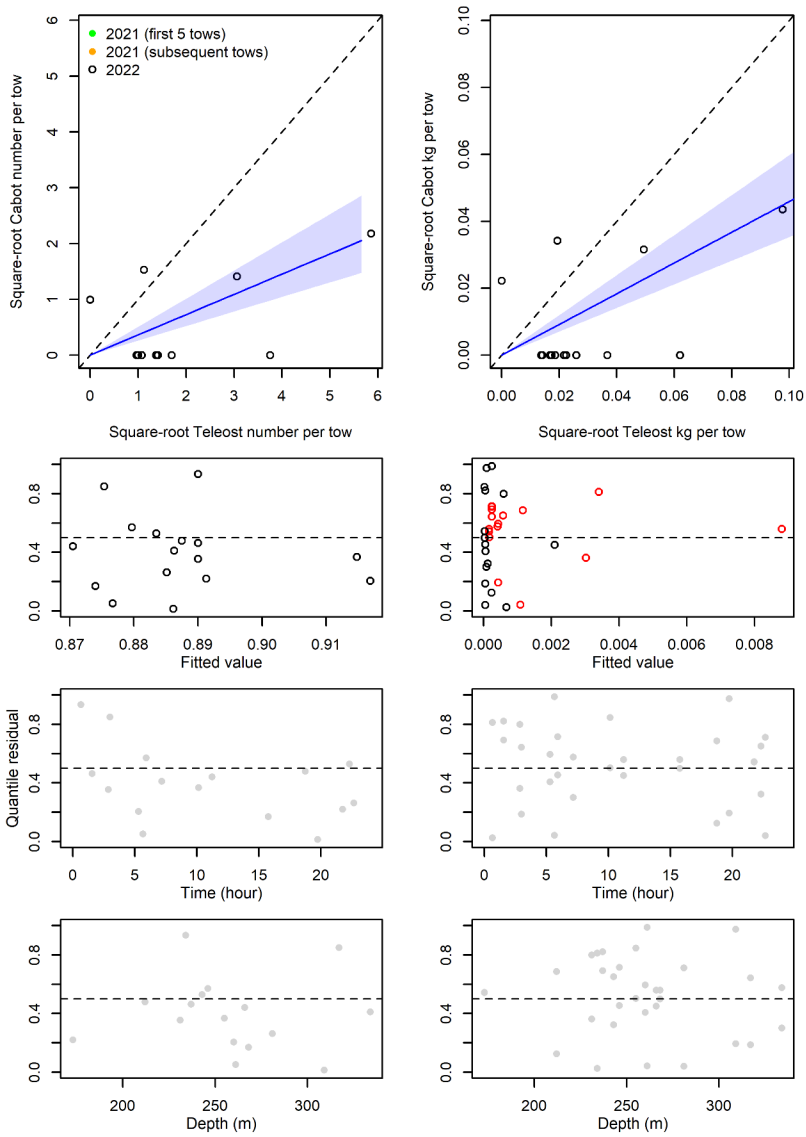

Figure 107.Visualisation of comparative fishing data, size-aggregated model predictions and residual plots for Epimeria loricata.

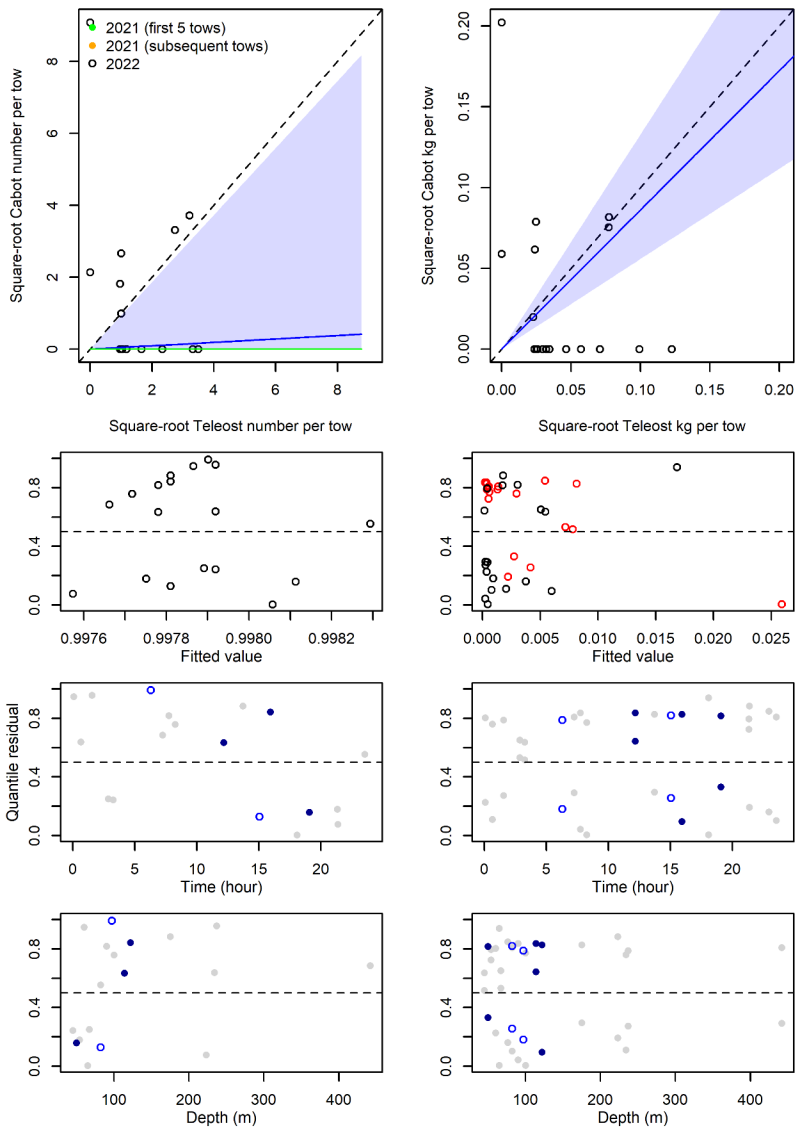

Figure 108.Visualisation of comparative fishing data, size-aggregated model predictions and residual plots for Eualus fabricii.

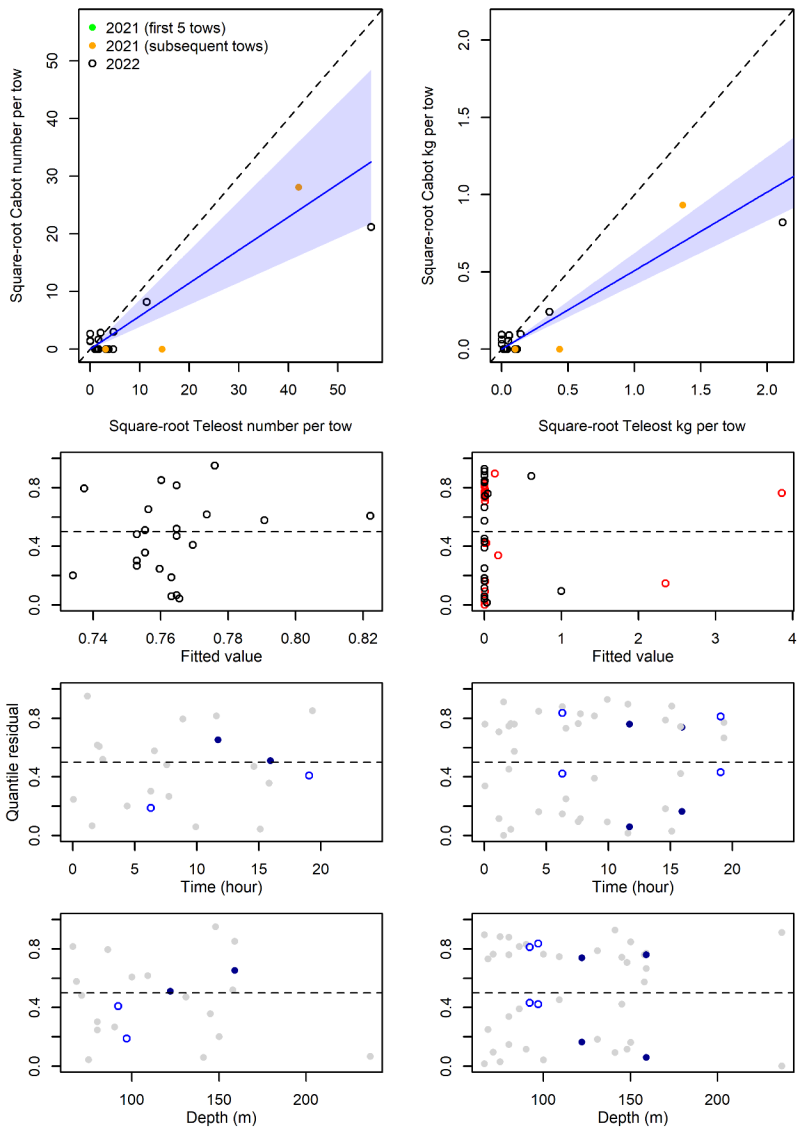

Figure 109.Visualisation of comparative fishing data, size-aggregated model predictions and residual plots for Eualus macilentus.

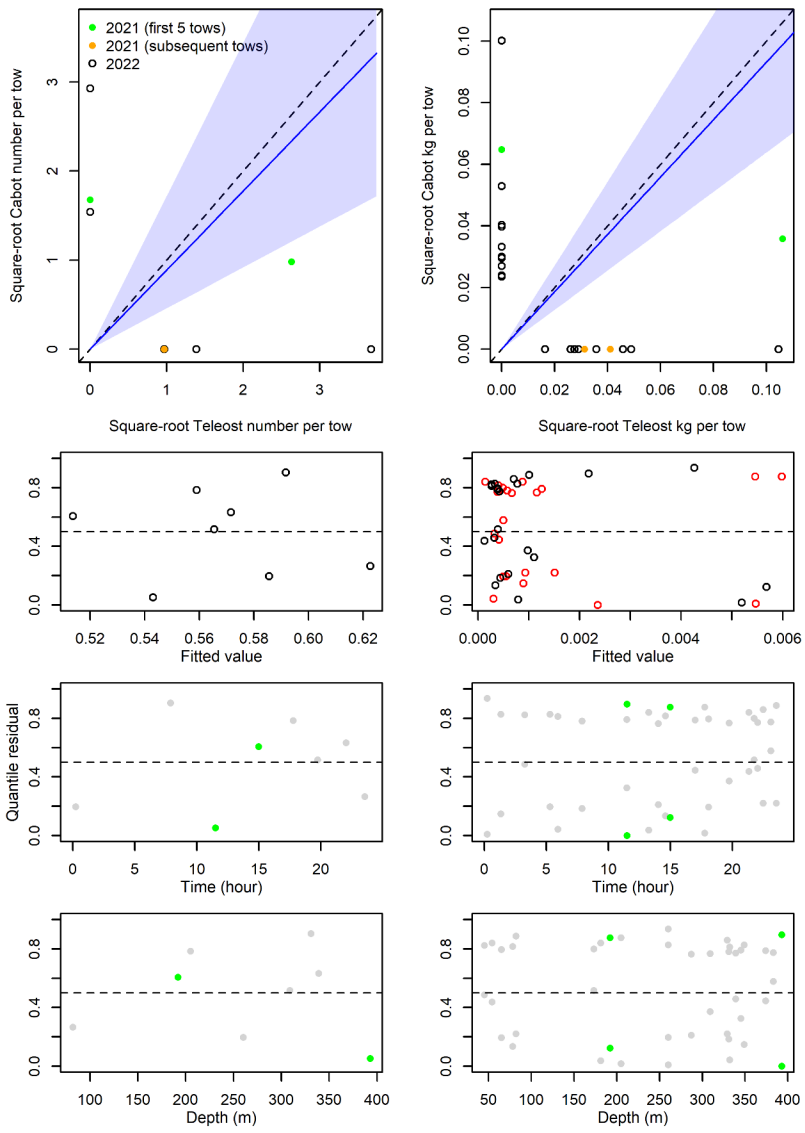

Figure 110.Visualisation of comparative fishing data, size-aggregated model predictions and residual plots for Spirontocaris sp.

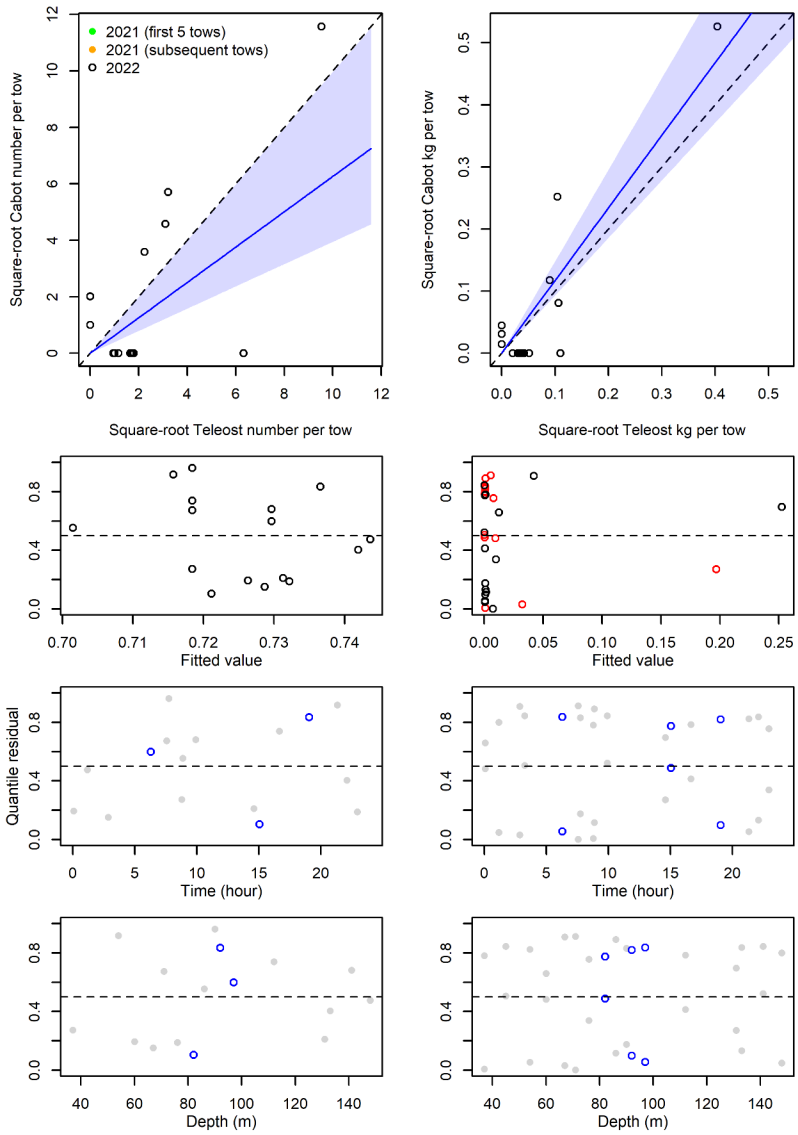

Figure 111.Visualisation of comparative fishing data, size-aggregated model predictions and residual plots for Spirontocaris spinus.

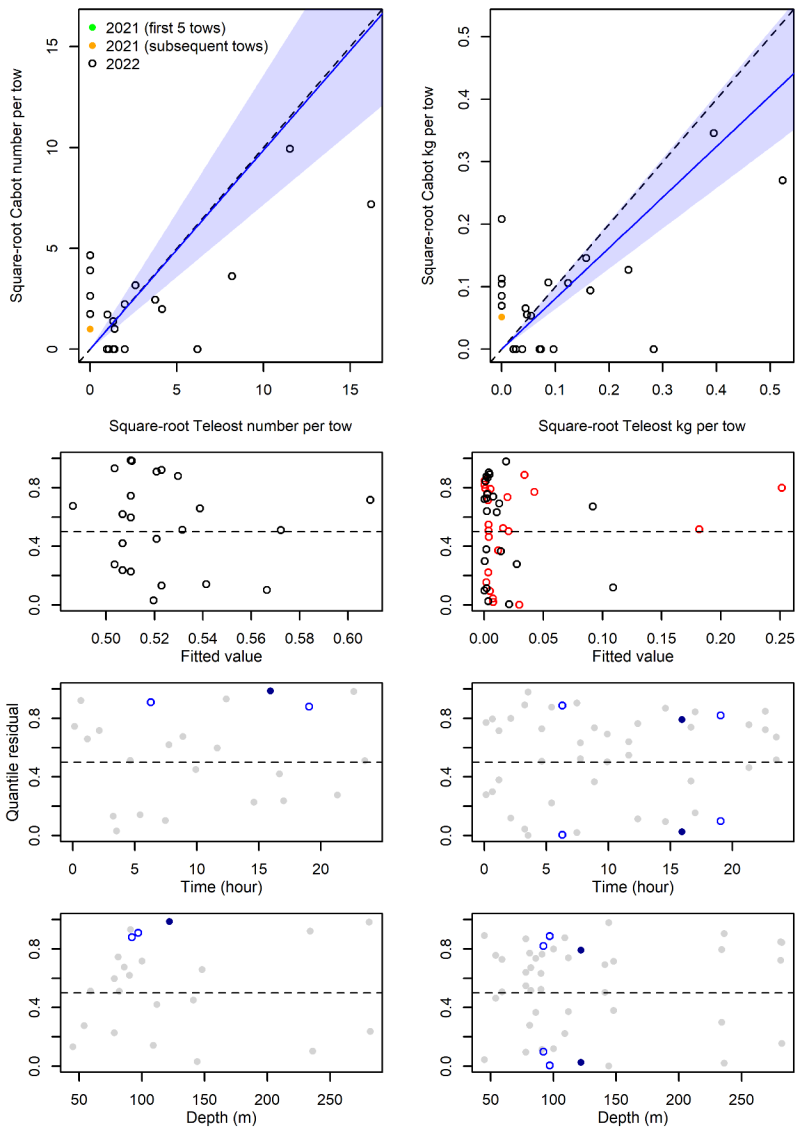

Figure 112.Visualisation of comparative fishing data, size-aggregated model predictions and residual plots for Sabinea septemcarinata.

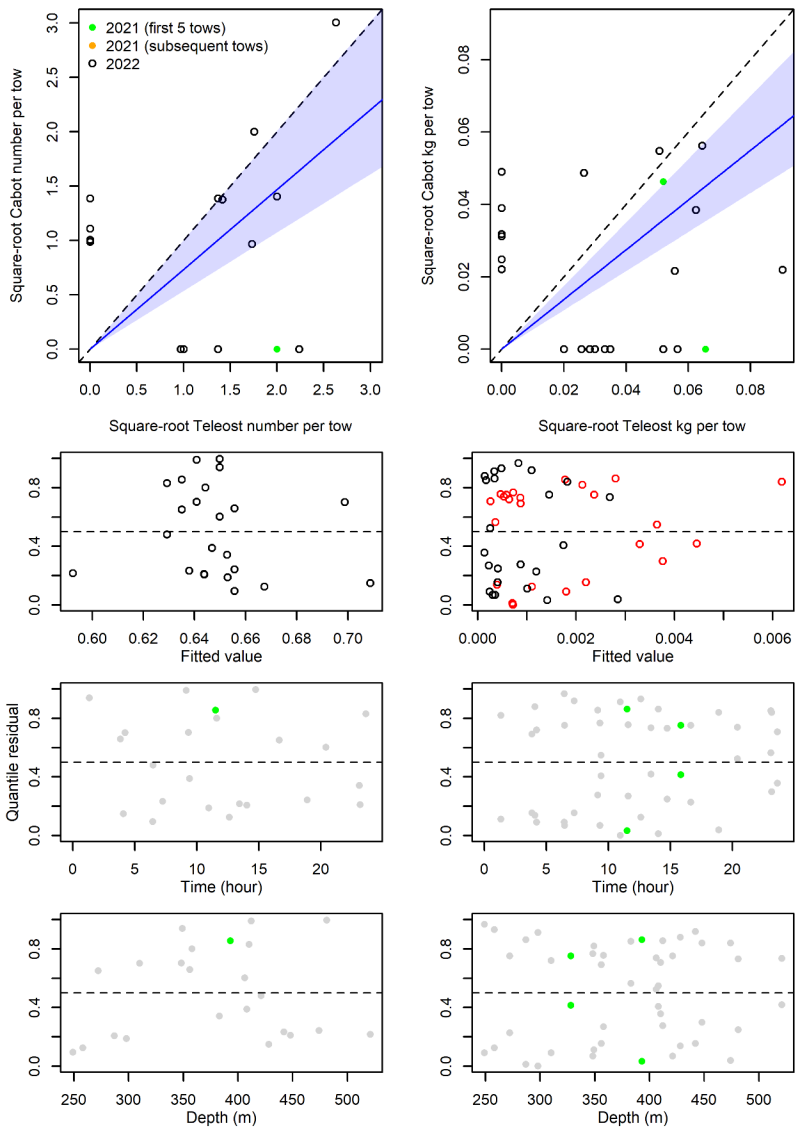

Figure 113.Visualisation of comparative fishing data, size-aggregated model predictions and residual plots for Munidopsis curvirostra.

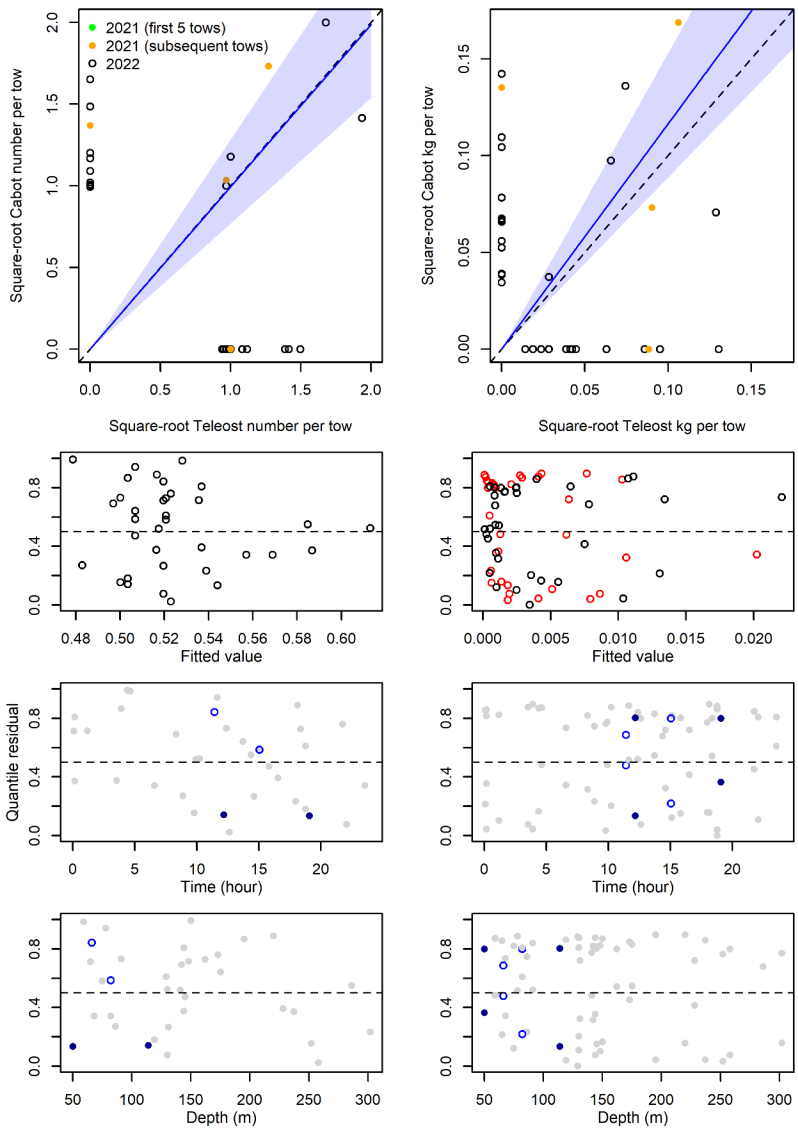

Figure 114.Visualisation of comparative fishing data, size-aggregated model predictions and residual plots for Pagurus sp.

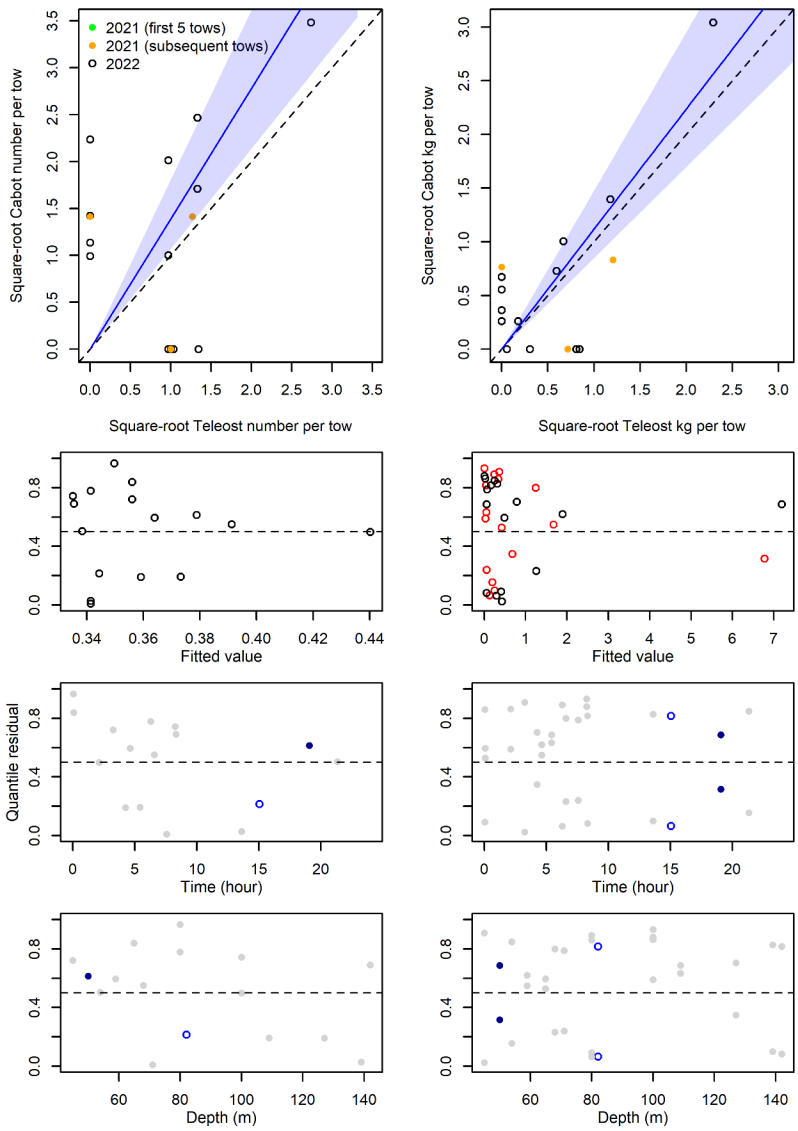

Figure 115.Visualisation of comparative fishing data, size-aggregated model predictions and residual plots for Cucumaria frondosa.

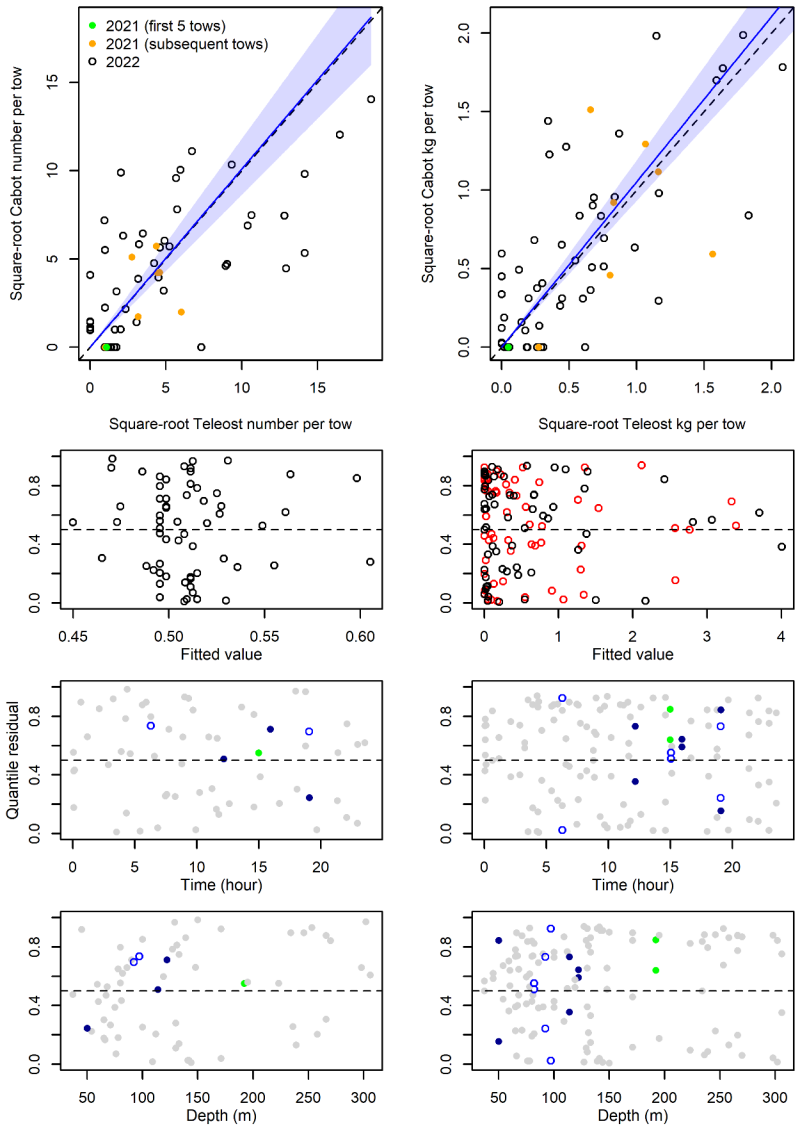

Figure 116.Visualisation of comparative fishing data, size-aggregated model predictions and residual plots for Strongylocentrotus sp.

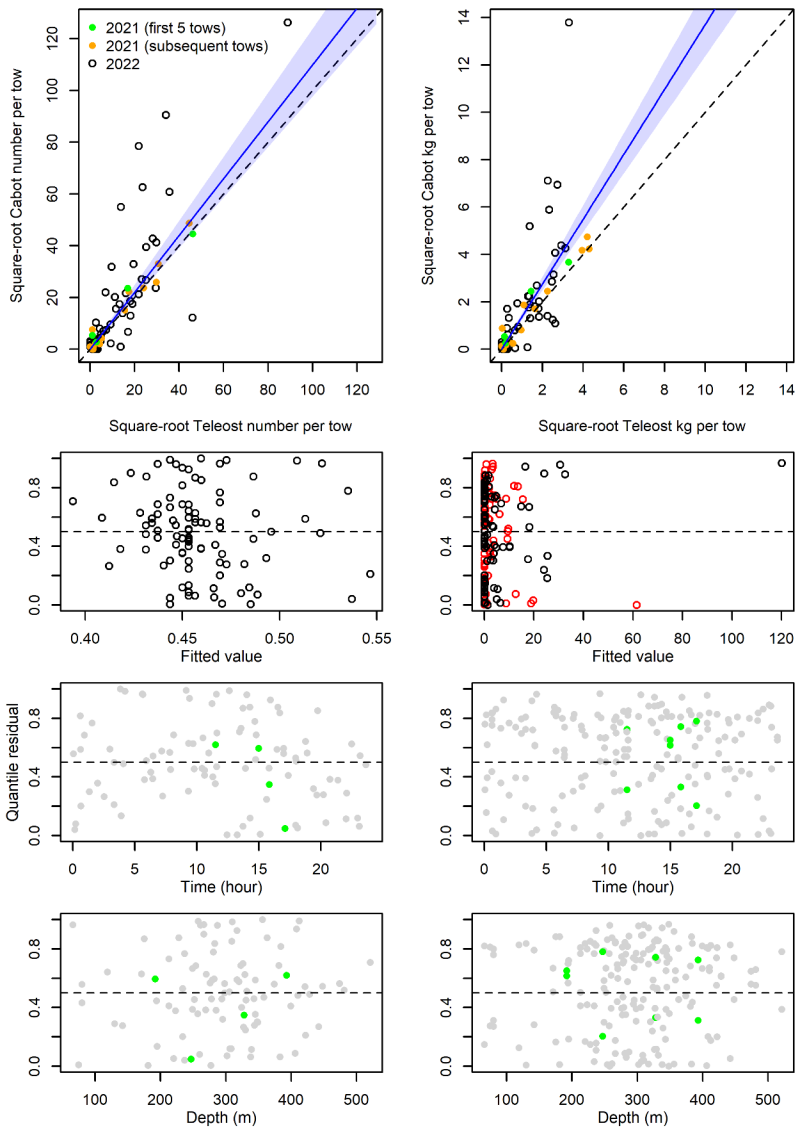

Figure 117.Visualisation of comparative fishing data, size-aggregated model predictions and residual plots for Brisaster fragilis.

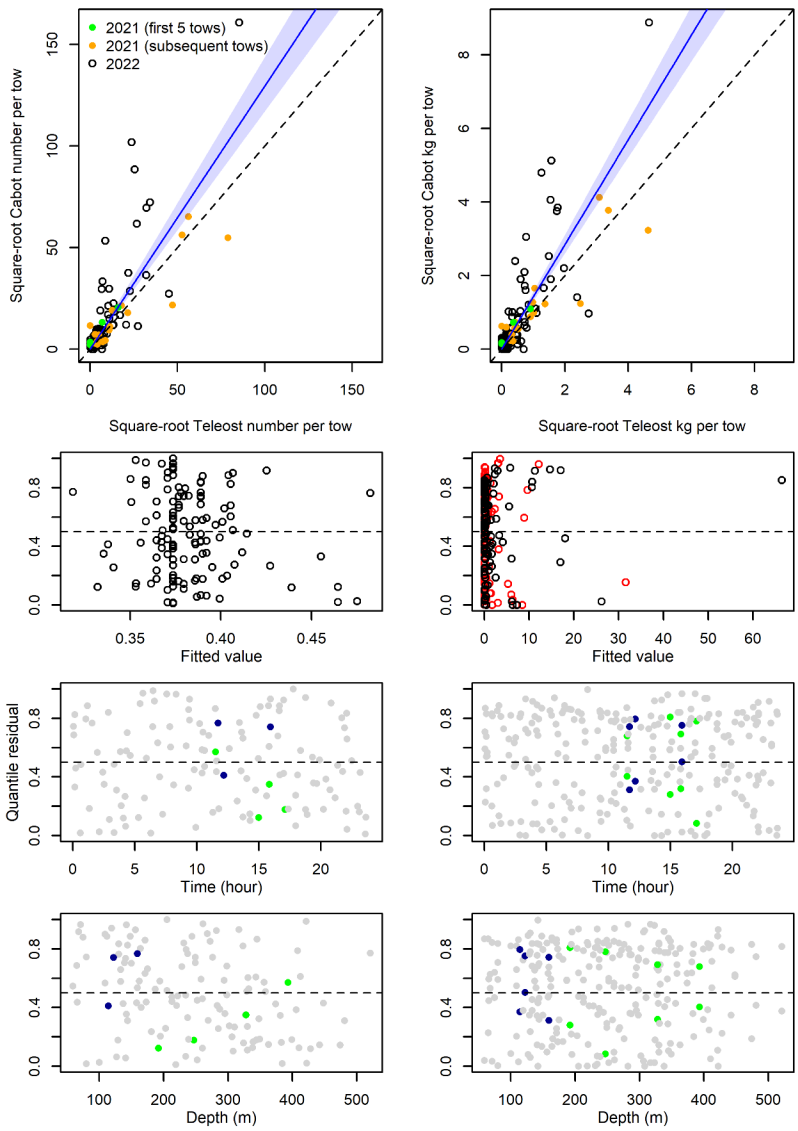

Figure 118.Visualisation of comparative fishing data, size-aggregated model predictions and residual plots for Ctenodiscus crispatus.

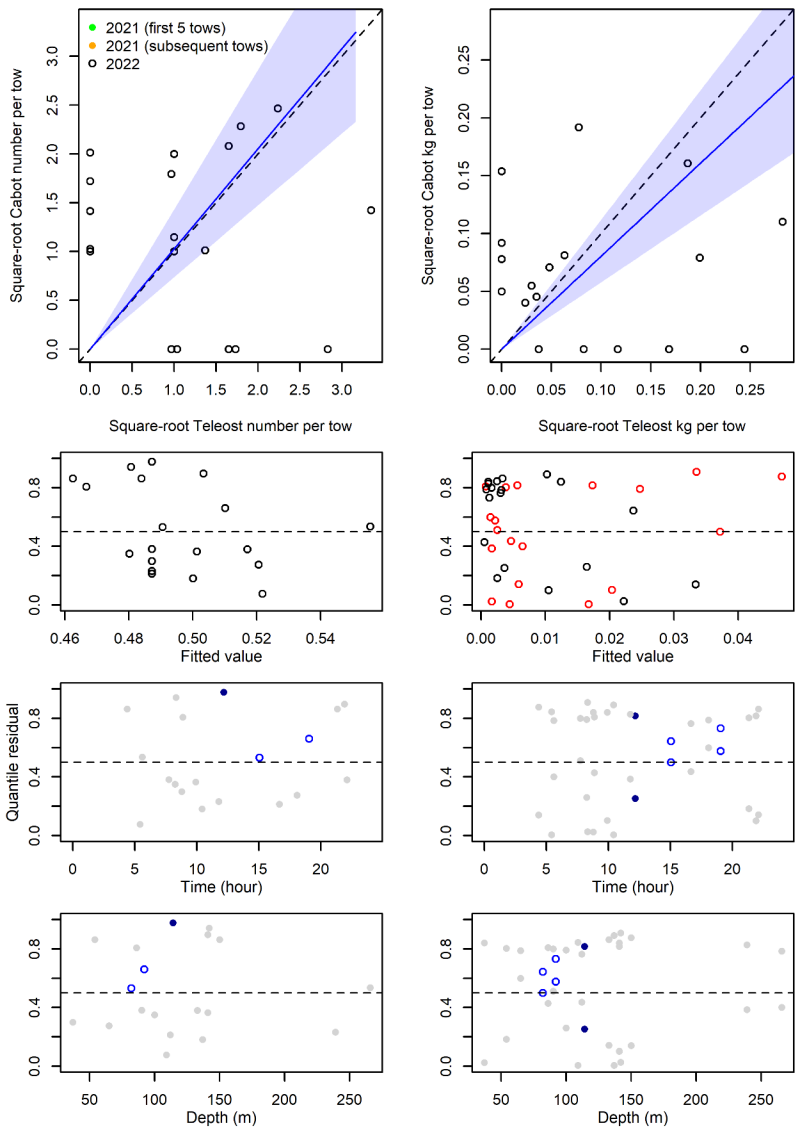

Figure 119.Visualisation of comparative fishing data, size-aggregated model predictions and residual plots for Pteraster militaris.

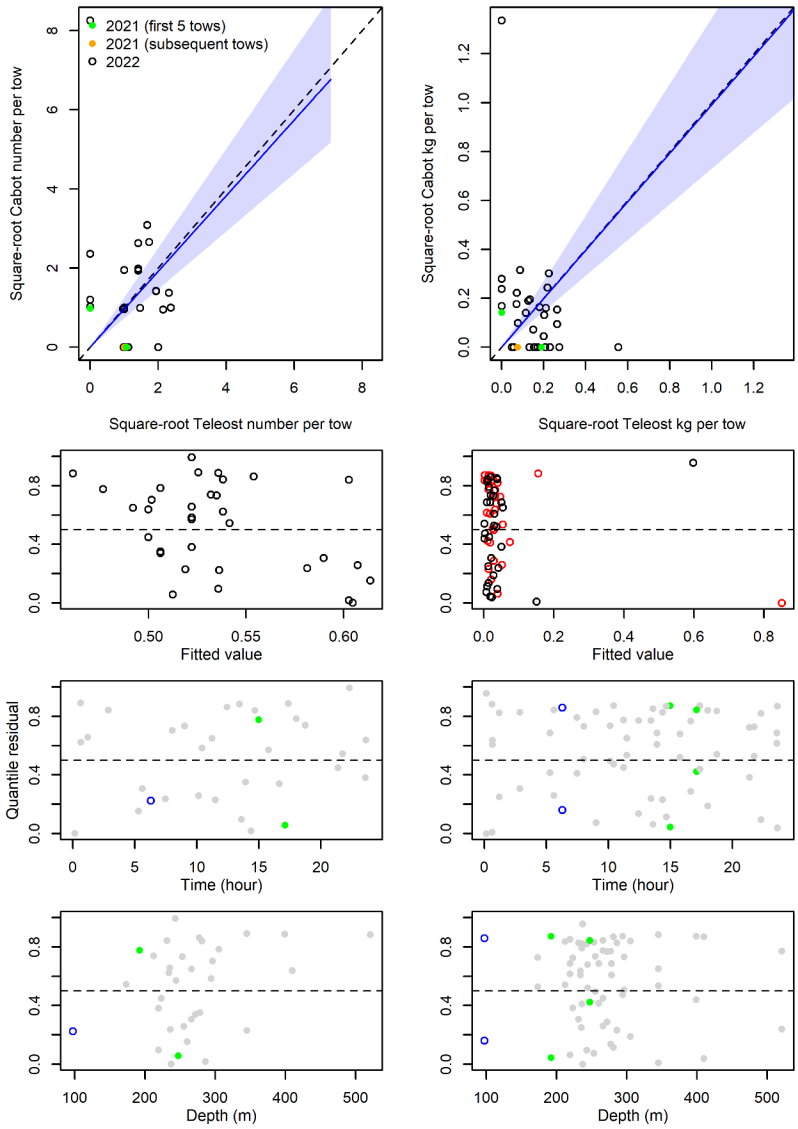

Figure 120.Visualisation of comparative fishing data, size-aggregated model predictions and residual plots for Ceramaster granularis.

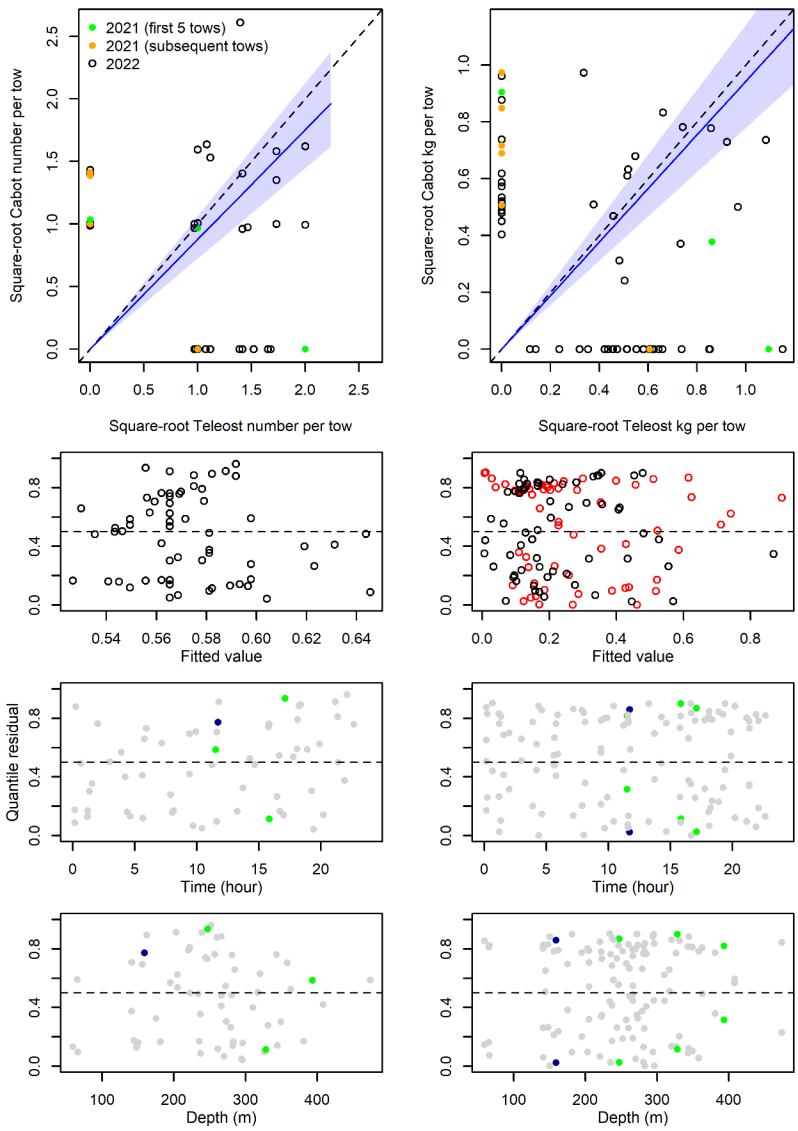

Figure 121.Visualisation of comparative fishing data, size-aggregated model predictions and residual plots for Hippasteria phrygiana.

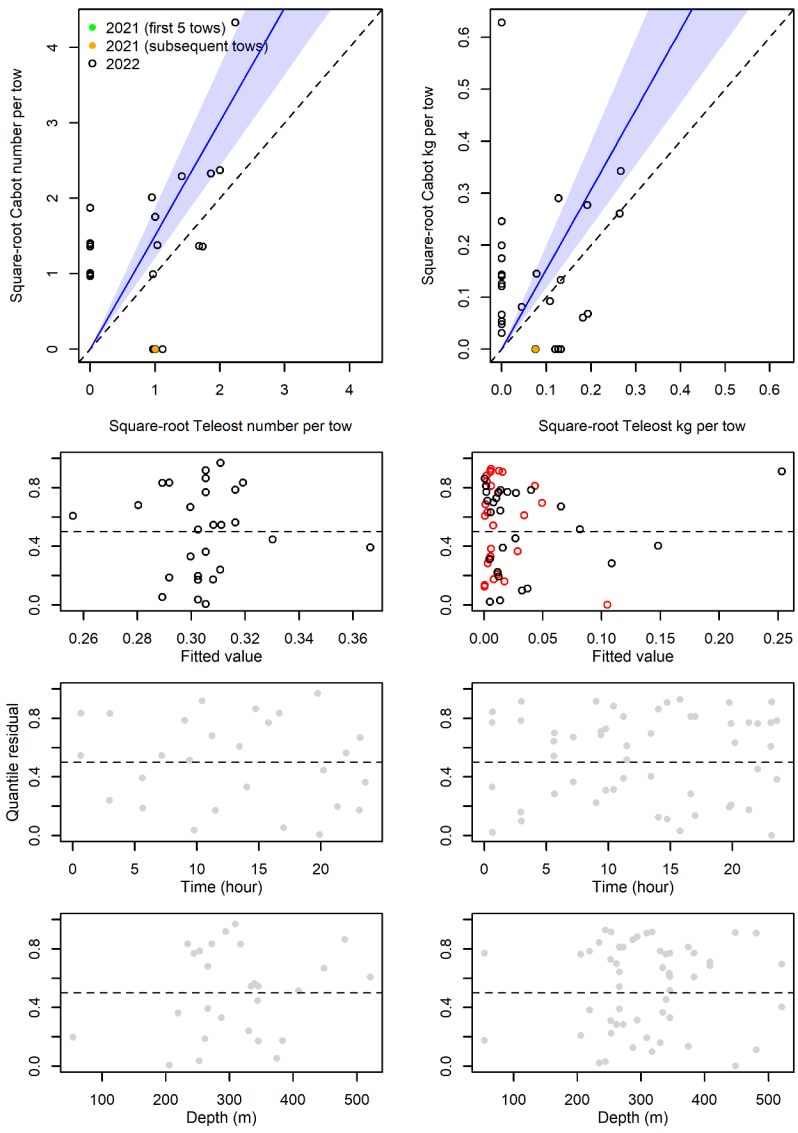

Figure 122.Visualisation of comparative fishing data, size-aggregated model predictions and residual plots for Pseudarchaster parelii.

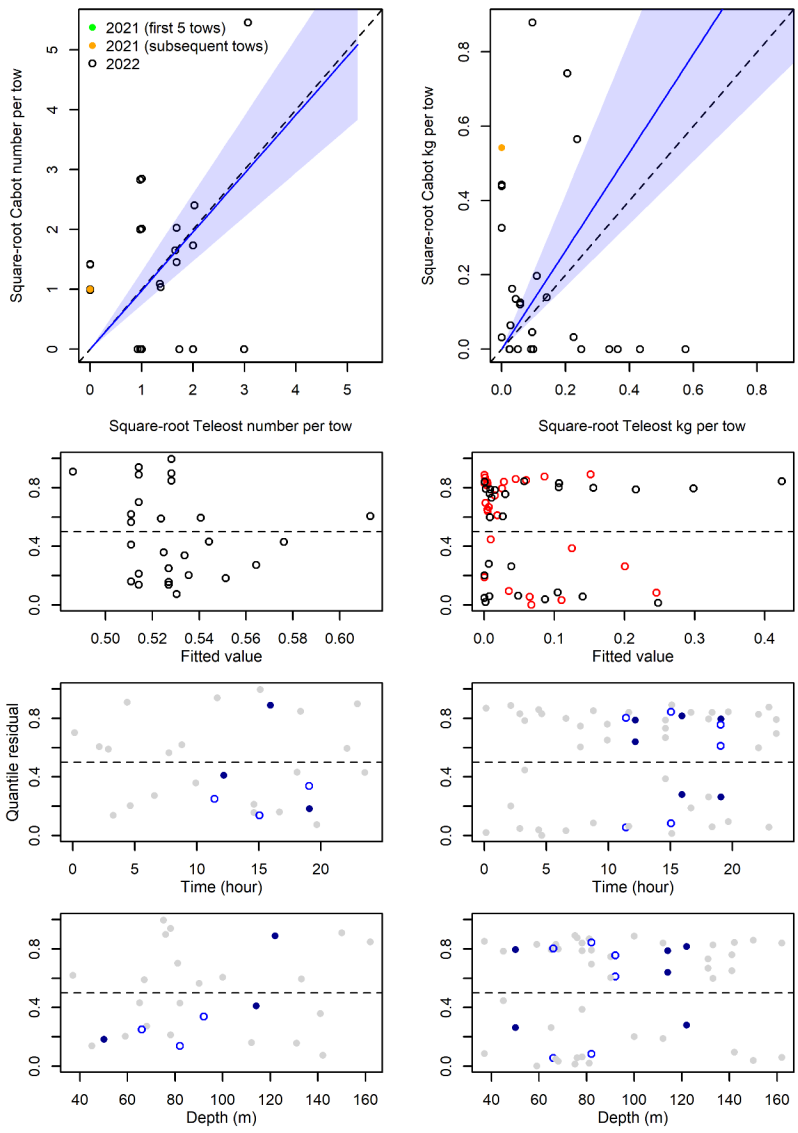

Figure 123.Visualisation of comparative fishing data, size-aggregated model predictions and residual plots for Crossaster papposus.

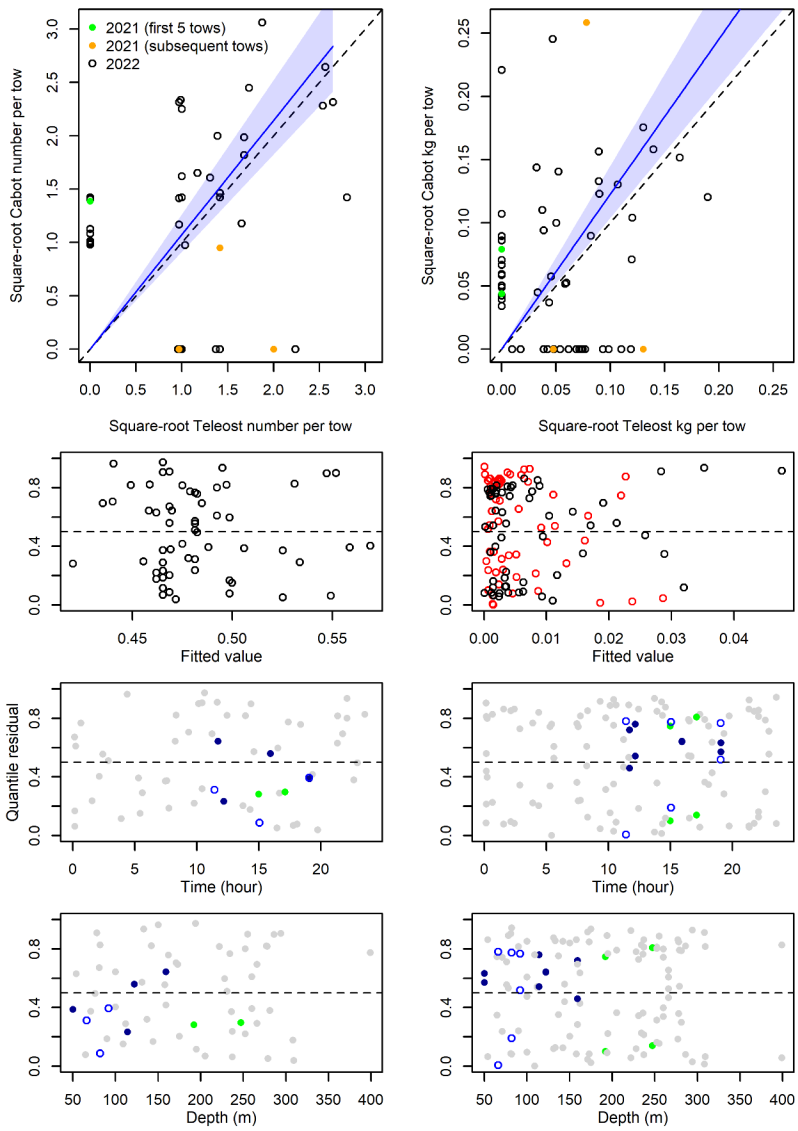

Figure 124.Visualisation of comparative fishing data, size-aggregated model predictions and residual plots for Henricia sp.

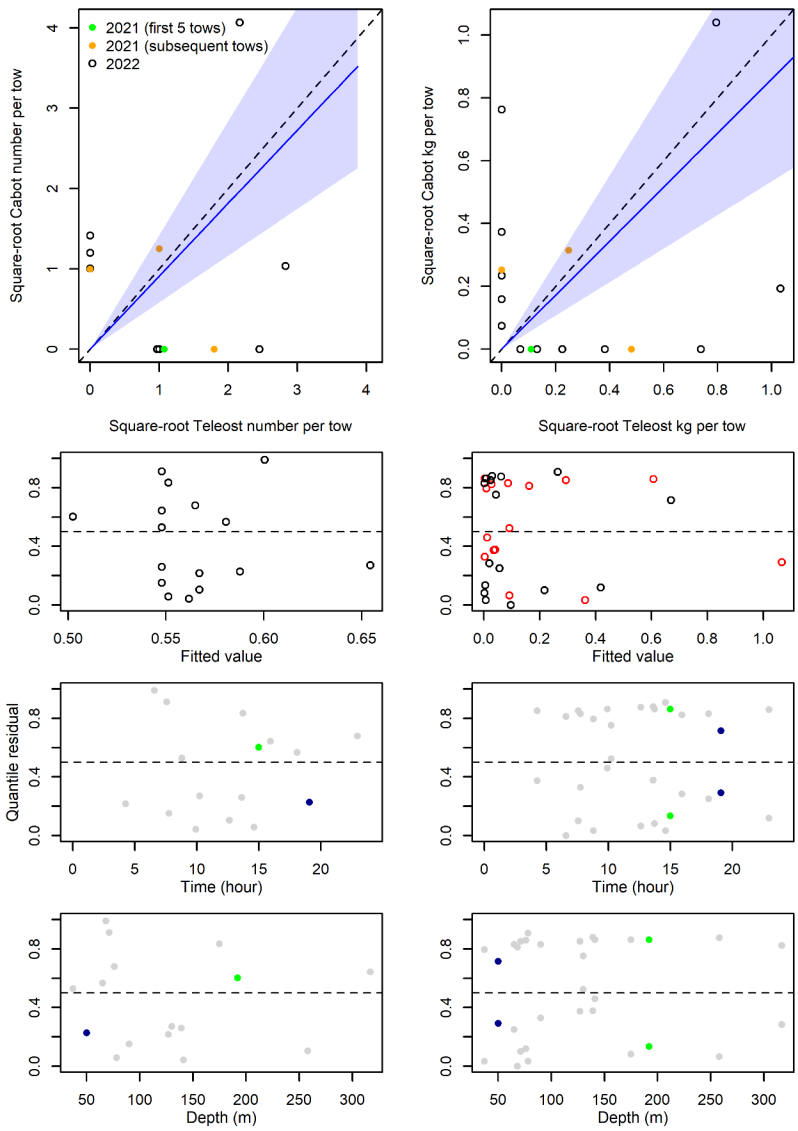

Figure 125.Visualisation of comparative fishing data, size-aggregated model predictions and residual plots for Leptasterias (Hexasterias) polaris.

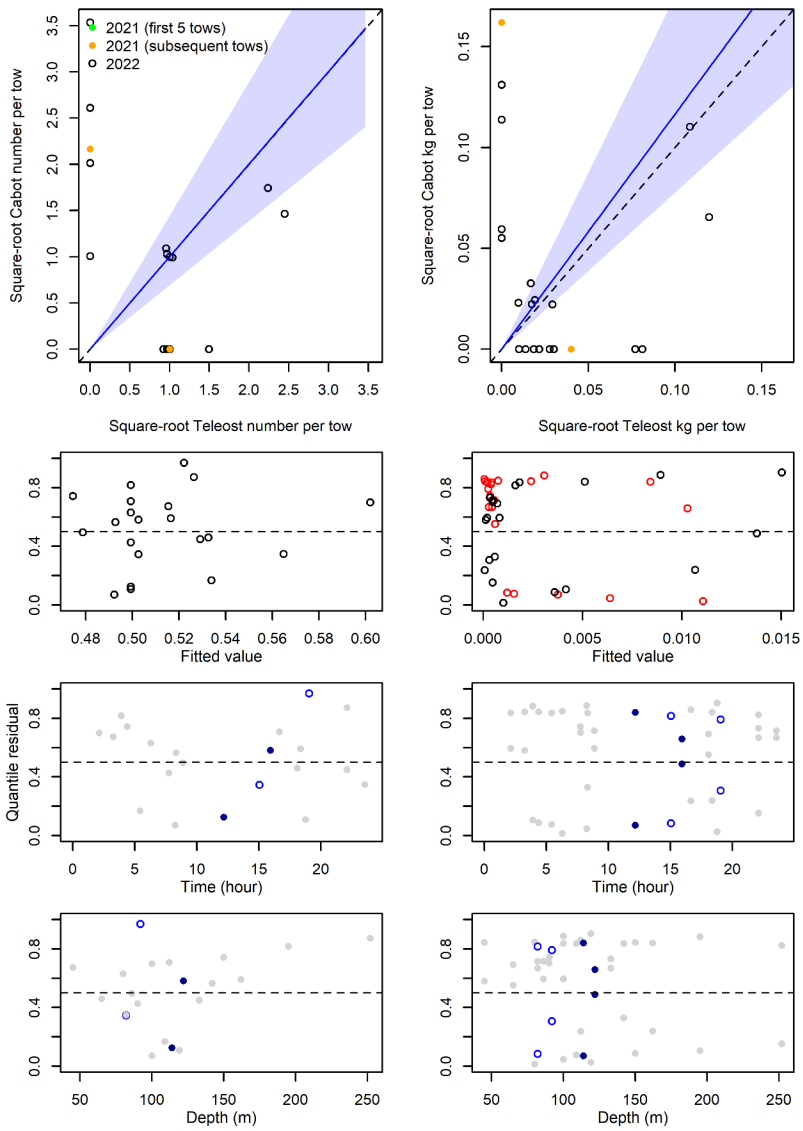

Figure 126.Visualisation of comparative fishing data, size-aggregated model predictions and residual plots for Leptasterias groenlandica.

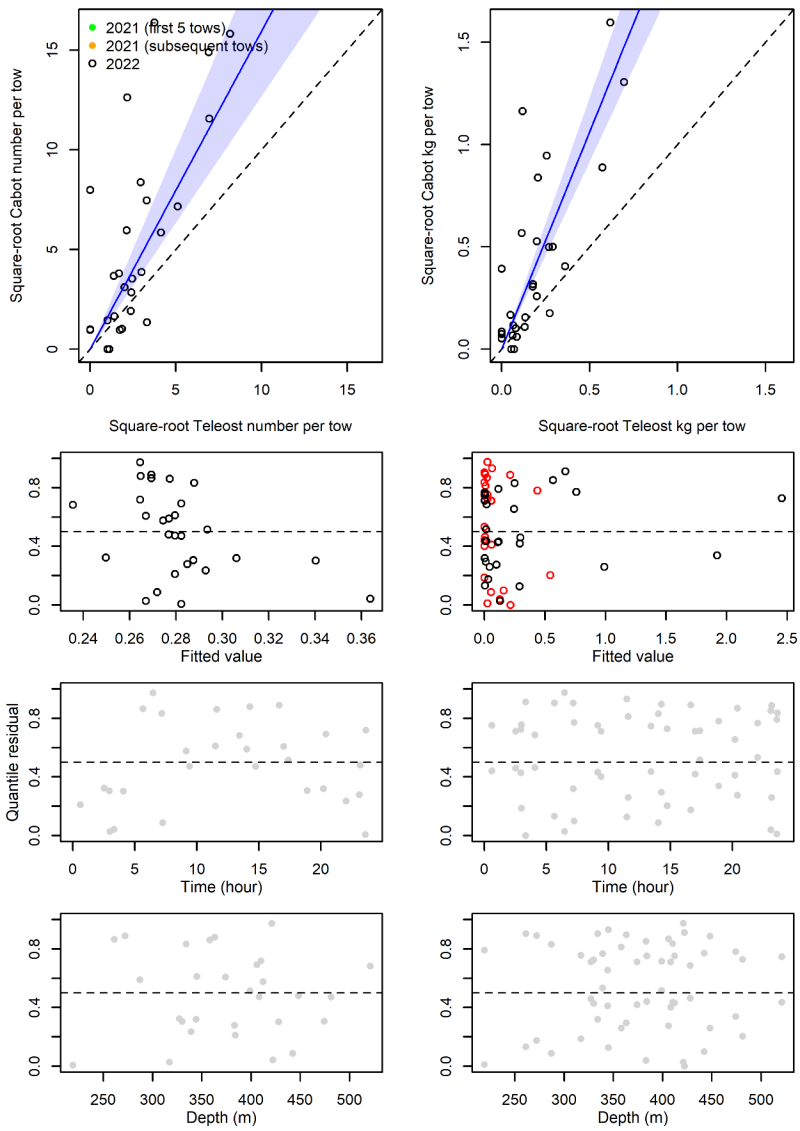

Figure 127.Visualisation of comparative fishing data, size-aggregated model predictions and residual plots for Psilaster andromeda.

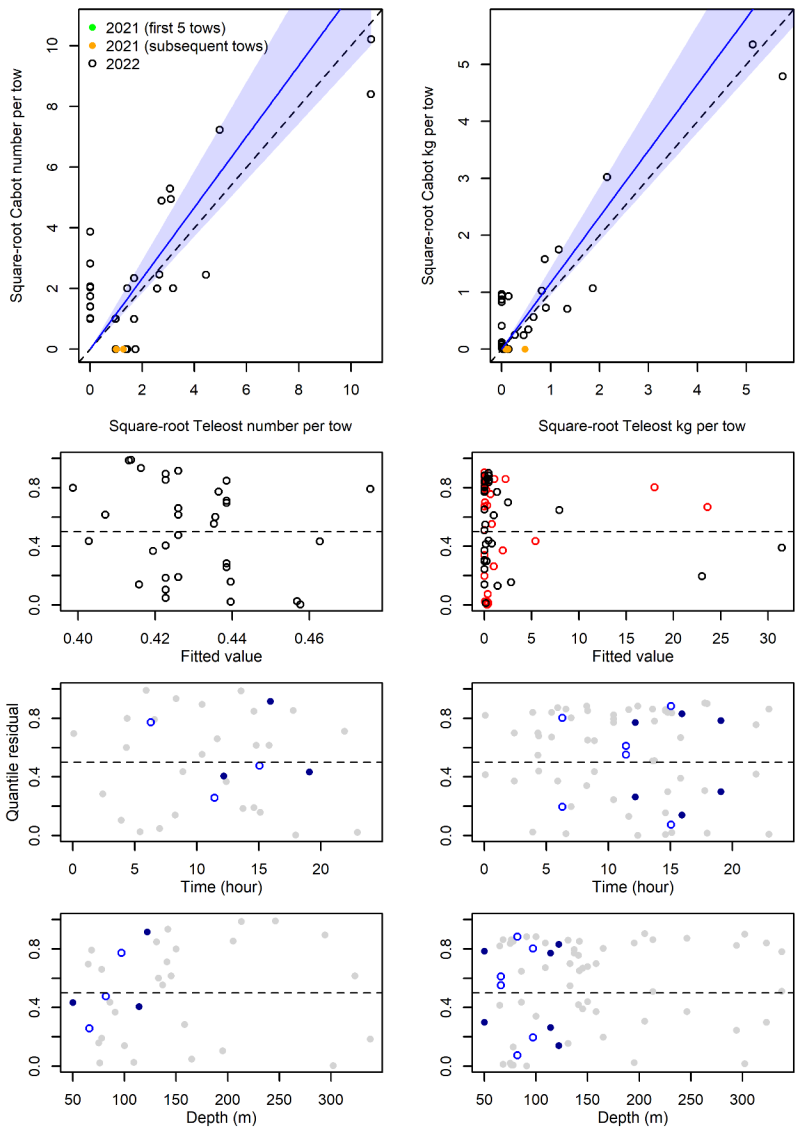

Figure 128.Visualisation of comparative fishing data, size-aggregated model predictions and residual plots for Gorgonocephalus sp.

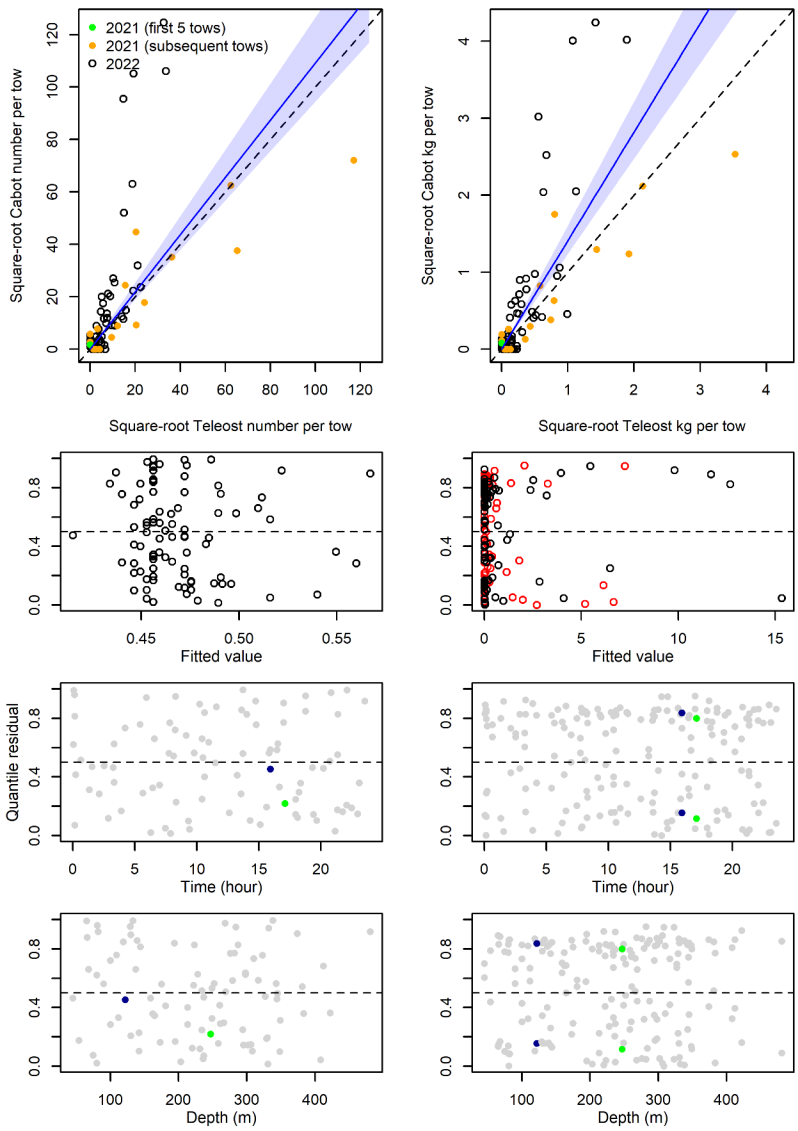

Figure 129.Visualisation of comparative fishing data, size-aggregated model predictions and residual plots for Ophiura sarsii.

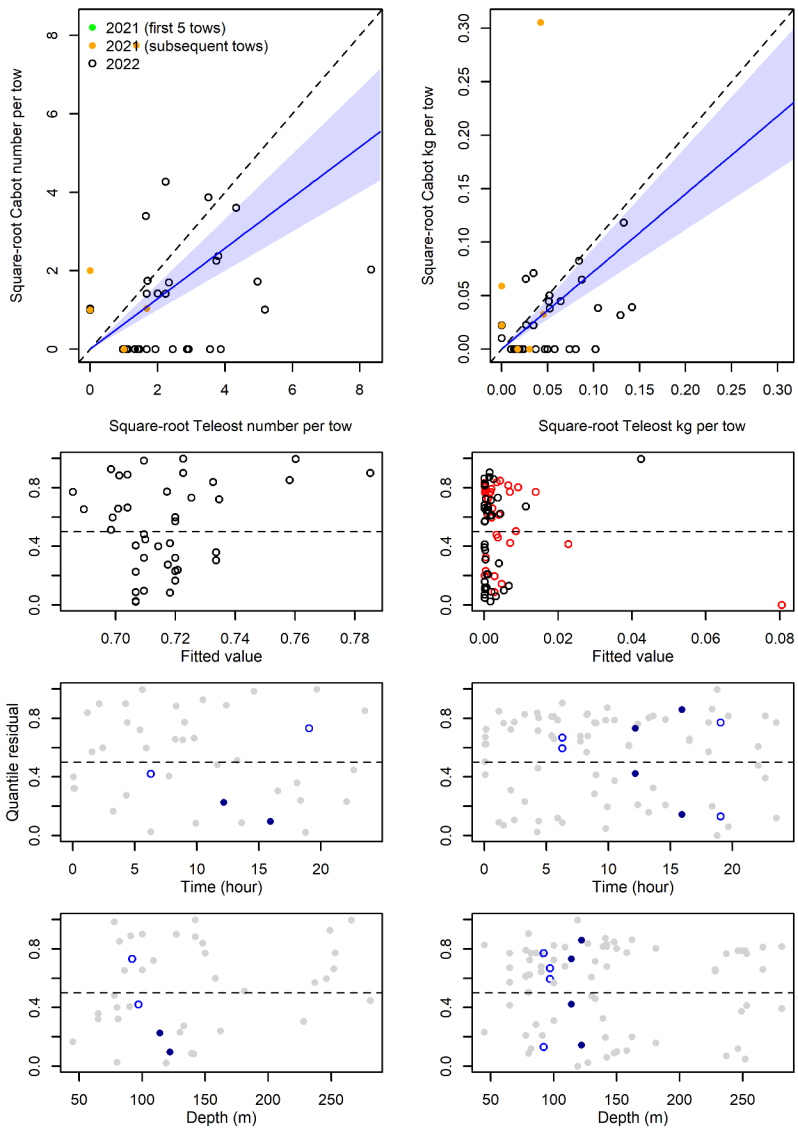

Figure 130.Visualisation of comparative fishing data, size-aggregated model predictions and residual plots for Ophiacantha bidentata.

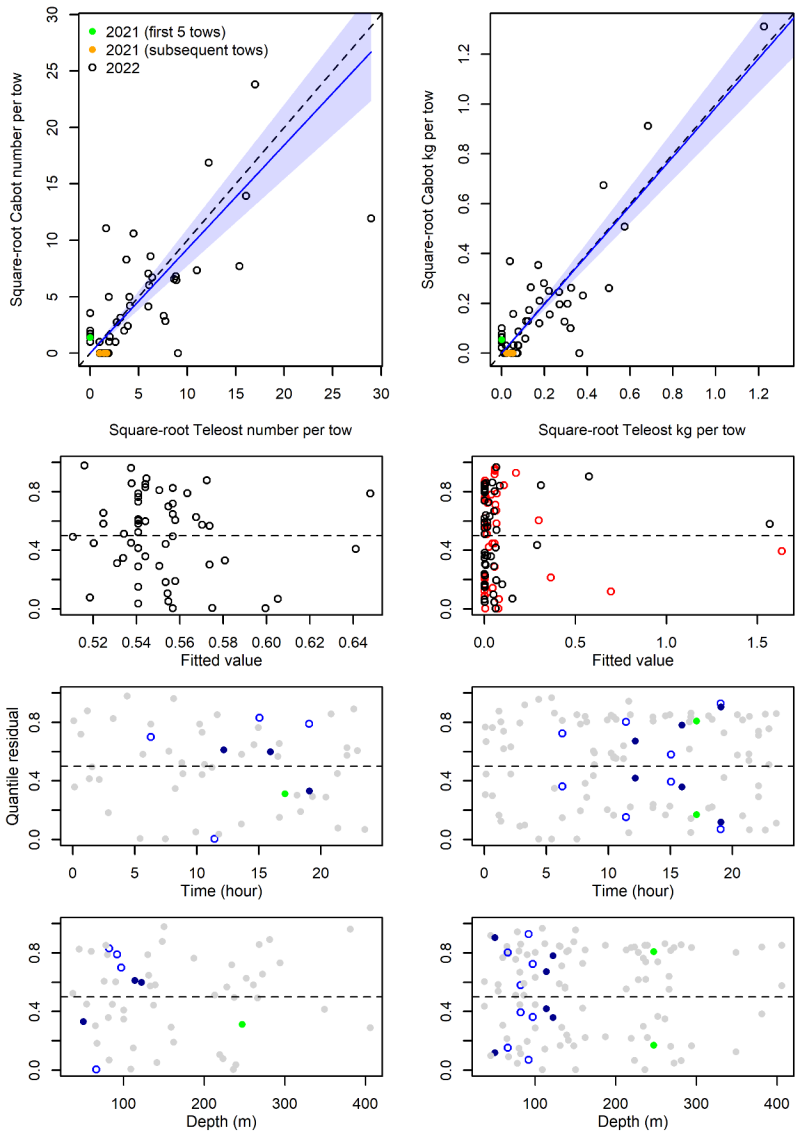

Figure 131.Visualisation of comparative fishing data, size-aggregated model predictions and residual plots for Ophiopholis aculeata.

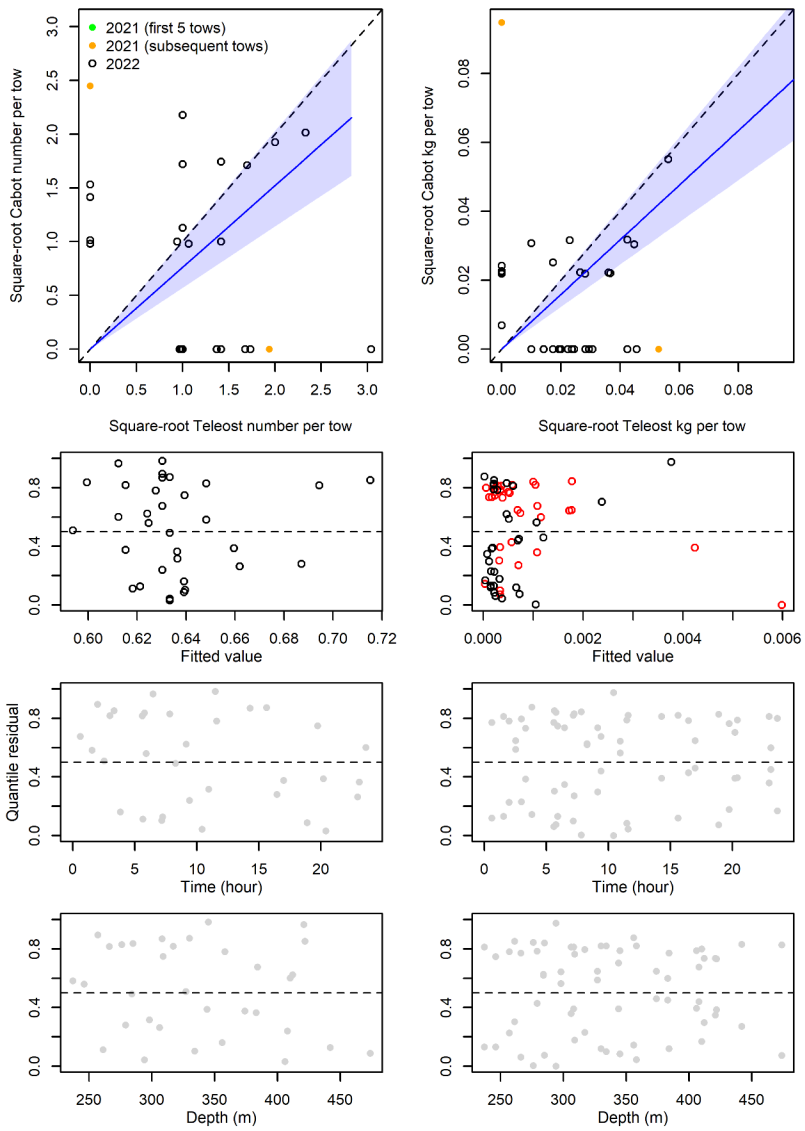

Figure 132.Visualisation of comparative fishing data, size-aggregated model predictions and residual plots for Ophioscolex glacialis.

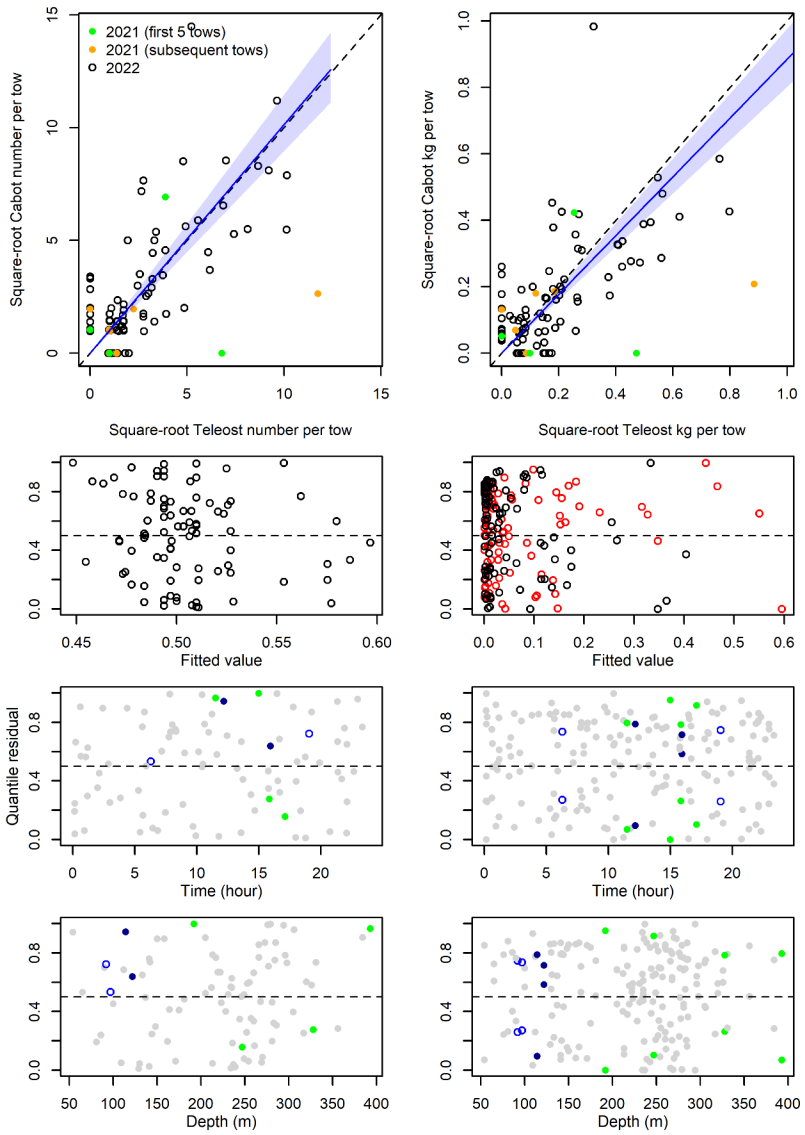

Figure 133.Visualisation of comparative fishing data, size-aggregated model predictions and residual plots for Ascidia sp.

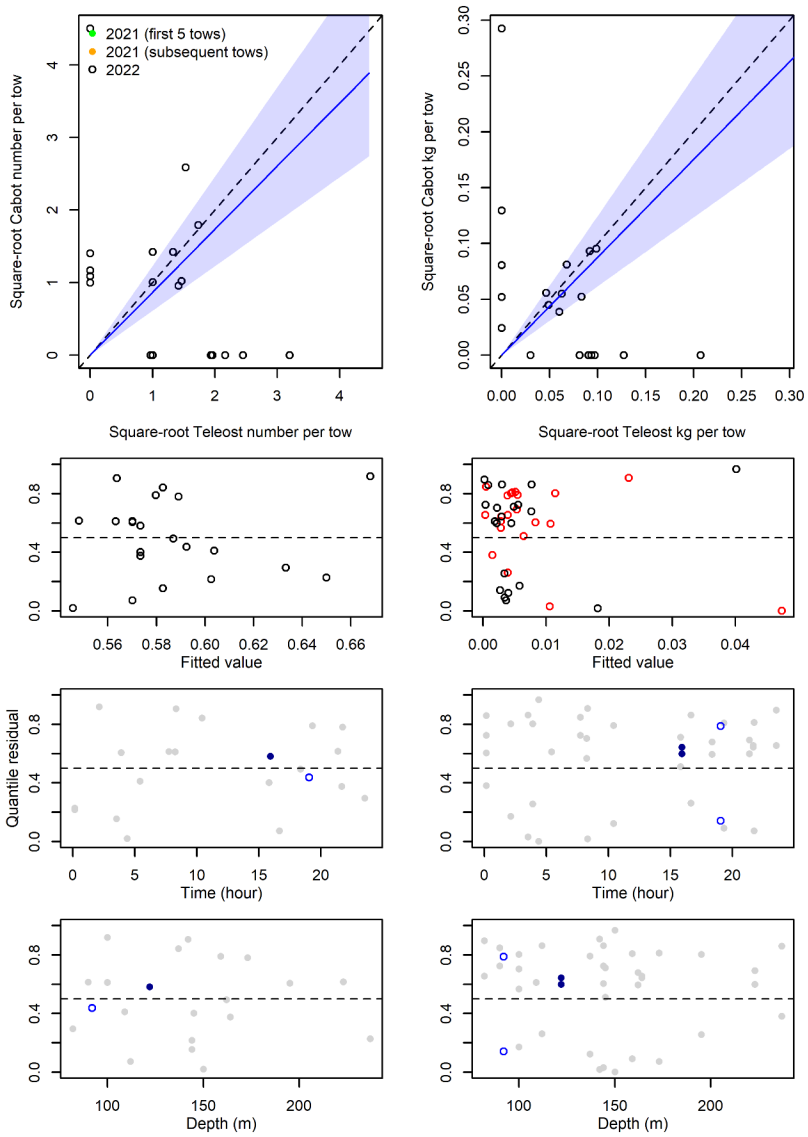

Figure 134.Visualisation of comparative fishing data, size-aggregated model predictions and residual plots for Eudistoma vitreum.

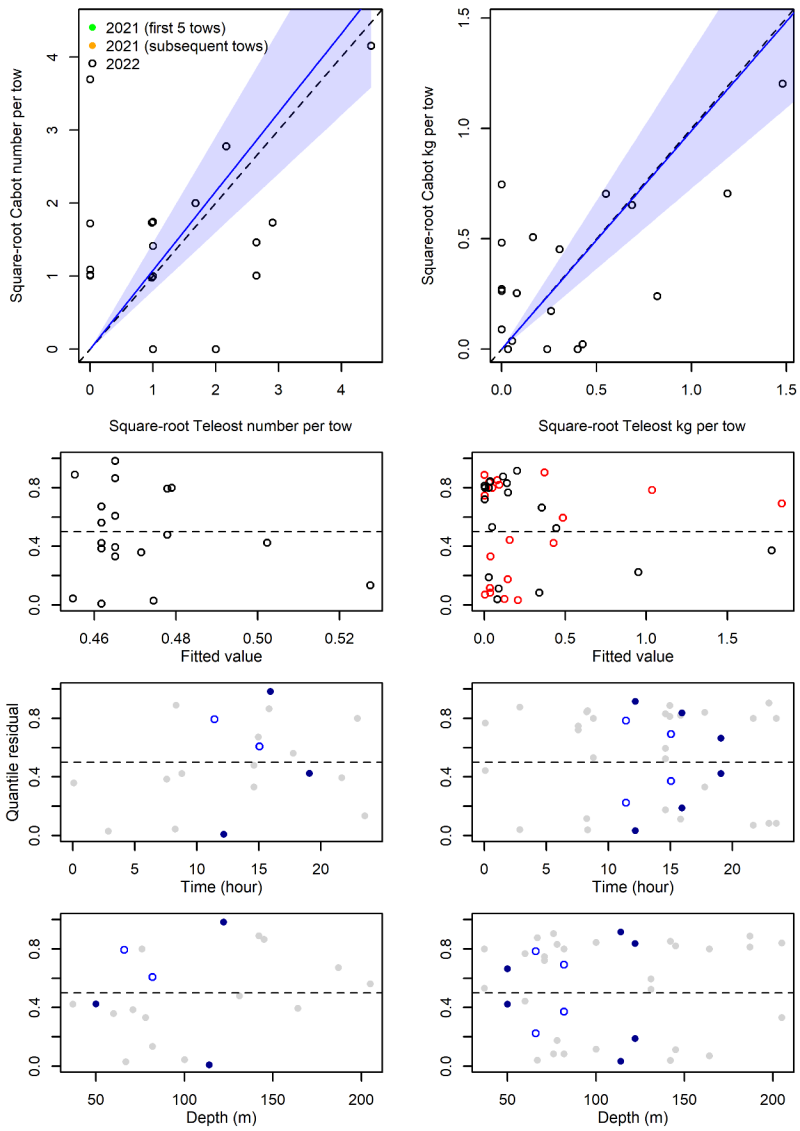

Figure 135.Visualisation of comparative fishing data, size-aggregated model predictions and residual plots for Boltenia ovifera.

9. APPENDICES

APPENDIX I - CAMPELEN 1800 GEAR CHANGES PRIOR TO 2020 COMPARATIVE FISHING

Modifications were made to the Campelen 1800 trawl prior to the commencement of comparative fishing in Atlantic Canada to make the survey trawl more user friendly and less susceptible to damage, and to reduce human resource requirement to acquire and resupply trawl parts. This trawl is used in three large bottom trawl-survey in Atlantic Canada, namely the spring and fall Newfoundland and Labrador survey, and the EnGSL survey.

The following changes were made to the trawl (refer to plan in Fig. A1):

1. Shortened Belly #2 **(CT19/CT25)** and Side Panel #5 **(CT31)** (from 255.5 to 199.5 meshes deep) to reduce damage, associated trawl repairs and construction costs.
2. Changed certain dimensions including the taping ratio of Belly #3 **(CT20/CT26)** in response to the shortening of Belly #2 (see Fig. A1 for details).
3. Strengthened protection of Lower Belly #1 **(CT24)** by splitting this panel into 3 sections which are laced together (usually the netting will tear in one section, typically the middle, if the tear is caused by rock or mud, and the sides of the belly will be okay). A “tear-stop” rope was also added between Belly #1 and Belly #2 to prevent further damage to the other bellies.
4. Lengthened Side Panels # 2 - **CT29** and Top Wing Bunt – **CT16B** (from 41.5 to 48.5 meshes) to reduce any slack netting that increases potential for damage, and to allow for easier repairs and construction.
5. Lengthened upper Bolshline **- CT34 (**from 13.53m to 13.70 meshes**)** to help with keeping the netting in shape on the top wings, and make the floats much easier to install and replace.

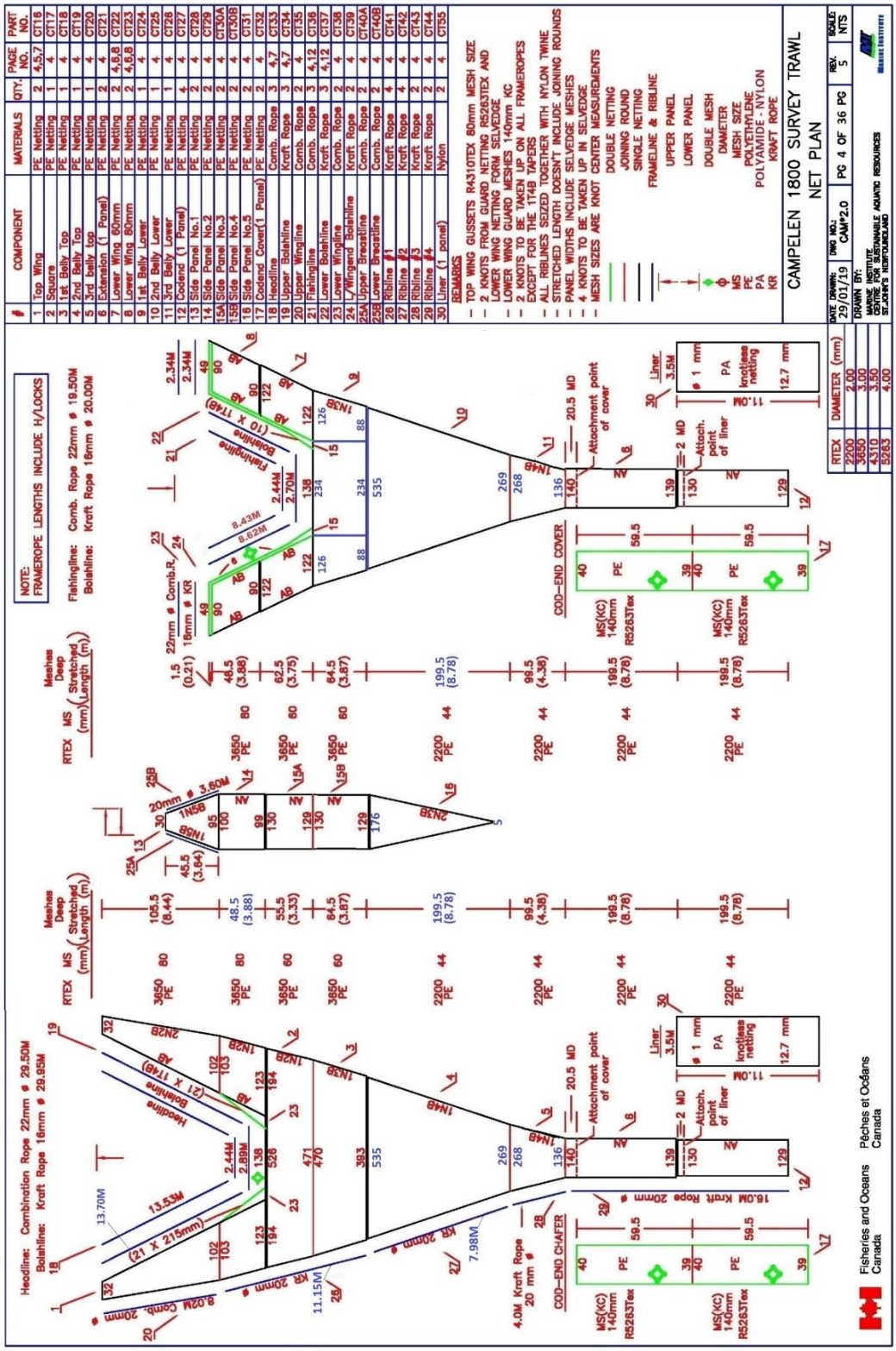

Figure A1. Net plan for the Campelen 1800 trawl

APPENDIX II – SWEPT AREA DETERMINATION

The geometry of the trawl when it is deployed on the bottom and fishing, namely the spread between the doors and between the wings, and the vertical opening, vary according to the vessel used and the fishing depth. The area swept by the trawl on the bottom is therefore variable from one tow to another. Scanmar sensors installed at different locations on the trawl continuously monitor the geometry of the trawl and data are recorded for each tow.

Average geometry data from 144 tows made on the John Cabot in 2022 are shown in Figure A2. The average spacing between the doors and between the wings increased with the fishing depth, stabilizing at depths of more than 250 m. In contrast, the vertical opening decreased according to the depth, again reaching an asymptote at depths greater than 250 m. Based on the 144 tows, for which the depths are collectively generally representative of depths available in the survey area, the average wingspread was 16.65 m, the average doorspread was 50.23 m and the average vertical opening was 3.13 m.

Although the wingspread varies according to depth and the type of substrate, the use of a constant wingspread is recommended in the calculations of survey swept-area abundance and biomass. This constant was derived by predicting the wingspead for each of the stations fished from 1990 to 2022 in the survey of the Estuary and northern Gulf survey (n = 7,264 tows) based on the depth of the station and the relationship between the wingspread and depth (Figure A2, panel A). The average wingspread for the modified Campelen 1800 trawl used with the CCGS John Cabot was estimated at 16.71 m. By comparison, the average wingspread for the Campelen 1800 trawl used on the CCGS Teleost was 16.94 m. These constants will therefore be used to determine the area swept by the trawl tow (average wingspread multiplied by the distance trawled) depending on the vessel.

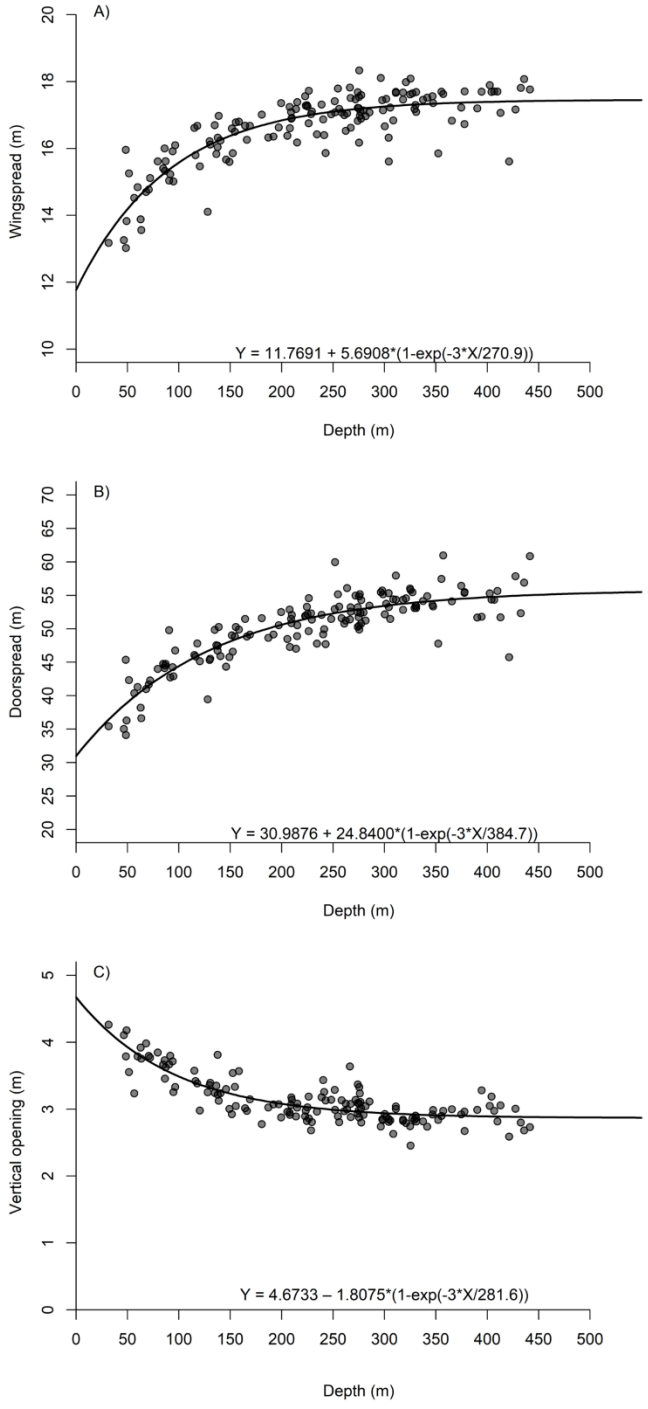

Figure A2. Wingspread (A), doorspread (B), and vertical opening (C) of the Campelen trawl as a function of depth for the 144 tows by the CCGS John Cabot in 2022.